Order Statistics in Wireless Communications

Diversity, Adaptation, and Scheduling in MIMO and OFDM Systems

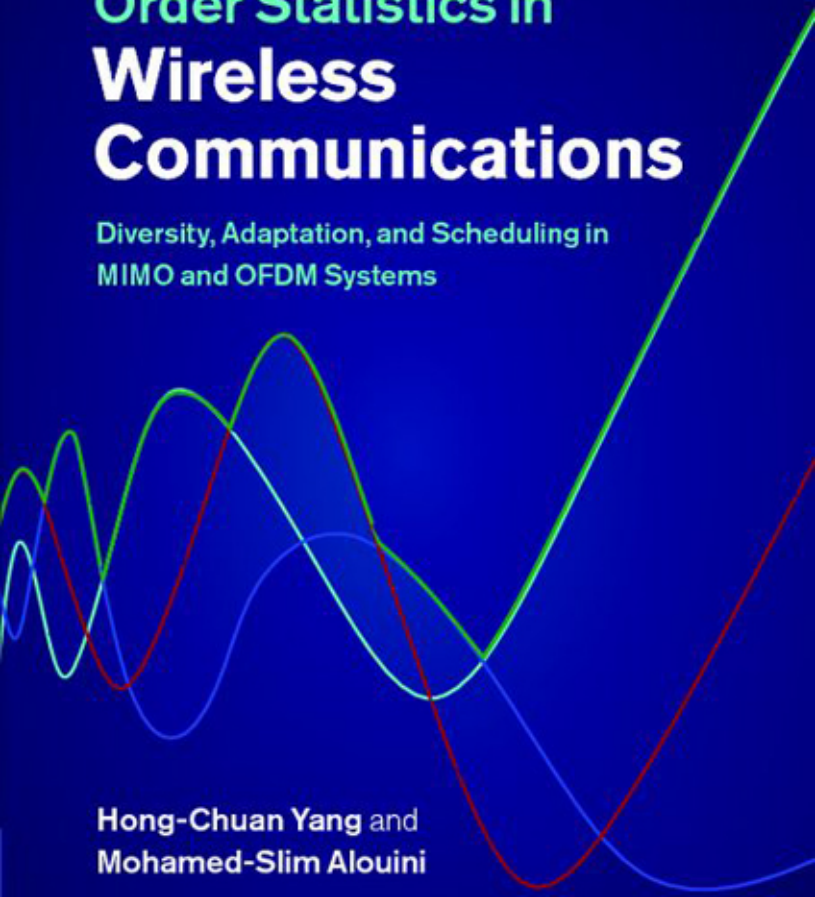

Hong-Chuan Yang and
Mohamed-Slim Alouini

CAMBRIDGE

CAMBRIDGE

more information - www.cambridge.org/9780521199254

Order Statistics in Wireless Communications

Diversity, Adaptation, and Scheduling in MIMO and OFDM Systems

Covering fundamental principles through to practical applications, this self-contained guide describes indispensable mathematical tools for the analysis and design of advanced wireless transmission and reception techniques in MIMO and OFDM systems. The analysis-oriented approach develops a thorough understanding of core concepts, and discussion of various example schemes shows how to apply these concepts in practice. The book focuses on techniques of advanced diversity combining, channel adaptive transmission, and multiuser scheduling, the foundations of future wireless systems for the delivery of highly spectrum-efficient wireless multimedia services. Bringing together conventional and novel results from a wide variety of sources, it will teach you to accurately quantify trade-offs between performance and complexity for different design options so that you can determine the most suitable design choice based on specific practical implementation constraints.

Hong-Chuan Yang is an Associate Professor in the Electrical and Computer Engineering Department at the University of Victoria, Canada. He has developed several mathematical tools for accurate performance evaluation of advanced wireless transmission technologies in fading environments, and his current research focuses on channel modeling, diversity techniques, system performance evaluation, cross-layer design, and energy-efficient communications.

Mohamed-Slim Alouini is a Professor of Electrical Engineering at King Abdullah University of Science and Technology (KAUST), Thuwal, Makkah Province, Saudi Arabia. A Fellow of the IEEE, he is a co-recipient of numerous best paper awards, including awards from ICC, Globecom, VTC, and PIMRC. His research interests include design and performance analysis of diversity combining techniques, MIMO techniques, multi-hop/cooperative communications, cognitive radio, and multi-resolution, hierarchical, and adaptive modulation schemes.

Order Statistics in Wireless Communications

Diversity, Adaptation, and Scheduling in MIMO and OFDM Systems

HONG-CHUAN YANG
University of Victoria, British Columbia, Canada

MOHAMED-SLIM ALOUINI
King Abdullah University of Science and Technology (KAUST), Saudi Arabia

CAMBRIDGE
UNIVERSITY PRESS

CAMBRIDGE UNIVERSITY PRESS
Cambridge, New York, Melbourne, Madrid, Cape Town,
Singapore, São Paulo, Delhi, Tokyo, Mexico City

Cambridge University Press
The Edinburgh Building, Cambridge CB2 8RU, UK

Published in the United States of America by Cambridge University Press, New York

www.cambridge.org
Information on this title: www.cambridge.org/9780521199254

First published 2011

Printed in the United Kingdom at the University Press, Cambridge

A catalogue record for this publication is available from the British Library

ISBN 978-0-521-19925-4 Hardback

To
Our Families

Contents

Preface

Order statistics is an important sub-discipline of statistical theory and finds applications in a vast variety of fields, with life science as the most notable example [1]. Over the years, order statistics has made an increasing number of appearances in design and analysis wireless communication systems, primarily because of the simple but effective engineering principle – "pick the best". For example, the diversity combining technique is an effective solution to improve the performance of wireless communication systems operating over fading channels by generating differently faded replicas of the same information-bearing signal. Selection combining (SC) [2, 3], which selects the replica with the best quality for further processing, is an attractive practical combining scheme and has been researched extensively in the literature. The performance analysis of the SC scheme entails the distribution functions of the largest random variables among multiple ones, which is available in conventional order statistics literature.

More recently, order statistics has also found application in the analysis and design of many emerging wireless transmission and reception techniques, such as advanced diversity combining techniques, channel adaptive transmission techniques, and multiuser scheduling techniques. These techniques are becoming the essential building blocks of future wireless systems for the delivery of multimedia services with high spectrum efficiency [4]. In particular, order statistics results have allowed for the accurate quantification of the trade-off of performance versus complexity among different design options, which will greatly facilitate the applications of these technologies in future wireless systems. At the same time, these applications to wireless system analysis provide new incentives for the further development of order statistic theory. In fact, the study of advanced diversity combining techniques has led to some new order statistics results [5, 6], in terms of the joint distribution functions of linear functions of ordered random variables.

The primary goal of this book is to provide a comprehensive and coherent treatment of the general subject of order statistics in wireless communications. By collecting the relevant results in the literature in a unified fashion, the book will serve as a useful resource for students and researchers to further exploit the potential of order statistics in the analysis and design of advanced wireless transmission technologies. It is our sincere hope that the book will build a solid foundation for readers to further explore the potential of order statistics in advanced wireless communication research. We also believe that the new wireless

communication research problems will in turn stimulate the future evolution of order statistics theory, which will benefit the solution of research problems in other research fields.

Diversity, adaptation, and scheduling are becoming three essential concepts in wireless communications [4]. Diversity combining can effectively mitigate the deleterious fading effect through the generation and exploration of differently faded replicas of the same information signal. Channel adaptation can acheive highly spectral and power-efficient transmission over fading channels by matching the transceiver parameters properly with the prevailing fading channel condition. Multiuser scheduling can explore the multiuser diversity gain inherent in multiuser systems for overall capacity benefit. These fundamental design principles manifest themselves in various transmission and reception technologies for both narrowband and wideband systems with single-antenna or multiple-antenna scenarios. In particular, both multiuser multiple-input–multiple-output (MIMO) systems and orthogonal frequency division multiple access (OFDMA) systems can apply user scheduling techniques to improve the overall system throughput.

Another goal of this book is to provide an in-depth analysis-oriented exposition of diversity combining, link adaptation, and user scheduling techniques. The uniqueness of our approach lies in the fact that for each design option of different techniques, we obtain the exact analytical expression of important performance metrics. Such analytical results build on accurate understanding of scheme design, careful statistical reasoning, and proper application of order statistics. Combined with the associated complexity quantification, the book will help foster a deep understanding of the underlying design principles and tradeoffs of different techniques. The readers will also benefit from the analytical methodologies, which may help them solve their specific research problem.

This book is intended for senior graduate students, researchers, and practising engineers in the field of wireless and mobile communications. Refs [4,7] may serve as suitable background references for this book. The material of this book has been used in a term-long graduate-level course on advanced wireless communications at the University of Victoria, Canada, and an intensive three-week short course at the Tsinghua University, China. It has proven to be an ideal venue for students to enhance their analytical skills as well as to expand their knowledge of advanced wireless transmission technologies.

The authors would like to acknowledge their current and past students, postdocs, and collaborators for their contributions in the works that have been included in this book. Specifically, the authors would like to thank Prof. Seyeong Choi, Prof. David Gesbert, Prof. Young-chai Ko, Prof. Geir Oien, Prof. Khalid A. Qaraqe, Dr. Peng Lu, Dr. Sung-Sik Nam, Dr. Ki-Hong Park, Dr. Lin Yang, Mr. Seung-Sik Eom, Mr. Noureddine Hamdi, Mr. Bengt Holter, and Mr. Le Yang. The authors want to thank Dr. Phil Meyler at Cambridge University Press whose remarkable talent identified the potential of this project. Finally, the valuable support from Ms. Sarah Finlay and Ms. Sabine Koch at Cambridge University Press during the preparation of the book is much appreciated.

References

[1] H. A. David, *Order Statistics*. New York, NY: John Wiley & Sons, Inc., 1981.

[2] W. C. Jakes, *Microwave Mobile Communications*. New York: Wiley, 1974.

[3] G. L. Stüber, *Principles of Mobile Communications*, 2nd ed. Norwell, MA: Kluwer Academic Publishers, 2000.

[4] A. J. Goldsmith, *Wireless Communications*. New York, NY: Cambridge University Press, 2005.

[5] H.-C. Yang, "New results on ordered statistics and analysis of minimum-selection generalized selection combining (GSC)," *IEEE Trans. Wireless Commun.*, vol. TWC-5, no. 7, pp. 1876–1885, July 2006.

[6] Y.-C. Ko, H.-C. Yang, S.-S. Eom and M.-S. Alouini, "Adaptive modulation with diversity combining based on output-threshold MRC," *IEEE Trans. Wireless Commun.*, vol. TWC-6, no. 10, pp. 3728–3737, October 2007.

[7] M. K. Simon and M.-S. Alouini, *Digital Communications over Generalized Fading Channels: A Unified Approach to Performance Analysis*. New York, NY: John Wiley & Sons, 2000.

Notation

General notation

$\mathbf{A}^H$	Hermitian transpose of matrix $\mathbf{A}$
$\mathrm{BER}_n^{-1}(\cdot)$	the inverse BER operation
$< BER >$	overall bit error rate of adaptive transmission system
$\overline{BER}_n$	average error rate of modulation mode n
$\mathbf{E}[\cdot]$	statistical expectation
$E_1(\cdot)$	exponential integral function of first order
$F_\gamma(\cdot)$	cumulative distribution function of γ
$I_0(\cdot)$	modified Bessel function of zero order
$J_0(\cdot)$	Bessel function of zero order
${\mathcal{L}_s}^{-1}(\cdot)$	inverse Laplace transform with respect to s
$\mathcal{M}_\gamma(\cdot)$	moment generating function of γ
$p_{X,Y}(\cdot)$	joint probability density function of X and Y
$p_{X\,\vert Y=y}(x)$	conditional probability density function of X given Y is equal to y
$p_\gamma(\cdot)$	probability density function of γ
$P_b(E)$	bit error rate
$\overline{P}_b$	average bit error rate
$P_E(\gamma)$	instantaneous error probability for given SNR γ
$\overline{P}_E$	average error rate
$PL(d)$ dB	path loss at distance d in dB
P_{out}	outage probability
$\Pr[\cdot]$	probability of an event
$P_s(E)$	symbol error rate
$\overline{P}_s$	average symbol error rate
$Q(\cdot)$	Gaussian Q-function
$Q_1(\cdot,\cdot)$	Marcum Q-function
$\Re\{\cdot\}$	real part of a complex number
s^*	complex conjugate of s
$tr\{\cdot\}$	trace of a matrix
$\mathcal{U}(\cdot)$	unit step function
$\mathbf{x}$	vector $\mathbf{x}$ (bold face lowercase letter)
$\|\mathbf{x}\|^2$	norm square of vector $\mathbf{x}$

$\mathbf{X}$	matrix $\mathbf{X}$ (bold face capital letter)
$\dot{\alpha}$	time derivative of the process α
$\gamma_{l:L}$	lth largest one among total L SNR values
$\overline{\gamma}$	average received SNR
$\tilde{\gamma}$	normalized SNR by its average
Γ_i	sum of the first i largest ordered SNRs
$\Gamma_{i:j}$	sum of the i largest SNRs among j ones
$\Gamma(\cdot)$	Gamma function
$\Gamma(\cdot,\cdot)$	incomplete Gamma function
Ω	short-term average channel power gain

Abbreviations

AAP	average access probability
AAR	average access rate
AAT	average access time
ABA-CBBI	adaptive beam activation based on CBBI
AFL	average feedback load
AMDC	joint adaptive modulation and diversity combining
ASE	average spectrum efficiency
ASK	amplitude shift keying
AT-GSC	absolute threshold GSC
AWGN	additive white Gaussian noise
AWT	average waiting time
BBI	best beam index
BBSI	best beam SINR and index
BER	bit error rate
BS	base station
CBBI	conditional best beam index feedback
CDF	cumulative distribution function
CLT	central limit theorem
CSI	channel state information
DPC	dirty paper coding
EDF	exceedance distribution function
EGC	equal gain combining
GEV	generalized extreme-value
GSC	generalized selection combining
GSEC	generalized switch and examine combining
GSECps	GSEC with post-examine selection
GSMuS	generalized selection multiuser scheduling
GWC-ZFBF	greedy weight clique ZFBF
i.i.d.	independent and identically distributed

i.n.d.	independent and non-identical distributed
ISI	intersymbol interference
LCR	level crossing rate
LOS	line of sight
MEC-GSC	minimum estimation and combining GSC
MGF	moment generation function
MIMO	multiple-input–multiple-output
MISO	multiple-input–single-output
MRC	maximum ratio combining
MSE	mean square error
MS-GSC	minimum selection GSC
NT-GSC	normalized threshold GSC
OC	optimum combining
OFDM	orthogonal frequency division multiplexing
OFDMA	orthogonal frequency division multiple access
OOBS	on–off based scheduling
OT-MRC	output threshold MRC
OT-GSC	output threshold GSC
PDF	probability density function
PMF	probability mass function
PSD	power spectral density
PSK	phase shift keying
QAM	quadrature amplitude modulation
QBBSI	BBSI schemes with quantized SINR feedback
QPSK	quadrature phase-shift keying
RMS	root mean square
RUB	random unitary beamforming
SBS	switched-based scheduling
SC	selection combining
SEC	switch and examine combining
SECps	switch and examine combining with post-examining selection
SHO	soft handover
SINR	signal to interference plus noise ratio
SNR	signal-to-noise ratio
SSC	switch and stay combining
STBC	space-time block code
SUP-ZFBF	successive projection ZFBF
TDD	time division duplexing
TDMA	time division multiple access
T-GSC	GSC with threshold test per branch
UWB	ultra wideband
WCDMA	wideband code division multiple access
ZFBF	zero-forcing beamforming

1 Introduction

The wireless communication industry has been and is still experiencing an exciting era of rapid development. New technologies and designs emerge on a regular basis. The timely adoption of these technologies in real-world systems relies heavily on the accurate prediction of their performance over general wireless fading channels and the associated system complexity. Theoretical performance and complexity analysis become invaluable in this process, because they can help circumvent the time-consuming computer simulation and expensive field test campaigns. These analytical results, usually in the form of elegant closed-form solutions, will also bring important insight into the dependence of the performance as well as complexity measures on system design parameters and, as such, facilitate the determination of the most suitable design choice in the face of practical implementation constraints.

Mathematical and statistical tools play a critical rule in the performance analysis of digital wireless communication systems over fading channels [1]. In fact, the proper utilization of these tools can help either simplify the existing results, which do not allow for efficient numerical evaluation, or render new analytical solutions that were previously deemed infeasible. One popular example is the application of moment generation function (MGF) in the performance analysis of digital communication system over fading channels [2]. With the unified MGF-based analytical framework, the error probability expressions, which usually involve an infinite integration of Gaussian Q-function, are simplified to a single integral of elementary functions with finite limits and, as such, facilitate convenient and accurate numerical evaluation.

Order statistics is an important sub-discipline of statistics theory [3]. Over the years, order statistics has made an increasing number of appearances in the design and analysis of wireless communication systems. Specifically, order statistics have been proven to be valuable tools during the performance analysis of advanced diversity techniques, adaptive transmission techniques, and multiuser scheduling techniques, where the simple but effective engineering principle of "selecting the best" frequently applies. This book aims at providing a coherent and systematic presentation of the applications of order statistics in wireless communication system analysis, which will prepare readers to further explore the potentials of ordered statistics in advanced wireless communication research.

1.1 Order statistics in wireless system analysis

The most common figure of merit governing the performance of a communication system is the signal-to-noise ratio (SNR). (For wireless transmission subject to certain interference, the modified matric signal to interference plus noise ratio (SINR) is often used.) The receiver output SNR, which can be directly related to the instantaneous error rate performance, serves as an excellent indicator of the fidelity of the detection process. As the result of the fading effect associated with multipath wireless channels, the receiver output SNR, usually denoted by γ, will randomly vary over time. In this scenario, the average performance measures should be employed, the evaluation of which would require the statistical distribution of γ. For example, the so-called outage probability performance measure, defined as the probability that the channel quality is too poor for reliable transmission, is calculated as the probability that γ falls below a certain specific threshold $\gamma_{\rm th}$, i.e.

$$P_{\rm out} = \int_0^{\gamma_{\rm th}} p_\gamma(\gamma){\rm d}\gamma, \tag{1.1}$$

where $p_\gamma(\cdot)$ is the probability density function (PDF) of γ. The average error rate of a wireless link can be calculated as

$$\overline{P}_E = \int_0^{\infty} P_E(\gamma) p_\gamma(\gamma){\rm d}\gamma, \tag{1.2}$$

where $P_E(\gamma)$ is the instantaneous error rate of the modulation scheme of interest for a given SNR value γ.

The PDF of γ for the conventional narrowband single-antenna link can be easily derived based on the adopted fading channel models. With the introduction of diversity, adaptation, and scheduling techniques, the statistics of the receiver output SNR become more challenging to obtain. Quite often, such analysis mandates some order statistics results, as the practical best-selection engineering principle frequently applies in the designs. As a classical example, the selection diversity combining technique uses the signal replica with the best quality, i.e. the highest instantaneous SNR, among several available ones for data detection [1]. As such, the receiver output SNR becomes the largest one of several branch SNRs, i.e. $\gamma_{\max} = \max\{\gamma_1, \gamma_2, \cdots\}$, the statistics characterization of which is readily available in traditional order statistics literature [4]. Specifically, the PDF of the largest one among L independent and identically distributed (i.i.d.) branch SNRs is given by

$$p_{\gamma_{\max}}(x) = L[F_\gamma(x)]^{K-1} p_\gamma(x), \tag{1.3}$$

where $F_\gamma(x)$ and $p_\gamma(x)$ are the common PDF and CDF of γ.

Recently, generalized selection combining (GSC) was proposed as an attractive combining scheme for broadband wireless systems (see for example [5–9]). The basic idea is to select L_c best diversity branches out of a total L available

ones, where $L_c < L$, and combine them in the optimal maximum ratio combining (MRC) fashion. The combiner output SNR with GSC becomes the sum of the L_c largest random variables among a total of L ones, the statistics of which were not immediately available over the general fading channel models. Furthermore, the analysis of adaptive combining schemes, where the receiver tries to utilize a minimum amount of combining operations to satisfy a certain threshold requirement, further requires the joint statistics of the partial sums of ordered random variables [10–12]. Such joint statistics also find application in the analysis of multiuser scheduling schemes for OFDMA and MIMO systems. In this book, we will provide a comprehensive treatment of the application of order statistics in the analysis of wireless communication systems and focus in particular on how conventional and new order statistics results help obtain the desired statistics of received output SNR. These statistical results can then be readily utilized to calculate various performance metric of interest by following the standard analytical procedure in [1, 2].

1.2 Diversity, adaptation, and scheduling

Many technologies have been developed to improve the quality and efficiency of wireless communication systems. While providing a coherent presentation of order statistics in wireless communications, we focus on three general classes of wireless techniques, namely diversity, adaptation, and scheduling, all of which are essential building blocks of current and emerging wireless systems and, as such, have received a significant amount of interest from both academia and industry. We adopt a unique analysis-oriented approach in presenting these technologies. Specifically, we present several practical designs for each technology and attack their exact performance and complexity analysis over general fading environment with the help of order statistics results. The primary objective is to accurately quantify the trade-off of performance versus complexity among different design options, which help foster a thorough and in-depth understanding of each technology.

Diversity combining techniques can effectively improve the performance of a wireless communication system operating over a fading environment. Conventional combining schemes have been well-documented in various textbooks on wireless communications [1, 13]. Over the past decade, there have been significant developments in the field of advanced diversity combining techniques for emerging broadband wireless systems. Motivated by the fact that a large number of available paths may exist whereas the system can only afford to process a limited number of paths due to the complexity and cost constraint, the common goal of these newly proposed combining schemes is to efficiently select a subset of strong diversity paths and combine them in the MRC fashion from those that are available [14–16]. The trade-off of performance versus complexity among different schemes mandates the exact analysis on each scheme. This book will provide a

comprehensive treatment of several representative advanced diversity-combining schemes.

Channel adaptive transmission and reception techniques can achieve high spectrum and/or power efficiency by effectively exploring the time-varying nature of wireless fading channels. Conventional adaptive transmission techniques vary various transmission parameters with the prevailing channel conditions to achieve highly spectral-efficient transmission while satisfying a certain error rate requirement [13]. With the recent development of adaptive diversity combining techniques, the amount of combining operation will also vary with the fading channel condition. The main objective of the new class of diversity techniques is to adaptively utilize the diversity combiner resource, in terms of active diversity branches and channel estimations, to achieve an overall complexity saving while satisfying a certain output performance requirement [10, 11]. The idea of adaptive combining can be applied to receive diversity, transmit diversity, and diversity in a multicell environment. Furthermore, receiver adaptive combining can also be designed jointly with adaptive transmission to reach a highly efficient transceiver design. This book will provide an analysis-oriented presentation of such designs and their underlying design trade-offs.

Multiuser scheduling can explore the diversity benefit inherent in multiuser wireless systems. The idea is to explore the independent variation of multiuser channels and schedule the users with the best channel conditions to transmit [17,18]. Multiuser scheduling has been shown to be able to acheive great throughput performance. The idea of multiuser scheduling has been incorporated into the emerging cellular system standards. This book will cover some recent developments in multiuser scheduling, including multiuser parallel scheduling [19], and scheduling in multiuser MIMO systems [20, 21]. We focus on those practical designs with low implementation complexity and which, as such, can be directly applied to practical wireless systems. Again, special effort will be made to quantify the various design trade-offs involved, which will benefit both academic research and practicing engineers.

1.3 Outline of the book

The primary focus of this book is the application of ordered statistics in the performance and complexity analysis of various wireless communication technologies. The book also covers three general classes of wireless technologies – namely, advanced diversity techniques, channel adaptive transmission, and reception techniques and multiuser scheduling techniques in the context of emerging MIMO–OFDM systems.

The book is organized as follows. We first summarize the basics of digital wireless communications over fading channels in Chapter 2, which provides the necessary background for the subsequent chapters. Then, the statistical results, more specifically the conventional and new results on the distribution functions

of random variables involving order statistics, are presented together with their derivations in Chapter 3. Chapter 4 concentrates on the analysis and design of advanced diversity combining techniques, whereas channel adaptive transmission and reception techniques are presented in Chapter 5. The concept of multiuser scheduling is explored in Chapter 6 and Chapter 7, in the context of OFDMA systems and multiuser MIMO system, respectively.

We strive to achieve an ideal balance between theory and practice. The detailed mathematical derivations for order statistics are grouped into one chapter so that other chapters will focus on the practical design insights. Such an arrangement will allow easy reading and convenient future referencing. Special emphasis will be placed on the important trade-off of performance versus complexity throughout the presentation. Whenever deemed necessary, the associated complexity measures are quantified and plotted together with the performance for clear trade-off illustration.

References

[1] G. L. Stüber, *Principles of Mobile Communications*, 2nd ed. Norwell, MA: Kluwer Academic Publishers, 2000.

[2] M. K. Simon and M.-S. Alouini, *Digital Communications over Generalized Fading Channels: A Unified Approach to Performance Analysis*. New York, NY: John Wiley & Sons, 2000.

[3] N. Balakrishnan and C. R. Rao, *Handbook of Statistics 17: Order Statistics: Applications*, 2nd ed. Amsterdam: North-Holland Elsevier, 1998.

[4] H. A. David, *Order Statistics*. New York, NY: John Wiley & Sons, Inc., 1981.

[5] N. Kong and L. B. Milstein, "Average SNR of a generalized diversity selection combining scheme," *IEEE Commun. Letters*, vol. 3, no. 3, p. 5759, March 1999, see also *Proc. IEEE Int. Conf. on Commun. (ICC'98)*, Atlanta, Georgia, pp. 1556–1560, June 1998.

[6] Y. Roy, J.-Y. Chouinard and S. A. Mahmoud, "Selection diversity combining with multiple antennas for MM-wave indoor wireless channels," *IEEE J. Select. Areas Commun.*, vol. SAC-14, no. 4, pp. 674–682, May 1998.

[7] M. Z. Win and J. H. Winters, "Virtual branch analysis of symbol error probability for hybrid selection/maximal-ratio combining in Rayleigh fading," *IEEE Trans. Commun.*, vol. COM-49, no. 11, pp. 1926–1934, November 2001.

[8] A. Annamalai and C. Tellambura, "Analysis of hybrid selection/maximal-ratio diversity combiner with Gaussian errors," *IEEE Trans. Wireless Commun.*, vol. TWC-1, no. 3, pp. 498–512, July 2002.

[9] Y. Ma and S. Pasupathy, "Efficient performance evaluation for generalized selection combining on generalized fading channels," *IEEE Trans. Wireless. Commun.*, vol. TWC-3, no. 1, pp. 29–34, January 2004.

[10] S. W. Kim, D. S. Ha and J. H. Reed, "Minimum selection GSC and adaptive low-power RAKE combining scheme," in *Proc. of IEEE Int. Symp. on Circuits and Systems. (ISCAS'03)*, Bangkok, Thailand, vol. 4, May 2003, pp. 357–360.

[11] H.-C. Yang, "New results on ordered statistics and analysis of minimum-selection generalized selection combining (GSC)," *IEEE Trans. Wireless Commun.*, vol. TWC-5, no. 7, pp. 1876–1885, July 2006.

[12] Y.-C. Ko, H.-C. Yang, S.-S. Eom and M. -S. Alouini, "Adaptive modulation with diversity combining based on output-threshold MRC," *IEEE Trans. Wireless Commun.*, vol. TWC-6, no. 10, pp. 3728–3737, October 2007.

[13] A. Goldsmith, *Wireless Communications*. Cambridge: Cambridge University Press, 2005.

[14] A. I. Sulyman and M. Kousa, "Bit error rate performance of a generalized diversity selection combining scheme in Nakagami fading channels," in *Proc. of IEEE Wireless Commun. and Networking Conf. (WCNC'00)*, Chicago, Illinois, September 2000, pp. 1080–1085.

[15] M. K. Simon and M.-S. Alouini, "Performance analysis of generalized selection combining with threshold test per branch (T-GSC)," *IEEE Trans. Veh. Technol.*, vol. VT-51, no. 5, pp. 1018–1029, September 2002.

[16] H.-C. Yang and M.-S. Alouini, "Generalized switch and examine combining (GSEC): A low-complexity combining scheme for diversity rich environments," *IEEE Trans. Commun.*, vol. COM-52, no. 10, pp. 1711–1721, October 2004.

[17] R. Knopp and P. Humblet, "Information capacity and power control in single-cell multiuser communications," in *Proc. IEEE Int. Conf. Commun. (ICC'95)*, Seattle, WA, vol. 1, pp. 331–335, June 1995.

[18] D. N. C. Tse,"Optimal power allocation over parallel Gaussian channels", in *Proc. Int. Symp. Inform. Theory (ISIT'97)*, Ulm, Germany, p. 27, June 1997.

[19] Y. Ma, J. Jin, and D. Zhang, "Throughput and channel access statistics of generalized selection multiuser scheduling," *IEEE Trans. Wireless Commun.*, vol. TWC-7, no. 8, pp. 2975–2987, August 2008.

[20] K. K. J. Chung, C.-S. Hwang and Y. K. Kim, "A random beamforming technique in MIMO systems exploiting multiuser diversity," *IEEE J. Select. Areas Commun.*, vol. SAC-21, no. 5, pp. 848–855, June 2003.

[21] M. Sharif and B. Hassibi, "On the capacity of MIMO broadcast channels with partial side information," *IEEE Trans. Inform. Theory*, vol. IT-51, no. 2, pp. 506–522, February 2005.

2 Digital communications over fading channels

2.1 Introduction

We present a brief summary of digital wireless communications in this chapter. The material will serve as a useful background for the advanced wireless technologies in later chapters. We first review the statistical fading channel models commonly used in wireless system analysis. After that, we discuss digital modulation schemes and their performance analysis over fading channels, including the well-known moment generating function (MGF)-based approach [1]. The basic concept of adaptive modulation and diversity combining will also be presented. While most of the materials of this chapter are reviews of classical results, which can be found in other wireless textbooks, this chapter provides for the first time a thorough treatment of various conventional threshold-based combining schemes, a class of combining scheme enjoying even lower complexity than selection combining (SC). The chapter concludes with a brief discussion of the transmit diversity technique. The discussion of this chapter is by no means comprehensive. The main objective is to introduce some common notation and system models for later chapters. For a thorough treatment of these subjects, the reader may refer to [1, 2].

2.2 Statistical fading channel models

Wireless channels rely on the physical phenomenon of electromagnetic wave propagation, due to the pioneering discoveries of Maxwell and Hertz. Radio waves propagate through several mechanisms, including direct line of sight (LOS), reflection, diffraction, scattering, etc. As such, there usually exist multiple propagation paths between the transmitters and the receivers, as illustrated in Fig. 2.1. In general, when the LOS path exists, as in microwave systems and certain indoor applications, the transmitted radio signal experiences less attenuation. On the other hand, if the LOS path does not exist, the radio signal can still reach the receiver through other mechanisms, but with severe attenuation.

The complicated propagation environment and the unpredictable nature of the propagation process make the modeling of wireless channels very challenging, especially considering the mobility of the transmitter and/or the receiver. To

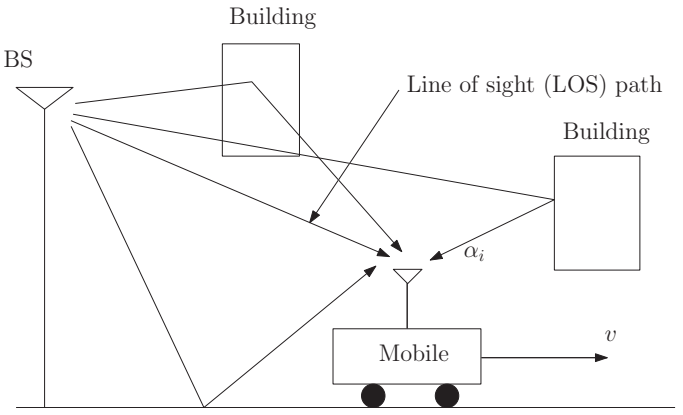

Figure 2.1 Multipath propagation.

avoid the modeling complication associated with the detailed propagation process, the wireless channel is usually characterized by three major effects: (i) path loss, for the general trend of power dissipation as propagation distance increases; (ii) shadowing, for the effects of large objects, such as buildings and trees, along the propagation path; and (iii) fading, resulting from the random superposition of signals from different propagation paths at the receiver. The received signal power variation due to these three effects is demonstrated in Fig. 2.2. In general, path loss and shadowing are called large-scale propagation effects, whereas fading is referred to as the small-scale effect, since the fading effect manifests itself in a much smaller time/spatial scale.

2.2.1 Path loss and shadowing

Path loss characterizes the general trend of power loss as the propagation distance increases. The linear *path loss* is defined as the ratio of the transmitted signal power P_t versus the received signal power P_r, i.e. $PL = P_t/P_r$. Among the different types of path loss models, the log-distance model is the most convenient for high-level system analysis [3]. Specifically, under the log-distance model, path loss at a distance d in dB scale is predicted using the following formula

$$PL(d)\text{dB} = PL(d_0)\text{dB} + 10\beta \log_{10}(d/d_0), \tag{2.1}$$

where d_0 is the reference distance, usually set to 1–10 m for indoor applications and 1 km for outdoor applications, $PL(d_0)$dB is the path loss at d_0 and β is the path loss exponent, which can be estimated by minimizing the mean square error (MSE) between the measurement data and the model. Note that the path loss model only captures the general trend of power dissipation, ignoring the effect of specific surrounding objects or multipaths.

Shadowing characterizes the blockage effect of large objects in the propagation environment. As the size, positioning, and properties of such objects are in

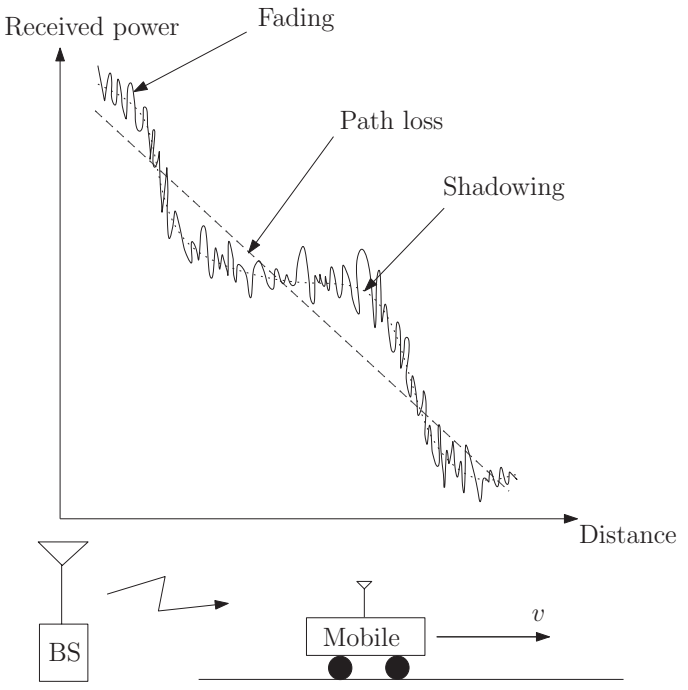

Figure 2.2 Received signal power.

general unknown, the shadowing effect has to be described in the statistical sense. The most popular shadowing model is the log-normal model, which has been emperically confirmed [4]. With the log-normal model, the path loss in dB scale at distance d, denoted by ψ_{dB}, is modeled as a Gaussian random variable with mean value $PL(d)$dB, given by appropriate path loss model, and variance σ_{dB}^2, which varies with the environment. As such, the PDF of ψ_{dB} is given by

$$p_{\psi_d B}(x) = \frac{1}{\sqrt{2\pi}\sigma_{dB}} \exp\left(-\frac{(x - PL(d)dB)^2}{2\sigma_{dB}^2}\right). \tag{2.2}$$

The log-normal model is so named as the path loss in linear scale ψ is a log-normal random variable, with PDF given by

$$p_{\psi}(x) = \frac{10/\ln(10)}{\sqrt{2\pi}x\sigma_{dB}} \exp\left(-\frac{(10\log_{10} x - PL(d)dB)^2}{2\sigma_{dB}^2}\right). \tag{2.3}$$

With the path loss and shadowing model, we can address some interesting system design problems, e.g. for a given transmitting power and target service area, what is the percentage of coverage after considering the path loss and shadowing effects. Assuming a location is covered if the received signal power after shadowing is above the threshold $P_{\min}$, the percentage of coverage can be calculated by averaging the probability that the received signal power at a

distance r is less than $P_{\min}$ over the target area. Mathematically, we have

$$C = \frac{1}{\pi R^2} \int_0^{2\pi} \int_0^R \Pr[P_r(r) > P_{\min}] r \mathrm{d}r \mathrm{d}\theta, \tag{2.4}$$

where R is the radius of the cell. Noting that the coverage probability under the combined log-distance path loss model and log-normal shadowing model is given by

$$\Pr[P_r(r) > P_{\min}] = \int_{-\infty}^{P_t - P_{\min}} p_{\psi_d B}(x) \mathrm{d}x, \tag{2.5}$$

the coverage percentage C can be shown to be given by

$$C = Q(a) + \exp\left(\frac{2-2ab}{b^2}\right) Q\left(\frac{2-ab}{b}\right) \tag{2.6}$$

where

$$a = \frac{P_{\min} - P_t + PL(d_0)\mathrm{dB} + 10\gamma \log_{10}(R/d_0)}{\sigma_{dB}}, b = \frac{10\gamma \log_{10}(e)}{\sigma_{dB}},$$

and $Q(\cdot)$ is the Gaussian Q-function[1], defined as

$$Q(x) = \frac{1}{\sqrt{2\pi}} \int_x^\infty e^{-\frac{t^2}{2}} \, \mathrm{d}t. \tag{2.7}$$

2.2.2 Multipath fading

Fading characterizes the effect of random superposition of signal copies arriving at the receiver from different propagation paths. These signal replicas may add together constructively or cancel one another, which leads to a large variation in received signal strength. To better demonstrate the process, let us assume the following bandpass signal is transmitted over a wireless channel

$$s(t) = \mathrm{Re}\{u(t) e^{j2\pi f_c t}\}, \tag{2.8}$$

where $u(t)$ is complex baseband envelope. Due to multipath propagation, the received signal becomes

$$r(t) = \mathrm{Re}\left\{ \sum_{n=0}^{N(t)} \alpha_n(t) u(t - \tau_n(t)) e^{j2\pi f_c (t - \tau_n(t)) + \phi_{D_n}(t)} \right\}. \tag{2.9}$$

where $N(t)$ is the number of paths, $\tau_n(t)$ is the delay, $\alpha_n(t)$ is the amplitude, and $\phi_{D_n}(t)$ is the phase shift, all for the nth path at time t. Note that the phase shift $\phi_{D_n}(t)$ is related to the Doppler frequency shift as $\phi_{D_n}(t) = \int_t 2\pi f_{D_n}(t) \mathrm{d}t$. After some manipulations while focusing on the complex baseband input and output

[1] The Gaussian Q-function is related to the complementary error function erfc$(\cdot)$ by $\mathrm{erfc}(x) = 2Q(\sqrt{2}x)$ and $Q(x) = \frac{1}{2}\mathrm{erfc}\left(\frac{x}{\sqrt{2}}\right)$.

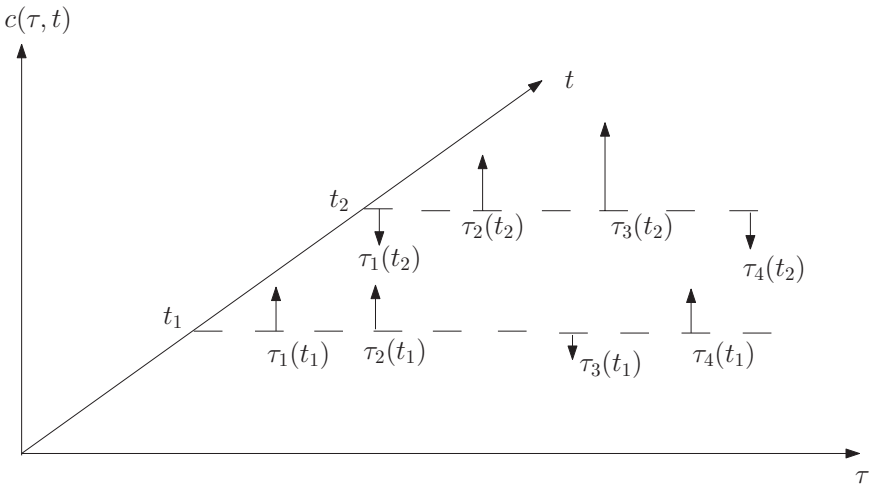

Figure 2.3 Impulse response of linear time variant channel.

relationship, the impulse response of the complex baseband wireless channel can be obtained as

$$c(\tau, t) = \sum_{n=0}^{N(t)} \alpha_n(t) e^{-j\phi_n(t)} \delta(\tau - \tau_n(t)), \tag{2.10}$$

where $\phi_n(t) = 2\pi f_c \tau_n(t) - \phi_{D_n}(t)$. As such, the wireless multipath channel is modeled as a linear time-variant system. Figure 2.3 illustrates the impulse response of the multipath fading channel. It follows that the wireless fading channels cause time-domain variation and power delay spread to the transmitted signal. Based on the relative severity of these effects with respect to the transmitted signal, the multipath fading channels can be classified to slow/fast fading and frequency flat/selective fading.

The so-called RMS (root mean square) delay spread, denoted by σ_T, is commonly used to quantify power spread along the delay axis introduced by the multipath channel. The definition of σ_T is based on the power delay profile, which describes the average signal power distribution along the delay axis and is mathematically given by $A_c(\tau) = \mathbf{E}_T[c^2(\tau, T)]$. Specifically, RMS delay spread σ_T can be calculated as

$$\sigma_T = \sqrt{\frac{\int_0^\infty (\tau - \mu_T)^2 A_c(\tau) \mathrm{d}\tau}{\int_0^\infty A_c(\tau) \mathrm{d}\tau}} = \sqrt{\frac{\sum_{n=0}^N \alpha_n^2 (\tau_n - \mu_T)^2}{\sum_{n=0}^N \alpha_n^2}} \tag{2.11}$$

where μ_T is the average delay spread, given by

$$\mu_T = \frac{\int_0^\infty \tau A_c(\tau) \mathrm{d}\tau}{\int_0^\infty A_c(\tau) \mathrm{d}\tau} = \frac{\sum_{n=0}^N \alpha_n^2 \tau_n}{\sum_{n=0}^N \alpha_n^2}. \tag{2.12}$$

If σ_T is large compared to the symbol period of the transmitted signal, then the delay spread will lead to significant intersymbol interference (ISI). Noting

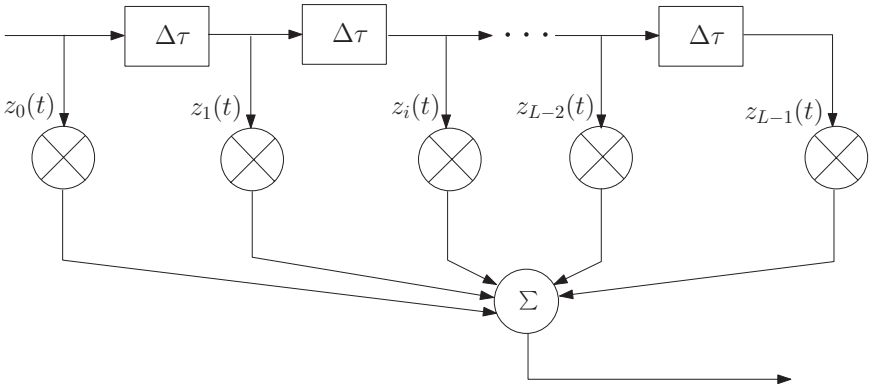

Figure 2.4 Tapped delay line channel model for selective fading.

that time-domain delay spread will translate to frequency selectiveness in the frequency-domain, the channel coherence bandwidth serves as an alternative metric for quantifying power spread along the delay axis. By definition, the channel coherence bandwidth, denoted by B_c, is the bandwidth over which the channel frequency response remains highly correlated. In particular, B_c satisfies: $A_C(\Delta f) = \mathbf{E}[C^*(f_1, t)C(f_2, t)] \approx 1$ for all $\Delta f = |f_1 - f_2| < B_c$. It can be intuitively expected that $B_c \propto 1/\sigma_T$. Correspondingly, the wireless channel is considered frequency-flat if $\sigma_T \ll T_s$, or equivalently, $B_c \gg B_s$, where B_s is the signal bandwidth. Otherwise, the wireless channel introduces selective fading.

Future wireless systems will use increasely wideband channels to provide high data rate multimedia services. As such, most emerging systems will be operating in a frequency-selective fading environment. The most popular model for selective fading is the tapped delay line model, which essentially models the wireless channel as a discrete-time filter. With this model, the channel impulse response is given by

$$c(\tau, t) = \sum_{i=0}^{L-1} z_i(t)\delta(\tau - i\triangle\tau), \tag{2.13}$$

where L is the total number of delay bins, also known as the length of the channel, $\triangle\tau$ is the width of the delay bin, and $z_i(t)$ is the composite time-varying gain of all paths in the ith bin. Figure 2.4 illustrates the tapped delay line model for selective fading channels. On the other hand, most current wireless technologies, such as diversity combining, multiuser scheduling, and multi-antenna transmission, are still designed based on frequency-flat fading channel models. The basic premise of such approaches is that the wideband frequency-selective channel can be converted into multiple parallel frequency-flat fading channels with the well-known multicarrier transmission/orthogonal frequency division multiplexing (OFDM) technique [2]. We follow the same approach and focus on the statistical channel model for a flat fading environment in the following subsections.

2.2.3 Frequency-flat fading

Frequency-flat fading corresponds to the scenario that the delay spread is small with respect to the transmit signal symbol period, i.e. $\sigma_T \ll T_s$. In this case, the multipath can be deemed to arrive at the receiver at the same time. The channel impulse response simplifies to

$$c(\tau, t) = \left(\sum_{n=0}^{N(t)} \alpha_n(t) e^{-j\phi_n(t)} \right) \delta(\tau) = z(t)\delta(\tau), \tag{2.14}$$

which means that the channel introduces a time-varying complex gain of $z(t) = \sum_{n=0}^{N(t)} \alpha_n(t) e^{-j\phi_n(t)}$. Correspondingly, the complex baseband input/output relation of the channel becomes

$$r(t) = z(t)u(t) + n(t), \tag{2.15}$$

where $u(t)$ is the transmitted complex envelope and $n(t)$ is the additive Gaussian noise. To develop further statistical models for the complex channel gain $z(t)$, we note that $z(t) = z_I(t) + jz_Q(t)$, where

$$z_I(t) = \sum_{n=0}^{N(t)} \alpha_n(t) \cos\phi_n(t), \;\; z_Q(t) = \sum_{n=0}^{N(t)} \alpha_n(t) \sin\phi_n(t). \tag{2.16}$$

As such, $z(t)$ can be modeled as a complex Gaussian random process with the application of central limit theorem (CLT). Starting from this basic result, we can arrive at the instantaneous statistics of the channel gain depending on whether an LOS component exists or not.

When there is no LOS component, the random process $z(t)$ can be assumed to have zero mean. With the additional assumption that $\phi_n(t)$ follows a uniform distribution over $[-\pi, \pi]$ and is independent of $\alpha_n(t)$, we can show that $z_I(t)$ and $z_Q(t)$ are independently Gaussian random variables with zero mean. It follows that the channel amplitude $|z(t)| = \sqrt{z_I(t)^2 + z_Q(t)^2}$ is Rayleigh distributed with distribution function

$$p_{|z|}(x) = \frac{x}{\sigma^2} \exp\left[-\frac{x^2}{2\sigma^2} \right], \tag{2.17}$$

where σ^2 is the common variance of $z_I(t)$ and $z_Q(t)$. The channel phase $\theta(t) = \arctan(z_Q(t)/z_I(t))$ is uniform distributed over $[0, 2\pi]$. We can further show that the channel power gain $|z(t)|^2$, which is proportional to the instantaneous received signal power, follows an exponential distribution with PDF given by

$$p_{z^2}(x) = \frac{1}{2\sigma^2} \exp\left[-\frac{x}{2\sigma^2} \right], x \geq 0, \tag{2.18}$$

where $2\sigma^2$ is the average channel power gain, depending upon the path loss/shadowing effects.

When the LOS component exists, $z_I(t)$ and $z_Q(t)$ become a Gaussian random process with nonzero mean. In this case, the instantaneous channel amplitude $|z| = \sqrt{z_I^2 + z_Q^2}$ follows a Rician distribution with distribution function

$$p_{|z|}(x) = \frac{x}{\sigma^2} \exp\left[-\frac{x^2 + s^2}{2\sigma^2}\right] I_0\left(\frac{xs}{\sigma^2}\right), \tag{2.19}$$

where $s^2 = \alpha_0^2$ is the channel power gain of the LOS component, $2\sigma^2$ is the average channel power gain of all non-LOS components, and $I_0(\cdot)$ is the modified Bessel function of zeroth order. Alternatively, the Rician distribution function is given in terms of the so-called Rician fading parameter $K = s^2/2\sigma^2$ and the total average power gain $\Omega = s^2 + 2\sigma^2$. It follows that we can show that the channel power gain $|z(t)|^2$ follows a non-central χ^2 distribution with distribution function

$$p_{|z|^2}(x) = \frac{K+1}{\Omega} \exp\left[-K - \frac{(K+1)x}{\Omega}\right] I_0\left(2\sqrt{\frac{K(K+1)x}{\Omega}}\right). \tag{2.20}$$

The Nakagami model is another statistical fading model for the LOS scenario and was developed from experimental measurements. Based on the Nakagami model, the channel amplitude is modeled as a random variable with distribution function

$$p_{|z|}(x) = \frac{2m^m x^{2m-1}}{\Gamma(m)\Omega} \exp\left[-\frac{mx^2}{\Omega}\right], \tag{2.21}$$

where $\Gamma(\cdot)$ is the Gamma function and $m \geq 1/2$ is the Nakagami fading parameter. It follows that the distribution function of the channel power gain under the Nakagami model is given by

$$p_{z^2}(x) = \left(\frac{m}{\Omega}\right)^m \frac{x^{m-1}}{\Gamma(m)} \exp\left[-\frac{mx}{\Omega}\right]. \tag{2.22}$$

With properly selected values for the Nakagami parameter m, the Nakagami model can apply to many fading scenarios. Specifically, when $m = 1$ (or $K = 0$ for the Rician fading model), we have Rayleigh fading. If m approaches ∞ (or K approaches ∞ for the Rician model), then the model corresponds to the no fading environment. The Nakagami model can well approximate Rician fading when $m = \frac{(K+1)^2}{2K+1}$. Finally, when $m < 1$, the Nakagami model applies a fading scenario that is more severe than Rayleigh fading.

An immediate application of these statistical models would be outage performance evaluation. Outage occurs when the instantaneous received signal power is too low for reliable information transmission. For transmission over fading channels, since the received signal power is proportional to the channel power gain, the outage probability can be calculated by evaluating the cumulative distribution function (CDF) of the channel power gain at a certain outage threshold, i.e. $P_{\text{out}} = \Pr[|z(t)|^2 < P_0]$, where P_0 is the normalized power outage threshold. For example, the outage probability of a point-to-point link under the Rician fading

model is given by

$$P_{\text{out}} = 1 - Q_1\left(\sqrt{2K}, \sqrt{\frac{2(1+K)}{\Omega}P_0}\right), \tag{2.23}$$

where $Q_1(\cdot,\cdot)$ is the Marcum Q-function, defined as

$$Q_1(\alpha,\beta) = \int_{\beta}^{\infty} x \exp\left(-\frac{x^2+\alpha^2}{2}\right) I_0(\alpha x)\mathrm{d}x. \tag{2.24}$$

Similarly, the outage probability under the Nakagami fading is

$$P_{\text{out}} = 1 - \frac{\Gamma\left(m, \frac{m}{\Omega}P_0\right)}{\Gamma(m)}, \tag{2.25}$$

where $\Gamma(\cdot,\cdot)$ is the incomplete Gamma function.

2.2.4 Channel correlation

In the design and analysis of different wireless technologies, we are also interested in the correlation of the wireless channel gains over space or time. For spatial correlation, we focus on the autocorrelation of the bandpass channel gain given by

$$\text{Re}\{z(t)e^{j2\pi f_c t}\} = z_I(t)\cos(2\pi f_c t) - z_Q(t)\sin(2\pi f_c t). \tag{2.26}$$

With the assumption of uniform scattering, i.e. the angle formed by the incident wave with the moving direction is uniformly distributed over $[0,\ 2\pi]$, we can show that the autocorrelation and cross-correlation function of the in-phase and quadrature components of the complex channel gain satisfy

$$\begin{aligned} A_{z_Q}(\tau) = A_{z_I}(\tau) = \frac{P_r}{2}J_0(2\pi f_D \tau); \\ A_{z_I,z_Q}(\tau) = 0, \end{aligned} \tag{2.27}$$

where $J_0(x)$ is the zero-order Bessel function. It follows that the autocorrelation function of $\text{Re}\{z(t)e^{j2\pi f_c t}\}$ is

$$A_z(\tau) = A_{z_I}(\tau)\cos(2\pi f_c \tau), \tag{2.28}$$

which is approximately zero if $f_D\tau \geq 0.4$, i.e. $v\tau \geq 0.4\lambda$. Based on this result, we arrive at a rule of thumb that channel gains become uncorrelated over a distance of half wavelength.

The time-domain variation of wireless channel gain is mainly due to the relative motion of transmitters and receivers.We usually use the so-called channel coherence time T_c to characterize the rate of such variation. The channel coherence time is defined as the time duration that the channel response remains highly correlated. In terms of the time-domain correlation of the wireless channel frequency response, $C(f,t+\Delta t)$, T_c should satisfy $\mathbf{E}[C^*(f,t)C(f,t+\Delta t)] \approx 1$ for all $\Delta t < T_c$. It can be shown, as one would intuitively expect, that T_c is inversely

proportional to the maximum Doppler shift $f_D = v/\lambda$ and approximately given by $T_c \approx 0.4/f_D$. If T_c is much greater than the symbol period T_s, then we claim that the transmitted signal experiences slow fading. Otherwise, the fading is considered to be fast. To meet the increasing demand for high data rate applications, most emerging wireless systems will be operating in a slow fading environment. In this context, a block fading channel model is often adopted in the design and analysis of various wireless technologies. In particular, the channel response is assumed to remain constant for the duration in the order of the channel coherence time and it becomes independent afterwards. While serving as an inaccurate approximation of the reality, the block fading channel model greatly facilitates the description and understanding of new wireless technologies, especially those based on channel estimation and feedback. We will adopt the same model in the following chapters unless otherwise noted.

2.3 Digital wireless communications

Most emerging wireless systems employ digital modulation schemes. Digital modulation schemes offer the following advantages among many others: (i) facilitate source/channel coding for efficient transmission and error protection; (ii) provide better immunity to additive noise and interference; and (iii) achieve higher spectrum efficiency with guaranteed error performance through adaptive transmission. While the fundamental process of digital modulation is essentially a mapping from bit/bit sequences (obtained after source/channel coding and digitization if necessary) to different sinusoidal waveforms, i.e.

$$\{d_j\}_{j=1}^{n} \Longrightarrow A(i)\cos(2\pi f(i)t + \theta(i)), i = 1, 2, \cdots, 2^n, \tag{2.29}$$

different modulation schemes lead to different trade-offs among spectrum efficiency, power efficiency, error performance, as well as implementation complexity. The desired properties of a modulation scheme for wireless systems include: (i) high spectral efficiency to better explore the limited spectrum resource; (ii) high power efficiency to preserve the valuable power resource of the battery-powered mobile terminals; (iii) robustness to the impairments introduced by multipath fading; and (iv) low implementation complexity to reduce the overall system cost. Usually, these are conflicting requirements. Therefore, the best choice would be that resulting in the most desirable trade-off.

2.3.1 Linear bandpass modulation

In this context, we focus the class of linear bandpass modulation schemes, which are widely used in current and emerging wireless systems. With these modulation schemes, the information is carried using either the amplitude and/or phase of the sinusoidal waveform. In particular, the modulated symbols over the ith symbol

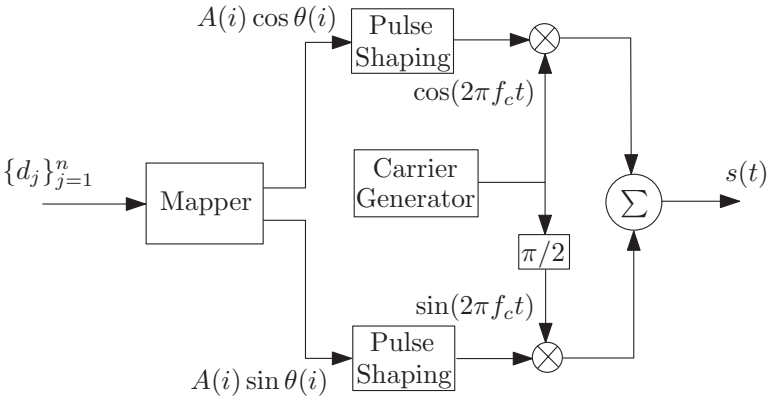

Figure 2.5 Demodulator structure of linear modulation schemes.

period can be written as

$$s(t) = A(i)\cos(2\pi f_c t + \theta(i)),\ (i-1)T_s \le t \le iT_s, \tag{2.30}$$

where f_c is the carrier frequency, $A(i)$ and $\theta(i)$ are information-carrying amplitude and phase. Both amplitude-shift keying (ASK), with constant $\theta(i)$, and phase-shift keying (PSK), with constant $A(i)$, are special cases of this general modulation type. Applying the trigonometric relationship, we can also write the modulation symbol of the linear modulation scheme into the in-phase/quadrature representation as

$$s(t) = s_I(i)\cos 2\pi f_c t - s_Q(i)\sin 2\pi f_c t, \tag{2.31}$$

where $s_I(i) = A(i)\cos\theta(i)$ is the in-phase component and $s_Q(i) = A(i)\sin\theta(i)$ is the quadrature component. The in-phase/quadrature representation is convenient for the understanding of the actual modulator implementation, the generic structure of which is shown in Fig. 2.5. Note that different modulation schemes will differ only in the mapping from bits to in-phase/quadrature components. Such properties will greatly facilitate the implementation of adaptive modulation schemes. Finally, the modulation symbol can be written into the complex envelope format as

$$s(t) = \mathrm{Re}\{(s_I(i) + js_Q(i))e^{j2\pi f_c t}\}, \tag{2.32}$$

where $s_I(i) + js_Q(i)$ is the complex baseband symbol, which varies from one symbol period to another.

The signal space concept is useful to understanding the demodulation process of digital modulation schemes. All linear modulation schemes share the same basis for their modulated symbols, which are given by

$$\phi_1(t) = \sqrt{\frac{2}{T_s}}\cos(2\pi f_c t),\ \text{and}\ \phi_2(t) = \sqrt{\frac{2}{T_s}}\sin(2\pi f_c t). \tag{2.33}$$

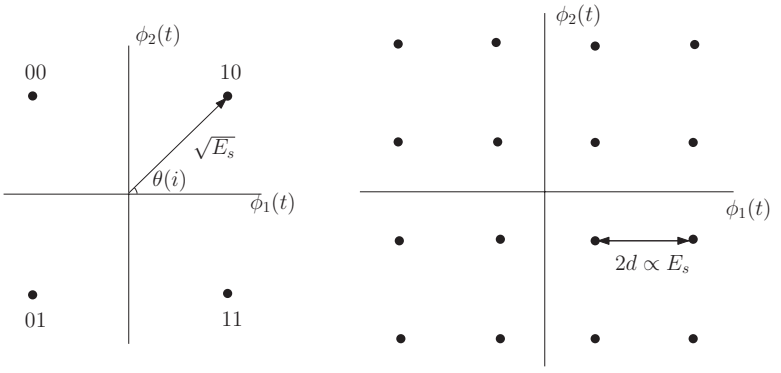

(a) QPSK (b) 16-QAM

Figure 2.6 Sample symbol constellation for linear bandpass modulation.

The modulated symbols become points in the two-dimensional plane defined by these two orthonormal bases. The collection of all possible symbol points form a constellation. Different modulation schemes differ by their constellation structure. As an illustration, the constellations of a square quadrature amplitude modulation (QAM) with $M = 4$ and $M = 16$ are plotted in Fig. 2.6. The coordinates of the constellation points are given by

$$s_{iI} = \sqrt{\frac{T_s}{2}} A(i) \cos\theta(i), \;\; s_{iQ} = \sqrt{\frac{T_s}{2}} A(i) \cos\theta(i), \qquad i = 1, 2, \cdots M. \tag{2.34}$$

Noting that the energy of the ith symbol can be calculated as

$$E_{s_i} = \int_0^{T_s} s^2(t) \mathrm{d}t = \frac{A(i)^2 T_s}{2},$$

the coordinates simplify to

$$s_{iI} = \sqrt{E_{s_i}} \cos\theta(i), \;\; s_{iQ} = \sqrt{E_{s_i}} \cos\theta(i). \tag{2.35}$$

The demodulator will first calculate the projection of the received signal over one symbol period, $r(t)$, $(i-1)T_s \le t \le iT_s$, onto the symbol space defined by the orthonormal basis and obtain the sufficient statistics for the detection of the transmit symbols, which are given by

$$r_I = \int_0^{T_s} r(t)\phi_1(t)\mathrm{d}t, \;\; r_Q = \int_0^{T_s} r(t)\phi_2(t)\mathrm{d}t. \tag{2.36}$$

The maximum likelihood detection rule is to detect the symbol s_i if the point (r_I, r_Q) is the closest to (s_{iI}, s_{iQ}). The structure of the demodulator is shown in Fig. 2.7.

Detection error occurs when the additive noise causes the received symbol to be closer to a symbol different from that which is transmitted. Therefore, the error performance of digital modulation scheme depends heavily on the ratio of

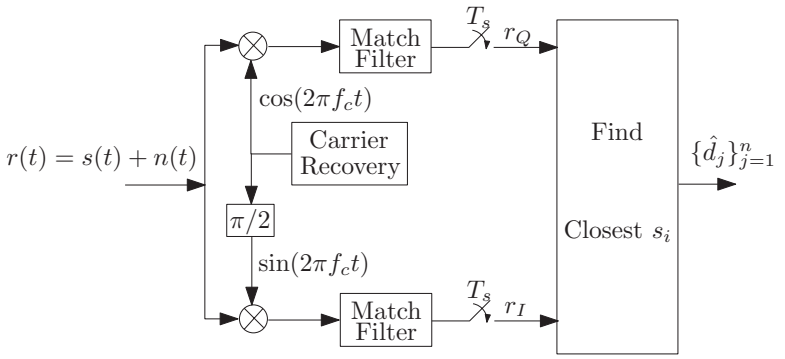

Figure 2.7 Demodulator structure of linear modulation schemes.

received signal power over noise power over signal bandwidth B. For additive white Gaussian noise (AWGN) channels, where the received signal $r(t)$ is related to the transmitted signal $s(t)$ simply by

$$r(t) = s(t) + n(t), \tag{2.37}$$

where $n(t)$ is the Gaussian random process with mean zero and power spectral density (PSD) $N_0/2$, the received signal power is $P_r = E_s/T_s$ and the noise power $N = N_0/2 \cdot 2B = N_0 B$. It follows that the SNR per symbol can be determined as

$$\text{SNR} = \frac{P_r}{N} = \frac{E_s}{N_0 B T_s}. \tag{2.38}$$

The product of BT_s varies only with the pulse-shaping function used and, as such, can be assumed to be constant. As such, the main figure of merit is the ratio of E_s/N_0, which is commonly referred to as received SNR per symbol and denoted by γ_s. For example, it can be shown that the error rate of the binary PSK (BPSK) modulation scheme over AWGN channel is given by

$$P_b(E) = Q\left(\sqrt{2\gamma_s}\right), \tag{2.39}$$

where $Q(\cdot)$ is the Gaussian Q-function. In addition, the symbol error probability of quadrature phase shift keying (QPSK) or equivalently, 4-QAM, over AWGN channel can be shown to be given by

$$P_s(E) = 1 - [1 - Q\left(\sqrt{2\gamma_b}\right)]^2 \approx 2Q\left(\sqrt{2\gamma_b}\right), \tag{2.40}$$

where $\gamma_b = E_b/N_0$ is the received SNR per bit and related to γ_s as $\gamma_b = \gamma_s/\log M$. Finally, the symbol error probability of square M-QAM is

$$P_s(E) = 1 - \left[1 - \frac{2(M-1)}{M} Q\left(\sqrt{\frac{3\gamma_s}{M^2-1}}\right)\right]^2. \tag{2.41}$$

2.3.2 Performance analysis over fading channels

The complex baseband channel model for a flat fading channel is given by

$$r(t) = z(t)s(t) + n(t), \tag{2.42}$$

where $z(t)$ is the time-varying complex channel gain, the statistical characterization of which was discussed in previous sections. The instantaneous power of desired signal at the receiver can be shown to be given by $P_r = |z(t)|^2 \frac{E_s}{T_s}$ and will also vary randomly with $|z(t)|^2$. It follows that the instantaneous SNR becomes

$$\gamma_s = |z(t)|^2 \frac{E_s}{N_0}, \tag{2.43}$$

which also becomes a random variable. In this context, the instantaneous system performance will not reflect the overall system performance. Instead, we need to apply average performance measures, including the outage probability and the average error rate.

Performance measures

Outage occurs when the instantaneous received signal power is too low for reliable information transmission. Over fading channels, the system may experience outage even when the average received SNR, after considering path loss and shadowing effects, is very large. Equivalently, an outage event can also be defined in terms of the instantaneous SNR. Mathematically, the outage probability, denoted by P_{out}, is given by

$$P_{\text{out}} = \Pr[\gamma_s < \gamma_{\text{th}}], \tag{2.44}$$

where γ_{th} is the SNR threshold. For the flat fading scenario, the outage probability can be calculated using the CDF of the instantaneous SNR. For example, the outage probability for the Rician fading case is

$$P_{\text{out}} = 1 - Q_1\left(\sqrt{2K}, \sqrt{2(1+K)\gamma_{\text{th}}}\right), \tag{2.45}$$

where $Q_1(\cdot,\cdot)$ is the Marcum Q-function, and for Nakagami fading is

$$P_{\text{out}} = 1 - \frac{\Gamma\left(m, m\gamma_{\text{th}}\right)}{\Gamma(m)}, \tag{2.46}$$

where $\Gamma(\cdot,\cdot)$ is the incomplete Gamma function.

The average error rate performance can be evaluated by averaging the instantaneous error rate over the distribution of the SNR. Note that at any time instant, the fading channel can be viewed as an AWGN channel with SNR equal to $|z(t)|^2 \frac{E_s}{N_0}$. Therefore, the average error rate of a modulation scheme over a flat fading channel can be calculated by averaging the instantaneous error rate, which is the error rate of this modulation scheme over an AWGN channel with SNR γ, over the distribution function of γ. Mathematically, the average error

rate, denoted by $\overline{P}_E$, is given by

$$\overline{P}_E = \int_0^\infty P_E(\gamma) p_\gamma(\gamma) \mathrm{d}\gamma, \tag{2.47}$$

where $P_E(\gamma)$ is the error rate over the AWGN channel with SNR γ and $p_\gamma(\gamma)$ is the distribution function of γ.

As an example, let us consider the average error rate performance of the BPSK modulation scheme over Rayleigh fading channels. The instantaneous error rate of BPSK is equal to $Q\left(\sqrt{2\gamma}\right)$. For Rayleigh fading, the PDF of the received SNR γ can be shown to be given by

$$p_\gamma(\gamma) = \frac{1}{\overline{\gamma}} \exp\left(-\frac{\gamma}{\overline{\gamma}}\right), \gamma \geq 0, \tag{2.48}$$

where $\overline{\gamma} = 2\sigma^2 E_s/N_0$ is the average received SNR. Therefore, the average error rate of BPSK over Rayleigh fading can be calculated as

$$\begin{aligned} \overline{P}_b &= \int_0^\infty Q\left(\sqrt{2\gamma}\right) \frac{1}{\overline{\gamma}} \exp\left(-\frac{\gamma}{\overline{\gamma}}\right) \mathrm{d}\gamma \\ &= \frac{1}{2}\left(1 - \sqrt{\frac{\overline{\gamma}}{1+\overline{\gamma}}}\right). \end{aligned} \tag{2.49}$$

For other fading channel models and/or modulation schemes, we need to plug in different distribution functions and/or an instantaneous error rate expression and then perform the integration. It is worth noting that in most cases, we cannot obtain a close-form expression, partly because the instantaneous rate expression usually involves the Gaussian Q-function and its square, and must evaluate the integration through numerical methods. Since the integration involves the whole real axis, it is challenging to obtain very accurate results with numerical integration, where truncation is always required. In this context, a new analytical framework based on the MGF of random variables was proposed and extensively used in practice to achieve the accurate evaluation of the average error rate over general fading channels [1].

MGF-based approach for error rate analysis

The MGF of a nonnegative random variable γ is defined as

$$\mathcal{M}_\gamma(s) = \int_0^\infty p_\gamma(\gamma) e^{s\gamma} \mathrm{d}\gamma, \gamma \geq 0, \tag{2.50}$$

where s is a complex dummy variable and $p_\gamma(\cdot)$ is the PDF. Due to the similarity with the Laplace transform definition, we have $\mathcal{M}_\gamma(-s) = \mathcal{L}\{p_\gamma(\gamma)\}$. The MGF is so named because we can easily calculate the moments of random variable γ as

$$\mathbf{E}[\gamma^n] = \frac{d^n}{ds^n} \mathcal{M}_\gamma(s)|_{s=0}. \tag{2.51}$$

Fortunately, the MGF of the received SNR for most fading models are readily available in a compact closed form. For example, the MGF of Rayleigh faded

SNR is

$$\mathcal{M}_{\gamma_s}(s) = (1 - s\overline{\gamma}_s)^{-1}, \tag{2.52}$$

whereas those for Rician and Nakagami faded SNRs are given by

$$\mathcal{M}_{\gamma_s}(s) = \frac{1+K}{1+K-s\overline{\gamma}_s} e^{\frac{s\overline{\gamma}_s K}{1+K-s\overline{\gamma}_s}}, \tag{2.53}$$

and

$$\mathcal{M}_{\gamma_s}(s) = \left(1 - \frac{s\overline{\gamma}_s}{m}\right)^{-m}, \tag{2.54}$$

respectively.

The key starting point of the MGF-based approach is the alternative expression of the Gaussian Q-function and its square, which was obtained by Craig in the early 1990s, given by

$$Q(x) = \frac{1}{\pi}\int_0^{\pi/2} \exp\left[\frac{-x^2}{2\sin^2\phi}\right] \mathrm{d}\phi, x > 0. \tag{2.55}$$

$$Q^2(x) = \frac{1}{\pi}\int_0^{\pi/4} \exp\left[\frac{-x^2}{2\sin^2\phi}\right] \mathrm{d}\phi, x > 0. \tag{2.56}$$

Applying these alternative expressions, we can calculate the average error rate of most modulation schemes of interest over general fading channel models through the finite integration of basic functions. As an example, let us consider a generic class of modulation schemes whose instantaneous error rate takes the form $P_E(\gamma) = aQ\left(\sqrt{b\gamma}\right)$, where a and b are modulation-specific constants. With the conventional approach, the average error rate of this modulation scheme should be calculated as

$$\overline{P}_s = \int_0^{\infty} aQ\left(\sqrt{b\gamma_s}\right) p_{\gamma_s}(\gamma)\mathrm{d}\gamma. \tag{2.57}$$

Substituting the alternative expression of the Q-function and changing the order of integration, we can rewrite the average error rate as

$$\overline{P}_s = \frac{a}{\pi}\int_0^{\pi/2} \mathcal{M}_{\gamma_s}\left(\frac{-b}{2\sin^2\phi}\right) \mathrm{d}\phi, \tag{2.58}$$

where $\mathcal{M}_{\gamma_s}(\cdot)$ is the MGF of the received SNR under the fading model under consideration. Note that the resulting expression only involves the integration with respect to ϕ over the integral of $[0, \pi/2]$.

Figure 2.8 plots the average error rate of coherent BPSK and non-coherent BFSK over fading channels as the function of the average received SNR. For reference, the error rate of these modulation schemes over AWGN channels with received SNR equal to the average SNR over the fading case is also plotted on

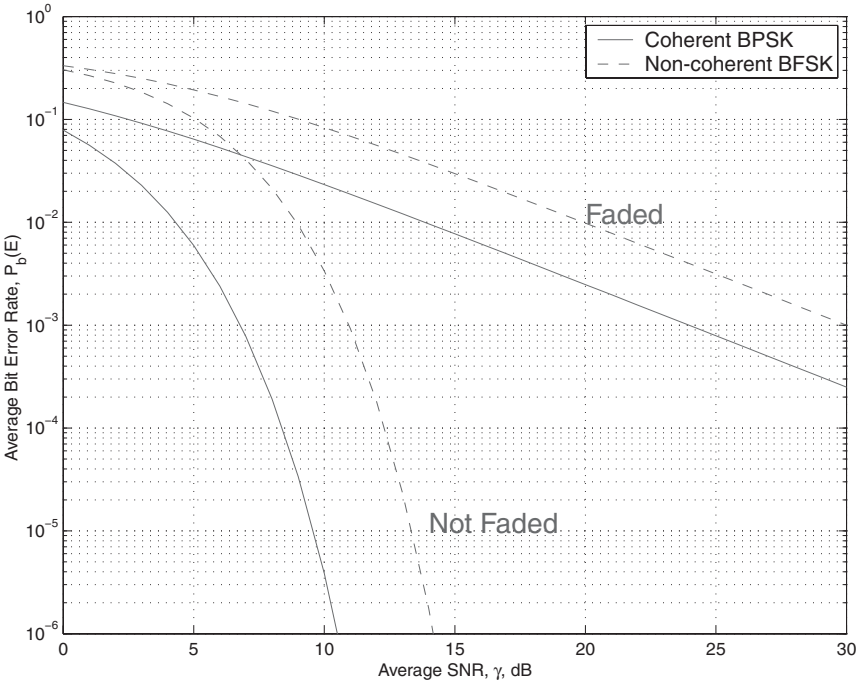

Figure 2.8 Error rate comparison between fading and non-fading environments.

the same figure. As we can see, the error performance degrades dramatically over fading channels. In particular, the error rate decreases in a log rate over the AWGN channel as the SNR increases, but in a linear rate in the fading case. As such, to achieve the same average error rate over fading channels, we need to maintain a much higher average SNR. An intuitive explanation of this phenomenon is that fading causes the frequent occurrence of very low received signal power due to destructive cancellation of different multipath signals. It is exactly from this perspective that diversity techniques try to improve the performance of wireless systems. Diversity has become one of the most essential concepts in wireless system design and implementation. We will elaborate more on it in the following sections.

2.3.3 Adaptive transmission

Adaptive transmission can achieve very high spectral and power efficiency over wireless fading channels with acceptable error rate performance [5–7]. The basic idea of adaptive transmission is to vary the transmission schemes/parameters, such as modulation mode, coding rate, or transmitting power, with the prevailing fading channel conditions. The system will exploit favorable channel conditions with higher data rate transmission at lower power levels and response to channel

degradation with reduced data rate or increased power level. As a result, the overall system throughput is maximized with controlled transmit power consumption while maintaining a certain desired error rate. As such, there has recently been a growing interest in this technique in both academia and industry to meet the increasing demand for highly spectrum-efficient transmission over wireless fading channels. Several adaptive transmission schemes have been incorporated in GSM/CDMA cellular systems and wireless LAN systems.

The availability of a certain channel state information (CSI) at the transmitter is the fundamental requirement of adaptive transmission techniques. It has been shown that with perfect CSI at the transmitter, there exists an optimal adaptive transmission scheme, involving continuous rate and power adaptation, that can achieve the Shannon capacity over fading channels. However, the provision of perfect CSI at the transmitter is a very challenging task in reality even for today's most advanced wireless systems. In addition, implementing continuous rate adaptation will entail prohibitively high complexity. As a result, while acknowledging a certain performance gap compared to the optimal scheme, most current wireless standards adopt adaptive transmission schemes employing discrete rate adaptation, which requires only limited CSI at the transmitter, achieved either through feedback signaling or by exploring the channel reciprocity. Among them, the constant-power variable-rate adaptive M-QAM scheme is of both theoretical and practical interest.

Constant-power variable-rate adaptive M-QAM

With the constant-power variable-rate adaptive M-QAM scheme, the system adaptively selects one of N different M-QAM modulation schemes based on the fading channel condition while using a fixed power level for transmission. Different M-QAM schemes differ by their constellation sizes. For squared M-QAM schemes, the constellation sizes are $M = 2^n,\ n = 1, 2, \cdots, N$, with size 2^n corresponding to a spectral efficiency of n bps/Hz based on the Nyquist criterion. The modulation schemes are chosen to achieve the highest spectral efficiency while maintaining the instantaneous error rate below a certain target value. Specifically, the value range of the channel quality indicator, usually the received SNR, is divided into $N + 1$ regions, with threshold values denoted by $0 < \gamma_{T_1} < \gamma_{T_2} < \cdots < \gamma_{T_N} < \infty$. When the received SNR γ falls into the nth region, i.e. $\gamma_{T_n} \leq \gamma < \gamma_{T_{n+1}}$, the constellation size 2^n will be selected for transmission. For practical implementation, the modulation mode selection is carried out at the receiver after estimating the received SNR. The receiver will then feed back the mode selection result to the transmitter over the control channels, which entails a feedback load of only $\lceil \log_2 N \rceil$ bits.

The threshold values are set such that the instantaneous error rate of the chosen modulation mode is below a certain target value, denoted by BER_0. For example, instantaneous bit error rate (BER) of 2^n-QAM with two-dimensional Grey coding over AWGN channel with SNR γ can be approximately calculated

Table 2.1 Threshold values in dB for 2^n-ary QAM to satisfy 1%, 0.1%, and 0.01% bit error rate.

n	$\text{BER}_0 = 10^{-2}$	$\text{BER}_0 = 10^{-3}$	$\text{BER}_0 = 10^{-4}$
2	4.32	6.79	8.34
3	7.07	9.65	11.30
4	7.88	10.52	12.21
5	10.84	13.58	15.30
6	11.95	14.77	16.52
7	15.40	18.01	19.79
8	16.40	19.38	21.20

as [6, eq. (28)]

$$\text{BER}_n(\gamma) = \frac{1}{5}\exp\left(-\frac{3\gamma}{2(2^n-1)}\right),\ n = 1, 2, \cdots, N. \tag{2.59}$$

As such, the threshold values can be calculated, for a target BER value of BER_0, as

$$\gamma_{T_n} = -\frac{2}{3}\ln(5\ \text{BER}_0)(2^n - 1);\ n = 0, 1, 2, \cdots, N. \tag{2.60}$$

Alternatively, we can solve for the threshold values by inverting the exact BER expression for square M-QAM [8] as

$$\gamma_{T_n} = \text{BER}_n^{-1}(\text{BER}_0), \tag{2.61}$$

where $\text{BER}_n^{-1}(\cdot)$ is the inverse BER expression. The threshold values for the target BER of 10^{-2}, 10^{-3}, and 10^{-4} cases are summarized in Table 2.1.

Performance analysis over fading channels

The performance of an adaptive M-QAM system can be evaluated in terms of the average spectral efficiency and the average error rate. In particular, the average spectral efficiency of the adaptive M-QAM scheme under consideration can be calculated as [6, eq. (33)]

$$\eta = \sum_{n=1}^{N} n\ P_n, \tag{2.62}$$

where P_n is the probability of using the nth constellation size. With the application of an appropriate fading channel model, P_n can be calculated using the distribution function of the received SNR as

$$P_n = \int_{\gamma_{T_n}}^{\gamma_{T_{n+1}}} p_\gamma(x)\mathrm{d}x, \tag{2.63}$$

where $p_\gamma(\cdot)$ denotes the PDF of the received SNR. The average BER of the adaptive modulation system can be calculated as [6, eq. (35)]

$$< BER >= \frac{1}{\eta} \sum_{n=1}^{N} n \, \overline{BER}_n, \tag{2.64}$$

where $\overline{BER}_n$ is the average error rate of using modulation mode n, given by

$$\overline{BER}_n = \int_{\gamma_{T_n}}^{\gamma_{T_{n+1}}} BER_n(x) p_\gamma(x) \mathrm{d}x, \tag{2.65}$$

where $BER_n(\gamma)$ is the instantaneous BER of modulation mode n with SNR γ, the approximate expression of which was given in (2.60).

2.4 Diversity combining techniques

Diversity combining techniques can effectively improve the performance of wireless communication systems over fading channels. The basic idea is to somehow receive the same data signal over multiple independent channels. Since the probability that these independent channels simultaneously experience deep fade is low, by properly combining these replicas together, we can improve the quality of the received signal and achieve better performance. The independent channels can be implemented in several ways, including using different frequencies, using different time slots, using different antennas, or using different codewords, etc. In general, the antenna diversity and path diversity approaches are more attractive as they provide diversity benefit without introducing redundancy into the transmit signal. We will base our following discussion mainly on the antenna reception diversity approach.

2.4.1 Antenna reception diversity

The generic structure of the diversity combiner is shown in Fig. 2.9. Specifically, the diversity combiner will generate its output signal by properly combining the signal replicas received from L diversity paths. Note that the detection will be performed based on the combiner output signal. As such, the statistics of the combiner output, denoted by γ_c, dictates the overall performance of the system. The design objective of the diversity combiner is to maximize the quality of the combined signal under a given complexity constraint. Four traditional combining schemes are selection combining (SC), threshold combining, maximal ratio combining (MRC), and equal gain combining (EGC). There is a trade-off of performance versus complexity among different combining scheme, as each scheme requires a different amount of channel state information of each diversity path and entails a different level of hardware complexity while leading to different performance improvement. To accurately quantify these trade-offs, we

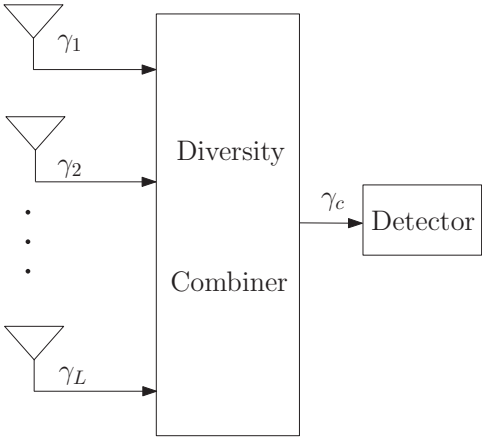

Figure 2.9 Antenna reception diversity system.

need to accurately evaluate the performance of these combining schemes. In the following, we will briefly explain the basic ideas of these combining schemes and elaborate more on how to analyze the performance of the resulting system based on the statistics of γ_c.

For the sake of clarity, we assume in the following that the diversity paths experience independent and identically distributed (i.i.d.) flat fading. The complex channel gains of the ith diversity path, denoted by $z_i = a_i e^{j\theta_i}$, vary independently with one another over time. As such, the received SNR corresponding to the ith diversity path is given by $\gamma_i = a_i^2 \frac{E_b}{N_0}$, which are independent and identically distributed random variables and can serve as the channel quality indicator of each path. The performance of the diversity system will depend on the statistics of the combiner output SNR γ_c. In particular, the outage probability, which now becomes the probability that γ_c is smaller than a threshold γ_{th}, is given by

$$P_{\text{out}} = \Pr[\gamma_c < \gamma_{\text{th}}] = F_{\gamma_c}(\gamma_{\text{th}}), \tag{2.66}$$

where $F_{\gamma_c}(\cdot)$ denotes the CDF of the combined SNR γ_c. The average error rate performance of diversity systems can be evaluated by averaging the instantaneous BER over the distribution of γ_c as

$$\overline{P}_E = \int_0^\infty P_E(\gamma) p_{\gamma_c}(\gamma) \mathrm{d}\gamma, \tag{2.67}$$

where $p_{\gamma_c}(\cdot)$ denotes the PDF of the combined SNR γ_c, respectively. As such, we need to derive the statistics of the combiner output SNR based on the combiner mode of operation as well as the statistics of the individual path SNR.

Selection combining (SC) is the most popular low-complexity combining scheme. With SC, the diversity path with the highest SNR is used for data detection. The mode of operation is illustrated in Fig. 2.10. The combiner needs to estimate the SNR of all available diversity paths and select the best one. The combiner output SNR with SC is then mathematically given by

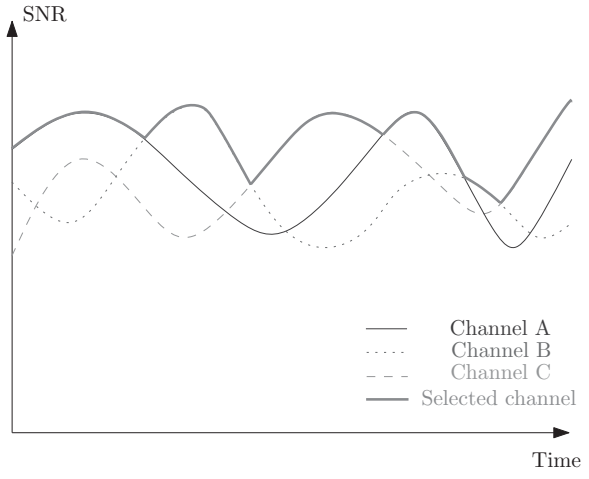

Figure 2.10 Selection combining over three diversity paths.

$\gamma_c = \max\{\gamma_1, \gamma_2, \cdots, \gamma_L\}$. Therefore, the combiner output SNR is the largest one of L different random variables. The statistics of γ_c can be easily obtained from the basic order statistic results. As an example, the PDF of γ_c can be obtained, with i.i.d. fading assumption on different diversity paths, as

$$p_{\gamma_c}(\gamma) = L[F_\gamma(\gamma)]^{L-1} p_\gamma(\gamma), \tag{2.68}$$

where $F_\gamma(\cdot)$ and $p_\gamma(\cdot)$ denote the common CDF and PDF of the path SNRs. The outage probability can be easily calculated as

$$P_{\text{out}} = [F_\gamma(\gamma_{\text{th}})]^L. \tag{2.69}$$

While SC has relative low receiver complexity as it only needs to process the signal from one diversity path, SC always requires the estimation of all available diversity paths.

Maximum ratio combining (MRC) is the optimal linear combining scheme in a noise-limited environment. The basic idea is to generate the combiner output signal as a linear combination of the received signal from different diversity paths such that the SNR of the combined signal is maximized. Mathematically speaking, the combined signal is given by

$$r_c(t) = \sum_{i=1}^{L} w_i r_i(t) = \sum_{i=1}^{L} w_i a_i e^{j\theta_i} s(t) + \sum_{i=1}^{L} w_i n_i(t), \tag{2.70}$$

where $r_i(t) = a_i e^{j\theta_i} s(t) + n_i(t), i = 1, 2, \cdots, L$ is the received signal from the ith path, and w_i represents the weights for the ith path, which need to be chosen optimally. It can be shown that the optimal weights w_i should be proportional to the complex conjugate of the complexity channel gain of the ith path,

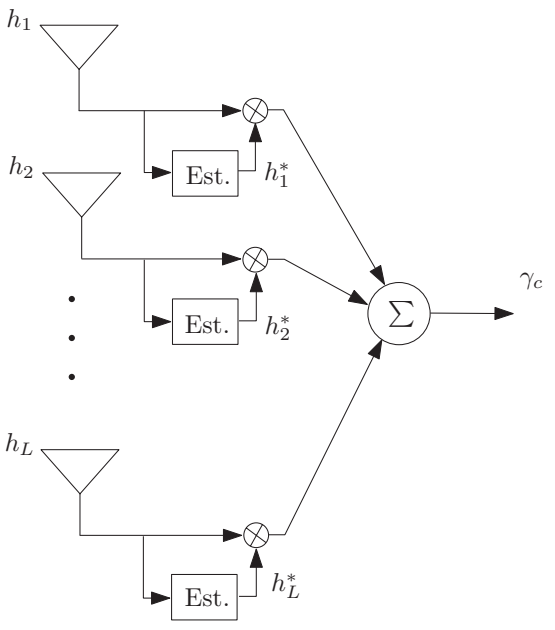

Figure 2.11 Structure of an MRC-based diversity combiner.

i.e. $a_i e^{-j\theta_i}$, which will lead to the maximum combiner output SNR given by

$$\gamma_c = \sum_{i=1}^{L} \gamma_i. \tag{2.71}$$

The structure of an MRC combiner is shown in Fig. 2.11.

For the performance evaluation of an MRC scheme, we need to determine the statistics of the sum of L random variables for the subsequent performance analysis. When the path SNRs are independent random variables, the MGF-based approach can readily apply. Note that the MGF of the sum of independent random variables is the product of the MGFs of individual random variables. As such, the MGF of the combined SNR with MRC over independent fading paths can be written as

$$\mathcal{M}_{\gamma_c}(s) = \prod_{i=1}^{L} \mathcal{M}_{\gamma_i}(s), \tag{2.72}$$

where $\mathcal{M}_{\gamma_i}(s)$ is the MGF of the ith path SNR. For convenience, we summarize in Table 2.2 the distribution functions of the individual path SNRs under three popular fading channel models. In Table 2.2, $\overline{\gamma}$ is the common average SNR per branch, $\Gamma(\cdot)$ is the Gamma function [9, sec. 8.31], $I_0(\cdot)$ is the modified Bessel function of the first kind with zero order [9, sec. 8.43], $\Gamma(\cdot,\cdot)$ is the incomplete Gamma function [9, sec. 8.35], and $Q_1(\cdot,\cdot)$ is the first-order Marcum Q-function [10]. As an example, for the i.i.d. Rayleigh fading scenario, the MGF

Table 2.2 Statistics of the fading signal SNR γ for the three fading models under consideration.

Model	Rayleigh	Rice	Nakagami-m
Parameter	·	$K \geq 0$	$m \geq \frac{1}{2}$
PDF, $p_\gamma(x)$	$\frac{1}{\overline{\gamma}} e^{-\frac{x}{\overline{\gamma}}}$	$\frac{(1+K)}{\overline{\gamma}} e^{-K-\frac{1+K}{\overline{\gamma}}x} I_0\left(2\sqrt{\frac{1+K}{\overline{\gamma}}Kx}\right)$	$(\frac{m}{\overline{\gamma}})^m \frac{x^{m-1}}{\Gamma(m)} e^{-\frac{m\,x}{\overline{\gamma}}}$
CDF, $F_\gamma(x)$	$1 - e^{-\frac{x}{\overline{\gamma}}}$	$1 - Q_1\left(\sqrt{2K}, \sqrt{\frac{2(1+K)}{\overline{\gamma}}x}\right)$	$1 - \frac{\Gamma\left(m, \frac{m}{\overline{\gamma}}x\right)}{\Gamma(m)}$
MGF, $\mathcal{M}_\gamma(s)$	$(1 - s\overline{\gamma})^{-1}$	$\frac{1+K}{1+K-s\overline{\gamma}} e^{\frac{s\overline{\gamma}K}{1+K-s\overline{\gamma}}}$	$\left(1 - \frac{s\overline{\gamma}}{m}\right)^{-m}$

of the combined SNR with MRC is given by

$$\mathcal{M}_{\gamma_c}(s) = \prod_{i=1}^{L} (1 - s\overline{\gamma})^{-1}, \tag{2.73}$$

which leads to the PDF of the combined SNR, after proper inverse Laplace transform, as

$$p_{\gamma_c}(\gamma) = \frac{\gamma^{L-1} e^{-\gamma/\overline{\gamma}}}{\overline{\gamma}^L (L-1)!}. \tag{2.74}$$

Both results can apply to the average error rate analysis over Rayleigh fading channels.

The equal gain combining (EGC) scheme has slightly lower complexity than the MRC. With EGC, the combined signal is still the linear combination of the signals received from different paths. But the weight for the ith path with EGC becomes $e^{-j\theta_i}$, which is simpler than that for MRC. As such, the receiver with EGC needs only to estimate the channel phase of each diversity path. In general, it is more challenging to estimate the channel phase than the channel amplitude. Therefore, EGC entails higher implementation complexity than SC. Furthermore, SC needs only to process the currently selected path, whereas the MRC and EGC receiver needs to process all L available paths.

2.4.2 Threshold combining and its variants

Threshold combining is another type of combining scheme with even lower complexity than SC [11–13]. With threshold combining, the receiver needs only to monitor the quality of the currently used branch. Dual-branch switch and stay combining (SSC) is the most well-known example of threshold combining [14,15]. With SSC, the receiver estimates the SNR of the currently used branch and compares it with a fixed threshold, denoted by γ_T. If the estimated SNR is greater or equal to γ_T, then the receiver continues to use the current branch. Otherwise, the receiver will switch to the other branch and use it for data reception, regardless

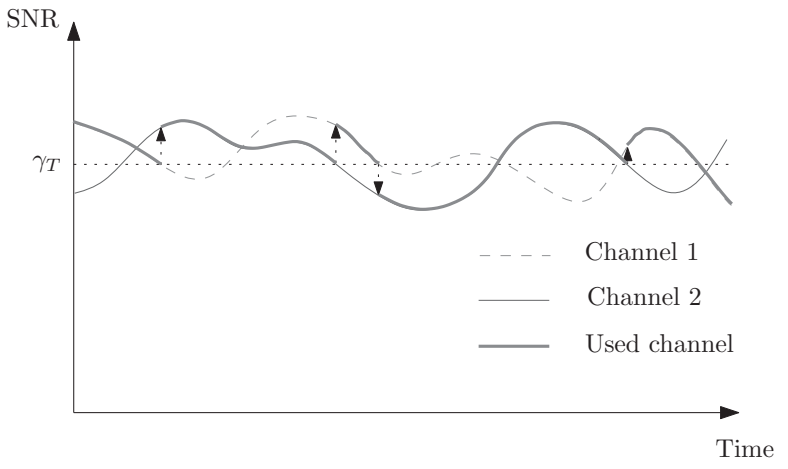

Figure 2.12 Mode of operation of dual branch switch and stay combining.

of its quality. The mode of operation of SSC is illustrated in Fig. 2.12 and can be mathematically summarized, assuming γ_1 is the SNR of the currently used branch, as

$$\gamma_c = \begin{cases} \gamma_1, & \gamma_1 \geq \gamma_T; \\ \gamma_2, & \gamma_1 < \gamma_T. \end{cases} \tag{2.75}$$

To derive the statistics of the combined SNR with SSC, we can start by applying the total probability theorem and writing the CDF of the combined SNR as

$$F_{\gamma_c}(\gamma) = \Pr[\gamma_1 < \gamma, \gamma_1 \geq \gamma_T] + \Pr[\gamma_2 < \gamma, \gamma_1 < \gamma_T]. \tag{2.76}$$

With the i.i.d. fading path assumption, the CDF can be obtained, in terms of the common CDF of individual path SNR, as

$$F_{\gamma_c}(\gamma) = \begin{cases} F_\gamma(\gamma_T)F_\gamma(\gamma) + F_\gamma(\gamma) - F_\gamma(\gamma_T), & \gamma \geq \gamma_T; \\ F_\gamma(\gamma_T)F_\gamma(\gamma), & \gamma < \gamma_T. \end{cases} \tag{2.77}$$

It follows that the PDF of the combined SNR with SSC is given by

$$p_{\gamma_c}(\gamma) = \begin{cases} F_\gamma(\gamma_T)p_\gamma(\gamma) + p_\gamma(\gamma), & \gamma \geq \gamma_T; \\ F_\gamma(\gamma_T)p_\gamma(\gamma), & \gamma < \gamma_T. \end{cases} \tag{2.78}$$

The generic expression of the average error rate for a certain modulation scheme can be calculated as

$$\overline{P}_E = F_\gamma(\gamma_T)\int_0^\infty P_E(\gamma)p_\gamma(\gamma)\mathrm{d}\gamma + \int_{\gamma_T}^\infty P_E(\gamma)p_\gamma(\gamma)\mathrm{d}\gamma. \tag{2.79}$$

The statistics of the combined SNR for more general scenario with path correlation and/or unbalanced paths can also be obtained by applying a Markov chain based approach [16].

In the multiple branch scenario, SSC was generalized to switch and examine combining (SEC) [17], which can exploit the diversity benefit of extra paths. The receiver with SEC will examine the quality of the switched-to path and switch again if it finds that the quality of that path is unacceptable. This process is continued until either an acceptable path is found or all paths have been examined. The mode of operation of L-branch SEC can be summarized with the following mathematical relationship, assuming the first branch is the currently used branch,

$$\gamma_c = \begin{cases} \gamma_1, & \gamma_1 \geq \gamma_T; \\ \gamma_2, & \gamma_1 < \gamma_T, \gamma_2 \geq \gamma_T; \\ \gamma_3, & \gamma_1 < \gamma_T, \gamma_2 < \gamma_T, \gamma_3 \geq \gamma_T; \\ \vdots & \vdots \\ \gamma_L, & \gamma_i < \gamma_T, i = 1, 2, \cdots, L-1. \end{cases} \tag{2.80}$$

It follows with the i.i.d. fading assumption, that the CDF of SEC output SNR is given by

$$F_{\gamma_c}(x) = \begin{cases} [F_\gamma(\gamma_T)]^{L-1} F_\gamma(x), \ x < \gamma_T; \\ \sum_{j=0}^{L-1} [F_\gamma(x) - F_\gamma(\gamma_T)][F_\gamma(\gamma_T)]^j \\ \quad + [F_\gamma(\gamma_T)]^L, \ x \geq \gamma_T. \end{cases} \tag{2.81}$$

The PDF and MGF of the combined SNR with L-branch SEC can then be routinely obtained and applied to its performance analysis over fading channels.

Figure 2.13 compares the average error rate performance of SC, SSC/SEC, and MRC. As we can see, MRC achieves the best performance and the performance gap increases as the number of diversity paths increase. The performance gain of MRC comes with higher hardware complexity and power consumption. Note that the receiver needs to know the complete complex channel gain, including the amplitude and phase, for each diversity path in order to determine the optimal branch weights for MRC. With SC, the receiver only requires the amplitude or power gain of all diversity branches. We can also see that the complexity saving of threshold combining over SC scheme comes at the cost of high average error rate, even with the optimal value of the switching threshold.

Another variant of threshold combining is the so-called switch and examine combining with post-examining selection (SECps) [18]. Similar to SSC/SEC schemes, the receiver with SECps tries to use an acceptable diversity path by examining as many paths as necessary. However, when no acceptable path is

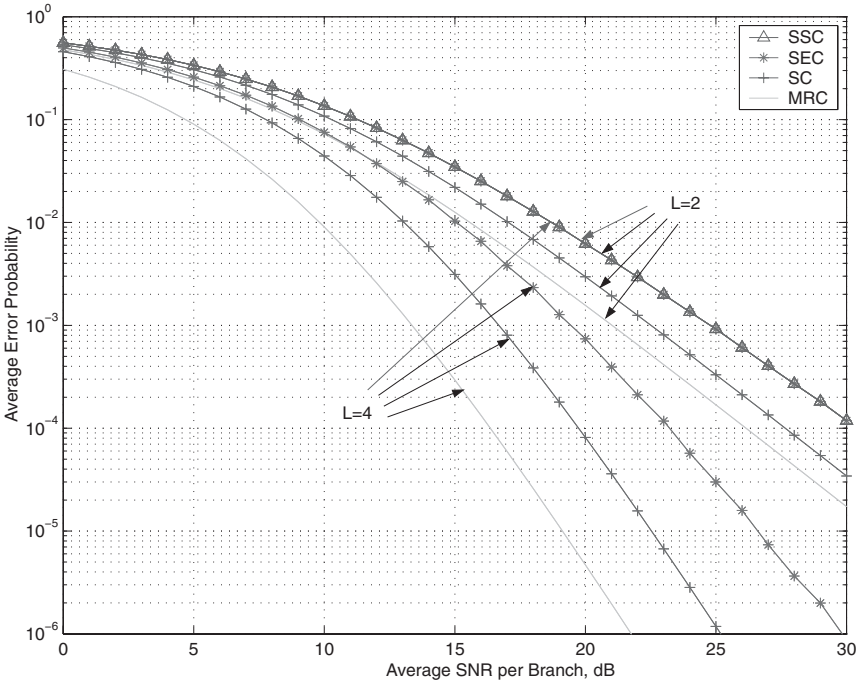

Figure 2.13 Average error rate comparison of conventional diversity combining schemes [17]. © 2003 IEEE.

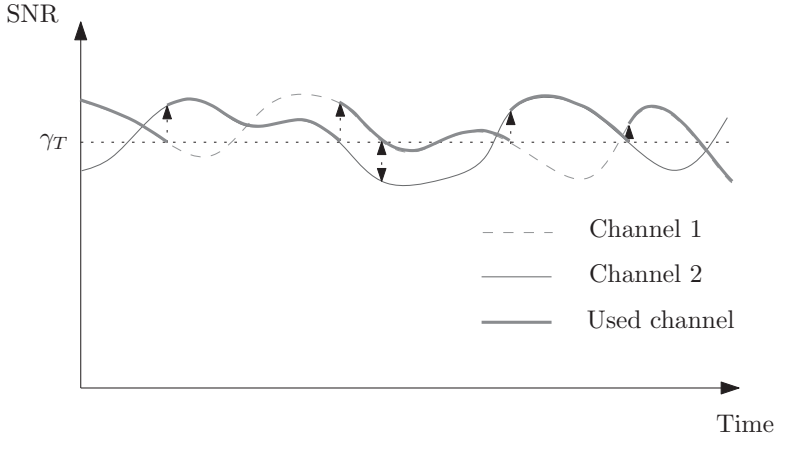

Figure 2.14 Mode of operation of SECps scheme over dual diversity branches.

found after examining all available ones, the receiver with SECps will use the best unacceptable one. The operation of SECps for the dual branch case is illustrated in Fig. 2.14. Note that compared with the dual SSC scheme, the SECps scheme will lead to a better output signal when both branches are unacceptable.

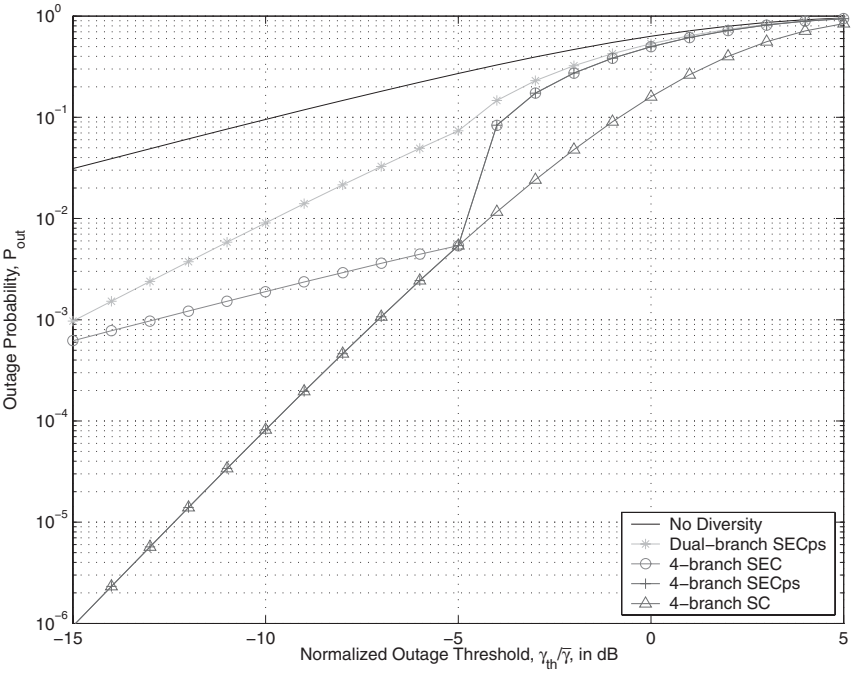

Figure 2.15 Outage probability of L-branch SECps as a function of normalized outage threshold $\gamma_{\rm th}/\overline{\gamma}$ in comparison with SEC and SC ($\gamma_T/\overline{\gamma} = -5$ dB) [18]. © 2006 IEEE.

The mode of operation of L-branch SECps can be summarized as

$$\gamma_c = \begin{cases} \gamma_1, & \gamma_1 \geq \gamma_T; \\ \gamma_2, & \gamma_1 < \gamma_T, \gamma_2 \geq \gamma_T; \\ \gamma_3, & \gamma_1 < \gamma_T, \gamma_2 < \gamma_T, \gamma_3 \geq \gamma_T; \\ \vdots & \vdots \\ \max\{\gamma_1, \gamma_2, \cdots, \gamma_L\}, & \gamma_i < \gamma_T, i = 1, 2, \cdots, L-1. \end{cases} \tag{2.82}$$

Consequently, the CDF of the combined SNR with SECps over i.i.d. fading paths can be obtained as

$$F_{\gamma_c}(x) = \begin{cases} 1 - \sum_{i=0}^{L-1} [F_\gamma(\gamma_T)]^i [1 - F_\gamma(x)], & x \geq \gamma_T; \\ [F_\gamma(x)]^L, & x < \gamma_T. \end{cases} \tag{2.83}$$

which can be applied to the outage performance evaluation. Figure 2.15 shows the outage performance of SECps in a multi-branch scenario. As we can see, as the number of diversity paths increases from 2 to 4, the outage performance of SECps improves considerably. While comparing the outage performance of 4-branch SECps with 4-branch SEC and SC, we can see that SECps has the same outage probability as SC when $\gamma_{\rm th} \leq \gamma_T$ and as SEC when $\gamma_{\rm th} > \gamma_T$. Intuitively,

Table 2.3 Complexity comparison of dual-branch SECps, SSC, and SC in terms of operations needed for combining decision over Rayleigh fading paths [18].

Schemes	Average number of channel estimations	Probability of branch switching
Dual-branch SC	2	0.5
Dual-branch SSC	1	$1 - e^{-\frac{\gamma_T}{\bar{\gamma}}} \in [0, 1)$
Dual-branch SECps	$2 - e^{-\frac{\gamma_T}{\bar{\gamma}}} \in [1, 2)$	$\frac{1}{2} - \frac{1}{2}e^{-2\frac{\gamma_T}{\bar{\gamma}}}$

when $\gamma_{\text{th}} \leq \gamma_T$, the receiver with SECps experiences outage only when the SNR of all diversity paths falls below γ_T and their maximum is smaller than γ_{th}, which is equivalent to the case of SC. On the other hand, when $\gamma_{\text{th}} > \gamma_T$, the receiver with SECps experiences outage when the SNR of the first acceptable path is smaller than γ_{th} or when the SNR of all diversity paths falls below γ_T, which is the same as the case of conventional SEC.

To summarize this section, we quantitatively compare the complexity of SC, SEC and SECps in terms of the average number of path estimations and the probability of branch switching. Based on its mode of operation, the average number of path estimations needed by SECps is given by

$$N_E^{\text{SECps}} = 1 + \sum_{i=1}^{L-1} [F_\gamma(\gamma_T)]^i = \frac{1 - [F_\gamma(\gamma_T)]^L}{1 - F_\gamma(\gamma_T)}. \tag{2.84}$$

Note that the SC scheme always needs L path estimations, i.e. $N_E^{\text{SC}} = L$. The receiver with conventional SEC needs to estimate at most $L - 1$ paths because when the first $L - 1$ paths are found unacceptable, the receiver will use the last path for reception. Therefore, SEC requires less path estimations than SECps, i.e. $N_E^{\text{SEC}} = 1 + \sum_{i=1}^{L-2} [P_\gamma(\gamma_T)]^i$. As a result, we have $N_E^{\text{SEC}} \leq N_E^{\text{SECps}} \leq N_E^{\text{SC}}$. On the other hand, the probability of branch switching with SECps, denoted by P_{SW}^{SECps}, can be shown to be given by

$$P_{SW}^{\text{SECps}} = F_\gamma(\gamma_T) - \int_0^{\gamma_T} p_\gamma(x)[F_\gamma(x)]^{L-1} \, \mathrm{d}x. \tag{2.85}$$

It is easy to see that the receiver with SC switches paths with a probability of $(L-1)/L$ over identically faded diversity paths, i.e. $P_{SW}^{\text{SC}} = (L-1)/L$. Meanwhile, the receiver with L-branch SEC switches paths whenever the current path becomes unacceptable (i.e. $\gamma_1 \leq \gamma_T$). As such, the switching probability with SEC is $P_{SW}^{\text{SEC}} = P_\gamma(\gamma_T)$. Consequently, we have $P_{SW}^{\text{SECps}} < P_{SW}^{\text{SEC}}$ and $P_{SW}^{\text{SECps}} < P_{SW}^{\text{SEC}}$. Table 2.3 summarizes these results for the $L = 2$ case.

2.4.3 Transmit diversity

When there are multiple transmit antennas and a single receive antenna, as is often the case in cellular downlink transmission, we can apply transmit diversity techniques to obtain diversity benefit. If the appropriate CSI corresponding

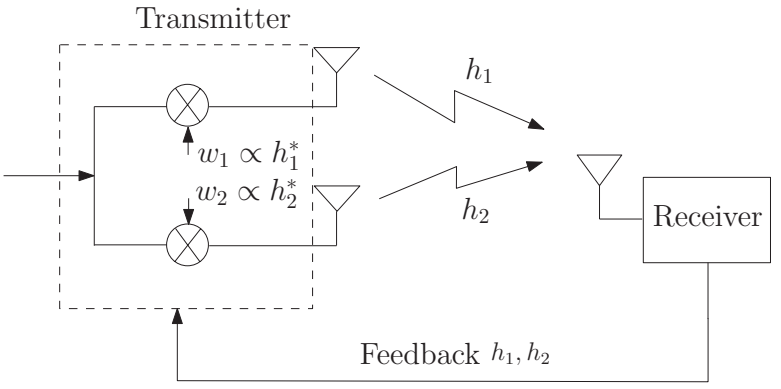

Figure 2.16 Closed loop transmit diversity based on MRC.

to different transmit antenna is available at the transmitter side, then we easily apply the conventional combining schemes discussed in the previous subsection. For example, if the complete complex gain $a_i e^{j\theta_i}$ for the channel from the ith transmit antenna to the receive antenna is available at the transmitter, we can implement the so-called transmit MRC by multiplying the transmit signal by a weight w_i, which is proportional to $a_i e^{-j\theta_i}$, before transmitting it on the ith antenna. To satisfy the total transmit energy constraint, we can chose the amplitude of w_i as

$$|w_i| = \frac{a_i}{\sqrt{\sum_{j=1}^{L} a_j^2}}, \tag{2.86}$$

which leads to $\sum_{i=1}^{L} |w_i|^2 = 1$. After propagating through the fading channels, the signal transmitted from different antennas will add up coherently at the receiver and each is weighted proportional to the amplitude of channel gain. As such, the SNR of the received signal is the same as the combiner output SNR with received MRC, i.e. $\gamma_c = \sum_{i=1}^{L} \gamma_i$. Figure 2.16 illustrates the structure of the MRC-based transmit diversity system with perfect CSI. Note that the requirement of complete CSI at the transmitter side can be challenging to satisfy in practice systems, considering the fact that they usually entail the channel estimation and feedback from the receiver. From this perspective, the low-complexity combining schemes including SC and threshold combining are more attractive, as much less channel information is required for their implementation. For example, the receiver with transmit SC only needs to inform the transmitter which antenna leads to the highest receive SNR and therefore should be used, which results in $\lceil \log_2 L \rceil$ bits of feedback load. With transmitter SSC, the receiver only needs to feed back one bit of information to indicate whether the transmitter should switch antenna or not.

When no CSI can be made available at the transmitter side, we can still explore the diversity benefit inherent in the multiple transmit antennas through a class of linear coding schemes, termed space-time block codes [19]. While the code design

for more than two transmit antennas scenario is available, the particular design for the dual transmit antenna case, widely recognized as Alamouti's scheme [20], is of great practical importance. Unlike other designs, Alamouti's scheme achieves full diversity gain over fading channels without incurring any rate loss. The scheme transmits two complex data symbols (s_1, s_2) over two symbol periods using two antennas as follows. In the first symbol period, s_1 from antenna 1 and s_2 from antenna 2. In the second symbol period, $-s_2^*$ from antenna 1 and s_1^* from antenna 2. Assuming that channel gains corresponding to the i transmit antenna $h_i = a_i e^{j\theta_i}$, $i = 1, 2$ remain constant during the two symbol periods, the received symbols over two symbol periods are

$$\begin{aligned} y_1 &= h_1 s_1 + h_2 s_2 + n_1 \\ y_2 &= h_1(-s_2^*) + h_2 s_1^* + n_2, \end{aligned} \tag{2.87}$$

where n_1 and n_2 are additive Gaussian noise collected by the receiver. After taking the complex conjugate of y_2, we can rewrite the two equations into matrix form as

$$\begin{bmatrix} y_1 \\ y_2^* \end{bmatrix} = \begin{bmatrix} h_1 & h_2 \\ h_2^* & -h_1^* \end{bmatrix} \begin{bmatrix} s_1 \\ s_2 \end{bmatrix} + \begin{bmatrix} n_1 \\ n_2^* \end{bmatrix}. \tag{2.88}$$

With the estimated channel gains, the receiver can perform detection on

$$\begin{bmatrix} z_1 \\ z_2 \end{bmatrix} = \begin{bmatrix} h_1 & h_2 \\ h_2^* & -h_1^* \end{bmatrix}^H \begin{bmatrix} y_1 \\ y_2^* \end{bmatrix} \tag{2.89}$$

where $[\cdot]^H$ denotes the Hermitian transpose. Due to the special structure of the matrix, we have

$$\begin{bmatrix} z_1 \\ z_2 \end{bmatrix} = (a_1^2 + a_2^2) \begin{bmatrix} s_1 \\ s_2 \end{bmatrix} + \begin{bmatrix} \tilde{n}_1 \\ \tilde{n}_2 \end{bmatrix}, \tag{2.90}$$

where $\tilde{n}_i$ can be shown to be zero-mean Gaussian with variance $(a_1^2 + a_2^2)N_0$. As such, we can show that the effective SNR of z_i for the detection of s_i is

$$\gamma_i = (a_1^2 + a_2^2)\frac{E_s}{2N_0} = \frac{1}{2}(\gamma_1 + \gamma_2). \tag{2.91}$$

Therefore, Alamouti's scheme achieves the same diversity gain as received MRC except for a 3 dB power loss due to the fact that each symbol is transmitted twice. The key advantage of Alamouti's scheme is that absolutely no CSI is required at the transmitter side. As a result, this scheme has been included in several wireless standards.

2.5 Summary

In this chapter, we reviewed the basics of digital wireless communications, including channel modeling, digital bandpass modulation, and performance analysis.

Several basic performance improvement techniques, such as adaptive modulation, diversity combining, and transmit diversity were also discussed. While most of the materials in this chapter are intended as the background for later chapters, we also present some trade-off analysis of different variants of threshold combining. Specifically, we introduce the general performance analysis procedure and sample complexity measures, which will apply to the analysis of advanced wireless technologies in later chapters.

2.6 Bibliography notes

For a more detailed discussion on most of the subjects in this chapter, the reader can refer to the popular textbook of A. Goldsmith [2]. Simon and Alouini's book [1] provides a thorough and in-depth coverage of digital transmission schemes for fading channel and their performance evaluation. Ref. [21] gives a complete overview of the OFDM technology and its application in wireless systems. The reader can refer to [19] for more general space-time code designs. The Markov chain-based analysis of the different implementation option of the switch and stay combining scheme and their analysis over a general fading channel is available in [16].

References

[1] M. K. Simon and M.-S. Alouini, *Digital Communications over Generalized Fading Channels*, 2nd ed. New York, NY: John Wiley & Sons, 2004.

[2] A. J. Goldsmith, *Wireless Communications*. New York, NY: Cambridge University Press, 2005.

[3] G. L. Stüber, *Principles of Mobile Communications*, 2nd ed. Norwell, MA: Kluwer Academic Publishers, 2000.

[4] W. C. Jakes, *Microwave Mobile Communication*, 2nd ed. Piscataway, NJ: IEEE Press, 1994.

[5] A. J. Goldsmith and S.-G. Chua, "Adaptive coded modulation for fading channels," *IEEE Trans. Commun.*, vol. COM-46, no. 5, pp. 595–602, May 1998.

[6] M.-S. Alouini and A. J. Goldsmith, "Adaptive modulation over Nakagami fading channels," *Kluwer J. Wireless Commun.*, vol. 13, nos. 1–2, pp. 119–143, 2000.

[7] K. J. Hole, H. Holm, and G. E. Oien, "Adaptive multidimensional coded modulation over flat fading channels," *IEEE J. Select. Areas Commun.*, vol. SAC-18, no. 7, pp. 1153–1158, July 2000.

[8] K. Cho and D. Yoon, "On the general BER expression of one- and two-dimensional amplitude modulation," *IEEE Trans. Commun.*, vol. 50, no. 7, pp. 1074–1080, July 2002.

[9] I. S. Gradshteyn and I. M. Ryzhik, *Table of Integrals, Series, and Products*, 5th ed. San Diego, CA: Academic Press, 1994.

[10] A. H. Nuttall, "Some integrals involving the Q_M function," *IEEE Trans. on Information Theory*, vol. 21, no. 1, pp. 95–96, January 1975.

[11] M. A. Blanco and K. J. Zdunek, "Performance and optimization of switched diversity systems for the detection of signals with Rayleigh fading," *IEEE Trans. Commun.*, vol. COM-27, no. 12, pp. 1887–1895, December 1979.

[12] A. A. Abu-Dayya and N. C. Beaulieu, "Analysis of switched diversity systems on generalized-fading channels," *IEEE Trans. Commun.*, vol. COM-42, no. 11, pp. 2959–2966, November 1994.

[13] ——, "Switched diversity on microcellular Ricean channels," *IEEE Trans. Veh. Technol.*, vol. VT-43, no. 4, pp. 970–976, November 1994.

[14] Y.-C. Ko, M.-S. Alouini, and M. K. Simon, "Analysis and optimization of switched diversity systems," *IEEE Trans. Veh. Technol.*, vol. VT-49, no. 5, pp. 1569–1574, September 2000, see also Y.-C. Ko, M.-S. Alouini, and M. K. Simon, "Correction to analysis and optimization of switched diversity systems," *IEEE Trans. Veh. Technol.*, vol. VT-51, pp. 216, January 2002.

[15] C. Tellambura, A. Annamalai and V. K. Bhargava, "Unified analysis of switched diversity systems in independent and correlated fading channel," *IEEE Trans. Commun.*, vol. COM-49, no. 11, pp. 1955–1965, November 2001.

[16] H.-C. Yang and M.-S. Alouini, "Markov chain and performance comparison of switched diversity systems," *IEEE Trans. Commu.*, vol. COM-52, no. 7, pp. 1113–1125, July 2004.

[17] H.-C. Yang and M.-S. Alouini, "Performance analysis of multibranch switched diversity systems," *IEEE Trans. Commun.*, vol. COM-51, no. 5, pp. 782–794, May 2003.

[18] H.-C. Yang and M.-S. Alouini, "Improving the performance of switched diversity with post-examining selection," *IEEE Trans. Wireless Commun.*, vol. TWC-5, no. 1, pp. 67–71, January 2006.

[19] A. Paulraj, R. Nabar and D. Gore, *Introduction to Space-Time Wireless Communications*. Cambridge: Cambridge University Press, 2003.

[20] S. M. Alamouti, "A simple transmitter diversity scheme for wireless communications," *IEEE J. Select. Areas Commun.*, vol. 16, no. 8, pp. 1451–458, October 1998.

[21] R. Prasad, *OFDM for Wireless Communication Systems*. Boston, MA: Artech House Publishers, 2004.

3 Distributions of order statistics

3.1 Introduction

The previous chapter shows that the performance analysis of wireless communication systems requires the statistics of the signal-to-noise ratio (SNR) at the receiver. In the analysis of many advanced wireless communication techniques in later chapters, we will make use of some order statistical results. This chapter summarizes these results and their derivations for easy reference. Specifically, we first review the basic distribution functions of ordered random variables. After that, we derive some new order statistics results, including the joint distribution functions of partial sums of ordered random variables, for which we also present a novel analytical framework based on the moment generating function (MGF). The chapter is concluded with a discussion on the limiting distributions of extremes. Whenever appropriate, we use the exponential random variable special case as an illustrative example. Note that we focus on those order statistics results that will be employed in later chapters in the performance and complexity analysis of different wireless technologies. For a more thorough treatment of order statistics, the readers are referred to [1, 2].

3.2 Basic distribution functions

Order statistics deals with the distributions and statistical properties of the new random variables obtained after ordering the realizations of some random variables. Let γ_j's, $j = 1, 2, \cdots, L$ denote L independent and identically distributed (i.i.d.) nonnegative random variables with common PDF $p_\gamma(\cdot)$ and CDF $F_\gamma(\cdot)$. Let $\gamma_{l:L}$ denote the random variable corresponding to the lth largest observation of the L original random variables, such that $\gamma_{1:L} \geq \gamma_{2:L} \geq \cdots \geq \gamma_{L:L}$. $\gamma_{l:L}$ is also called lth order statistics. The ordering process is illustrated in Fig. 3.1.

3.2.1 Marginal and joint distributions

As an immediate result of the ordering process, these order statistics are no longer identically distributed [1]. The PDF of $\gamma_{l:L}$, $l = 1, 2, \cdots, L$, can be shown

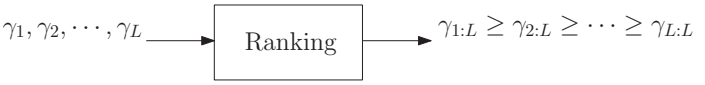

Figure 3.1 Ordering random variables.

to be given by

$$p_{\gamma_{l:L}}(x) = \frac{L!}{(L-l)!(l-1)!}[F_\gamma(x)]^{L-l}[1-F_\gamma(x)]^{l-1}p_\gamma(x). \tag{3.1}$$

The PDF of the largest random variable, $\gamma_{1:L}$, and the smallest random variable, $\gamma_{L:L}$, can be obtained as

$$p_{\gamma_{1:L}}(x) = L[F_\gamma(x)]^{L-1}p_\gamma(x), \tag{3.2}$$

and

$$p_{\gamma_{L:L}}(x) = L[1-F_\gamma(x)]^{L-1}p_\gamma(x), \tag{3.3}$$

respectively.

Another consequence of the ordering operation is that the ordered random variables are dependent of one another. Specifically, the joint PDF of two arbitrary order statistics, $\gamma_{l:L}$ and $\gamma_{k:L}$, $l < k$, can be shown to be given by [1]

$$\begin{aligned} p_{\gamma_{l:L},\gamma_{k:L}}(x,y) = {} & \frac{L!}{(l-1)!(k-l-1)!(L-k)!}\left(1-F_\gamma(x)\right)^{l-1}p_\gamma(x) \\ & \times\left(F_\gamma(x)-F_\gamma(y)\right)^{k-l-1}p_\gamma(y)\left(F_\gamma(y)\right)^{L-k}, \end{aligned} \tag{3.4}$$

which is clearly not equal to the product of the marginal PDFs, $p_{\gamma_{l:L}}(x)$ and $p_{\gamma_{k:L}}(x)$. Furthermore, while the joint PDF of the L-original random variables can be written as the product of individual PDFs, because of the independence property, as

$$p_{\gamma_1,\gamma_2,\cdots,\gamma_L}(x_1,x_2,\cdots,x_L) = \prod_{i=1}^{L} p_\gamma(x_i), \tag{3.5}$$

the joint PDF of the L-ordered random variables becomes

$$p_{\gamma_{1:L},\gamma_{2:L},\cdots,\gamma_{L:L}}(x_1,x_2,\cdots,x_L) = L!\prod_{i=1}^{L} p_\gamma(x_i), \quad x_1 \geq x_2 \geq \cdots \geq x_L. \tag{3.6}$$

3.2.2 Conditional distributions

Now let us consider the distribution of an ordered random variable given the realization of another ordered random variable [1]. These results are summarized in the following two theorems.

Theorem 3.1. *The conditional distribution of the jth order statistics, $\gamma_{j:L}$, given that the lth order statistics $\gamma_{l:L}$ is equal to y, where $j > l$, is the distribution of*

the $L-j$th order statistics of $L-l$ i.i.d. random variables γ_j^-, whose PDF is the truncated PDF of the original random variable γ on the right at y, i.e.

$$p_{\gamma_{j:L}|\gamma_{l:L}=y}(x) = p_{\gamma^-_{L-j:L-l}}(x), \tag{3.7}$$

where the PDF of γ_j^- is given by

$$p_{\gamma_j^-}(x) = \frac{p_\gamma(x)}{F_\gamma(y)}, x \le y. \tag{3.8}$$

Proof. By definition, the conditional PDF of $\gamma_{j:L}$ given $\gamma_{l:L} = y$ is

$$p_{\gamma_{j:L}|\gamma_{l:L}=y}(x) = \frac{p_{\gamma_{j:L},\gamma_{l:L}}(x,y)}{p_{\gamma_{l:L}}(y)}. \tag{3.9}$$

After substituting (3.4) and (3.1) into (3.9) and some manipulations, we can show that

$$p_{\gamma_{j:L}|\gamma_{l:L}=y}(x) = \frac{(L-l)!}{(j-l-1)!(L-j)!}\left(1-\frac{F_\gamma(x)}{F_\gamma(y)}\right)^{j-l-1}\frac{p_\gamma(x)}{F_\gamma(y)}\left(\frac{F_\gamma(x)}{F_\gamma(y)}\right)^{L-j}, \tag{3.10}$$

which is the PDF of the $L-j$th order statistics of $L-l$ i.i.d. random variables with distribution function $p_\gamma(x)/F_\gamma(y)$ $(x \le y)$. □

Theorem 3.2. *The conditional distribution of the jth order statistics, $\gamma_{j:L}$, given that the lth order statistics $\gamma_{l:L}$ is equal to y, where $j < l$, is the same as the distribution of the jth order statistics of $l-1$ i.i.d. random variables γ_j^+, whose PDF is the truncated PDF of the original random variable γ on the left at y, i.e.*

$$p_{\gamma_{j:L}|\gamma_{l:L}=y}(x) = p_{\gamma^+_{j:l-1}}(x), \tag{3.11}$$

where the PDF of γ_j^+ is given by

$$p_{\gamma_j^+}(x) = \frac{p_\gamma(x)}{1-F_\gamma(y)},\ x \ge y. \tag{3.12}$$

The theorem can be similarly proved as Theorem 3.1 [3]. These two theorems establish that order statistics of samples from a continuous distribution form a reversible Markov chain. Specifically, the distribution of $\gamma_{j:L}$ given that $\gamma_{l:L} = y$ with $j < l$ is independent of $\gamma_{l+1:L}, \gamma_{l+2:L}, \cdots, \gamma_{L:L}$ and the distribution of $\gamma_{j:L}$ given that $\gamma_{l:L} = y$ with $j > l$ is independent of $\gamma_{l-1:L}, \gamma_{l-2:L}, \cdots, \gamma_{1:L}$. These results become very useful in the derivation of the following sections.

3.3 Distribution of the partial sum of largest order statistics

In the analysis of certain advance diversity combining schemes, we require the statistics of the sum of the largest order statistics, i.e. $\sum_{i=1}^{L_s}\gamma_{i:L}$, where $L_s < L$

[4–7]. The direct calculation of such a distribution function can be very tedious [8], as the largest L_s order statistics $\gamma_{i:L}, i = 1, 2, \cdots, L_s$ are correlated random variables with distribution function

$$p_{\gamma_{1:L},\gamma_{2:L},\cdots,\gamma_{L_s:L}}(x_1, x_2, \cdots, x_{L_s}) = \frac{L!}{(L-L_s)!}[F_\gamma(x_{L_s})]^{L-L_s}\prod_{i=1}^{L_s} p_\gamma(x_i), \quad x_1 \geq x_2 \geq \cdots \geq x_{L_s}. \tag{3.13}$$

3.3.1 Exponential special case

When γ_i are i.i.d. exponential random variables, i.e. the PDF of γ_i is commonly given by

$$p_\gamma(x) = \frac{1}{\overline{\gamma}} e^{-\frac{x}{\overline{\gamma}}}, \qquad x \geq 0, \tag{3.14}$$

where $\overline{\gamma}$ is the common mean, we can invoke the classical result by Sukhatme to convert the sum of correlated random variables to the sum of independent random variables [4, 9].

Theorem 3.3. *The spacings between ordered exponential random variables $x_l = \gamma_{l:L} - \gamma_{l+1:L}$, $l = 1, 2, \cdots, L$, are independently exponential random variables with distribution functions given by*

$$p_{x_l}(x) = \frac{l}{\overline{\gamma}} e^{-lx/\overline{\gamma}}, \ x \geq 0. \tag{3.15}$$

Proof. Omitted. □

The sum of the largest order statistics can be rewritten as

$$\begin{aligned}\sum_{i=1}^{L_s}\gamma_{i:L} &= \sum_{i=1}^{L_s}\sum_{l=i}^{L} x_l \\ &= x_1 + 2x_2 + \cdots + L_s x_{L_s} + L_s x_{L_s+1} + \cdots + L_s x_L,\end{aligned} \tag{3.16}$$

which becomes the sum of independent random variables. We can then follow the moment generating function (MGF) approach to derive the statistics of the sum. Specifically, the MGF of lx_k can be shown to be given by

$$\mathcal{M}_{lx_k}(s) = \int_0^\infty p_{lx_k}(x)e^{sx}\mathrm{d}x = \left(1 - \frac{s\overline{\gamma}l}{k}\right)^{-1}. \tag{3.17}$$

Consequently, the MGF of the partial sum $\sum_{i=1}^{L_s}\gamma_{i:L}$ can be obtained as the product of individual MGF as

$$\mathcal{M}_{\sum_{i=1}^{L_s}\gamma_{i:L}}(s) = (1 - s\overline{\gamma})^{-L_s}\prod_{l=L_s+1}^{L}\left(1 - \frac{s\overline{\gamma}L_s}{l}\right)^{-1}. \tag{3.18}$$

Finally, the PDF and CDF of $\sum_{i=1}^{L_s} \gamma_{i:L}$ can be routinely obtained after applying proper inverse Laplace transform, for which closed-form results can be obtained. For example, the PDF of $\sum_{i=1}^{L_s} \gamma_{i:L}$ is given by

$$p_{\sum_{i=1}^{L_s} \gamma_{i:L}}(x) = \frac{L!}{(L-L_s)!L_s!} e^{-\frac{x}{\overline{\gamma}}} \left[\frac{x^{L_s-1}}{\overline{\gamma}^{L_s}(L_s-1)!} + \frac{1}{\overline{\gamma}} \sum_{l=1}^{L-L_s} (-1)^{L_s+l-1} \frac{(L-L_s)!}{(L-L_s-l)!l!} \left(\frac{L_s}{l}\right)^{L_s-1} \times \left(e^{-\frac{lx}{L_s\overline{\gamma}}} - \sum_{m=0}^{L_s-2} \frac{1}{m!} \left(-\frac{lx}{L_s\overline{\gamma}}\right)^m \right) \right]. \tag{3.19}$$

3.3.2 General case

The statistics of $\sum_{i=1}^{L_s} \gamma_{i:L}$ becomes more challenging to obtain when the γ_is are not exponentially distributed. Existing solutions usually involve several folds of integration, which does not lead to convenient mathematical evaluation [5]. Based on the results in the previous section, we propose an alternative approach to obtain the statistics of $\sum_{i=1}^{L_s} \gamma_{i:L}$ for the general case. The basic idea is to treat the partial sum as the sum of two correlated random variables as

$$\sum_{i=1}^{L_s} \gamma_{i:L} = \sum_{i=1}^{L_s-1} \gamma_{i:L} + \gamma_{L_s:L}. \tag{3.20}$$

Then, the PDF of $\sum_{i=1}^{L_s} \gamma_{i:L}$ can be obtained from the joint PDF of $\gamma_{L_s:L}$ and $\sum_{i=1}^{L_s-1} \gamma_{i:L} \equiv y_{L_s}$, denoted by $p_{\gamma_{L_s:L}, y_{L_s}}(\cdot,\cdot)$ as

$$p_{\sum_{i=1}^{L_s} \gamma_{i:L}}(x) = \int_0^\infty p_{\gamma_{L_s:L}, y_{L_s}}(x-y, y)\mathrm{d}y. \tag{3.21}$$

We now derive the general result of the joint PDF of the lth order statistics, $\gamma_{l:L}$, and the partial sum of the first $l-1$ order statistics, $y_l = \sum_{j=1}^{l-1} \gamma_{j:L}$, $p_{\gamma_{l:L}, y_l}(\cdot,\cdot)$. Note that while the γ_js are independent random variables, y_l and $\gamma_{l:L}$ are correlated random variables. Applying the Bayesian formula, we can write $p_{\gamma_{l:L}, y_l}(\cdot,\cdot)$ as

$$p_{\gamma_{l:L}, y_l}(x,y) = p_{\gamma_{l:L}}(x) \times p_{y_l|\gamma_{l:L}=x}(y), \tag{3.22}$$

where $p_{\gamma_{l:L}}(\cdot)$ is the PDF of the lth order statistics, given in (3.1), and $p_{y_l|\gamma_{l:L}=x}(\cdot)$ is the conditional PDF of the sum of the first $l-1$ order statistics given that $\gamma_{l:L}$ is equal to x. The conditional PDF $p_{y_l|\gamma_{l:L}=x}(\cdot)$ can be determined with the help of the following corollary of Theorem 3.2 [10].

Corollary 3.1. *The conditional PDF of the sum of the first $l-1$ order statistics of L i.i.d. random variables ($l \leq L$), given that the lth order statistics is equal to y, is the same as the distribution of the sum of $l-1$ different i.i.d. random variables whose PDF is the truncated PDF of the original random variable on*

the left at y, i.e.

$$p_{\gamma_l|\gamma_{l:L}=y}(x) = p_{\sum_{j=1}^{L=l-1}\gamma_j^+}(x), \tag{3.23}$$

where the PDF of γ_j^+ was given in (3.12).

Proof. Theorem 3.2 states that given that the lth order statistics $\gamma_{l:L} = y$, the conditional distribution of the jth order statistics with $j < l$ is the same as the distribution of the jth order statistics of $l-1$ different i.i.d. random variables whose PDF is the truncated PDF of the original random variable on the left at y, as shown in (3.12). Therefore, the distribution of the sum of the first $l-1$ order statistics of L i.i.d. random variables given that the lth order statistics $\gamma_{l:L} = y$ is the same as the distribution of the sum of the $l-1$ order statistics of $l-1$ i.i.d. random variables with the truncated distribution. The proof of this corollary is completed by noting that the ordering operation does not affect the statistics of the sum of the random variables. □

Based on the above corollary, the conditional PDF in (3.22) can be obtained as the PDF of the sum of $l-1$ i.i.d. random variables. The MGF approach can also apply, which is demonstrated for the exponential r. v. case in the following example.

Example 3.1: When γ_i are i.i.d. exponentially distributed with CDF given by

$$F_\gamma(x) = 1 - e^{-\frac{x}{\overline{\gamma}}}, \qquad \gamma \geq 0, \tag{3.24}$$

the truncated PDF in (3.12) specializes to

$$p_{\gamma_j^+}(y) = \frac{1}{\overline{\gamma}} e^{-\frac{x-y}{\overline{\gamma}}}, \ x \geq y. \tag{3.25}$$

The corresponding MGF of γ_j^+ can be shown to be given by

$$M_{\gamma_j^+}(t) = \int_0^{+\infty} p_{\gamma_j^+}(y) e^{sx} \mathrm{d}x = \frac{1}{1 - s\overline{\gamma}} e^{sy}. \tag{3.26}$$

Consequently, the MGF of the sum of $l-1$ i.i.d. random variable γ_j^+ can be shown to be given by

$$M_{\sum_{j=1}^{l-1}\gamma_j^+}(t) = [M_{\gamma_j^+}(t)]^{l-1} = \frac{1}{(1 - s\overline{\gamma})^{l-1}} e^{(l-1)sx}, \tag{3.27}$$

which is also the MGF of the conditional random variable. After carrying out a proper inverse Laplace transform, we can obtain the conditional PDF of the sum of the first $l-1$ order statistics $p_{\gamma_l|\gamma_{l:L}=y}(\cdot)$ as

$$\begin{aligned} p_{\gamma_l|\gamma_{l:L}=y}(x) &= p_{\sum_{j=1}^{l-1}\gamma_j^+}(x) \\ &= \frac{1}{(l-2)!\overline{\gamma}^{l-1}} [x - (l-1)y]^{(l-2)} e^{-\frac{x-(l-1)y}{\overline{\gamma}}}, \ x \geq (l-1)y. \end{aligned} \tag{3.28}$$

Finally, we can obtain a generic expression of the joint PDF $p_{\gamma_{l:L},y_l}(\cdot,\cdot)$ after appropriate substitution into (3.22) as

$$p_{\gamma_{l:L},y_l}(x,y) = \frac{L!}{(L-l)!(l-1)!}[F_\gamma(x)]^{L-l}[1-F_\gamma(x)]^{l-1}p_\gamma(x)\; p_{\sum_{j=1}^{l-1}\gamma_j^+}(y). \tag{3.29}$$

Note that since the random variable γ_js are nonnegative and $\gamma_{j:L} \geq \gamma_{l:L}$ for all $j = 1, 2, \cdots, l-1$, we have $y_l = \sum_{j=1}^{i-1}\gamma_{j:L} \geq (l-1)\gamma_{l:L}$. Therefore, the support of the joint PDF $p_{\gamma_{l:L},y_l}(x,y)$ is the region $x > 0, y > (l-1)x$.

For the exponential r. v. special case, noting that the PDF of the lth order statistics of L i.i.d. exponential random variables specializes to

$$p_{\gamma_{l:L}}(x) = \frac{L!}{\overline{\gamma}(l-1)!}\sum_{j=0}^{L-l}\frac{(-1)^j}{(L-l-j)!j!}\; e^{-\frac{(l+j)x}{\overline{\gamma}}}, \tag{3.30}$$

we obtain the joint PDF of $\gamma_{l:L}$ and y_l, by substituting (3.30) and (3.28) into (3.22), as

$$p_{\gamma_{l:L},y_l}(x,y) = \sum_{j=0}^{L-l}\frac{(-1)^j L!}{(L-l-j)!(l-1)!(l-2)!j!\overline{\gamma}^l}[y-(l-1)x]^{(l-2)}e^{-\frac{y+(j+1)x}{\overline{\gamma}}}, \quad x \geq 0,\; y \geq (l-1)x. \tag{3.31}$$

As an illustration, the joint PDF of $\gamma_{l:L}$ and y_l for exponential special case, as given in (3.31), is plotted in Fig. 3.2. Note that since $l = 3$ here, the joint PDF is equal to zero when $y_l < 2\gamma_{l:L}$.

3.4 Joint distributions of partial sums

In this section, we generalize the result in previous section by deriving the joint distributions of partial sums of order statistics [3]. We consider two scenarios depending on whether all ordered random variables are involved or not.

3.4.1 Cases involving all random variables

We first investigate the three-dimensional joint PDF $p_{y_l,\gamma_{l:L},z_l}(y,\gamma,z)$, where y_l is the sum of the first $l-1$ order statistics, i.e. $y_l = \sum_{j=1}^{l-1}\gamma_{j:L}$, and z_l is the sum of the last $L-l$ order statistics, i.e. $z_l = \sum_{j=l+1}^{L}\gamma_{j:L}$. The definition of y_l and z_l is illustrated below.

$$\overbrace{\gamma_{1:L},\cdots,\gamma_{l-1:L}}^{y_l=\sum_{i=1}^{l-1}\gamma_{i:L}},\gamma_{l:L},\overbrace{\gamma_{l+1:L},\cdots,\gamma_{L:L}}^{z_l=\sum_{i=l+1}^{k-1}\gamma_{i:L}}. \tag{3.32}$$

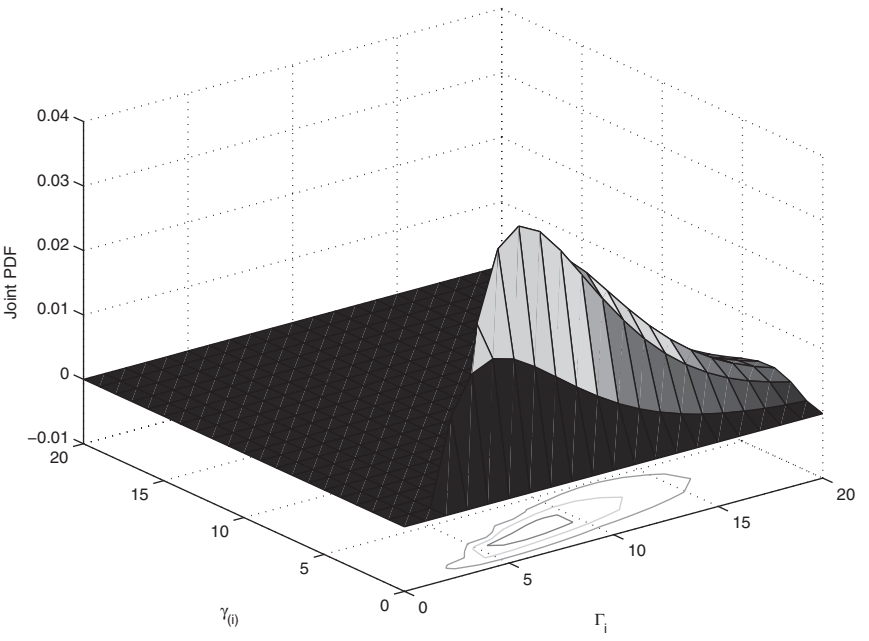

Figure 3.2 Joint PDF of Γ_{i-1} and $\gamma_{(i)}$ for the exponential random variable case ($L = 6$, $i = 3$, and $\overline{\gamma} = 6$ dB) [3]. © 2006 IEEE.

Applying twice the Bayesian rule, we can write this joint PDF $p_{y_l,\gamma_{l:L},z_l}(y,\gamma,z)$ as the product of the PDF of $\gamma_{l:L}$ and two conditional PDFs as follows

$$p_{y_l,\gamma_{l:L},z_l}(y,\gamma,z) = p_{\gamma_{l:L}}(\gamma) \times p_{z_l|\gamma_{l:L}=\gamma}(z) \times p_{y_l|\gamma_{l:L}=\gamma,z_l=z}(y). \tag{3.33}$$

The generic expression of $p_{\gamma_{l:L}}(\cdot)$ was given in (3.1) in terms of the common PDF and CDF of γ_i, $p_\gamma(\gamma)$ and $P_\gamma(\gamma)$. As noted earlier, the order statistics of samples from a continuous distribution form a Markov chain, the conditional distribution of the jth order statistics of L i.i.d. random samples, given that the lth order statistics is equal to γ ($j < l$) and that the sum of the last $L - l$ order statistics is equal to z, is the same as the conditional distribution of the jth order statistics given only that the lth order statistics is equal to γ, i.e.

$$p_{\gamma_{j:L}|\gamma_{l:L}=\gamma,\sum_{k=l+1}^{L}\gamma_{k:L}=z}(y) = p_{\gamma_{j:L}|\gamma_{l:L}=\gamma}(y). \tag{3.34}$$

With the application of Corollary 1, we have

$$p_{y_l|\gamma_{l:L}=\gamma,z_l=z}(y) = p_{\sum_{j=1}^{l-1}\gamma_j^+}(y),\ y > (l-1)\gamma, \tag{3.35}$$

where the PDF of γ_j^+ was given in (3.12)

The conditional PDF $p_{z_l|\gamma_{l:L}=\gamma}(z)$ can be determined with the help of the following corollary [3].

Corollary 3.2. *The conditional distribution of the sum of the last $L-l$ order statistics of L i.i.d. random samples ($l \leq L$), given that the lth order statistics is equal to γ, is the same as the distribution of the sum of $L-l$ different i.i.d. random variables whose PDF is the PDF of the original (unordered) random variable truncated on the right of γ, i.e.*

$$p_{z_l|\gamma_{l:L}=\gamma}(z) = p_{\sum_{j=1}^{L-l}\gamma_j^-}(z),\ z < (L-l)\gamma, \tag{3.36}$$

where the PDF of γ_j^- is given by

$$p_{\gamma_j^-}(x) = \frac{p_\gamma(x)}{F_\gamma(\gamma)}, \qquad 0 < x < \gamma. \tag{3.37}$$

Proof. Based on Theorem 3.1, the distribution of the sum of the last $L-l$ order statistics of L i.i.d. random variables given that the lth order statistics $\gamma_{l:L} = \gamma$ is the same as the distribution of the sum of $L-l$ order statistics of $L-l$ i.i.d. random variables with truncated distribution. The proof is completed by noting that the ordering operation does not affect the statistics of the sum of random variables. □

Finally, we obtain the joint PDF $p_{y_l,\gamma_{l:L},z_l}(y,\gamma,z)$ as

$$\begin{aligned} &p_{y_l,\gamma_{l:L},z_l}(y,\gamma,z) = p_{\gamma_{l:L}}(\gamma)p_{\sum_{j=1}^{L-l}\gamma_j^-}(z)p_{\sum_{j=1}^{l-1}\gamma_j^+}(y), \\ &\gamma > 0, y > (l-1)\gamma, z < (L-l)\gamma. \end{aligned} \tag{3.38}$$

Example 3.2: When γ_i are i.i.d. exponentially distributed, $p_{\gamma_j^-}(x)$ defined in (3.37) specializes to

$$p_{\gamma_j^-}(x) = \frac{\frac{1}{\overline{\gamma}}e^{-\frac{x}{\overline{\gamma}}}}{1-e^{-\frac{\gamma}{\overline{\gamma}}}},\ x < \gamma, \tag{3.39}$$

Following again the MGF approach, we can obtain the closed-form expression for $p_{z_l|\gamma_{l:L}=\gamma}(\cdot)$ as

$$p_{\sum_{j=1}^{L-l}\gamma_j^-}(z) = \sum_{i=0}^{L-l}\binom{L-l}{i}\frac{e^{-z/\overline{\gamma}}}{(1-e^{-\gamma/\overline{\gamma}})^{L-l}}\frac{(-1)^i(z-i\gamma)^{L-l-1}}{\overline{\gamma}^{L-l}(L-l-1)!}\mathcal{U}(z-i\gamma), \tag{3.40}$$

where $\mathcal{U}(\cdot)$ is the unit step function.

It follows, after properly substituting (3.14), (3.24), (3.28), and (3.36) into (3.38), we can obtain a closed-form expression for the joint PDF $p_{y_l,\gamma_{l:L},z_l}(y,\gamma,z)$

as

$$p_{y_l,\gamma_{l:L},z_l}(y,\gamma,z) = \frac{L!}{(L-l)!(l-1)!\overline{\gamma}^L}\frac{[y-(l-1)\gamma]^{l-2}}{(l-2)!(L-l-1)!}e^{-\frac{y+\gamma+z}{\overline{\gamma}}}\mathcal{U}(y-(l-1)\gamma) \times \sum_{i=0}^{L-l}\binom{L-l}{i}(-1)^i(z-i\gamma)^{L-l-1}\mathcal{U}(z-i\gamma), \quad \gamma>0, y>(l-1)\gamma, z<(L-l)\gamma. \tag{3.41}$$

We can apply the three-dimensional joint PDF of partial sums derived above to obtain the joint PDF of the lth order statistics and the sum of the remaining $L-1$ order statistics. Specifically, setting $l=1$, (3.38) reduces to the joint PDF of the largest random variable and the sum of the remaining ones, denoted by $p_{\gamma_{1:L},z_1}(\gamma,z)$, which is given by

$$p_{\gamma_{1:L},z_1}(\gamma,z) = p_{\gamma_{1:L}}(\gamma)p_{\sum_{j=1}^{L-1}\gamma_j}(z), \qquad \gamma>0, z<(L-l)\gamma. \tag{3.42}$$

For the general case where $1<l<L$, we can obtain the joint PDF of $\gamma_{l:L}$ and $\sum_{i\neq l}\gamma_{i:L}$, while noting that the latter is equal to y_l+z_l, as

$$p_{\gamma_{l:L},y_l+z_l}(\gamma,w) = \int_0^{(L-l)\gamma} p_{y_l,\gamma_{l:L},z_l}(w-z,\gamma,z)\mathrm{d}z, \quad y>(l-1)\gamma. \tag{3.43}$$

These joint PDFs are useful in the performance analysis of different wireless transmission technologies in later chapters.

3.4.2 Cases only involving the largest random variables

We now consider the joint PDFs involving only the first k-ordered random variables, i.e. $\gamma_{l:L}$, $l=1,2,\cdots,k$. More specifically, we are interested in obtaining the joint PDF of the lth largest random variable ($l<k$) and the sum of the remaining $k-1$ ones, which is denoted by $\sum_{j=1,j\neq l}^{k}\gamma_{j:L}$ [11]. Note that the case of $l=k$ has been addressed in the previous section.

We first consider the general case where $1<l<k-1$. In this case, we start with the joint PDF of the following four random variables, $y_l,\gamma_{l:L},z_l^k,\gamma_{k:L}$, where y_l and z_l^k are partial sums defined based on the first k order statistics, as

$$\overbrace{\gamma_{1:L},\cdots,\gamma_{l-1:L}}^{y_l=\sum_{i=1}^{l-1}\gamma_{i:L}},\gamma_{l:L},\overbrace{\gamma_{l+1:L},\cdots,\gamma_{k-1:L}}^{z_l^k=\sum_{i=l+1}^{k-1}\gamma_{i:L}},\gamma_{k:L},\gamma_{k+1:L},\cdots,\gamma_{L:L}. \tag{3.44}$$

Applying the Bayesian rule twice, the 4D joint PDF under consideration, $p_{y_l,\gamma_{l:L},z_l^k,\gamma_{k:L}}(y,\gamma,z,\beta)$, can be written as

$$p_{y_l,\gamma_{l:L},z_l^k,\gamma_{k:L}}(y,\gamma,z,\beta) = p_{\gamma_{l:L},\gamma_{k:L}}(\gamma,\beta)\cdot p_{y_l|\gamma_{l:L}=\gamma,\gamma_{k:L}=\beta}(y) \times p_{z_l^k|\gamma_{l:L}=\gamma,\gamma_{k:L}=\beta,y_l=y}(z), \tag{3.45}$$

where $p_{\gamma_{l:L},\gamma_{k:L}}(\cdot,\cdot)$ is the joint PDF of $\gamma_{l:L}$ and $\gamma_{k:L}$, the generic expression of which was given in (3.4). As shown earlier, ordered random variables satisfy the Markovian property. Therefore, the conditional PDFs $p_{y_l|\gamma_{l:L}=\gamma,\gamma_{k:L}=\beta}(y)$, and $p_{z_l^k|\gamma_{l:L}=\gamma,\gamma_{k:L}=\beta,y_l=y}(z)$ are equivalent to $p_{y_l|\gamma_{l:L}=\gamma}(y)$, and $p_{z_l^k|\gamma_{l:L}=\gamma,\gamma_{k:L}=\beta}(z)$, respectively. With the application of Corollary 1, we obtain the conditional PDF $p_{y_l|\gamma_{l:L}=\gamma,\gamma_{k:L}=\beta}(y)$ as

$$\begin{aligned} p_{y_l|\gamma_{l:L}=\gamma,\gamma_{k:L}=\beta}(y) &= p_{y_l|\gamma_{l:L}=\gamma}(y) \\ &= p_{\sum_{i=1}^{l-1}\gamma_i^+}(y), \quad 0<(l-1)\gamma<y, \end{aligned} \tag{3.46}$$

where γ_i^+ is the random variable with truncated distribution given in (3.12).

The conditional PDF $p_{z_l^k|\gamma_{l:L}=\gamma,\gamma_{k:L}=\beta,y_l=y}(z)$, or equivalently $p_{z_l^k|\gamma_{l:L}=\gamma,\gamma_{k:L}=\beta}(z)$, can be determined with the help of the following corollary [11].

Corollary 3.3. *The conditional distribution of the sum of $k-l+1$ order statistics, i.e. $\sum_{i=l+1}^{k-1}\gamma_{i:L}$, given that the lth order statistics is equal to γ and the kth order statistics is equal to β, is the same as the distribution of the sum of $k-l+1$ different i.i.d. random variables whose PDF is the truncated PDF of the original random variable on the right at γ and on the left at β, i.e.*

$$\begin{aligned} p_{z_l^k|\gamma_{l:L}=\gamma,\gamma_{k:L}=\beta}(z) &= p_{\sum_{i=1}^{k-l-1}\gamma_i^{\pm}}(z), \\ &\qquad 0<\beta<\frac{z}{k-l-1}<\gamma, \end{aligned} \tag{3.47}$$

where $\gamma_i^{\pm}$ denotes the random variable with PDF

$$p_{\gamma_i^{\pm}}(x)=\frac{p_\gamma(x)}{F_\gamma(\gamma)-F_\gamma(\beta)},\ \beta\le x\le\gamma.$$

The results can be proved easily after sequentially applying Corollary 1 and Corollary 2.

Finally, after substituting (3.4), (3.46), and (3.47) into (3.45), we obtain the generic expression of the joint PDF $p_{y_l,\gamma_{l:L},z_l^k,\gamma_{k:L}}(y,\gamma,z,\beta)$ as

$$\begin{aligned} p_{y_l,\gamma_{l:L},z_l^k,\gamma_{k:L}}(y,\gamma,z,\beta) &= p_{\gamma_{l:L},\gamma_{k:L}}(\gamma,\beta)\cdot p_{\sum_{i=1}^{l-1}\gamma_i^+}(y)\cdot p_{\sum_{i=1}^{k-l-1}\gamma_i^{\pm}}(z), \\ &\qquad 0<\beta<\gamma, y>(l-1)\gamma, \beta<\frac{z}{k-l-1}<\gamma. \end{aligned} \tag{3.48}$$

In the case of $k=1$, it is sufficient to consider the 3D joint PDF of $p_{\gamma_{1:L},z_1^k,\gamma_{k:L}}(\gamma,z,\beta)$, which can be written as

$$p_{\gamma_{1:L},z_1^k,\gamma_{k:L}}(\gamma,z,\beta)=p_{\gamma_{1:L},\gamma_{k:L}}(\gamma,\beta)\cdot p_{z_1^k|\gamma_{1:L}=\gamma,\gamma_{k:L}=\beta}(z). \tag{3.49}$$

Applying Corollary 3, the 3D joint PDF can be obtained as

$$\begin{aligned} &p_{\gamma_{1:L},z_1^k,\gamma_{k:L}}(\gamma,z,\beta)=p_{\gamma_{1:L},\gamma_{k:L}}(\gamma,\beta)\cdot p_{\sum_{i=1}^{k-2}\gamma_i^{\pm}}(z), \\ &0<\beta<\gamma,(k-2)\beta<z<(k-2)\gamma. \end{aligned} \tag{3.50}$$

When $l = k-1$, the 3D joint PDF of interest becomes $p_{y_{k-1},\gamma_{k-1:L},\gamma_{k:L}}(y,\gamma,\beta)$, which can be written, after applying the Bayesian rule, as

$$p_{y_{k-1},\gamma_{k-1:L},\gamma_{k:L}}(y,\gamma,\beta) = p_{\gamma_{k-1:L},\gamma_{k:L}}(\gamma,\beta)\cdot p_{y_{k-1}|\gamma_{k-1:L}=\gamma,\gamma_{k:L}=\beta}(y). \tag{3.51}$$

It follows, after proper substitution, $p_{y_{k-1},\gamma_{k-1:L},\gamma_{k:L}}(y,\gamma,\beta)$ can be shown to be given by

$$\begin{aligned} &p_{y_{k-1},\gamma_{k-1:L}\,\gamma_{k:L}}(y,\gamma,\beta) = p_{\gamma_{k-1:L},\gamma_{k:L}}(\gamma,\beta)\cdot p_{\sum_{i=1}^{k-2}\gamma_i^{+}}(y), \\ &0<\beta<\gamma, y>(k-2)\gamma. \end{aligned} \tag{3.52}$$

The 3D joint PDFs $p_{\gamma_{1:L},z_1^k,\gamma_{k:L}}(\gamma,z,\beta)$ and $p_{y_{k-1},\gamma_{k-1:L}\,\gamma_{k:L}}(y,\gamma,\beta)$ for the exponential random variable special case can be similarly obtained after proper submissions into (3.50) and (3.52).

Example 3.3: When γ_i are i.i.d. exponential random variables, it can be also shown that $p_{\gamma_i^{\pm}}(x)$ specializes to

$$p_{\gamma_i^{\pm}}(x) = \frac{e^{-x/\overline{\gamma}}}{\overline{\gamma}\left(e^{-\beta/\overline{\gamma}}-e^{-\gamma/\overline{\gamma}}\right)}, \quad \beta\le x\le\gamma, \tag{3.53}$$

The corresponding MGF is given by

$$\mathcal{M}_{\gamma_i^{\pm}}(s) = \int_{\beta}^{\gamma} p_{\gamma_i^{\pm}}(x)e^{sx}\mathrm{d}x = \frac{e^{s\beta-\beta/\overline{\gamma}}-e^{s\gamma-\gamma/\overline{\gamma}}}{(e^{-\beta/\overline{\gamma}}-e^{-\gamma/\overline{\gamma}})(1-s\overline{\gamma})}. \tag{3.54}$$

Noting that the MGF of $\sum_{i=1}^{k-l-1}\gamma_i^{\pm}$ is equal to $[\mathcal{M}_{\gamma_i^{\pm}}(s)]^{k-l-1}$, we can obtain the closed-form expression for (3.47) by taking the inverse Laplace transform as

$$\begin{aligned} &p_{z_l^k|\gamma_{l:L}=\gamma,\gamma_{k:L}=\beta,y_l=y}(z) = \mathcal{L}^{-1}\{[\mathcal{M}_{\gamma_i^{\pm}}(s)]^{k-l-1}\} \\ &= \sum_{j=0}^{k-l-1}\binom{k-l-1}{j}\frac{(-1)^j e^{-z/\overline{\gamma}}[z-\beta(k-l-j-1)-\gamma j]^{k-l-2}}{[(e^{-\beta/\overline{\gamma}}-e^{-\gamma/\overline{\gamma}})\overline{\gamma}]^{k-l-1}(k-l-2)!} \\ &\times\mathcal{U}(z-\beta(k-l-j-1)-\gamma j), \\ &\quad (k-l-1)\beta<z<(k-l-1)\gamma. \end{aligned} \tag{3.55}$$

Meanwhile, the joint PDF of $\gamma_{l:L}$ and $\gamma_{k:L}$ given in (3.4) becomes

$$\begin{aligned} p_{\gamma_{l:L},\gamma_{k:L}}(x,y) = &\frac{L!}{(l-1)!(k-l-1)!(L-k)!\overline{\gamma}^2}e^{-\frac{lx+y}{\overline{\gamma}}} \\ &\times\left(e^{-\frac{y}{\overline{\gamma}}}-e^{-\frac{x}{\overline{\gamma}}}\right)^{k-l-1}\cdot\left(1-e^{-\frac{y}{\overline{\gamma}}}\right)^{L-k}, \end{aligned} \tag{3.56}$$

After substituting (3.28),(3.55), and (3.56) into (3.48), we can obtain a closed-form expression for the 4D joint PDF, $p_{y_l,\gamma_{l:L},z_l^k,\gamma_{k:L}}(y,\gamma,z,\beta)$, for the exponential random variable case as

$$\begin{aligned}
&p_{y_l,\gamma_{l:L},z_l^k,\gamma_{k:L}}(y,\gamma,z,\beta) \qquad (3.57)\\
&= \frac{L!e^{-(y+\gamma+z+\beta)/\overline{\gamma}}(1-e^{-\beta/\overline{\gamma}})^{L-k}[y-(l-1)\gamma]^{l-2}}{(L-k)!(k-l-1)!(k-l-2)!(l-1)!(l-2)!\overline{\gamma}^k}\\
&\times \sum_{j=0}^{k-l-1}\binom{k-l-1}{j}(-1)^j[b-\beta(k-l-j-1)-\gamma j]^{k-l-2}\\
&\times\mathcal{U}(\gamma)\mathcal{U}(\gamma-\beta)\mathcal{U}(y-(l-1)\gamma)\mathcal{U}(z-\beta(k-l-j-1)-\gamma j),\\
&\quad (k-l-1)\beta < z < (k-l-1)\gamma.
\end{aligned}$$

Remark: We notice from the above three examples that the derivation of the joint PDFs often involves the statistics of the sum of some truncated random variables. For convenience, we summarize the PDF and MGF of the truncated random variables corresponding to the received SNR of the three most popular fading channel models in Table 3.1.

With these multiple dimensional joint PDFs available, we can readily derive the joint PDF of any partial sums involving the largest k-ordered random variables. For example, we can obtain the joint PDF of $Y = y_l + \gamma_{l:L}$ and $Z = z_l^k + \gamma_{k:L}$, $p_{Y,Z}(y,z)$as

$$p_{Y,Z}(y,z) = \int_0^{\frac{z}{k-l}}\int_{\frac{z}{k-l}}^{\frac{y}{l}} p_{y_l,\gamma_{l:L},z_l^k,\gamma_{k:L}}(y-\gamma,\gamma,z-\beta,\beta)\mathrm{d}\gamma\mathrm{d}\beta, \quad y > \frac{l}{k-l}z. \tag{3.58}$$

In addition, the joint PDF $\gamma_{l:L}$ and $W = y_l + z_l^k + \gamma_{k:L}$, denoted by $p_{\gamma_{l:L},W}(\gamma,w)$, can be calculated as

$$p_{\gamma_{l:L},W}(\gamma,w) = \begin{cases} \displaystyle\int_{(k-2)w/(k-1)}^{(k-2)\gamma} p_{\gamma_{1:L},z_1^k,\gamma_{k:L}}(\gamma,z,w-z)\mathrm{d}z, & l=1;\\ \displaystyle\int_0^{\gamma}\int_{(k-l-1)\beta}^{(k-l-1)\gamma} & \\ \quad p_{y_l,\gamma_{l:L},z_l^k,\gamma_{k:L}}(w-z-\beta,\gamma,z,\beta)\mathrm{d}z\mathrm{d}\beta, & 1<l<k-1;\\ \displaystyle\int_0^{\gamma} p_{y_{k-1},\gamma_{k-1:L}\gamma_{k:L}}(w-\beta,\gamma,\beta)\mathrm{d}\beta, & l=k-1. \end{cases} \tag{3.59}$$

Note that only finite integrations of the joint PDFs are involved in these calculations. Therefore, even though a closed-form expression is tedious to obtain, this joint probability can be easily calculated with mathematical software, such as Mathematica and Maple.

Table 3.1 Truncated MGFs for the three fading models under consideration.

$M_{\gamma^+}(s)$ where γ^+ has PDF $p_{\gamma_j^+}(x) = \frac{p_\gamma(x)}{1-P_\gamma(\gamma_T)},\ x \geq \gamma_T$.	
Rayleigh	$\frac{1}{1-s\overline{\gamma}} e^{s\gamma_T}$
Rice	$\frac{1+K}{1+K-s\overline{\gamma}} e^{\frac{s\overline{\gamma}K}{1+K-s\overline{\gamma}}} \frac{Q_1\left(\sqrt{\frac{2K(1+K)}{1+K-s\overline{\gamma}}}, \sqrt{2(1+K-s\overline{\gamma})\frac{\gamma_T}{\overline{\gamma}}}\right)}{Q_1\left(\sqrt{2K}, \sqrt{2(1+K)\frac{\gamma_T}{\overline{\gamma}}}\right)}$
Nakagami-m	$\left(1-\frac{s\overline{\gamma}}{m}\right)^{-m} \frac{\Gamma\left(m, \frac{m\gamma_T}{\overline{\gamma}} - s\gamma_T\right)}{\Gamma\left(m, \frac{m\gamma_T}{\overline{\gamma}}\right)}$

$M_{\gamma^-}(s)$ where γ^- has PDF $p_{\gamma_j^-}(x) = \frac{p_\gamma(x)}{P_\gamma(\gamma_T)},\quad 0 < x < \gamma_T$.	
Rayleigh	$\frac{1}{1-s\overline{\gamma}} \frac{1-e^{s\gamma_T - \frac{\gamma_T}{\overline{\gamma}}}}{1-e^{-\frac{\gamma_T}{\overline{\gamma}}}}$
Rice	$\frac{1+K}{1+K-s\overline{\gamma}} e^{\frac{s\overline{\gamma}K}{1+K-s\overline{\gamma}}} \frac{1-Q_1\left(\sqrt{\frac{2K(1+K)}{1+K-s\overline{\gamma}}}, \sqrt{2(1+K-s\overline{\gamma})\frac{\gamma_T}{\overline{\gamma}}}\right)}{1-Q_1\left(\sqrt{2K}, \sqrt{2(1+K)\frac{\gamma_T}{\overline{\gamma}}}\right)}$
Nakagami-m	$\left(1-\frac{s\overline{\gamma}}{m}\right)^{-m} \frac{1-\Gamma\left(m, \frac{m\gamma_T}{\overline{\gamma}} - s\gamma_T\right)/\Gamma(m)}{1-\Gamma\left(m, \frac{m\gamma_T}{\overline{\gamma}}\right)/\Gamma(m)}$

$M_{\gamma^\pm}(s)$ where $\gamma^\pm$ has $p_{\gamma_i^\pm}(x) = \frac{p_\gamma(x)}{P_\gamma(\gamma_{T_1}) - P_\gamma(\gamma_{T_2})},\ \gamma_{T_2} \leq x \leq \gamma_{T_1}$.	
Rayleigh	$\frac{1}{1-s\overline{\gamma}} \frac{e^{s\gamma_{T_2} - \frac{\gamma_{T_2}}{\overline{\gamma}}} - e^{s\gamma_{T_1} - \frac{\gamma_{T_1}}{\overline{\gamma}}}}{e^{-\frac{\gamma_{T_2}}{\overline{\gamma}}} - e^{-\frac{\gamma_{T_1}}{\overline{\gamma}}}}$
Rice	$\frac{\frac{1+K}{1+K-s\overline{\gamma}} e^{\frac{s\overline{\gamma}K}{1+K-s\overline{\gamma}}} Q_1\left(\sqrt{\frac{2K(1+K)}{1+K-s\overline{\gamma}}}, \sqrt{2(1+K-s\overline{\gamma})\frac{\gamma_{T_2}}{\overline{\gamma}}}\right)}{Q_1\left(\sqrt{2K}, \sqrt{2(1+K)\frac{\gamma_{T_2}}{\overline{\gamma}}}\right) - Q_1\left(\sqrt{2K}, \sqrt{2(1+K)\frac{\gamma_{T_1}}{\overline{\gamma}}}\right)} - \frac{\frac{1+K}{1+K-s\overline{\gamma}} e^{\frac{s\overline{\gamma}K}{1+K-s\overline{\gamma}}} Q_1\left(\sqrt{\frac{2K(1+K)}{1+K-s\overline{\gamma}}}, \sqrt{2(1+K-s\overline{\gamma})\frac{\gamma_{T_1}}{\overline{\gamma}}}\right)}{Q_1\left(\sqrt{2K}, \sqrt{2(1+K)\frac{\gamma_{T_2}}{\overline{\gamma}}}\right) - Q_1\left(\sqrt{2K}, \sqrt{2(1+K)\frac{\gamma_{T_1}}{\overline{\gamma}}}\right)}$
Nakagami-m	$\left(1-\frac{s\overline{\gamma}}{m}\right)^{-m} \frac{\Gamma\left(m, \frac{m\gamma_{T_2}}{\overline{\gamma}} - s\gamma_{T_2}\right) - \Gamma\left(m, \frac{m\gamma_{T_1}}{\overline{\gamma}} - s\gamma_{T_1}\right)}{\Gamma\left(m, \frac{m\gamma_{T_2}}{\overline{\gamma}}\right) - \Gamma\left(m, \frac{m\gamma_{T_1}}{\overline{\gamma}}\right)}$

3.5 MGF-based unified analytical framework for joint distributions

In this section, we present a unified analytical framework to determine the joint statistics of partial sums of ordered RVs using an MGF-based approach [15]. More specifically, we extend the result in [12–14], which only derives the joint MGF of the selected individual order statistics and the sum of the remaining ones, and systematically solves for the joint statistics of arbitrary partial sums of ordered RVs. The main advantage of the proposed MGF-based unified framework is that it applies not only to the cases when all the K-ordered RVs are considered, but also to those cases when only the K_s ($K_s < K$) best RVs are involved. For each scenario, we present some selected examples to illustrate the derivation procedure.

3.5.1 General steps

The proposed analytical framework adopts a general two-step approach:

(i) obtain the analytical expressions of the joint MGF of partial sums (not necessarily the partial sums of interest as will be seen later);
(ii) apply the proper inverse Laplace transform to derive the joint PDF of partial sums (additional integration may be required to obtain the desired joint PDF).

To facilitate the inverse Laplace transform calculation, the joint MGF from step (i) should be made as compact as possible. An observation made in [13–15] involving the interchange of multiple integrals of ordered RVs becomes useful in the following analysis. Suppose, for example, that we need to evaluate a multiple integral over the range $\gamma_a \geq \gamma_1 \geq \gamma_2 \geq \gamma_3 \geq \gamma_4 \geq \gamma_b$. More specifically, let

$$I = \int_{\gamma_b}^{\gamma_a} \mathrm{d}\gamma_1 \int_{\gamma_b}^{\gamma_1} \mathrm{d}\gamma_2 \int_{\gamma_b}^{\gamma_2} \mathrm{d}\gamma_3 \int_{\gamma_b}^{\gamma_3} \mathrm{d}\gamma_4 \;\; p\left(\gamma_1, \gamma_2, \gamma_3, \gamma_4\right). \tag{3.60}$$

It can be shown that by interchanging the order of integration, while ensuring each pair of integration limits is chosen to be as tight as possible, the multiple integral in (3.60) can be rewritten into the following equivalent representations,

$$\begin{aligned}
I &= \int_{\gamma_b}^{\gamma_a} \mathrm{d}\gamma_4 \int_{\gamma_4}^{\gamma_a} \mathrm{d}\gamma_3 \int_{\gamma_3}^{\gamma_a} \mathrm{d}\gamma_2 \int_{\gamma_2}^{\gamma_a} \mathrm{d}\gamma_1 \;\; p\left(\gamma_1, \gamma_2, \gamma_3, \gamma_4\right) \\
&= \int_{\gamma_b}^{\gamma_a} \mathrm{d}\gamma_2 \int_{\gamma_b}^{\gamma_2} \mathrm{d}\gamma_3 \int_{\gamma_b}^{\gamma_3} \mathrm{d}\gamma_4 \int_{\gamma_2}^{\gamma_a} \mathrm{d}\gamma_1 \;\; p\left(\gamma_1, \gamma_2, \gamma_3, \gamma_4\right) \\
&= \int_{\gamma_b}^{\gamma_a} \mathrm{d}\gamma_3 \int_{\gamma_3}^{\gamma_a} \mathrm{d}\gamma_1 \int_{\gamma_b}^{\gamma_3} \mathrm{d}\gamma_4 \int_{\gamma_3}^{\gamma_1} \mathrm{d}\gamma_2 \;\; p\left(\gamma_1, \gamma_2, \gamma_3, \gamma_4\right) \\
&= \int_{\gamma_b}^{\gamma_a} \mathrm{d}\gamma_1 \int_{\gamma_b}^{\gamma_1} \mathrm{d}\gamma_4 \int_{\gamma_4}^{\gamma_1} \mathrm{d}\gamma_3 \int_{\gamma_3}^{\gamma_1} \mathrm{d}\gamma_2 \;\; p\left(\gamma_1, \gamma_2, \gamma_3, \gamma_4\right) \\
&= \int_{\gamma_b}^{\gamma_a} \mathrm{d}\gamma_4 \int_{\gamma_4}^{\gamma_a} \mathrm{d}\gamma_1 \int_{\gamma_4}^{\gamma_1} \mathrm{d}\gamma_3 \int_{\gamma_3}^{\gamma_1} \mathrm{d}\gamma_2 \;\; p\left(\gamma_1, \gamma_2, \gamma_3, \gamma_4\right).
\end{aligned} \tag{3.61}$$

The general rule is that the integration limits should be selected as tight as possible using the remaining variables. For example, in the first equation of (3.61), the variables are integrated in the order of γ_1, γ_2, γ_3, and γ_4. Based on the given inequality condition $\gamma_a \geq \gamma_1 \geq \gamma_2 \geq \gamma_3 \geq \gamma_4 \geq \gamma_b$, the integration limit of γ_1 should be from γ_2 to γ_a, because γ_2 is the tightest among the remaining RVs. Similarly, the integration limit γ_3 is from γ_4 to γ_a, because γ_1 and γ_2 were already integrated out.

After obtaining the joint MGF in a compact form, we can derive the joint PDF of a selected partial sum through an inverse Laplace transform. For most of our cases of interest, the joint MGF involves basic functions, for which the inverse Laplace transform can be calculated analytically. In the worst case, we may rely on the Bromwich contour integral. The final joint PDF involves at

most one single one-dimensional contour integration, which can be easily and accurately evaluated numerically with the help of the integral tables [16, 17] or using standard mathematical packages such as Mathematica and Matlab.

The general steps can be directly applied when all K-ordered RVs are considered and the RVs in the partial sums are continuous. When these conditions do not hold, we need to apply some extra steps in the analysis in order to obtain a valid joint MGF. Specifically, when only the best K_s ($K_s < K$)-ordered RVs are involved in the partial sums, we should consider the K_sth order statistics $\gamma_{K_s:K}$ separately. When the RVs involved in a partial sum are not continuous, i.e. are separated by the other RVs, we need to divide this partial sum into smaller sums. Without such separation, we cannot find the valid integration limit when calculating the joint MGF. In both cases, when the joint PDF of the new partial sums are derived, we need to perform another finite integration to obtain the desired joint PDF.

3.5.2 Illustrative examples

In the following, we present several examples to illustrate the proposed analytical framework. Our focus is on how to obtain a compact expression of the joint MGFs, which can be greatly simplified with the application of the following functions and relations.

Common functions

(i) A mixture of a CDF and an MGF $c(\gamma, \lambda)$:

$$c(\gamma, \lambda) = \int_0^{\gamma} \mathrm{d}x \; p(x) \exp(\lambda x), \tag{3.62}$$

where $p(x)$ denotes the PDF of the RV of interest. Note that $c(\gamma, 0) = c(\gamma)$ is the CDF and $c(\infty, \lambda)$ leads to the MGF. Here, the variable γ is real, while λ can be complex.

(ii) A mixture of an exceedance distribution function (EDF) and an MGF, $e(\gamma, \lambda)$:

$$e(\gamma, \lambda) = \int_{\gamma}^{\infty} \mathrm{d}x \; p(x) \exp(\lambda x). \tag{3.63}$$

Note that $e(\gamma, 0) = e(\gamma)$ is the EDF while $e(0, \lambda)$ gives the MGF.

(iii) An interval MGF $\mu(\gamma_a, \gamma_b, \lambda)$:

$$\mu(\gamma_a, \gamma_b, \lambda) = \int_{\gamma_a}^{\gamma_b} \mathrm{d}x \; p(x) \exp(\lambda x). \tag{3.64}$$

Note that $\mu(0, \infty, \lambda)$ gives the MGF.

The functions defined in (3.62), (3.63) and (3.64) are related as follows

$$\begin{aligned} c(\gamma,\lambda) &= e(0,\lambda) - e(\gamma,\lambda) \qquad (3.65)\\ &= c(\infty,\lambda) - e(\gamma,\lambda) \\ e(\gamma,\lambda) &= c(\infty,\lambda) - c(\gamma,\lambda) \qquad (3.66)\\ &= e(0,\lambda) - c(\gamma,\lambda) \\ \mu(\gamma_a,\gamma_b,\lambda) &= c(\gamma_b,\lambda) - c(\gamma_a,\lambda) \qquad (3.67)\\ &= e(\gamma_a,\lambda) - e(\gamma_b,\lambda). \end{aligned}$$

Simplifying relationship

(i) Integral I_m defined as

$$\begin{aligned} I_m \;=& \int_0^{\gamma_{m-1:K}} \mathrm{d}\gamma_{m:K}\; p(\gamma_{m:K}) \exp(\lambda\gamma_{m:K}) \\ &\times \int_0^{\gamma_{m:K}} \mathrm{d}\gamma_{m+1:K} p(\gamma_{m+1:K}) \exp(\lambda\gamma_{m+1:K}) \\ &\times \int_0^{\gamma_{m+1:K}} \mathrm{d}\gamma_{m+2:K} p(\gamma_{m+2:K}) \exp(\lambda\gamma_{m+2:K}) \\ &\cdots \int_0^{\gamma_{K-1:K}} \mathrm{d}\gamma_{K:K} p(\gamma_{K:K}) \exp(\lambda\gamma_{K:K}), \end{aligned} \qquad (3.68)$$

can be expressed in terms of the function $c(\gamma,\lambda)$ as

$$I_m = \frac{1}{(K-m+1)!}\left[c(\gamma_{m-1:K},\lambda)\right]^{(K-m+1)}. \qquad (3.69)$$

(ii) Integral I'_m defined as

$$\begin{aligned} I'_m \;=& \int_{\gamma_{m+1:K}}^{\infty} \mathrm{d}\gamma_{m:K}\; p(\gamma_{m:K}) \exp(\lambda\gamma_{m:K}) \\ &\int_{\gamma_{m:K}}^{\infty} \mathrm{d}\gamma_{m-1:K} p(\gamma_{m-1:K}) \exp(\lambda\gamma_{m-1:K}) \\ &\times \int_{\gamma_{m-1:K}}^{\infty} \mathrm{d}\gamma_{m-2:K} p(\gamma_{m-2:K}) \exp(\lambda\gamma_{m-2:K}) \\ &\cdots \int_{\gamma_{2:K}}^{\infty} \mathrm{d}\gamma_{1:K} p(\gamma_{1:K}) \exp(\lambda\gamma_{1:K}), \end{aligned} \qquad (3.70)$$

can be expressed in terms of the function $e(\gamma,\lambda)$ as

$$I'_m = \frac{1}{m!}\left[e(\gamma_{m+1:K},\lambda)\right]^m. \qquad (3.71)$$

(iii) Integral $I''_{a,b}$ defined as

$$\begin{aligned} I''_{a,b} &= \int_{\gamma_{b:K}}^{\gamma_{a:K}} \mathrm{d}\gamma_{b-1:K}\; p\left(\gamma_{b-1:K}\right) \exp\left(\lambda\gamma_{b-1:K}\right) \\ &\int_{\gamma_{b-1:K}}^{\gamma_{a:K}} \mathrm{d}\gamma_{b-2:K} p\left(\gamma_{b-2:K}\right) \exp\left(\lambda\gamma_{b-2:K}\right) \\ &\times \int_{\gamma_{b-2:K}}^{\gamma_{a:K}} \mathrm{d}\gamma_{b-3:K} p\left(\gamma_{b-3:K}\right) \exp\left(\lambda\gamma_{b-3:K}\right) \\ &\cdots \int_{\gamma_{a+2:K}}^{\gamma_{a:K}} \mathrm{d}\gamma_{a+1:K} p\left(\gamma_{a+1:K}\right) \exp\left(\lambda\gamma_{a+1:K}\right), \end{aligned} \tag{3.72}$$

can be expressed in terms of the function $\mu\left(\cdot,\cdot\right)$ as

$$I''_{a,b} = \frac{1}{(b-a-1)!}\left[\mu\left(\gamma_{b:K},\gamma_{a:K},\lambda\right)\right]^{(b-a-1)} \qquad \text{for } a < b. \tag{3.73}$$

The proof of this simplifying relationship can be found in the Appendix of this chapter.

Let us first consider the joint PDF of $\sum_{n=1}^{m} \gamma_{n:K}$ and $\sum_{n=m+1}^{K} \gamma_{n:K}$, which involves all K-ordered random variables. Let $Z_1 = \sum_{n=1}^{m} \gamma_{n:K}$ and $Z_2 = \sum_{n=m+1}^{K} \gamma_{n:K}$ for convenience. The following theorem presents the joint PDF of Z_1 and Z_2.

Theorem 3.4. *The two-dimensional joint PDF of Z_1 and Z_2 can be calculated as*

$$\begin{aligned} & p_{Z_1,Z_2}\left(z_1,z_2\right) = \mathcal{L}^{-1}_{S_1,S_2}\left\{MGF_{Z_1,Z_2}\left(-S_1,-S_2\right)\right\} \\ &= \frac{K!}{(K-m)!\,(m-1)!} \int_0^{\infty} \mathrm{d}\gamma_{m:K} \Bigg[p\left(\gamma_{m:K}\right) \\ &\times \mathcal{L}^{-1}_{S_1}\left\{\exp\left(-S_1\gamma_{m:K}\right)\left[e\left(\gamma_{m:K},-S_1\right)\right]^{(m-1)}\right\} \\ &\times \mathcal{L}^{-1}_{S_2}\left\{\left[c\left(\gamma_{m:K},-S_2\right)\right]^{(K-m)}\right\}\Bigg] \qquad \text{for } z_1 \geq \frac{m}{K-m} z_2. \end{aligned} \tag{3.74}$$

Proof. The second-order MGF of Z_1 and Z_2 is given by the expectation

$$\begin{aligned} & MGF_{Z_1,Z_2}\left(\lambda_1,\lambda_2\right) = E\left\{\exp\left(\lambda_1 Z_1 + \lambda_2 Z_2\right)\right\} \\ &= K! \int_0^{\infty} \mathrm{d}\gamma_{1:K} p\left(\gamma_{1:K}\right) \exp\left(\lambda_1\gamma_{1:K}\right) \cdots \int_0^{\gamma_{m-1:K}} \mathrm{d}\gamma_{m:K} p\left(\gamma_{m:K}\right) \exp\left(\lambda_1\gamma_{m:K}\right) \\ &\times \int_0^{\gamma_{m:K}} \mathrm{d}\gamma_{m+1:K} p\left(\gamma_{m+1:K}\right) \exp\left(\lambda_2\gamma_{m+1:K}\right) \cdots \int_0^{\gamma_{K-1:K}} \mathrm{d}\gamma_{K:K} p\left(\gamma_{K:K}\right) \exp\left(\lambda_2\gamma_{K:K}\right). \end{aligned} \tag{3.75}$$

After applying (3.69), the MGF can be rewritten into the following form.

$$MGF_{Z_1,Z_2}(\lambda_1,\lambda_2) = K!\int_0^{\infty} \mathrm{d}\gamma_{1:K}\, p(\gamma_{1:K}) \exp(\lambda_1\gamma_{1:K}) \times \cdots \int_0^{\gamma_{m-1:K}} \mathrm{d}\gamma_{m:K}\, p(\gamma_{m:K}) \exp(\lambda_1\gamma_{m:K}) \frac{1}{(K-m)!} [c(\gamma_{m:K},\lambda_2)]^{(K-m)}. \tag{3.76}$$

Changing the order of integration based on the principle of (3.61), we can rewrite (3.76) as

$$MGF_{Z_1,Z_2}(\lambda_1,\lambda_2) = \frac{K!}{(K-m)!}\int_0^{\infty} \mathrm{d}\gamma_{m:K}\, p(\gamma_{m:K}) \exp(\lambda_1\gamma_{m:K}) \times [c(\gamma_{m:K},\lambda_2)]^{(K-m)} \int_{\gamma_{m:K}}^{\infty} \mathrm{d}\gamma_{m-1:K}\, p(\gamma_{m-1:K}) \exp(\lambda_1\gamma_{m-1:K}) \times \cdots \int_{\gamma_{2:K}}^{\infty} \mathrm{d}\gamma_{1:K}\, p(\gamma_{1:K}) \exp(\lambda_1\gamma_{1:K}). \tag{3.77}$$

Finally, applying (3.71), we can obtain the second-order MGF of Z_1 and Z_2 as

$$MGF_{Z_1,Z_2}(\lambda_1,\lambda_2) = \frac{K!}{(K-m)!\,(m-1)!} \int_0^{\infty} \mathrm{d}\gamma_{m:K}\, p(\gamma_{m:K}) \exp(\lambda_1\gamma_{m:K}) [c(\gamma_{m:K},\lambda_2)]^{(K-m)} [e(\gamma_{m:K},\lambda_1)]^{(m-1)}. \tag{3.78}$$

The desired two-dimensional joint PDF of $Z_1 = \sum_{n=1}^{m} \gamma_{n:K}$ and $Z_2 = \sum_{n=m+1}^{K} \gamma_{n:K}$ can be obtained after proper inverse Laplace transform.

□

For the exponential random variable special case, with the help of the inverse Laplace transform pair [16]

$$\mathcal{L}_s^{-1}\left\{\left(\frac{1}{s+a}\right)^n\right\} = \frac{1}{(n-1)!}t^{n-1}e^{-at}, \quad t \geq 0, n = 1,2,3,\ldots, \tag{3.79}$$

and the Laplace transform property [16]

$$\mathcal{L}_s^{-1}\left\{e^{-as}F(s)\right\} = f(t-a)\,U(t-a), \quad a > 0, \tag{3.80}$$

we can obtain the following compact expression for the joint PDF of Z_1 and Z_2, as

$$p_{Z_1,Z_2}(z_1,z_2) = \begin{cases} \frac{K!}{(K-m)!(K-m-1)!(m-1)!(m-2)!\bar{\gamma}^K}\exp\left(-\frac{z_1+z_2}{\bar{\gamma}}\right) \\ \times\int_0^\infty \mathrm{d}\gamma_{m:K}\Bigg[\left[z_1-m\gamma_{m:K}\right]^{m-2}U\left(z_1-m\gamma_{m:K}\right) \\ \times\sum_{j=0}^{K-m}(-1)^j\binom{K-m}{j}\left[z_2-j\gamma_{m:K}\right]^{K-m-1}U\left(z_2-j\gamma_{m:K}\right)\Bigg], & m\geq 2; \\ \frac{K!}{(K-1)!(K-2)!\bar{\gamma}^K}\exp\left(-\frac{z_1+z_2}{\bar{\gamma}}\right) \\ \times\sum_{j=0}^{K-1}(-1)^j\binom{K-1}{j}\left[z_2-jz_1\right]^{K-2}U\left(z_2-jz_1\right), & m=1. \end{cases} \quad (3.81)$$

We now consider the joint PDF of $\gamma_{m:K}$ and $\sum_{\substack{n=1\\n\neq m}}^{K_s}\gamma_{n:K}$, which involves the K_s largest ordered random variables among a total K ones. Note also that depending on the value of m, the ordered random variables involved in the summation may be discontinuous. In these cases, we may need to first consider the joint PDF of some new partial sums. The results are summarized in the following theorem.

Theorem 3.5. *The joint PDF of $\gamma_{m:K}$ and $\sum_{\substack{n=1\\n\neq m}}^{K_s}\gamma_{n:K}$ can be obtained as*

$$p_{\gamma_{m:K},\sum_{\substack{n=1\\n\neq m}}^{K_s}\gamma_{n:K}}(x,y) = \begin{cases} \int_{\binom{K_s-2}{K_s-1}y}^{(K_s-2)x} p_{\gamma_{1:K},\sum_{n=2}^{K_s-1}\gamma_{n:K},\gamma_{K_s:K}}(x,z_2,y-z_2)\,\mathrm{d}z_2, & m=1, \\ \int_0^x\int_{(m-1)x}^{y-(K_s-m)z_4} p_{\sum_{n=1}^{m-1}\gamma_{n:K},\gamma_{m:K},\sum_{n=m+1}^{K_s-1}\gamma_{n:K},\gamma_{K_s:K}}(z_1,x,y-z_1-z_4,z_4)\,\mathrm{d}z_1\mathrm{d}z_4, & 1<m<K_s-1, \\ \int_{(K_s-2)x}^{y} p_{\sum_{n=1}^{K_s-2}\gamma_{n:K},\gamma_{K_s-1:K},\gamma_{K_s:K}}(z_1,x,y-z_1)\,\mathrm{d}z_1, & m=K_s-1, \\ p_{\gamma_{K_s:K},\sum_{n=1}^{K_s-1}\gamma_{n:K}}(x,y), & m=K_s, \end{cases} \quad (3.82)$$

where the joint PDFs involved are given by, for $m=1$,

$$p_{\gamma_{1:K},\sum_{n=2}^{K_s-1}\gamma_{n:K},\gamma_{K_s:K}}(z_1,z_2,z_3) = \frac{K!}{(K_s-2)!}p(z_1)\,p(z_3)\left[c(z_3)\right]^{(K-K_s)}U(z_1-z_3)\,\mathcal{L}_{S_2}^{-1}\left\{\left[\mu(z_3,z_1,-S_2)\right]^{(K_s-2)}\right\},$$
$$z_3<z_1,\ (K_s-2)z_3<z_2<(K_s-2)z_1, \quad (3.83)$$

for $1 < m < K_s - 1$,

$$
\begin{aligned}
&p_{\sum_{n=1}^{m-1}\gamma_{n:K},\gamma_{m:K},\sum_{n=m+1}^{K_s-1}\gamma_{n:K},\gamma_{K_s:K}}(z_1,z_2,z_3,z_4)\\
&=\frac{K!}{(K_s-m-1)!\,(m-1)!}p(z_2)\,p(z_4)\,[c(z_4)]^{(K-K_s)}\,U(z_2-z_4)\\
&\times\mathcal{L}_{S_1}^{-1}\left\{[e(z_2,-S_1)]^{(m-1)}\right\}\mathcal{L}_{S_3}^{-1}\left\{[\mu(z_4,z_2,-S_3)]^{(K_s-m-1)}\right\},\\
&z_4<z_2,\ (m-1)z_2<z_1,\ (K_s-m-1)\,z_4<z_3<(K_s-m-1)\,z_2, \qquad (3.84)
\end{aligned}
$$

for $m = K_s - 1$,

$$
\begin{aligned}
&p_{\sum_{n=1}^{K_s-2}\gamma_{n:K},\gamma_{K_s-1:K},\gamma_{K_s:K}}(z_1,z_2,z_3)\\
&=\frac{K!}{(K_s-2)!}p(z_2)\,p(z_3)\,[c(z_3)]^{(K-K_s)}\,U(z_2-z_3)\,\mathcal{L}_{S_1}^{-1}\left\{[e(z_2,-S_1)]^{(K_s-2)}\right\},\\
&z_3<z_2,\ z_1>(K_s-2)\,z_2, \qquad (3.85)
\end{aligned}
$$

for $m = K_s$,

$$
\begin{aligned}
&p_{\gamma_{K_s:K},\sum_{n=1}^{K_s-1}\gamma_{n:K}}(z_1,z_2)\\
&=\frac{K!}{(K_s-1)!}p(z_1)\,[c(z_1)]^{(K-K_s)}\,\mathcal{L}_{S_2}^{-1}\left\{[e(z_1,-S_2)]^{(K_s-1)}\right\},\\
&z_2\geq(K_s-1)\,z_1, \qquad (3.86)
\end{aligned}
$$

where $U(\cdot)$ *is the unit step function.*

Proof. The proof is presented in the Appendix of this chapter. □

Note that (3.82) involves only finite integrations of higher-dimensional joint PDFs, for which the closed-form expression can usually be obtained. For example, for the exponential random variable special case, the joint PDFs involved in (3.82) can be shown to be given by, for $m = 1$,

$$
\begin{aligned}
&p_{\gamma_{1:K},\sum_{n=2}^{K_s-1}\gamma_{n:K},\gamma_{K_s:K}}(z_1,z_2,z_3) \qquad (3.87)\\
&=\frac{K!}{(K-K_s)!\,(K_s-2)!\,(K_s-3)!\bar{\gamma}^{K_s}}\exp\left(-\frac{z_1+z_2+z_3}{\bar{\gamma}}\right)\\
&\times\left[1-\exp\left(-\frac{z_3}{\bar{\gamma}}\right)\right]^{K-K_s}U(z_1-z_3)\\
&\times\sum_{j=0}^{K_s-2}\left[(-1)^j\binom{K_s-2}{j}[z_2-(K_s-2-j)\,z_3-jz_1]^{K_s-3}\right.\\
&\left.\times U(z_2-(K_s-2-j)\,z_3-jz_1)\right], \qquad (3.88)
\end{aligned}
$$

for $1 < m < K_s - 1$,

$$
\begin{aligned}
&p_{\sum_{n=1}^{m-1}\gamma_{n:K},\gamma_{m:K},\sum_{n=m+1}^{K_s-1}\gamma_{n:K},\gamma_{K_s:K}}(z_1,z_2,z_3,z_4)\\
&=\frac{K!}{(K-K_s)!\,(K_s-m-1)!\,(K_s-m-2)!\,(m-1)!\,(m-2)!\bar{\gamma}^{K_s}}\\
&\times\exp\left(-\frac{z_1+z_2+z_3+z_4}{\bar{\gamma}}\right)\left[1-\exp\left(-\frac{z_4}{\bar{\gamma}}\right)\right]^{K-K_s}[z_1-(m-1)\,z_2]^{m-2}\\
&\times\sum_{j=0}^{K_s-m-1}\left[(-1)^j\binom{K_s-m-1}{j}[z_3-(K_s-m-1-j)\,z_4-jz_2]^{K_s-m-2}\right.\\
&\left.\times U(z_2-z_4)\,U(z_1-(m-1)\,z_2)\,U(z_3-(K_s-m-1-j)\,z_4-jz_2)\right]. \quad (3.89)
\end{aligned}
$$

for $m = K_s - 1$,

$$
\begin{aligned}
&p_{\sum_{n=1}^{K_s-2}\gamma_{n:K},\gamma_{K_s-1:K},\gamma_{K_s:K}}(z_1,z_2,z_3)\\
&=\frac{K!}{(K-K_s)!\,(K_s-2)!\,(K_s-3)!\bar{\gamma}^{K_s}}\exp\left(-\frac{z_1+z_2+z_3}{\bar{\gamma}}\right)\\
&\times\left[1-\exp\left(-\frac{z_3}{\bar{\gamma}}\right)\right]^{K-K_s}[z_1-(K_s-2)\,z_2]^{K_s-3}\,U(z_2-z_3)\\
&\times U(z_1-(K_s-2)\,z_2). \quad (3.90)
\end{aligned}
$$

for $m = K_s$,

$$
\begin{aligned}
&p_{\gamma_{K_s:K},\sum_{n=1}^{K_s-1}\gamma_{n:K}}(z_1,z_2)\\
&=\frac{K!}{(K-K_s)!\,(K_s-1)!\,(K_s-2)!\bar{\gamma}^{K_s}}\exp\left(-\frac{z_1+z_2}{\bar{\gamma}}\right)\\
&\times\left[1-\exp\left(-\frac{z_1}{\bar{\gamma}}\right)\right]^{K-K_s}[z_2-(K_s-1)\,z_1]^{K_s-2}\,U(z_2-(K_s-1)\,z_1). \quad (3.91)
\end{aligned}
$$

Therefore, the desired joint PDF can be evaluated easily numerically with the help of integral tables [16, 17] or using standard mathematical packages such as Mathematica or Matlab, etc.

3.6 Limiting distributions of extreme order statistics

The limiting distribution of the largest order statistics from L i.i.d. samples can be useful in the asymptotic analysis of multiuser wireless systems. It has

been established that the limiting distribution of $\gamma_{1:L}$, i.e. $\lim_{L\to+\infty} F_{\gamma_{1:L}}(x)$, if it exists, must be one of the following three types [1, 18]:

- Fréchet distribution with CDF

$$F^{(1)}(x) = \exp(-x^{-\alpha}), x > 0, \alpha > 0; \tag{3.92}$$

- Weibull distribution with CDF

$$F^{(2)}(x) = \begin{cases} \exp[-(-x)^{\alpha}], & x \le 0, \alpha > 0, \\ 1, & x > 0; \end{cases} \tag{3.93}$$

- Gumbel distribution with CDF

$$F^{(3)}(x) = \exp(-e^{-x}). \tag{3.94}$$

Specifically, there exist constants $a_L > 0$ and b_L such that

$$\lim_{L\to+\infty} P_{\gamma_{1:L}}(a_L x + b_L) = F^{(i)}(x), \ i = 1, 2, \text{ or } 3. \tag{3.95}$$

Note that these three distributions are members of the family of generalized extreme-value (GEV) distribution with CDF given by

$$F^{GEV}(x) = \exp\left\{-\left[1 + \xi\left(\frac{x-\mu}{\sigma}\right)\right]^{-1/\xi}\right\}, \tag{3.96}$$

where ξ, μ, and σ are constant parameters. Specifically, when $\xi = 0$, the CDF of the GEV distribution simplifies to

$$F^{GEV}(x) = \exp\left(-e^{-\frac{x-\mu}{\sigma}}\right), \tag{3.97}$$

which is of the Gumbel type. Furthermore, setting $\xi > 0$ and $\xi < 0$ will lead to Fréchet and Weibull types, respectively.

The type of the limiting distribution depends on the properties of the distribution functions of the original unordered random variables. It can be shown that if the distribution functions of γ_i satisfy

$$\lim_{x\to+\infty} \frac{x p_{\gamma}(x)}{1 - F_{\gamma}(x)} = \alpha, \tag{3.98}$$

for some constant $\alpha > 0$, then the limiting distribution of $\gamma_{1:L}$ will be of the Fréchet type. This indicates that for some constant $a_L > 0$, we have

$$\lim_{L\to+\infty} F_{\gamma_{1:L}}(a_L x) = F^{(1)}(x), \tag{3.99}$$

where a_L can be computed by solving $1 - P_\gamma(a_L) = 1/L$ based on the characteristic of extremes. If, instead, the following condition is satisfied by the distribution of γ_i

$$\lim_{x \to +\infty} \frac{1 - F_\gamma(x)}{p_\gamma(x)} = \alpha, \tag{3.100}$$

where the constant $\alpha > 0$, then the limiting distribution of $\gamma_{1:L}$ will be of the Gumbel type. More specifically, we have

$$\lim_{L \to +\infty} F_{\gamma_{1:L}}(x) = F^{(3)}\left(\frac{x - b_L}{a_L}\right) = \exp\left(-e^{-\frac{x-b_L}{a_L}}\right), \tag{3.101}$$

where the constant b_L and a_L can be computed by sequentially solving equations $1 - F_\gamma(b_L) = 1/L$ and $1 - F_\gamma(a_L + b_L) = 1/(eL)$.

Example 3.4: When γ_is follow i.i.d. exponential distribution with PDF $p_\gamma(x) = e^{-x}$, we can easily verify that the condition in (3.100) holds and, as such, the limiting distribution of $\gamma_{1:L}$ is of the Gumbel type. Applying the results in (3.101), we can show that $a_L = 1$ and $b_L = \log L$. Finally, we have

$$\lim_{L \to +\infty} F_{\gamma_{1:L} - \log L}(x) = \lim_{L \to +\infty} \Pr[\gamma_{1:L} < \log L + x] = \exp\left(-e^{-x}\right). \tag{3.102}$$

3.7 Summary

In this chapter, the relevant order statistics results were presented in a systematic fashion. Starting from the basic distribution functions of order random variables, we derived the distribution functions of the partial sum and the joint distribution function of several partial sums, first using the successive conditioning approach then with the MGF-based analytical framework. The results were applied to the exponential random variable special case for illustration whenever feasible.

3.8 Bibliography notes

For more thorough coverage of order statistics, the reader may refer to the book by David [1]. Section 9.11.2 of [19] addresses the distribution function of the sum of the largest order statistics for non-identically distributed original random variables. Ref. [12] presents more illustrative examples for the MGF-based

analytical framework for the joint distribution function of several partial sums.

Appendix to chapter 3. Order statistics

Proof of the simplifying relationship involving I_m

In this subsection, we prove the following relationship by induction.

$$I_m = \frac{1}{(K-m+1)!}\left[c\left(\gamma_{m-1:K},\lambda\right)\right]^{(K-m+1)}. \tag{3.103}$$

Let us first consider the case $m = K$. Noting that $p\left(\gamma_{K:K}\right)\exp\left(\lambda\gamma_{K:K}\right) = c'\left(\gamma_{K:K},\lambda\right)$, it is easy to show that

$$\begin{aligned}\int_0^{\gamma_{K-1:K}} \mathrm{d}\gamma_{K:K}\, p\left(\gamma_{K:K}\right)\exp\left(\lambda\gamma_{K:K}\right) &= \int_0^{\gamma_{K-1:K}} \mathrm{d}\gamma_{K:K}\, c'\left(\gamma_{K:K},\lambda\right) \\ &= c\left(\gamma_{K:K},\lambda\right)\Big|_0^{\gamma_{K-1:K}} \\ &= c\left(\gamma_{K-1:K},\lambda\right).\end{aligned} \tag{3.104}$$

Now let us assume the relationship in (3.103) holds for $K \geq m \geq k$, and consider the case $m = k-1$. Starting from the definition of I_m, we have

$$\begin{aligned}I_{k-1} = &\int_0^{\gamma_{k-2:K}} \mathrm{d}\gamma_{k-1:K}\, p\left(\gamma_{k-1:K}\right)\exp\left(\lambda\gamma_{k-1:K}\right) \int_0^{\gamma_{k-1:K}} \mathrm{d}\gamma_{k:K}\, p\left(\gamma_{k:K}\right)\exp\left(\lambda\gamma_{k:K}\right) \\ &\cdots \int_0^{\gamma_{K-1:K}} \mathrm{d}\gamma_{K:K}\, p\left(\gamma_{K:K}\right)\exp\left(\lambda\gamma_{K:K}\right) \\ = &\int_0^{\gamma_{k-2:K}} \mathrm{d}\gamma_{k-1:K}\, c'\left(\gamma_{k-1:K},\lambda\right)\frac{1}{(K-k+1)!}\left[c\left(\gamma_{k-1:K},\lambda\right)\right]^{(K-k+1)}.\end{aligned} \tag{3.105}$$

Applying integration by part, we have

$$\begin{aligned}I_{k-1} = &\frac{1}{(K-k+1)!}\left[c\left(\gamma_{k-1:K},\lambda\right)\right]^{(K-k+2)}\Big|_0^{\gamma_{k-2:K}} \\ &- \int_0^{\gamma_{k-2:K}} \mathrm{d}\gamma_{k-1:K}\frac{1}{(K-k)!}\left[c\left(\gamma_{k-1:K},\lambda\right)\right]^{(K-k+1)} c'\left(\gamma_{k-1:K},\lambda\right).\end{aligned} \tag{3.106}$$

It follows after some rearrangement of terms and manipulation that

$$\int_0^{\gamma_{k-2:K}} \mathrm{d}\gamma_{k-1:K} \left[c\left(\gamma_{k-1:K}, \lambda\right)\right]^{(K-k+1)} c'\left(\gamma_{k-1:K}, \lambda\right) \tag{3.107}$$
$$= \frac{1}{(K-k+2)} \left[c\left(\gamma_{k-2:K}, \lambda\right)\right]^{(K-k+2)}$$

Substituting (3.107) into (3.106), we can finally show

$$\begin{aligned} I_{k-1} &= \frac{1}{(K-k+1)!} \left[c\left(\gamma_{k-2:K}, \lambda\right)\right]^{(K-k+2)} \\ &\quad - \frac{1}{(K-k)!} \frac{1}{(K-k+2)} \left[c\left(\gamma_{k-2:K}, \lambda\right)\right]^{(K-k+2)} \\ &= \frac{1}{(K-k+2)!} \left[c\left(\gamma_{k-2:K}, \lambda\right)\right]^{(K-k+2)}. \end{aligned} \tag{3.108}$$

We can now conclude that the relationship in (3.103) holds for m.

The simplifying relationship involving I'_m and $I''_{a,b}$, given in (3.71) and (3.73), respectively, can be proved similarly.

Derivation of the joint PDF of $\gamma_{m:K}$ and $\sum_{\substack{n=1 \\ n \neq m}}^{K_s} \gamma_{n:K}$ among K-ordered RVs

In this Appendix, we derive the joint PDF of $\gamma_{m:K}$ and $\sum_{\substack{n=1 \\ n \neq m}}^{K_s} \gamma_{n:K}$ among K-ordered RVs by considering four cases: (i) $m = 1$, (ii) $1 < m < K_s - 1$, (iii) $m = K_s - 1$, and (iv) $m = K_s$ separately.

(i) $m = 1$

In this case, we need to consider the random variable $\gamma_{K_s:K}$ separately. As such, we start by calculating the three-dimensional joint MGF of $Z_1 = \gamma_{1:K}$, $Z_2 = \sum_{n=2}^{K_s-1} \gamma_{n:K}$, and $Z_3 = \gamma_{K_s:K}$ as

$$\begin{aligned} &MGF\left(\lambda_1, \lambda_2, \lambda_3\right) = E\left\{\exp\left(\lambda_1 Z_1 + \lambda_2 Z_2 + \lambda_3 Z_3\right)\right\} \\ &= K! \int_0^{\infty} \mathrm{d}\gamma_{1:K} p\left(\gamma_{1:K}\right) \exp\left(\lambda_1 \gamma_{1:K}\right) \int_0^{\gamma_{1:K}} \mathrm{d}\gamma_{2:K} p\left(\gamma_{2:K}\right) \exp\left(\lambda_2 \gamma_{2:K}\right) \\ &\times \cdots \int_0^{\gamma_{K_s-2:K}} \mathrm{d}\gamma_{K_s-1:K} p\left(\gamma_{K_s-1:K}\right) \exp\left(\lambda_2 \gamma_{K_s-1:K}\right) \\ &\times \int_0^{\gamma_{K_s-1:K}} \mathrm{d}\gamma_{K_s:K} p\left(\gamma_{K_s:K}\right) \exp\left(\lambda_3 \gamma_{K_s:K}\right) \left[c\left(\gamma_{K_s:K}\right)\right]^{(K-K_s)}. \end{aligned} \tag{3.109}$$

With the help of (3.61) and (3.73), we can simplify the three-dimensional MGF to

$$MGF(\lambda_1,\lambda_2,\lambda_3) = K!\int_0^\infty \mathrm{d}\gamma_{K_s:K}\, p(\gamma_{K_s:K}) \exp(\lambda_3\gamma_{K_s:K}) [c(\gamma_{K_s:K})]^{(K-K_s)} \times \int_{\gamma_{K_s:K}}^\infty \mathrm{d}\gamma_{1:K}\, p(\gamma_{1:K}) \exp(\lambda_1\gamma_{1:K}) \frac{1}{(K_s-2)!} [\mu(\gamma_{K_s:K},\gamma_{1:K},\lambda_2)]^{(K_s-2)}. \tag{3.110}$$

The joint PDF of $Z_1 = \gamma_{1:K}$, $Z_2 = \sum_{n=2}^{K_s-1} \gamma_{n:K}$ and $Z_3 = \gamma_{K_s:K}$ can then be calculated after applying proper inverse Laplace transform to (3.110) as

$$\begin{aligned} & p_{\gamma_{1:K},\sum_{n=2}^{K_s-1}\gamma_{n:K},\gamma_{K_s:K}}(z_1,z_2,z_3) = \mathcal{L}^{-1}_{S_1,S_2,S_3}\{MGF_Z(-S_1,-S_2,-S_3)\} \\ &= \frac{K!}{(K_s-2)!}\int_0^\infty \mathrm{d}\gamma_{K_s:K}\, p(\gamma_{K_s:K})\, \mathcal{L}^{-1}_{S_3}\{\exp(-S_3\gamma_{K_s:K})\}[c(\gamma_{K_s:K})]^{(K-K_s)} \\ &\quad \times \int_{\gamma_{K_s:K}}^\infty \mathrm{d}\gamma_{1:K}\, p(\gamma_{1:K})\, \mathcal{L}^{-1}_{S_1}\{\exp(-S_1\gamma_{1:K})\} \\ &\quad \times \mathcal{L}^{-1}_{S_2}\left\{[\mu(\gamma_{K_s:K},\gamma_{1:K},-S_2)]^{(K_s-2)}\right\} \\ &= \frac{K!}{(K_s-2)!} p(z_1)\, p(z_3)\, [c(z_3)]^{(K-K_s)}\, U(z_1-z_3) \\ &\quad \times \mathcal{L}^{-1}_{S_2}\left\{[\mu(z_3,z_1,-S_2)]^{(K_s-2)}\right\}. \end{aligned} \tag{3.111}$$

Finally, the desired two-dimensional joint PDF of $\gamma_{m:K}$ and $\sum_{\substack{n=1\\n\neq m}}^{K_s} \gamma_{n:K}$ can be calculated as

$$p_{\gamma_{m:K},\sum_{\substack{n=1\\n\neq m}}^{K_s}\gamma_{n:K}}(x,y) = \int_{\left(\frac{K_s-2}{K_s-1}\right)y}^{(K_s-2)x} p_{\gamma_{1:K},\sum_{n=2}^{K_s-1}\gamma_{n:K},\gamma_{K_s:K}}(x,z_2,y-z_2)\,\mathrm{d}z_2. \tag{3.112}$$

(ii) $1 < m < K_s - 1$

In this case, we divide the partial sum $\sum_{\substack{n=1\\n\neq m}}^{K_s} \gamma_{n:K}$ into three parts by considering $\gamma_{K_s:K}$ and discontinuous ordered random variables separately. In

particular, we first calculate the four-dimensional MGF of $Z_1 = \sum_{n=1}^{m-1} \gamma_{n:K}$, $Z_2 = \gamma_{m:K}$, $Z_3 = \sum_{n=m+1}^{K_s-1} \gamma_{n:K}$ and $Z_4 = \gamma_{K_s:K}$ as

$$\begin{aligned}
MGF(\lambda_1,\lambda_2,\lambda_3,\lambda_4) &= K! \int_0^{\infty} \mathrm{d}\gamma_{1:K}\, p(\gamma_{1:K}) \exp(\lambda_1 \gamma_{1:K}) \\
&\cdots \int_0^{\gamma_{m-2:K}} \mathrm{d}\gamma_{m-1:K}\, p(\gamma_{m-1:K}) \exp(\lambda_1 \gamma_{m-1:K}) \\
&\times \int_0^{\gamma_{m-1:K}} \mathrm{d}\gamma_{m:K}\, p(\gamma_{m:K}) \exp(\lambda_2 \gamma_{m:K}) \\
&\times \int_0^{\gamma_{m:K}} \mathrm{d}\gamma_{m+1:K}\, p(\gamma_{m+1:K}) \exp(\lambda_3 \gamma_{m+1:K}) \\
&\cdots \int_0^{\gamma_{K_s-2:K}} \mathrm{d}\gamma_{K_s-1:K}\, p(\gamma_{K_s-1:K}) \exp(\lambda_3 \gamma_{K_s-1:K}) \\
&\times \int_0^{\gamma_{K_s-1:K}} \mathrm{d}\gamma_{K_s:K}\, p(\gamma_{K_s:K}) \exp(\lambda_4 \gamma_{K_s:K}) \left[c(\gamma_{K_s:K})\right]^{(K-K_s)}.
\end{aligned} \tag{3.113}$$

With the help of (3.61), (3.103), (3.71), and (3.73), we can arrive at the follow compact expression for the MGF.

$$\begin{aligned}
MGF(\lambda_1,\lambda_2,\lambda_3,\lambda_4) &= \frac{K!}{(K_s-m-1)!\,(m-1)!} \\
&\times \int_0^{\infty} \mathrm{d}\gamma_{K_s:K}\, p(\gamma_{K_s:K}) \exp(\lambda_4 \gamma_{K_s:K}) \left[c(\gamma_{K_s:K})\right]^{(K-K_s)} \\
&\times \int_{\gamma_{K_s:K}}^{\infty} \mathrm{d}\gamma_{m:K}\, p(\gamma_{m:K}) \exp(\lambda_2 \gamma_{m:K}) \left[e(\gamma_{m:K},\lambda_1)\right]^{(m-1)} \\
&\times \left[\mu(\gamma_{K_s:K},\gamma_{m:K},\lambda_3)\right]^{(K_s-m-1)}.
\end{aligned} \tag{3.114}$$

Similar to the previous case, we can calculate the four-dimensional joint PDF of $Z_1 = \sum_{n=1}^{m-1} \gamma_{n:K}$, $Z_2 = \gamma_{m:K}$, $Z_3 = \sum_{n=m+1}^{K_s-1} \gamma_{n:K}$ and $Z_4 = \gamma_{K_s:K}$ by applying

an inverse Laplace transform, yielding

$$
\begin{aligned}
&p_{\sum_{n=1}^{m-1}\gamma_{n:K},\gamma_{m:K},\sum_{n=m+1}^{K_s-1}\gamma_{n:K},\gamma_{K_s:K}}(z_1,z_2,z_3,z_4) = \\
&\frac{K!}{(K_s-m-1)!\,(m-1)!}\int_0^\infty \mathrm{d}\gamma_{K_s:K}\,p\left(\gamma_{K_s:K}\right)\mathcal{L}_{S_4}^{-1}\left\{\exp\left(-S_4\gamma_{K_s:K}\right)\right\}) \\
&\times\left[c\left(\gamma_{K_s:K}\right)\right]^{(K-K_s)}\int_{\gamma_{K_s:K}}^\infty \mathrm{d}\gamma_{m:K}\left[p\left(\gamma_{m:K}\right)\mathcal{L}_{S_2}^{-1}\left\{\exp\left(-S_2\gamma_{m:K}\right)\right\}\right. \\
&\left.\times\mathcal{L}_{S_1}^{-1}\left\{\left[e\left(\gamma_{m:K},-S_1\right)\right]^{(m-1)}\right\}\mathcal{L}_{S_3}^{-1}\left\{\left[\mu\left(\gamma_{K_s:K},\gamma_{m:K},-S_3\right)\right]^{(K_s-m-1)}\right\}\right] \\
&= \frac{F}{(K_s-m-1)!\,(m-1)!}p\left(z_2\right)p\left(z_4\right)\left[c\left(z_4\right)\right]^{(K-K_s)}U\left(z_2-z_4\right) \\
&\times\mathcal{L}_{S_1}^{-1}\left\{\left[e\left(z_2,-S_1\right)\right]^{(m-1)}\right\}\mathcal{L}_{S_3}^{-1}\left\{\left[\mu\left(z_4,z_2,-S_3\right)\right]^{(K_s-m-1)}\right\}. \qquad (3.115)
\end{aligned}
$$

Finally, the desired two-dimensional joint PDF of $\gamma_{m:K}$ and $\sum_{\substack{n=1\\n\neq m}}^{K_s}\gamma_{n:K}$ can be calculated as

$$
\begin{aligned}
&p_{\gamma_{m:K},\sum_{\substack{n=1\\n\neq m}}^{K_s}\gamma_{n:K}}(x,y) \qquad (3.116)\\
&= \int_0^x\int_{(m-1)x}^{y-(K_s-m)z_4} p_{\sum_{n=1}^{m-1}\gamma_{n:K},\gamma_{m:K},\sum_{n=m+1}^{K_s-1}\gamma_{n:K},\gamma_{K_s:K}}(z_1,x,y-z_4,z_4)\,\mathrm{d}z_1\mathrm{d}z_4.
\end{aligned}
$$

(iii) $m = K_s - 1$

In this case, we can start with the three-dimensional MGF of $Z_1 = \sum_{n=1}^{K_s-2}\gamma_{n:K}$, $Z_2 = \gamma_{K_s-1:K}$, and $Z_3 = \gamma_{K_s:K}$, which is given by

$$
\begin{aligned}
&MGF\left(\lambda_1,\lambda_2,\lambda_3\right) = K!\int_0^\infty \mathrm{d}\gamma_{1:K}\,p\left(\gamma_{1:K}\right)\exp\left(\lambda_1\gamma_{1:K}\right) \\
&\times\int_0^{\gamma_{K_s-2:K}} \mathrm{d}\gamma_{K_s-1:K}\,p\left(\gamma_{K_s-1:K}\right)\exp\left(\lambda_2\gamma_{K_s-1:K}\right) \\
&\times\int_0^{\gamma_{K_s-1:K}} \mathrm{d}\gamma_{K_s:K}\,p\left(\gamma_{K_s:K}\right)\exp\left(\lambda_3\gamma_{K_s:K}\right)\left[c\left(\gamma_{K_s:K}\right)\right]^{(K-K_s)}. \qquad (3.117)
\end{aligned}
$$

The three-dimensional MGF can be simplified, with the help of (3.61) and (3.71), to

$$MGF\left(\lambda_1,\lambda_2,\lambda_3\right)=\frac{K!}{(K_s-2)!} \tag{3.118}$$
$$\times\int_0^\infty \mathrm{d}\gamma_{K_s:K}\,p\left(\gamma_{K_s:K}\right)\exp\left(\lambda_3\gamma_{K_s:K}\right)\left[c\left(\gamma_{K_s:K}\right)\right]^{(K-K_s)}$$
$$\times\int_{\gamma_{K_s:K}}^\infty \mathrm{d}\gamma_{K_s-1:K}\,p\left(\gamma_{K_s-1:K}\right)\exp\left(\lambda_2\gamma_{K_s-1:K}\right)\left[e\left(\gamma_{K_s-1:K},\lambda_1\right)\right]^{(K_s-2)}.$$

The corresponding three-dimensional joint PDF of $\sum_{n=1}^{K_s-2}\gamma_{n:K}$, $\gamma_{K_s-1:K}$ and $\gamma_{K_s:K}$ is then given by

$$p_{\sum_{n=1}^{K_s-2}\gamma_{n:K},\gamma_{K_s-1:K},\gamma_{K_s:K}}\left(z_1,z_2,z_3\right)=\frac{K!}{(K_s-2)!} \tag{3.119}$$
$$p\left(z_2\right)p\left(z_3\right)\left[c\left(z_3\right)\right]^{(K-K_s)}U\left(z_2-z_3\right)\mathcal{L}_{S_1}^{-1}\left\{\left[e\left(z_2,-S_1\right)\right]^{(K_s-2)}\right\}.$$

Finally, the desired two-dimensional joint PDF of $\gamma_{m:K}$ and $\sum_{\substack{n=1\\n\neq m}}^{K_s}\gamma_{n:K}$ can be obtained as

$$p_{\gamma_{m:K},\sum_{\substack{n=1\\n\neq m}}^{K_s}\gamma_{n:K}}\left(x,y\right)=\int_0^x p_{\sum_{n=1}^{K_s-2}\gamma_{n:K},\gamma_{K_s-1:K},\gamma_{K_s:K}}\left(y-z_3,x,z_3\right)\mathrm{d}z_3. \tag{3.120}$$

(iv) $m=K_s$

For this case, we can consider directly the two-dimensional MGF of $\gamma_{m:K}$ and $\sum_{\substack{n=1\\n\neq m}}^{K_s}\gamma_{n:K}$, which is given by

$$MGF\left(\lambda_1,\lambda_2\right)=K!\int_0^\infty \mathrm{d}\gamma_{1:K}\,p\left(\gamma_{1:K}\right)\exp\left(\lambda_2\gamma_{1:K}\right)$$
$$\cdots\int_0^{\gamma_{K_s-2:K}} \mathrm{d}\gamma_{K_s-1:K}\,p\left(\gamma_{K_s-1:K}\right)\exp\left(\lambda_2\gamma_{K_s-1:K}\right)$$
$$\times\int_0^{\gamma_{K_s-1:K}} \mathrm{d}\gamma_{K_s:K}\,p\left(\gamma_{K_s:K}\right)\exp\left(\lambda_1\gamma_{K_s:K}\right)\left[c\left(\gamma_{K_s:K}\right)\right]^{(K-K_s)}. \tag{3.121}$$

With the help of (3.61) and (3.71), we can simplify the MGF to

$$MGF\left(\lambda_1,\lambda_2\right)=\frac{K!}{(K_s-1)!}\int_0^\infty d\gamma_{K_s:K}\,p\left(\gamma_{K_s:K}\right)\exp\left(\lambda_1\gamma_{K_s:K}\right)\\ \times\left[c\left(\gamma_{K_s:K}\right)\right]^{(K-K_s)}\left[e\left(\gamma_{K_s:K},\lambda_2\right)\right]^{(K_s-1)}. \tag{3.122}$$

The desired two-dimensional joint PDF of $\gamma_{K_s:K}$ and $\sum_{n=1}^{K_s-1}\gamma_{n:K}$ can be obtained, by applying an inverse Laplace transform, as

$$p_{\gamma_{m:K},\sum\limits_{\substack{n=1\\n\neq m}}^{K_s}\gamma_{n:K}}(z_1,z_2)\\ =\frac{K!}{(K_s-1)!}p\left(z_1\right)\left[c\left(z_1\right)\right]^{(K-K_s)}\mathcal{L}_{S_2}^{-1}\left\{\left[e\left(z_1,-S_2\right)\right]^{(K_s-1)}\right\}. \tag{3.123}$$

References

[1] H. A. David, *Order Statistics.* New York, NY: John Wiley & Sons, Inc., 1981.

[2] N. Balakrishnan and C. R. Rao, *Handbook of Statistics 17: Order Statistics: Applications*, 2nd ed. Amsterdam: North-Holland Elsevier, 1998.

[3] Y.-C. Ko, H.-C. Yang, S.-S. Eom and M.-S. Alouini, "Adaptive modulation and diversity combining based on output-threshold MRC," *IEEE Trans. Wireless Commun.*, vol. 6, no. 10, pp. 3728–3737, October 2007.

[4] M.-S. Alouini and M. K. Simon, "An MGF-based performance analysis of generalized selective combining over Rayleigh fading channels," *IEEE Trans. Commun.*, vol. 48, no. 3, pp. 401–415, March 2000.

[5] Y. Ma and C. C. Chai, "Unified error probability analysis for generalized selection combining in Nakagami fading channels," *IEEE J. Select. Areas Commun.*, vol. 18, no. 11, pp. 2198–2210, November 2000.

[6] M. Z. Win and J. H. Winters, "Virtual branch analysis of symbol error probability for hybrid selection/maximal-ratio combining Rayleigh fading," *IEEE Trans. Commun.*, vol. 49, no. 11, pp. 1926–1934, 2001.

[7] A. Annamalai and C. Tellambura, "Analysis of hybrid selection/maximal-ratio diversity combiners with Gaussian errors," *IEEE Trans. Wireless Commun.*, vol. 1, no. 3, pp. 498–511, July 2002.

[8] Y. Roy, J.-Y. Chouinard and S. A. Mahmoud, "Selection diversity combining with multiple antennas for MM-wave indoor wireless channels," *IEEE J. Select. Areas Commun.*, vol. SAC-14, no. 4, pp. 674–682, May 1998.

[9] P. V. Sukhatme, "Tests of significance for samples of the population with two degrees of freedom," *Ann. Eugenics*, vol. 8, p. 5256, 1937.

[10] H.-C. Yang, "New results on ordered statistics and analysis of minimum-selection generalized selection combining (GSC)," *IEEE Trans. Wireless Commun.*, vol. 5, no. 7, pp. 1876–1885, 2006.

[11] S. Choi, M.-S. Alouini, K. A. Qaraqe and H.-C. Yang, "Finger replacement method for RAKE receivers in the soft handover region," *IEEE Trans. Wireless Commun.*, vol. TWC-7, no. 4, pp. 1152–1156, 2008.

[12] A. H. Nuttall, "An integral solution for the joint PDF of order statistics and residual sum," NUWC-NPT, Technical Report, October 2001.

[13] ——, "Joint probability density function of selected order statistics and the sum of the remaining random variables," NUWC-NPT, Technical Report, January 2002.

[14] A. H. Nuttall and P. M. Baggenstoss, "Joint distributions for two useful classes of statistics, with applications to classification and hypothesis testing," *IEEE Trans. Signal Processing*, submitted for publication. [Online]. Available: http://www.npt.nuwc.navy.mil/Csf/papers/order.pdf

[15] S. Nam, M.-S. Alouini and H.-C. Yang, "An MGF-based unified framework to determine the joint statistics of partial sums of ordered random variables," *IEEE Trans. on Inform. Theory*, vol. IT-56, no. 11, pp. 5655–5672, November 2010.

[16] M. Abramowitz and I. A. Stegun, *Handbook of Mathematical Functions*. New York, NY: Dover Publications, 1972.

[17] I. S. Gradshteyn and I. M. Ryzhik, *Table of Integrals, Series, and Products*, 6th ed. San Diego, CA: Academic Press, 2000.

[18] N. T. Uzgoren, "The asymptotic development of the distribution of the extreme values of a sample," in *Studies in Mathematics and Mechanics Presented to Richard von Mises*. New York, NY: Academic, 1954, pp. 346–353.

[19] M. K. Simon and M.-S. Alouini, *Digital Communications over Generalized Fading Channels*, 2nd ed. New York, NY: John Wiley & Sons, 2004.

4 Advanced diversity techniques

4.1 Introduction

Diversity combining can considerably improve the performance of wireless system operating over fading channels [1, 2]. In general, the performance gain increases as the number of diversity branches increases, although with a diminishing gain. These results have motivated the recent development of several wideband wireless systems, where a large number of diversity paths exist. Examples include wideband code division multiple access (WCDMA) systems [3], ultra wideband (UWB) systems [4], and millimeter (MM)-wave systems [5]. While huge diversity benefits can be explored in the resulting diversity-rich environment, it is critical to exploit those benefits efficiently [6]. In particular, MRC is well-known to be the optimal combining scheme in a noise-limited environment. However, applying MRC in such a diversity-rich environment will entail very high system complexity. Note that we need to implement a receiver chain for each resolvable diversity path. In addition, processing all the diversity paths will lead to very high processing power consumption.

In this chapter, we present several advanced combining schemes for diversity-rich environments. The general principle of these schemes is to select a proper subset of good diversity paths among those available and then combine them in an optimal MRC fashion. Specifically, these schemes will determine the path subset using the best-selection process or thresholding, or a combination of both. As expected intuitively, different schemes will lead to different performance versus complexity trade-offs. Based on accurate mathematical analysis, sometimes with the help of the order statistics results from the previous chapter, we are able to obtain the exact statistics of the combiner output SNR with these schemes, which are then utilized to quantify the trade-off study between performance and complexity between them. For analytical tractability and clarity, we adopt an independent flat-fading channel model for the available diversity paths.

4.2 Generalized selection combining (GSC)

GSC is one of the most widely studied low-complexity schemes for diversity-rich environments, which is also known as hybrid selection and maximum ratio

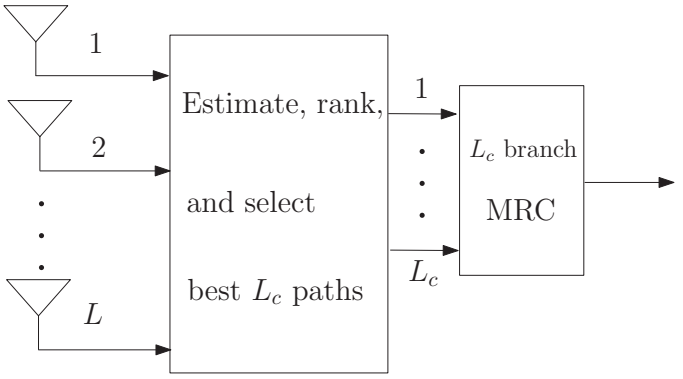

Figure 4.1 Structure of a GSC-based diversity combiner.

combining scheme (see for example [3–5,7–15]). The basic idea is to select a subset of the best paths and then combine them in the MRC fashion. The rationale is that applying MRC to the weak paths will bring little additional performance benefit, while entailing extra hardware complexity of additional RF chains. In addition, the channel estimation of weak paths can be unreliable, which further limits the benefit of applying MRC to them, as imperfect channel estimation will considerably degrade the performance of MRC [16, 17]. The structure of a GSC combiner is shown in Fig. 4.1, which consists of the concardination of a multi-branch selection combiner and a conventional MRC combiner. The immediate benefit with pre-selection is that only an L_c-branch MRC is needed with GSC.

The mode of operation of a GSC combiner can be summarized as follows: (i) Receiver first estimates the SNRs of all L available diversity paths, which may correspond to the resolved paths for UWB and WCDMA systems or the antenna branches in an MM-wave system; (ii) Receiver will then rank the SNRs and select the L_c strongest paths, i.e. those with the highest SNR; (iii) Receiver finally determines the MRC weights for those selected paths, which entails the full channel estimation (amplitude and phase) of the selected paths, and starts actual data reception. Note that unlike the conventional MRC combiner, where the receiver needs to estimate the complex channel gains for all diversity paths, the receiver with GSC only needs to estimate the complete channel states of those selected paths. The path selection process only requires the received signal power to be estimated.

4.2.1 Statistics of output SNR

To evaluate the performance of the GSC combiner, we need the statistics of the combined SNR γ_c, which is given by

$$\gamma_c = \sum_{i=1}^{L_c} \gamma_{i:L}, \tag{4.1}$$

where $\gamma_{i:L}$ is the ith largest one among total L SNRs. Based on the order statistics results in the previous chapter, we can obtain the closed-form expression of the MGF of the combined SNR with GSC for the i.i.d. Rayleigh fading scenario as

$$\mathcal{M}_{\gamma_c}(s) = (1 - s\overline{\gamma})^{-L_c} \prod_{l=L_c+1}^{L} \left(1 - \frac{s\overline{\gamma}L_c}{l}\right)^{-1}. \tag{4.2}$$

With the MGF of γ_c, we can directly apply the MGF-based approach to evaluate the average error rate performance. In particular, the average error rate of M-ary phase-shift-keying (M-PSK) signals is given by [18]

$$\overline{P}_s = \frac{1}{\pi} \int_0^{\frac{(M-1)\pi}{M}} \mathcal{M}_{\gamma_c}\left(-\frac{g_{\mathrm{PSK}}}{\sin^2\phi}\right) \mathrm{d}\phi, \tag{4.3}$$

where $g_{\mathrm{PSK}} = \sin^2(\pi/M)$. The PDF and CDF of γ_c with GSC can be derived routinely after taking the proper inverse Laplace transform. In particular, the CDF of γ_c with GSC is given in the following closed-form expression [10]

$$\begin{aligned} F_{\gamma_c}(x) = \frac{L!}{(L-L_c)!L_c!} \Bigg\{ & 1 - e^{-\frac{x}{\overline{\gamma}}} \sum_{k=0}^{L_c-1} \frac{1}{k!} \left(\frac{x}{\overline{\gamma}}\right)^k \\ & + \sum_{l=1}^{L-L_c} (-1)^{L_c+l-1} \frac{(L-L_c)!}{(L-L_c-l)!l!} \left(\frac{L_c}{l}\right)^{L_c-1} \\ & \times \Bigg[\left(1 + \frac{l}{L_c}\right)^{-1} \left[1 - e^{-\left(1+\frac{l}{L_c}\right)\frac{x}{\overline{\gamma}}}\right] \\ & - \sum_{m=0}^{L_c-2} \left(-\frac{l}{L_c}\right)^m \left(1 - e^{-\frac{x}{\overline{\gamma}}} \sum_{k=0}^{m} \frac{1}{k!} \left(\frac{x}{\overline{\gamma}}\right)^k\right) \Bigg] \Bigg\}, \end{aligned} \tag{4.4}$$

which can be directly applied to calculate the outage performance of GSC.

For more general fading channel models, the statistical distribution function of γ_c can still be obtained with the order statistics result in the previous chapter, although the closed-form expression may be not available. Specifically, the combiner output SNR with GSC can be viewed as the sum of two correlated random variables: the sum of the first $L_c - 1$ largest SNRs $\sum_{i=1}^{L_c-1} \gamma_{i:L}$, denoted by Γ_{L_c-1}, and the L_cth largest path SNR $\gamma_{L_c:L}$. It follows that the PDF of combiner output SNR γ_c can be written in terms of the joint PDF of Γ_{L_c-1} and $\gamma_{L_c:L}$ as

$$p_{\gamma_c}(x) = \int_0^{\infty} p_{\Gamma_{L_c-1},\gamma_{L_c:L}}(x-y, y)\mathrm{d}y. \tag{4.5}$$

The generic expression of the joint PDF $p_{\Gamma_{L_c-1},\gamma_{L_c:L}}(\cdot,\cdot)$ has been derived in the previous chapter.

For the general independent and non-identical distributed (i.n.d.) fading channel case, the MGF of the combined SNR with GSC can be obtained as

$$\mathcal{M}_{\gamma_c}(s) = \sum_{\substack{n_1,\cdots,n_{L_c-1} \\ n_1<n_2<\cdots<n_{L_c-1}}} \sum_{n_{L_c}} \int_0^\infty e^{-sx} p_{n_{L_c}}(x) \times \left[\prod_{l=1}^{L_c-1} \mathcal{M}_{n_l}(s,x)\right] \left[\prod_{l'=L_c+1}^{L} F_{n'_l}(x)\right] \mathrm{d}x, \tag{4.6}$$

where $n_i \in \{1, 2, \cdots, L_c\}$, $i = 1, \cdots, L_c$, are the index of the ith selected branches, $p_{n_{L_c}}(x)$ is the PDF of the L_cth selected branch SNR, $F_{n'_l}(x)$ is the SNR CDF of the remain branches and $\mathcal{M}_{n_l}(s,x)$ is the truncated MGF of the lth selected branch SNR [15, eq. (4)]. Note that summation $\sum_{\substack{n_1,\cdots,n_{L_c-1} \\ n_1<n_2<\cdots<n_{L_c-1}}}$ is carrying over all possible index sets of the largest $L_c - 1$ branch SNRs out of the total L branches and $\sum_{n_{L_c}}$ over the possible indexes of L_cth selected branch.

4.3 GSC with threshold test per branch (T-GSC)

The GSC scheme discussed in the previous section can be viewed as a natural combination of SC and MRC. While maintaining a fixed low-hardware complexity, the GSC combiner may discard diversity paths with good quality or include some weak paths. To alleviate the above-mentioned shortcomings of the conventional GSC scheme, GSC with threshold test per branch (T-GSC) was proposed and studied in [19, 20]. With T-GSC, the combining decision on a particular path is based on the comparison result of its SNR against a preseleted threshold. Specifically, if the path SNR is above the threshold, the path will be combined in an MRC fashion. Otherwise, it will be discarded. As such, T-GSC will combine a variable number of diversity paths over time. Note that as the T-GSC combiner may need to combine all L diversity paths in the MRC fashion, T-GSC has the same hardware complexity as the conventional MRC scheme. However, T-GSC can save the receiver processing power by only combining those paths with good-enough quality.

Depending on how the SNR threshold is chosen, there are two T-GSC schemes, i.e. absolute threshold GSC (AT-GSC) and normalized threshold GSC (NT-GSC) [20,21]. With AT-GSC, the ith diversity path is combined if $\gamma_i \geq \gamma_T$, where γ_T is a fixed threshold. With NT-GSC, however, the threshold γ_T is normalized against the best path SNR, i.e.

$$\gamma_T = \eta \max_l \{\gamma_l\},$$

where $0 < \eta < 1$ is the normalized threshold [22,23]. Note that with AT-GSC, it may happen in the worst case scenario that no path is combined, whereas with NT-GSC, such a problem is avoided as at least the best path will be selected. On the other hand, the NT-GSC scheme requires the additional complexity of

Table 4.1 MGF $M_{\gamma_l'}(\cdot)$ for the three fading models under consideration.

Model	$M_{\gamma_l'}(s)$
Rayleigh	$1 - e^{-\frac{\gamma_T}{\overline{\gamma}}} + \frac{1}{1-t\overline{\gamma}} e^{t\gamma_T - \frac{\gamma_T}{\overline{\gamma}}}$
Rice	$1 - Q_1\left(\sqrt{2K}, \sqrt{2(1+K)\frac{\gamma_T}{\overline{\gamma}}}\right) + \frac{1+K}{1+K-t\overline{\gamma}} e^{\frac{t\overline{\gamma}K}{1+K-t\overline{\gamma}}}$ $\times Q_1\left(\sqrt{\frac{2K(1+K)}{1+K-t\overline{\gamma}}}, \sqrt{2(1+K-t\overline{\gamma})\frac{\gamma_T}{\overline{\gamma}}}\right)$
Nakagami-m	$1 - \frac{\Gamma\left(m, \frac{m\gamma_T}{\overline{\gamma}}\right)}{\Gamma(m)} + \left(1 - \frac{t\overline{\gamma}}{m}\right)^{-m} \frac{\Gamma\left(m, \frac{m\gamma_T}{\overline{\gamma}} - t\gamma_T\right)}{\Gamma(m)}$

determining the instantaneous best path, which involves the comparison of different estimated path SNRs. In the following, we present the major steps in obtaining the statistics of the output SNR with both T-GSC schemes.

4.3.1 Statistics of output SNR

AT-GSC

Based on the mode of operation of the AT-GSC scheme, the combiner can be viewed as an L-branch MRC combiner with input SNRs given by

$$\gamma_l' = \begin{cases} \gamma_l, & \gamma_l \geq \gamma_{\text{th}}; \\ 0, & 0 \leq \gamma_l < \gamma_{\text{th}}, \end{cases} \tag{4.7}$$

where γ_l is the SNR of the lth diversity path. The combiner output SNR is equal to the sum of these L input SNRs, i.e. $\gamma_c = \sum_{l=1}^{L} \gamma_l'$. With the i.i.d. assumption, we can easily calculate the MGF of γ_c as the product of the MGFs of γ_l'. It can be shown that the PDF of γ_l' can be given by

$$p_{\gamma_l'}(\gamma) = \begin{cases} F_{\gamma_l}(\gamma_T)\delta(\gamma), & \gamma = 0; \\ p_{\gamma_l}(\gamma), & \gamma \geq \gamma_T, \end{cases} \tag{4.8}$$

where $F_{\gamma_l}(\cdot)$ and $p_{\gamma_l}(\cdot)$ are the CDF and PDF of the lth path SNRs, respectively. It follows that the MGF of γ_l' can be obtained as

$$\mathcal{M}_{\gamma_l'}(s) = F_{\gamma_l}(\gamma_T) + \int_{\gamma_T}^{\infty} p_{\gamma_l}(\gamma) e^{s\gamma} \mathrm{d}\gamma. \tag{4.9}$$

For most popular fading channel models, the closed-form expression of $\mathcal{M}_{\gamma_l'}(\cdot)$ is available. Table 4.1 summarizes these results for the three fading-channel models under consideration. Finally, the MGF of the combined SNR with AT-GSC is given by

$$\mathcal{M}_{\gamma_c}(s) = \prod_{l=1}^{L} \mathcal{M}_{\gamma_l'}(s) = \prod_{l=1}^{L} F_{\gamma_l}(\gamma_T) + \int_{\gamma_T}^{\infty} p_{\gamma_l}(\gamma) e^{s\gamma} d\gamma. \tag{4.10}$$

The PDF and CDF of the combined SNR can be obtained routinely after taking proper inverse Laplace transform and carrying out integration. With the statistics of the combined SNR, we can readily evaluate the performance of AT-GSC over fading channels.

NT-GSC

To derive the statistics of the combined SNR with NT-GSC, we consider L mutually exclusive events depending on how many diversity paths are combined [22]. Let $\gamma_{1:L} \geq \gamma_{2:L} \geq \cdots \geq \gamma_{L:L}$ denote the ordered path SNRs in descending order, where $\gamma_{1:L}$ corresponds to the largest among all L, i.e. $\gamma_{1:L} = \max_l\{\gamma_l\}$. It follows that L_c paths are combined with NT-GSC if and only if $\gamma_{1:L} \geq \gamma_{2:L} \geq \cdots \geq \gamma_{L_c:L} \geq \eta\gamma_{1:L} \geq \gamma_{L_c+1:L} \geq \cdots \geq \gamma_{L:L}$, which leads to the combiner output SNR being

$$\gamma_{c,L_c} = \sum_{i=1}^{L_c} \gamma_{i:L},\ L_c = 1, 2, \cdots, L. \tag{4.11}$$

Applying the total probability theorem, the distribution function of the combined SNR with NT-GSC can be obtained as the sum of the distribution functions for each individual event. In particular, the MGF of γ_c can be written as

$$\mathcal{M}_{\gamma_c}(s) = \sum_{L_c=1}^{L} \mathcal{M}_{\gamma_{c,L_c}}(s), \tag{4.12}$$

where $\mathcal{M}_{\gamma_{c,L_c}}(s)$ is the MGF for the event that L_c paths are combined and is given by

$$\begin{aligned}\mathcal{M}_{\gamma_{c,L_c}}(s) = &\int_0^\infty \mathrm{d}\gamma_{1:L} \int_{\eta\gamma_{1:L}}^{\gamma_{1:L}} \mathrm{d}\gamma_{2:L} \cdots \int_{\eta\gamma_{1:L}}^{\gamma_{L_c-1:L}} \mathrm{d}\gamma_{L_c:L} \int_0^{\eta\gamma_{1:L}} \mathrm{d}\gamma_{L_c+1:L} \\ &\int_0^{\gamma_{L_c+1:L}} \mathrm{d}\gamma_{L_c+2:L} \cdots \int_0^{\eta\gamma_{L-1:L}} e^{s\sum_{i=1}^{L_c}\gamma_{i:L}} \\ &p_{\gamma_{1:L},\gamma_{2:L},\cdots,\gamma_{L:L}}(\gamma_{1:L}, \gamma_{2:L}, \cdots, \gamma_{L:L})\mathrm{d}\gamma_{L:L},\end{aligned} \tag{4.13}$$

where $p_{\gamma_{1:L},\gamma_{2:L},\cdots,\gamma_{L:L}}(\cdot)$ is the joint PDF of the ordered path SNRs, given in the previous chapter. After proper substitution and carrying out the integration with the help of the following definition of partial MGF

$$\mathcal{M}_\gamma(s, x) = \int_x^\infty p_\gamma(\gamma) e^{s\gamma} \mathrm{d}\gamma, \tag{4.14}$$

we can obtain the MGF for the event that L_c paths are combined in the following compact form involving a single integral

$$\mathcal{M}_{\gamma_{c,L_c}}(s) = L_c \binom{L}{L_c} \int_0^\infty e^{s\gamma} p_\gamma(\gamma) [F_\gamma(\eta\gamma)]^{L-L_c} [\mathcal{M}_\gamma(s, \gamma) - \mathcal{M}_\gamma(s, \eta\gamma)]^{L_c-1} \mathrm{d}\gamma. \tag{4.15}$$

Note that the partial MGF $\mathcal{M}_\gamma(s, x)$ is related to the MGF defined in (4.9) as $\mathcal{M}_\gamma(s, \gamma_{\mathrm{th}}) = \mathcal{M}_{\gamma_l'}(s) - F_\gamma(\gamma_{\mathrm{th}})$. We can easily obtain the closed-form expression

of the partial MGF for three popular fading channel models directly from Table 4.1. The PDF and CDF of the combined SNR with NT-GSC can be obtained routinely.

4.3.2 Average number of combined paths

Both GSC and T-GSC will reduce the combiner complexity in terms of the number of active MRC branches. With GSC, the number of active MRC branches is fixed to $L_c < L$, whereas with T-GSC, the number of active branches is randomly varying. In particular, the probability that i branches will be active with AT-GSC is equal to

$$\Pr[N_c = i] = \binom{L}{i} [1 - F_\gamma(\gamma_T)]^i [F_\gamma(\gamma_T)]^{L-i}. \tag{4.16}$$

As such, the average number of combined paths with AT-GSC is given by

$$\overline{N}_c = \sum_{i=0}^{L} i \Pr[N_c = i] = L[1 - F_\gamma(\gamma_T)]. \tag{4.17}$$

Based on the mode of operation of NT-GSC, the probability $\Pr[N_c = i]$ with NT-GSC can be calculated as

$$\Pr[N_c = i] = \Pr[\gamma_{i:L} \geq \eta\gamma_{1:L} \geq \gamma_{i+1:L}], \tag{4.18}$$

which can be calculated using the joint PDF of $\gamma_{1:L}$, $\gamma_{i:L}$, and $\gamma_{i+1:L}$ as

$$\Pr[N_c = i] = \int_0^\infty \int_{\eta x}^{x} \int_0^{\eta x} p_{\gamma_{1:L},\gamma_{i:L},\gamma_{i+1:L}}(x, y, z) \mathrm{d}x\mathrm{d}y\mathrm{d}z. \tag{4.19}$$

After slightly generalized (3.4), the joint PDF $p_{\gamma_{1:L},\gamma_{i:L},\gamma_{i+1:L}}(\cdot,\cdot,\cdot)$ can be obtained as

$$\begin{aligned} p_{\gamma_{1:L},\gamma_{i:L},\gamma_{i+1:L}}(x, y, z) = {} & \frac{L!}{(i-2)!(L-i-1)!} p_\gamma(x) \\ & \times (F_\gamma(x) - F_\gamma(y))^{i-2} p_\gamma(y) p_\gamma(z) (F_\gamma(z))^{L-i-1}. \end{aligned} \tag{4.20}$$

4.4 Generalized switch and examine combining (GSEC)

Both GSC variants discussed in the previous section require the estimation of all available diversity paths, regardless of whether they are eventually used or not. The path estimation complexity can be further reduced with a switching-based mechanism during the path selection stage. Note that the main complexity saving of threshold combining schemes over selection combining is fewer path estimations. Generalized switch and examine combining (GSEC) is another low-complexity combining scheme that was proposed for a diversity-rich environment in this context [6]. The basic idea of GSEC is to extend the notion of switch and

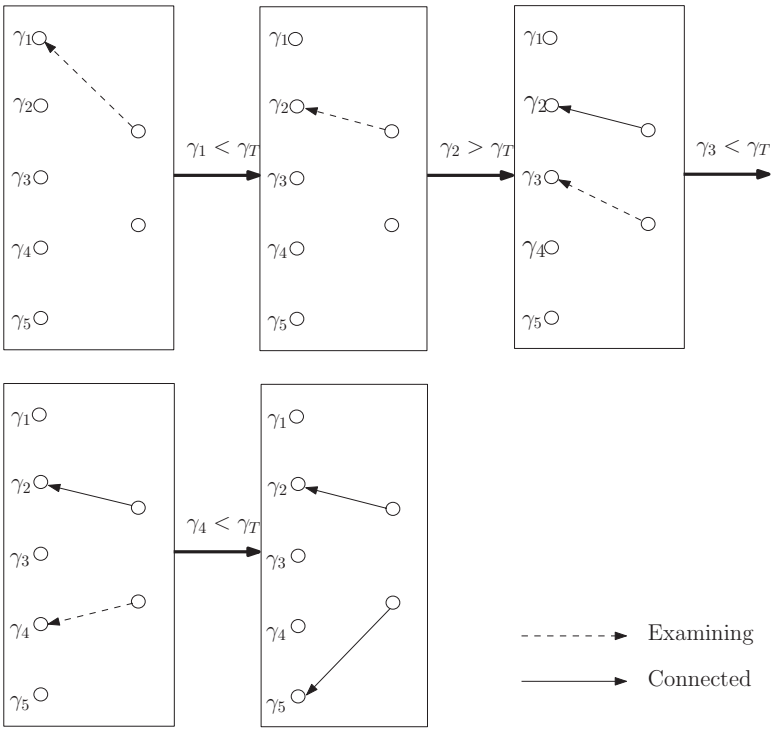

Figure 4.2 Sample operation of a GSEC-based diversity combiner.

examine combining studied in a previous chapter to multi-input-multi-output scenario and use it for multiple path selection before cascading with a traditional MRC combiner. As such, the GSEC scheme can also be viewed as hybrid switch and examine/maximum ratio combining.

Specifically, the receiver with GSEC tries to select L_c acceptable paths, i.e. those whose instantaneous SNR is above a pre-selected fixed threshold, out of a total of L available paths for subsequent MRC combining. Figure 4.2 illustrates a sample path selection process of a GSEC combiner. Specifically, the receiver with GSEC will sequentially estimate and compare the channel SNR of diversity paths against s_T until it finds L_c acceptable paths. After that, the receiver will stop path estimation. As such, the receiver with GSEC does not always need to estimate all L diversity paths, which manifest the major complexity saving of GSEC over GSC and T-GSC. If there are not enough acceptable paths even after examining all paths, the receiver will randomly select some unacceptable paths for MRC combining. Therefore, similar to GSC, GSEC always combines a fixed number of diversity branches. On the other hand, the path selection process with GSEC is much simpler than that of GSC, as the receiver does not need to rank all available diversity paths. Note that with GSC, the receiver needs to compare two estimated SNRs whereas with GSEC, only comparisons of an estimated SNR with a fixed threshold are necessary.

4.4.1 Statistics of output SNR

To accurately quantify the new trade-off of performance versus complexity introduced by the GSEC scheme, we need the statistical characterization of its combined SNR. In this section, we derive the generic expression of the MGF of the combined SNR with GSEC, which can be used to routinely obtain other distribution functions. Based on the mode of operation of GSEC, we note that the number of acceptable diversity paths that are eventually combined with GSEC only takes values from 0 to L_c. Since they are exclusive and disjoint events, we can apply the total probability theorem and write the MGF of combiner output γ_c in the following weighted sum form

$$\mathcal{M}_{\gamma_c}(s) = \sum_{i=0}^{L_c} \pi_i \, \mathcal{M}_{\gamma_c}^{(i)}(s), \tag{4.21}$$

where $\mathcal{M}_{\gamma_c}^{(i)}(\cdot)$ is the conditional MGF of γ_c given that exactly i out of L_c combined paths are acceptable and π_i is the probability that there are exactly i acceptable paths. With the i.i.d. fading assumption, it is not difficult to show that the π_is are mathematically given by

$$\pi_i = \begin{cases} \binom{L}{i} [F_\gamma(\gamma_T)]^{L-i}[1 - F_\gamma(\gamma_T)]^i, & i = 0, \cdots, L_c - 1; \\ \sum_{j=L_c}^{L} \binom{L}{j} [F_\gamma(\gamma_T)]^{L-j}[1 - F_\gamma(\gamma_T)]^j, & i = L_c, \end{cases} \tag{4.22}$$

where $P_\gamma(\cdot)$ is the common CDF of the received SNR on each diversity path and given in Table 2.2 for the three fading models under consideration.

The conditional MGF $\mathcal{M}_{\gamma_c}^{(i)}(\cdot)$ can be written as

$$\mathcal{M}_{\gamma_c}^{(i)}(s) = [\mathcal{M}_{\gamma^+}(s)]^i [\mathcal{M}_{\gamma^-}(s)]^{L_c - i}, \tag{4.23}$$

where $\mathcal{M}_{\gamma^+}(\cdot)$ denotes the MGF of a single-path SNR given that it is greater or equal to γ_T and $\mathcal{M}_{\gamma^-}(\cdot)$ denotes the MGF of a single-path SNR given that it is less than γ_T, both of which have been defined in the previous chapter. Their closed-form expressions for the three fading models under consideration are summarized in Table 3.1. Finally, after substituting (4.22) and (4.23) into (4.21), the generic expression for the MGF of the overall combiner output γ_c is given by

$$\begin{aligned} \mathcal{M}_{\gamma_c}(s) = &\sum_{i=0}^{L_c-1} \binom{L}{i} [P_\gamma(\gamma_T)]^{L-i}[1 - P_\gamma(\gamma_T)]^i [\mathcal{M}_{\gamma^+}(s)]^i [\mathcal{M}_{\gamma^-}(s)]^{L_c - i} \\ &+ \sum_{j=L_c}^{L} \binom{L}{j} [P_\gamma(\gamma_T)]^{L-j}[1 - P_\gamma(\gamma_T)]^j [\mathcal{M}_{\gamma^+}(s)]^{L_c}. \end{aligned} \tag{4.24}$$

When $L_c = L$, it can be shown, with the help of the following relationship

$$[1 - F_\gamma(\gamma_T)]\mathcal{M}_{\gamma^+}(s) + F_\gamma(\gamma_T)\mathcal{M}_{\gamma^-}(s) = \mathcal{M}_\gamma(s), \tag{4.25}$$

where $\mathcal{M}_\gamma(\cdot)$ is the common MGF of the received SNR, that (4.24) reduces to $[\mathcal{M}_\gamma(s)]^L$, i.e. the GSEC combiner is equivalent to an L branch MRC combiner, as expected. It can also be shown that when $L_c = 1$, (4.24) simplifies to the MGF of the output SNR of a traditional L branch SEC combiner [24, eq. (35)].

With the analytical expression of the MGF, we can readily derive the PDF and CDF of the combined SNR with GSEC through inverse Laplace transform and integration. As an example, the CDF γ_c over i.i.d. Rayleigh fading channel can be obtained as

$$\begin{aligned} F_{\gamma_c}(x) = & \sum_{i=0}^{L_c-1} \binom{L}{i} \left[1 - \exp\left(-\frac{\gamma_T}{\overline{\gamma}}\right)\right]^{L-L_c} \sum_{j=0}^{\min[L_c, \lfloor \frac{x}{\gamma_T} \rfloor]-i} \\ & \times \binom{L_c - i}{j} (-1)^j \exp\left(-\frac{(i+j)\gamma_T}{\overline{\gamma}}\right) \\ & \times \left[1 - \exp\left(-\frac{x - (i+j)\ \gamma_T}{\overline{\gamma}}\right) \sum_{k=0}^{L_c-1} \frac{1}{k!} \left(\frac{x - (i+j)\ \gamma_T}{\overline{\gamma}}\right)^k\right] \\ & + I_{L_c\gamma_T}(x) \sum_{j=L_c}^{L} \binom{L}{j} \left[1 - \exp\left(-\frac{\gamma_T}{\overline{\gamma}}\right)\right]^{L-j} \exp\left(-\frac{j\gamma_T}{\overline{\gamma}}\right) \\ & \times \left[1 - \exp\left(-\frac{x - L_c\ \gamma_T}{\overline{\gamma}}\right) \sum_{k=0}^{L_c-1} \frac{1}{k!} \left(\frac{x - L_c\ \gamma_T}{\overline{\gamma}}\right)^k\right], \end{aligned} \tag{4.26}$$

where $I_{L_c\gamma_T}(x)$ is an indicator function, which is equal to 1 if $x \geq L_c\gamma_T$ and zero otherwise.

4.4.2 Average number of path estimations

We now quantify the complexity of GSEC in terms of the average number of path estimations. Because of the subsequent MRC combining, the receiver with GSEC needs always to estimate at least L_c diversity paths. In the case that there are less than L_c acceptable paths among the total L ones, based on the mode of operation of GSEC, whenever the receiver encounters $L - L_c$ unacceptable paths, it will apply MRC to the remaining paths, which necessitates their full estimations. As a result, in this case, the receiver needs to estimate all L available diversity paths. It is not difficult to show that the probability that there are less than L_c acceptable paths is given by

$$P_B = \sum_{L-L_c+1}^{L} \binom{L}{k} [F_\gamma(\gamma_T)]^{L-k} [1 - F_\gamma(\gamma_T)]^k. \tag{4.27}$$

On the other hand, if there are at least L_c acceptable diversity paths, based on the mode of operation of GSEC, the combiner will stop examining paths whenever it has found L_c acceptable ones. In this case, the number of channel estimates during a guard period takes values from L_c to L. Note that the probability that k channel estimates are performed in a guard period, denoted by $P_A^{(k)}$, is equal to the probability that the L_cth acceptable path is the kth path examined, or equivalently, exactly $k - L_c$ ones of the first $k - 1$ examined paths, are unacceptable whereas the kth examined path is acceptable. It can be shown, with the assumption of i.i.d. diversity paths, that $P_A^{(k)}$ is mathematically given by

$$P_A^{(k)} = \binom{k-1}{k-L_c} [1 - F_\gamma(\gamma_T)]^{L_c} [F_\gamma(\gamma_T)]^{k-L_c}. \tag{4.28}$$

Finally, by combining these two mutually exclusive cases, we obtain the expression for the overall average number of channel estimates needed by GSEC during a guard period as

$$\begin{aligned} N_E &= \sum_{L_c}^{L} k\ P_A^{(k)} + L\ P_B \\ &= \sum_{k=L_c}^{L} k\ [1 - F_\gamma(\gamma_T)]^{L_c} \binom{k-1}{k-L_c} [F_\gamma(\gamma_T)]^{k-L_c} \\ &\quad + L \sum_{L-L_c+1}^{L} \binom{L}{k} [F_\gamma(\gamma_T)]^{L-k} [1 - F_\gamma(\gamma_T)]^k. \end{aligned} \tag{4.29}$$

In the case of $\gamma_T = 0$, since $F_\gamma(\gamma_T) = 0$, it can be shown that $N = L_c$, as expected. On the other hand, when $\gamma_T \to \infty$ and thus $F_\gamma(\gamma_T) = 1$, it can be similarly shown that $N = L$, also as expected.

4.4.3 Numerical examples

Figure 4.3 plots the average bit error probability of BPSK with GSEC as a function of the switching threshold for $L = 4$ and different values of L_c. It can be observed that there exists an optimal choice of the switching threshold in the minimum average error probability sense except for the $L_c = 4$ case, which corresponds to a traditional 4-branch MRC. The performance advantage of the optimal threshold diminishes and the value of the optimal threshold decreases as L_c increases.

Figure 4.4 compares the error performance of GSEC and GSC in a diversity-rich environment with $L = 12$ available diversity paths. GSEC is not as good as GSC performance-wise. We also note that as L_c increases, the performance gap between GSEC and GSC reduces significantly. This implies that GSEC can take advantage of additional diversity paths with a relative lower complexity compared to the competing GSC scheme. For instance, for a BER of 10^{-6}, there

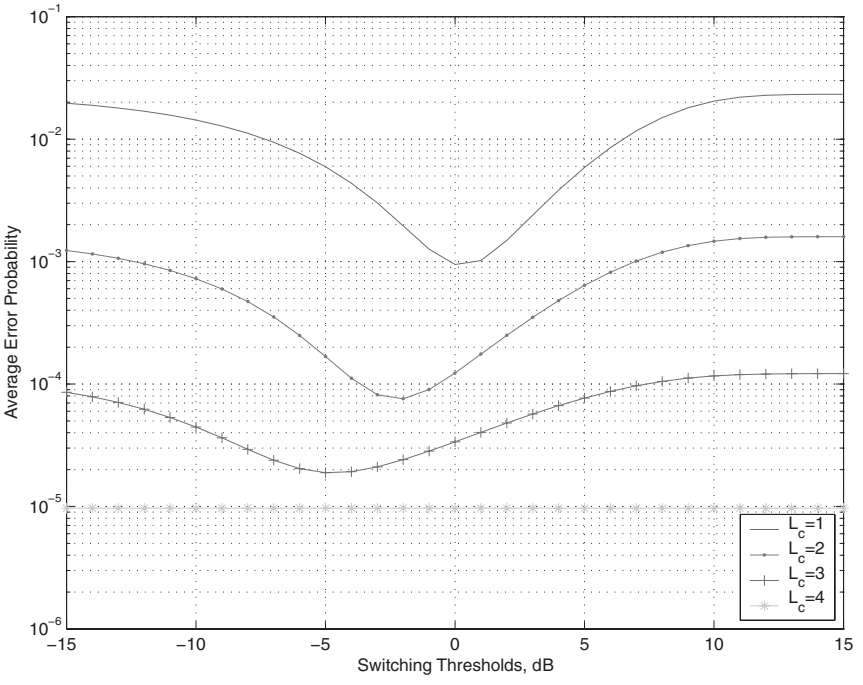

Figure 4.3 Average BER of BPSK with GSEC over $L = 4$ i.i.d. Rayleigh fading paths as a function of the common switching threshold γ_T ($\overline{\gamma} = 10$ dB) [6]. © 2004 IEEE.

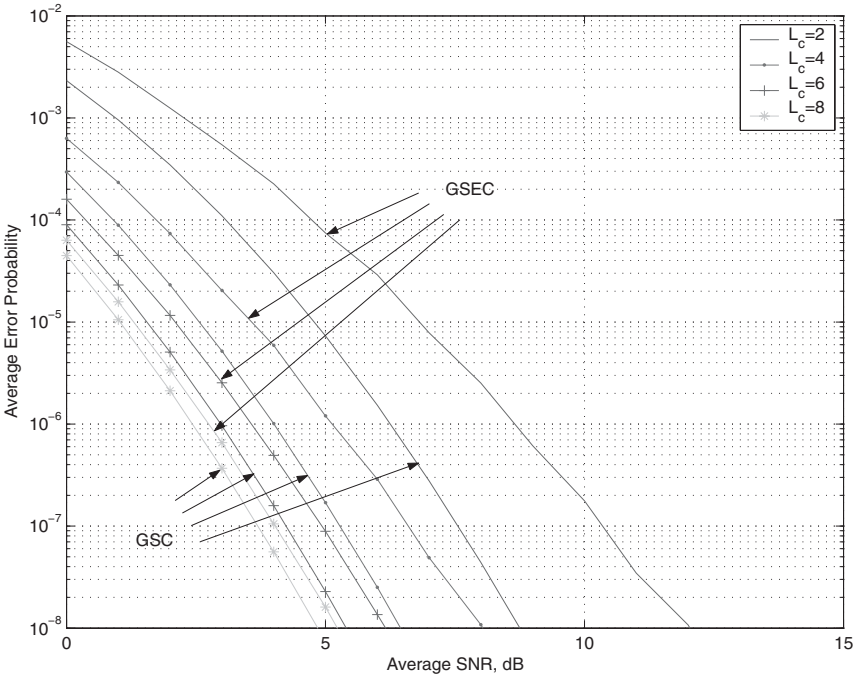

Figure 4.4 Error rate comparison of GSEC and GSC in diversity-rich environment, $L = 12$ [6]. © 2004 IEEE.

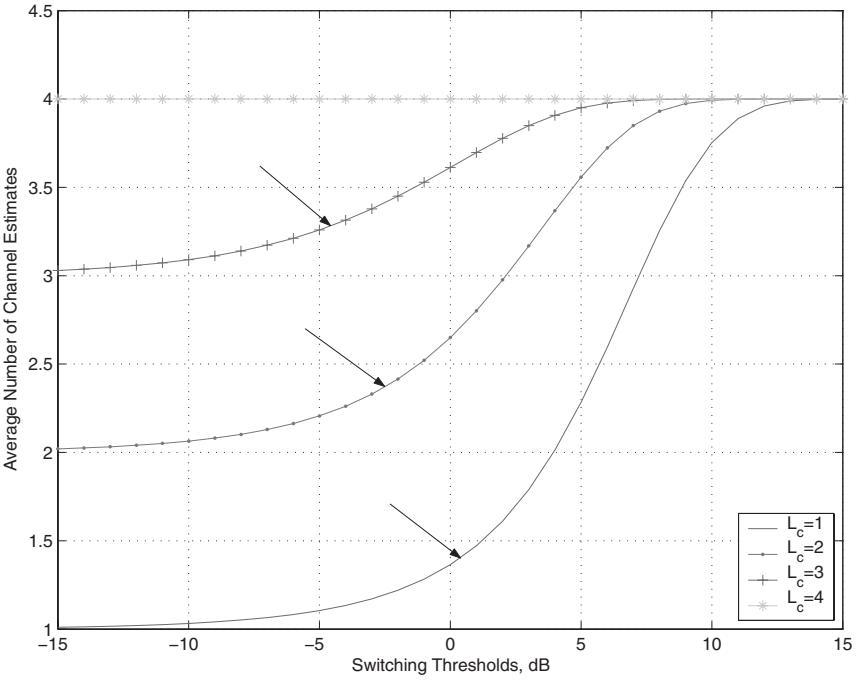

Figure 4.5 Average number of channel estimates of GSEC with $L = 4$ as function of the common switching threshold γ_T ($\overline{\gamma} = 10$ dB) [6]. © 2004 IEEE.

is only a 0.6 dB difference when $L_c = 6$. Notice that, in this scenario, the GSC combiner needs to perform approximately $L_c \times L = 12 \times 6 = 72$ comparisons in each guard period to select the 6 strongest paths, whereas GSEC requires at most $L = 12$ comparisons.

Figure 4.5 plots the average number of path estimates of GSEC with $L = 4$ as a function of the switching threshold for the Rayleigh fading case. As we can see, as the switching threshold γ_T increases, the number of path estimates N increases from L_c to L. Intuitively, because if the threshold is large, it becomes more difficult for the receiver to find acceptable paths and as such more paths need to be estimated. We also marked the optimal operating points for GSEC in terms of minimizing the average error rate, which were read from Fig. 4.3. Note that even for the best performance, GSEC does not need to estimate all the diversity paths, whereas for GSC all L diversity paths need to be estimated in each guard period.

4.5 GSEC with post-examining selection (GSECps)

The GSEC scheme works well when the channel condition is favorable and the receiver can find enough acceptable paths. When there are not enough acceptable

paths, however, GSEC will combine all the acceptable paths and some 'randomly' selected unacceptable paths. In this case, the selected unacceptable paths may have low instantaneous SNR, which degrades the performance of GSEC, especially in a low SNR region. Noting that in this case all diversity paths have been estimated anyway, a preferred alternative is to combine those unacceptable paths with the highest instantaneous SNRs.

With this observation in mind, an improved version of GSEC, termed the generalized switch and examine combining with post-examine selection (GSECps) was proposed [25]. In particular, the new scheme operates in exactly the same way as GSEC when there are enough acceptable paths. When the number of acceptable paths is smaller than the number of paths required, instead of combining some 'randomly' selected unacceptable paths as with GSEC, GSECps combines the best unacceptable paths together with all acceptable paths. Intuitively, we expect that GSECps can offer better performance than GSEC through the occasional selection of the best unacceptable paths while maintaining roughly the same complexity. Note that GSECps can also be viewed as the generalization of switch and examine combining with post-examine selection (SECps) scheme studied in Section 2.3 [26], since GSECps reduces to SECps when the number of paths to be combined is one.

Specifically, the mode of operation of GSEC can be summarized as follows. The receiver will sequentially estimate the instantaneous SNR of the available diversity paths and compare them with the fixed threshold γ_T to determine the acceptance of a path. Let L_a stand for the number of acceptable paths. If at least L_c paths are found to be acceptable, i.e. $L_a \geq L_a$, the receiver will combine the first L_c of them in the MRC fashion. Otherwise, the receiver will combine all the L_a acceptable paths, where $L_a < L_c$, and the strongest $L_c - L_a$ unacceptable paths. As we can see, when there are enough acceptable paths, i.e. $L_a \geq L_c$, GSECps will be equivalent to GSEC. On the other hand, when $L_a < L_c$, the receiver is essentially combining the L_c best paths of the L available paths, as is the case with GSC. Figure 4.6 presents a sample operation of the GSECps scheme.

4.5.1 Statistics of output SNR

We focus on the statistics of the combined SNR with GSECps over i.i.d. Rayleigh fading environment, for which the closed-form expressions for PDF, CDF and MGF of γ_c are obtained. Note that depending on whether or not there are L_c acceptable paths, we can apply the total probability theorem and write the CDF of γ_c in the following form

$$\begin{aligned} F_{\gamma_c}(x) &= \Pr[\gamma_c < x] \\ &= \pi_{L_c} \cdot \Pr[\gamma_c < x | L_a \geq L_c] + \Pr[\gamma_c < x, L_a < L_c], \end{aligned} \tag{4.30}$$

where π_{L_c} is the probability that there are at least L_c acceptable paths, which was given in (4.22), $\Pr[\gamma_c < x | L_a \geq L_c]$ is the conditional probability of the event

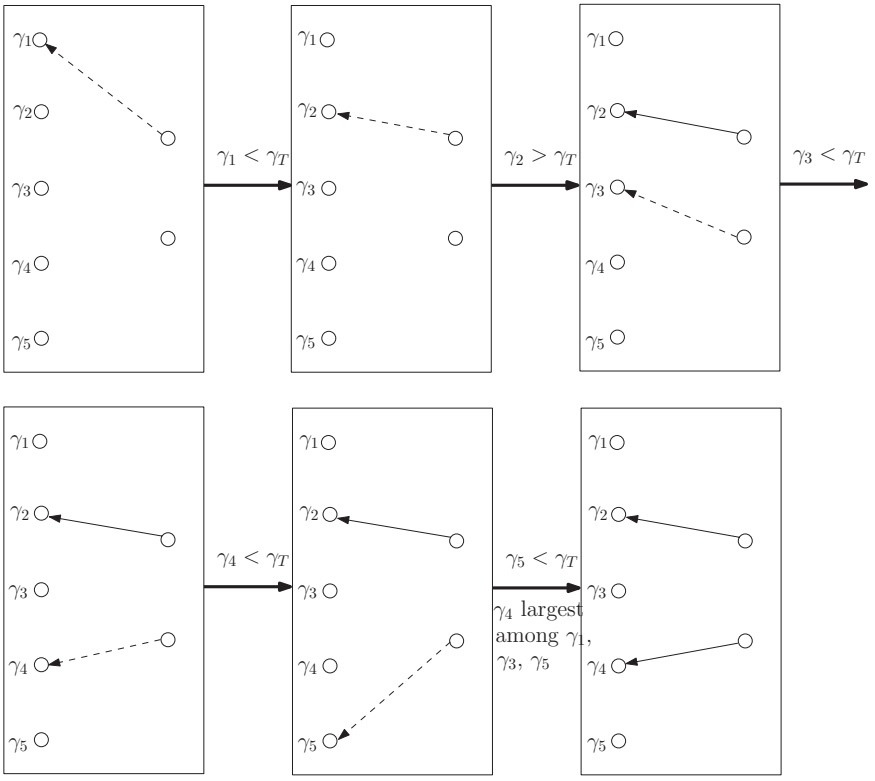

Figure 4.6 Sample operation of a GSECps-based diversity combiner.

$\gamma_c < x$ given that there are at least L_c acceptable paths, and $\Pr[\gamma_c < x, L_a < L_c]$ is the joint probability of the events $\gamma_c < x$ and $L_a < L_c$. Note that when $L_a \geq L_c$, GSECps combines L_c acceptable paths. As such, γ_c is the sum of L_c path SNRs that are greater than γ_T. Therefore, $\Pr[\gamma_c < x | L_a \geq L_c]$ can be shown to be given by [6, eq. (38)]

$$\Pr[\gamma_c < x | L_a \geq L_c] = 1 - e^{-\frac{x - L_c\gamma_T}{\overline{\gamma}}} \sum_{k=0}^{L_c-1} \frac{1}{k!} \left(\frac{x - L_c\gamma_T}{\overline{\gamma}} \right)^k, \; x \geq L_c\gamma_T. \quad (4.31)$$

Note that since $L_a \geq L_c$, the combined SNR γ_c is always greater than $L_c\gamma_T$.

To calculate $\Pr[\gamma_c < x, L_a < L_c]$, we first note that since there are less than L_c acceptable paths, the receiver will in effect combine L_c strongest paths. Therefore, we have

$$\gamma_c = \sum_{i=1}^{L_c} \gamma_{i:L}, \quad (4.32)$$

where $\gamma_{i:L}$ is the ith largest SNR of all L path SNRs. Let Γ_{L_c-1} denote the sum of the first $L_c - 1$ largest SNR, i.e. $\Gamma_{L_c-1} = \sum_{j=1}^{L_c-1} \gamma_{j:L}$. We can rewrite $\Pr[\gamma_c < x, L_a < L_c]$ while noting that $L_a < L_c$ holds if and only if the L_cth

largest SNR of all L path SNRs, $\gamma_{L_c:L}$, is less than γ_T, as

$$\Pr[\gamma_c < x, L_a < L_c] = \Pr[\Gamma_{L_c-1} + \gamma_{L_c:L} < x, \gamma_{L_c:L} < \gamma_T], \tag{4.33}$$

which can be computed with the joint PDF of $\gamma_{L_c:L}$ and Γ_{L_c-1}, denoted by $p_{\gamma_{L_c:L},\Gamma_{L_c-1}}(y,z)$. Based on the order statistics results in a previous chapter, $p_{\gamma_{L_c:L},\Gamma_{L_c-1}}(y,z)$ for i.i.d. Rayleigh fading environment can be obtained as [27, eq. (11)]

$$p_{\gamma_{L_c:L},\Gamma_{L_c-1}}(y,z) = \sum_{j=0}^{L-L_c} \frac{(-1)^j L![z-(L_c-1)y]^{L_c-2}}{(L-L_c-j)!(L_c-1)!(L_c-2)!j!\overline{\gamma}^{L_c}} e^{-\frac{z+(j+1)y}{\overline{\gamma}}}, \quad y \geq 0,\ z \geq (L_c-1)y. \tag{4.34}$$

Noting that the support of the joint PDF, $\Pr[\gamma_c < x, L_a < L_c]$ can be written as

$$\Pr[\Gamma_{L_c-1} + \gamma_{L_c:L} < x, \gamma_{L_c:L} < \gamma_T] = \int_0^{\min\{\gamma_T, \frac{x}{L_c}\}} \int_{(L_c-1)y}^{x-y} p_{\gamma_{L_c:L},\Gamma_{L_c-1}}(y,z)\,\mathrm{d}z\,\mathrm{d}y. \tag{4.35}$$

After substituting (4.34) into (4.35), carrying out the integration and appropriate simplifications, we have

$$\Pr[\gamma_c < x, L_a < L_c] = \begin{cases} F_{\gamma_c}(L_c\gamma_T) + \sum_{j=1}^{L-L_c}\sum_{k=0}^{L_c-2} A_{(j,k)} \\ \quad \times \left[e^{-\frac{j\gamma_T + L_c\gamma_T}{\overline{\gamma}}} \left(1 - \Gamma\big(L_c-1-k, \frac{x-L_c\gamma_T}{\overline{\gamma}}\big)\right) \right. \\ \quad \left. - \left(\Gamma\big(L_c-1-k, \frac{L_c\gamma_T}{\overline{\gamma}}\big) - \Gamma\big(L_c-1-k, \frac{x}{\overline{\gamma}}\big)\right)\right] \\ \quad + \binom{L}{L_c}\left[\left(\Gamma\big(L_c, \frac{L_c\gamma_T}{\overline{\gamma}}\big) - \Gamma\big(L_c, \frac{x}{\overline{\gamma}}\big)\right)\right. \\ \quad \left. - e^{-\frac{L_c\gamma_T}{\overline{\gamma}}}\left(1 - \Gamma\big(L_c, \frac{x-L_c\gamma_T}{\overline{\gamma}}\big)\right)\right],\ x \geq L_c\gamma_T; \\ F_{\gamma_c}(x), \qquad x < L_c\gamma_T, \end{cases} \tag{4.36}$$

where

$$F_{\gamma_c}(x) = \binom{L}{L_c}\left\{1 - \Gamma(L_c, x/\overline{\gamma}) + \sum_{l=1}^{L-L_c}(-1)^{L_c+l-1}\binom{L-L_c}{l}\left(\frac{L_c}{l}\right)^{L_c-1} \times \left[\frac{1-e^{-(1+l/L_c)(x/\overline{\gamma})}}{1+l/L_c} - \sum_{m=0}^{L_c-2}(\frac{-l}{L_c})^m\left(1-\Gamma(m+1, x/\overline{\gamma})\right)\right]\right\}, \tag{4.37}$$

$$A_{(j,k)} = \frac{(-1)^j L! {L_c}^k}{(L-L_c-j)!(L_c-1)!j!(-j)^{k+1}}, \tag{4.38}$$

and $\Gamma(n,x)$ is the incomplete Gamma function defined by

$$\Gamma(n,x)=\frac{1}{(n-1)!}\int_x^\infty t^{n-1}e^{-t}\mathrm{d}t. \tag{4.39}$$

Combining (4.22), (4.31), and (4.36), we obtain the closed-form expression of the CDF of the output SNR γ_c and, equivalently, the outage probability of GSECps.

Starting from the CDF of the combined SNR with GSECps, we can routinely derive the PDF and MGF. Specifically, after differentiation and some manipulations, the PDf of γ_c for i.i.d. Rayleigh fading channels is given by

$$\begin{aligned}
&p_{\gamma_c}(x)\\
&=\begin{cases}
\binom{L}{L_c}\left[\dfrac{x^{L_c-1}e^{-x/\overline{\gamma}}}{\overline{\gamma}^{L_c}(L_c-1)!}+\dfrac{1}{\overline{\gamma}}\displaystyle\sum_{l=1}^{L-L_c}(-1)^{L_c+l-1}\binom{L-L_c}{l}\left(\frac{L_c}{l}\right)^{L_c-1}\right.\\
\quad\left.\times\, e^{-x/\overline{\gamma}}\left(e^{-lx/L_c\overline{\gamma}}-\displaystyle\sum_{m=0}^{L_c-2}\frac{1}{m!}\Big(\frac{-lx}{L_c\overline{\gamma}}\Big)^m\right)\right],\ x<L_c\gamma_T\\
\pi_{L_c}\left[\dfrac{1}{(L_c-1)!\overline{\gamma}^{L_c}}(x-L_c\gamma_T)^{L_c-1}e^{-\frac{x-L_c\gamma_T}{\overline{\gamma}}}\right]\\
\quad+\displaystyle\sum_{j=1}^{L-L_c}\sum_{k=0}^{L_c-2}\frac{A_{(j,k)}\overline{\gamma}^{k+1-L_c}}{(L_c-2-k)!}e^{-x/\overline{\gamma}}\left(e^{\frac{-j\gamma_T}{\overline{\gamma}}}(x-L_c\gamma_T)^{L_c-2-k}-x^{L_c-2-k}\right)\\
\quad+\binom{L}{L_c}\dfrac{1}{(L_c-1)!\overline{\gamma}_c^{L}}e^{-\frac{x}{\overline{\gamma}}}\left(x^{L_c-1}-(x-L_c\gamma_T)^{L_c-1}\right),\ x\geq L_c\gamma_T
\end{cases}
\end{aligned} \tag{4.40}$$

where π_{L_c} and $A_{(j,k)}$ were defined in (4.22) and (4.38), respectively. The MGF of γ_c, denoted by $M_{\gamma_c}(t)$, can be shown to be given, for the i.i.d. Rayleigh fading case, by

$$\begin{aligned}
\mathcal{M}_{\gamma_c}(t)&=\binom{L}{L_c}\left\{\frac{1-\Gamma(L_c,(1-t\overline{\gamma})L_c\gamma_T/\overline{\gamma})}{(1-t\overline{\gamma})^{L_c}}+\sum_{l=1}^{L-L_c}(-1)^{L_c+l-1}\binom{L-L_c}{l}\right.\\
&\left.\times\left(\frac{L_c}{l}\right)^{L_c-1}\left[I(l,t)-\sum_{m=0}^{L_c-2}\Big(\frac{-l}{L_c}\Big)^m\frac{(1-\Gamma(m+1,(1-t\overline{\gamma})L_c\gamma_T/\overline{\gamma}))}{(1-t\overline{\gamma})^{m+1}}\right]\right\}\\
&+\sum_{j=1}^{L-L_c}\sum_{k=0}^{L_c-2}A_{(j,k)}\left[e^{-\frac{L_c\gamma_T+j\gamma_T}{\overline{\gamma}}}\frac{e^{L_c\gamma_T t}}{(1-t\overline{\gamma})^{L_c-1-k}}-\frac{\Gamma(L_c-1-k,(1-t\overline{\gamma})L_c\gamma_T/\overline{\gamma})}{(1-t\overline{\gamma})^{L_c-1-k}}\right]\\
&+\binom{L}{L_c}\left[\frac{\Gamma(L_c,(1-t\overline{\gamma})L_c\gamma_T/\overline{\gamma})}{(1-t\overline{\gamma})^{L_c}}-\frac{e^{L_c\gamma_T\left(t-\frac{1}{\overline{\gamma}}\right)}}{(1-t\overline{\gamma})^{L_c}}\right]+\pi_{L_c}e^{L_c\gamma_T t}\left(\frac{1}{1-t\overline{\gamma}}\right)^{L_c},
\end{aligned} \tag{4.41}$$

where

$$I(l,t)=\frac{1}{\overline{\gamma}t-\frac{L_c+l}{L_c}}\left[\exp\left(\frac{L_c\gamma_T(tL_c\overline{\gamma}-L_c-l)}{L_c\overline{\gamma}}\right)-1\right], \tag{4.42}$$

π_{L_c} and $A_{(j,k)}$ were defined in (4.22) and (4.38), respectively. With these closed-form results, we can readily evaluate the error performance of different modulation schemes with GSECps.

4.5.2 Complexity analysis

In this subsection, we calculate the average number of path estimations and comparisons needed by GSECps during path selection process over the i.i.d Rayleigh fading channel. This study allows a thorough complexity comparison among GSC, GSEC and GSECps.

Note that compared with conventional GSEC, GSECps adds a ranking process when $L_a < L_c$. Since the ranking process only involves comparisons, the average number of path estimations needed by GSECps, denoted by N, will be the same as GSEC, which was given in (4.29) in a previous section [6, eq. (27)]. For Rayleigh fading channels, (4.29) specializes to

$$\begin{aligned} N_E = &\sum_{k=L_c}^{L} k\binom{k-1}{k-L_c}\left[1-e^{-\frac{\gamma_T}{\bar{\gamma}}}\right]^{k-L_c} e^{-\frac{\gamma_T L_c}{\bar{\gamma}}} \\ &+ L\sum_{k=L-L_c+1}^{L}\binom{L}{k}\left[1-e^{-\frac{\gamma_T}{\bar{\gamma}}}\right]^{k} e^{-\frac{\gamma_T (L-k)}{\bar{\gamma}}}. \end{aligned} \tag{4.43}$$

To calculate the average number of comparisons of GSECps, we first note that every path examination involves one path estimation and one comparison. If $L_a \geq L_c$, according to the operation of GSECps, the receiver stops examining paths whenever it has found L_c acceptable paths. Therefore, in this case, the number of comparisons will be equal to the number of path examinations. Hence, the average number of comparisons for the $L_a \geq L_c$ case, denoted by N_A, can be shown to be given by

$$N_A = \sum_{k=L_c}^{L} k\binom{k-1}{k-L_c}\left[F_\gamma(\gamma_T)\right]^{k-L_c}\left[1-F_\gamma(\gamma_T)\right]^{L_c}. \tag{4.44}$$

On the other hand, when $L_a < L_c$, GSECps will first examine all L available paths. Therefore, the number of comparisons associated with path examinations is L. Then GSECps ranks the $L-L_a$ unacceptable paths to select $L_c - L_a$ paths with the highest instantaneous SNRs. It is not hard to show that the number of comparisons associated with the ranking process is $\sum_{k=1}^{L_c-L_a}(L-L_a-k)$. Therefore, for any L_a, $0 \leq L_a < L_c$, the number of comparisons is $L + \sum_{k=1}^{L_c-L_a}(L-L_a-k)$. Hence, the average number of comparisons for the $L_a < L_c$ case, denoted by N_B, is given by

$$N_B = \sum_{j=0}^{L_c-1}\Pr[L_a=j]\left[L + \sum_{k=1}^{L_c-j}(L-j-k)\right], \tag{4.45}$$

where $\Pr[L_a = j]$ is the probability that there are exactly j acceptable paths. It can be shown, with the assumption of i.i.d. fading paths, that $\Pr[L_a = j]$ is mathematically given by

$$\Pr[L_a = j] = \binom{L}{j} \left[F_\gamma(\gamma_T)\right]^{L-j} \left[1 - F_\gamma(\gamma_T)\right]^j. \tag{4.46}$$

By combining these two mutually exclusive cases, we obtain the expression for the overall average number of comparisons needed by GSECps over i.i.d. fading channels, denoted by N_C, as

$$\begin{aligned} N_C &= N_A + N_B \\ &= \sum_{k=L_c}^{L} k \binom{k-1}{k-L_c} \left[F_\gamma(\gamma_T)\right]^{k-L_c} \left[1 - F_\gamma(\gamma_T)\right]^{L_c} \\ &\quad + \sum_{L_a=0}^{L_c-1} \left[L + \sum_{k=1}^{L_c-L_a} (L - L_a - k)\right] \binom{L}{L_a} \left[F_\gamma(\gamma_T)\right]^{L-L_a} \left[1 - F_\gamma(\gamma_T)\right]^{L_a}. \end{aligned} \tag{4.47}$$

For Rayleigh fading channels, N_C specializes to

$$\begin{aligned} N_C &= \sum_{k=L_c}^{L} k \binom{k-1}{k-L_c} \left[1 - e^{-\frac{\gamma_T}{\overline{\gamma}}}\right]^{k-L_c} e^{-\frac{\gamma_T L_c}{\overline{\gamma}}} \\ &\quad + \sum_{L_a=0}^{L_c-1} \left[L + \sum_{k=1}^{L_c-L_a} (L - L_a - k)\right] \binom{L}{L_a} \left[1 - e^{-\frac{\gamma_T}{\overline{\gamma}}}\right]^{L-L_a} e^{-\frac{\gamma_T L_a}{\overline{\gamma}}}. \end{aligned} \tag{4.48}$$

For GSEC, there is no ranking process and, as such, the average number of comparisons needed is equal to the number of path examinations, which has been given in (4.43). For GSC, the number of comparisons is always $\sum_{k=1}^{L_c}(L-k)$ to select the strongest L_c paths through comparisons.

4.5.3 Numerical examples

In Fig. 4.7, we study the operation complexity of GSECps in comparison with GSEC and GSC. We set $L = 4$ and $L_c = 2$. In Fig. 4.7(a), we plot the average number of path estimations needed by the three schemes as a function of normalized switching threshold, $\gamma_T/\overline{\gamma}$. As expected, GSECps needs the same number of path estimations as GSEC and both schemes require fewer path estimations than GSC when the threshold is not too large. Only when γ_T is larger than $\overline{\gamma}$ by more than 5 dB will GSECps and GSEC need to estimate all four paths.

In Fig. 4.7(b), the average number of comparisons needed by these schemes during the path selection process is plotted as a function of the normalized switching threshold, $\gamma_T/\overline{\gamma}$. Note that GSC always performs roughly five comparisons to find the two best paths among the four available while the receiver with GSEC performs at most four comparisons between the path SNR and the

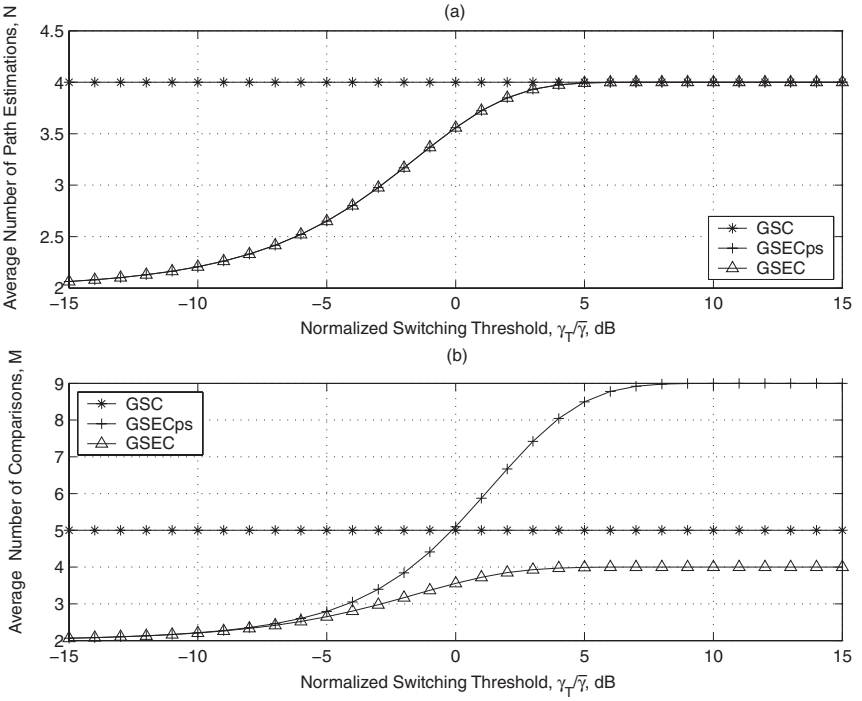

Figure 4.7 Operation complexity of GSECps in comparison with GSC and GSEC ($L = 4$ and $L_c = 2$): (a) average number of path estimations, (b) average number of comparisons [25]. © 2008 IEEE.

switching threshold. The number of comparisons needed by GSECps, however, increases from 2 to 9 in the worst case, which includes 4 comparisons between the instantaneous path SNR and the switching threshold and 5 more comparisons to find the two best unacceptable paths. While GSECps may need four more comparisons than GSC in the worst case, these extra comparisons involve a fixed threshold, and are therefore easy to implement. Moreover, as will be shown in the next subsection, GSECps can provide nearly the same performance as GSC when γ_T is slightly less than $\overline{\gamma}$, where the number of comparisons needed by GSECps is much less than GSC.

Figure 4.8 plots the average error rate of BPSK with GSEC, GSECps and GSC as a function of the average SNR per path with $\gamma_T = 3$ dB. Again, we set $L = 4$ and $L_c = 2$. It is easy to see that when the channel condition is poor, i.e. $\overline{\gamma}$ is small, GSECps has the same error performance as GSC. That is because it is more likely that there are not enough acceptable paths and GSECps operates the same as GSC by selecting the best unacceptable paths. As $\overline{\gamma}$ becomes larger, i.e. the channel condition is improving, the performance advantage of GSECps over GSEC decreases. Note that in this case, the probability of $L_a \geq L_c$ increases and GSECps behaves more like GSEC.

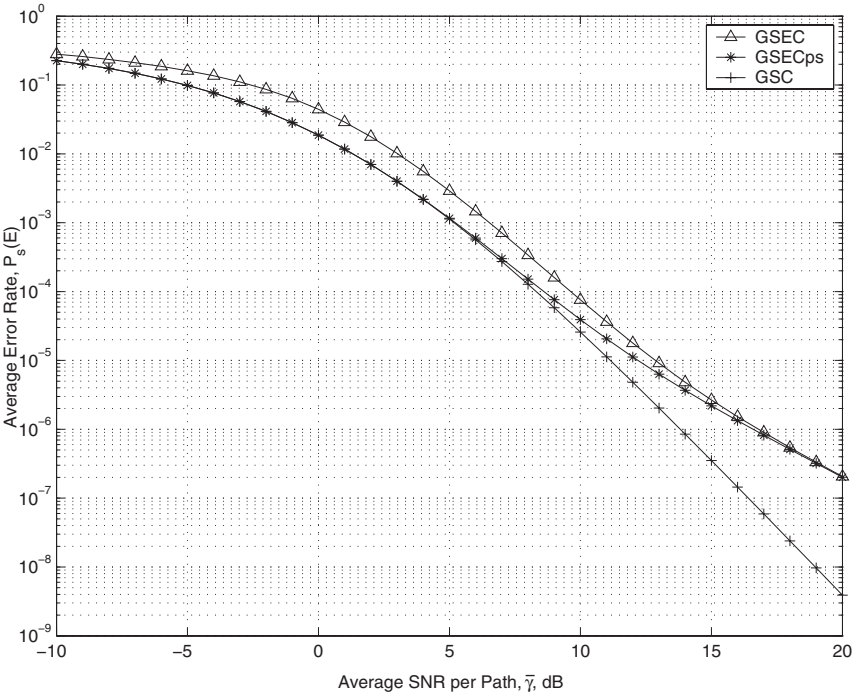

Figure 4.8 Average error rate of BPSK with GSC, GSEC, and GSECps over $L = 4$ i.i.d. Rayleigh fading channels as function of the average SNR per path ($\gamma_T = 3$ dB and $L_c = 2$) [25]. © 2008 IEEE.

In Fig. 4.9, we plot the average error rate of BPSK with the three schemes under consideration as a function of the normalized switching threshold, $\gamma_T/\overline{\gamma}$. It indicates that when γ_T is small, GSECps has the same error performance as GSEC because there are usually enough acceptable paths and GSECps operates more like GSEC. As γ_T increases, the performance of GSEC degrades while the performance of GSECps becomes the same as that of GSC.

Considering Fig. 4.9 together with Fig. 4.7, we can study the trade-off involved among GSECps, GSEC, and GSC. Comparing GSECps with GSEC, we observe that both schemes require the same number of path estimations while GSECps offers better error performance at the cost of slightly more comparison operations. In particular, if $\gamma_T/\overline{\gamma}$ is set to be -7 dB, where GSEC reaches its best error performance, GSECps still offers a 60% decrease in average error rate while requiring 0.05 more comparisons on average. Comparing GSECps with GSC, we can see that if we set $\gamma_T/\overline{\gamma} = -3$ dB, GSECps has nearly the same error performance as GSC, but needs fewer path estimations and comparisons. In conclusion, GSECps achieves better performance–complexity trade-off than both GSEC and GSC.

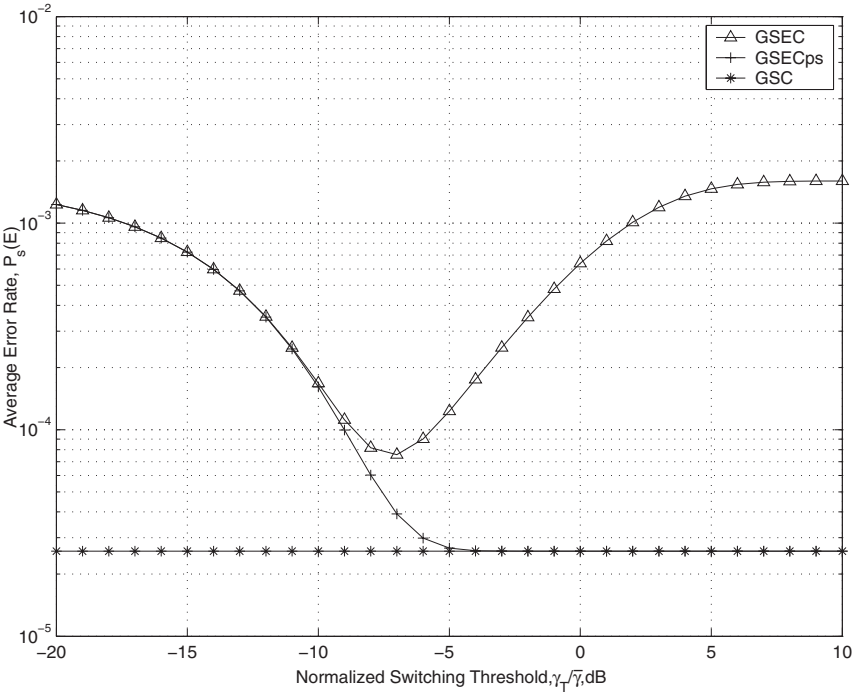

Figure 4.9 Average error rate of BPSK with GSC, GSEC, and GSECps over $L = 4$ i.i.d. Rayleigh fading channels as function of the normalized switching threshold $\gamma_T/\overline{\gamma}$ ($L_c = 2$) [25]. © 2008 IEEE.

4.6 Summary

In this chapter, we studied four representative advanced diversity combining schemes for a diversity-rich environment. The common basic idea is to reduce the combiner hardware complexity and/or processing power by only combining a proper selected path subset in the optimal MRC fashion. We derived the exact statistics of their combiner output SNR, which are in turn applied to the performance analysis of these schemes over a generalized fading channel. Whenever feasible, we also quantified the associated complexity of each scheme in terms of the average number of active MRC branches and the average number of path estimations. Selected numerical examples were presented and discussed to illustrate the trade-off among different schemes.

4.7 Bibliography notes

Win and Winters [11] present a virtual branch-based method to analyze the performance of the GSC scheme over fading channels. The analysis of GSC over

general correlated fading has also been addressed (see for example [15, 28]). The GSC scheme has also been designed based on the log-likelihood ratio of each diversity branch [29]. The idea of a hybrid combining scheme was also considered for the EGC scheme in [30]. A modified version of the AT-GSC scheme, which eliminates the error state of no path selection, was proposed and studied by Chen and Tellambura [31]. Xiao and Dong propose a modified version of the NT-GSC scheme and present a new analytical method for the performance analysis of both GSC and NT-GSC [23]. Femenias [32] propose a generalized sort, switch, and examine combining (GSSEC) scheme and compared it with GSC and GSEC schemes.

References

[1] W. C. Jakes, *Microwave Mobile Communication*, 2nd ed. Piscataway, NJ: IEEE Press, 1994.

[2] G. L. Stüber, *Principles of Mobile Communications*, 2nd ed. Norwell, MA: Kluwer Academic Publishers, 2000.

[3] N. Kong, T. Eng and L. B. Milstein, "A selection combining scheme for RAKE receivers," in *Proc. IEEE Int. Conf. Univ. Personal Comm. ICUPC'95*, Tokyo, Japan, November 1995, pp. 426–429.

[4] M. Z. Win and Z. A. Kostić, "Virtual path analysis of selective Rake receiver in dense multipath channels," *IEEE Commun. Letters*, vol. 3, no. 11, pp. 308–310, November 1999.

[5] Y. Roy, J.-Y. Chouinard and S. A. Mahmoud, "Selection diversity combining with multiple antennas for MM-wave indoor wireless channels," *IEEE J. Select. Areas Commun.*, vol. SAC-14, no. 4, pp. 674–682, May 1998.

[6] H.-C. Yang and M.-S. Alouini, "Generalized switch and examine combining (GSEC): a low-complexity combining scheme for diversity rich environments," *IEEE Trans. Commun.*, vol. COM-52, no. 10, pp. 1711–1721, October, 2004.

[7] K. J. Kim, S. Y. Kwon, E. K. Hong and K. C. Whang, "Comments on 'Comparison of diversity combining techniques for Rayleigh-fading channels'," *IEEE Trans. Commun.*, vol. COM-46, no. 9, pp. 1109–1110, September 1998.

[8] M.-S. Alouini and M. K. Simon, "Performance of coherent receivers with hybrid SC/MRC over Nakagami-m fading channels," *IEEE Trans. Veh. Technol.*, vol. VT-48, no. 4, pp. 1155–1164, July 1999.

[9] M. Z. Win and J. H. Winters, "Analysis of hybrid selection/maximal-ratio combining in Rayleigh fading," *IEEE Trans. Commun.*, vol. COM-47, no. 12, pp. 1773–1776, December 1999. See also *Proceedings of IEEE International Conference on Communications (ICC'99)*, Vancouver, British Columbia, Canada, pp. 6–10, June 1999.

[10] M.-S. Alouini and M. K. Simon, "An MGF-based performance analysis of generalized selective combining over Rayleigh fading channels," *IEEE Trans. Commun.*, vol. COM-48, no. 3, pp. 401–415, March 2000.

[11] M. Z. Win and J. H. Winters, "Virtual branch analysis of symbol error probability for hybrid selection/maximal-ratio combining in Rayleigh fading," *IEEE Trans. Commun.*, vol. COM-49, no. 11, pp. 1926–1934, November 2001.

[12] Y. Ma and C. Chai, "Unified error probability analysis for generalized selection combining in Nakagami fading channels," *IEEE J. Select. Areas Commun.*, vol. SAC-18, no. 11, pp. 2198–2210, November 2000.

[13] A. F. Molisch, M. Z. Win and J. H. Winters, "Capacity of MIMO systems with antenna selection," in *Proc. of IEEE Int. Conf. on Commun. (ICC'01)*, Helsinki, Finland, vol. 2, pp. 570–574, June 2001.

[14] A. Annamalai and C. Tellambura, "Analysis of hybrid selection/maximal-ratio diversity combiner with Gaussian errors," *IEEE Trans. Wireless Commun.*, vol. TWC-1, no. 3, pp. 498–512, July 2002.

[15] Y. Ma and S. Pasupathy, "Efficient performance evaluation for generalized selection combining on generalized fading channels," *IEEE Trans. Wireless. Commun.*, Vol. 3, no. 1, pp. 29–34, January 2004.

[16] M. J. Gans, "The effect of Gaussian error in maximal ratio combiners," *IEEE Trans. Commun. Technol.*, vol. COM-19, no. 4, pp. 492–500, August 1971.

[17] B. R. Tomiuk, N. C. Beaulieu and A. A. Abu-Dayya, "General forms for maximal ratio diversity with weighting errors," *IEEE Trans. Commun.*, vol. COM-47, no. 4, pp. 488–492, April 1999. See also *Proc. IEEE Pacific Rim Conf. on Communications, Computers and Signal Processing (PACRIM'99)*, Victoria, BC, Canada, pp. 363–368, May 1995.

[18] M. K. Simon and M.-S. Alouini, *Digital Communications over Generalized Fading Channels: A Unified Approach to Performance Analysis*. New York, NY: John Wiley & Sons, 2000.

[19] A. I. Sulyman and M. Kousa, "Bit error rate performance of a generalized diversity selection combining scheme in Nakagami fading channels," in *Proc. of IEEE Wireless Commun. and Networking Conf. (WCNC'00)*, Chicago, Illinois, September 2000, pp. 1080–1085.

[20] M. K. Simon and M.-S. Alouini, "Performance analysis of generalized selection combining with threshold test per branch (T-GSC)," *IEEE Trans. Veh. Technol.*, vol. VT-51, no. 5, pp. 1018 –1029, September 2002.

[21] A. Annamalai, G. Deora and C. Tellambura, "Unified analysis of generalized selection diversity with normalized threshold test per branch," in *Proc. of IEEE Wireless Commun. and Networking Conf. (WCNC'03)*, New Orleans, Louisiana, vol. 2, March 2003, pp. 752–756.

[22] X. Zhang and N. C. Beaulieu, "SER and outage of thresholdbased hybrid selection/maximal-ratio combining over generalized fading channels," *IEEE Trans. Commun.*, vol. 52, no. 12, pp. 2143–2153, December 2004.

[23] L. Xiao and X. Dong, "Unified analysis of generalized selection combining with normalized threshold test per branch," *IEEE Trans. Wireless Commun.*, vol. 5, no. 8, pp. 2153–2163, August 2006.

[24] H.-C. Yang and M.-S. Alouini, "Performance analysis of multibranch switched diversity systems," *IEEE Trans. Commun.*, vol. COM-51, no. 5, pp. 782–794, May 2003.

[25] H.-C. Yang and L. Yang, "Tradeoff analysis of performance and complexity on GSECps diversity combining scheme," *IEEE Trans. on Wireless Commun.*, vol. TWC-7, no. 1, pp. 32–36, January 2008.

[26] H.-C. Yang and M.-S. Alouini, "Improving the performance of switched diversity with post-examining selection," *IEEE Trans. Wireless Commun.*, vol. TWC-5, no. 1, pp. 67–71, January 2006.

[27] H.-C. Yang, "New results on ordered statistics and analysis of minimum-selection generalized selection combining (GSC)," *IEEE Trans. Wireless Commun.*, vol. TWC-5, no. 7, July 2006. See also the conference version in *Proc. of IEEE Int. Conf. on Commun. (ICC'05)*.

[28] R. K. Mallik and M. Z. Win, "Analysis of hybrid selection/maximal-ratio combining in correlated Nakagami fading," vol. COM-50, no. 8, pp. 1372–1383, August, 2002.

[29] S. W. Kim, Y. G. Kim and M. K. Simon, "Generalized selection combining based on the log-likelihood ratio," *IEEE Trans. Commun.*, vol. COM-52, no. 4, pp. 521–524, April 2004.

[30] Y. Ma and J. Jin, "Unified performance analysis of hybrid-selection/equal-gain combining," *IEEE Trans. Veh. Technol.*, vol. VT-56, no. 4, pp. 1866–1873, July 2007.

[31] Y. Chen and C. Tellambura, "A new hybrid generalized selection combining scheme and its performance over fading channels," *Proc. IEEE Wireless Commun. Net. Conf. (WCNC'04)*, Atlanta, Georgia, vol. 2, pp. 926–932, March 2004.

[32] G. Femenias, "Performance analysis of generalized sort, switch, and examine combining," *IEEE Trans. Commun.*, vol. COM-54, no. 12, pp. 2137–2143, December 2006.

5 Adaptive transmission and reception

5.1 Introduction

Most conventional diversity techniques target the worst-case scenario [1]. The general principle is to perform a fixed set of combining operations on differently faded replicas such that the combiner output signal exhibits a better quality. This basic design principle manifests itself in the conventional MRC, EGC, and SC schemes as well as those more recent advanced combining schemes discussed in the previous chapter, such as GSC, T-GSC, and GSEC. While this approach has proven to be very effective in improving the performance of wireless communication systems, especially when the channel experiences deep fades, it may lead to an inefficient utilization of the receiver processing resource when the channel becomes more favorable. Note that the same set of combining operations will still be performed even though the system performance may be acceptable with fewer combining operations in this case. This observation motivates the recent interest in adaptive diversity combining for receiver power-saving purposes.

The basic idea of adaptive combining schemes is to adaptively utilize the diversity combiner resource in such a way that the combiner output signal satisfies a certain quality requirement. The generic structure of the adaptive diversity receiver is shown in Fig. 5.1. Specifically, the receiver will just perform enough combining operations such that the quality of the combiner output signal becomes acceptable. For example, minimum selection GSC (MS-GSC) [2–4] is one of the first adaptive combining schemes. With MS-GSC, the receiver combines the least number of best diversity branches such that the SNR of the combiner output signal exceeds a certain predetermined threshold. Other sample adaptive combining schemes include output threshold MRC (OT-MRC), output threshold GSC (OT-GSC) [5], and minimum estimation and combining GSC (MEC-GSC) [6].

It is worth mentioning that these adaptive combining schemes can also be viewed as the generalization of the conventional SSC scheme [1]. Recall that with the SSC scheme, the receiver continues to use its current diversity branch as long as its SNR is above a certain threshold (i.e. no combining operation). When the SNR of the current branch is below the threshold, the receiver switches to the other branch (the simplest combining operation) and uses it for data reception. As such, SSC is one of the simplest adaptive combining schemes.

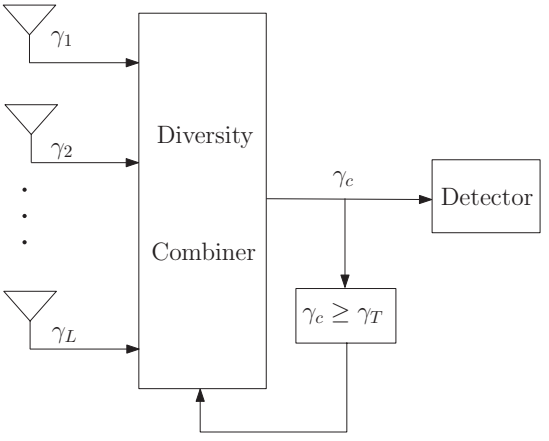

Figure 5.1 Structure of an adaptive diversity receiver.

The aforementioned adaptive combining schemes, such as MS-GSC or OT-MRC, will perform more complex combining operations if necessary. Note also that these adaptive schemes differ from those threshold-based combining schemes discussed in the previous chapter, e.g. the T-GSC and GSEC schemes [7–9], in that the threshold checking is performed on the combiner output rather than on each individual branch. SSC/SEC schemes appear in both categories as the output SNR with these schemes is the SNR of the current used branch.

In the following sections, we first present and study three representative adaptive combining schemes, namely OT-MRC, MS-GSC, and OT-GSC. We carry out a thorough and accurate performance versus complexity trade-off analysis on each of them with the help of the order statistics results. After that, we illustrate the general applicability of the adaptive combining idea by considering adaptive transmit diversity systems [10] and RAKE finger management schemes [11]. We will show that the adaptive combining principle can bring significant complexity saving at the cost of little or no performance loss. Finally, we investigate the joint design of adaptive diversity combining with adaptive modulation. Specifically, noting that both adaptive modulation and adaptive combining utilize some predetermined threshold in their operation, we naturally combine them and arrive at three different joint adaptive modulation and diversity combining (AMDC) schemes [12]. The performance and efficiency of each schemes are accurately quantified and illustrated using selected numerical examples.

5.2 Output-threshold MRC

With OT-MRC, the receiver tries to increase the combined SNR γ_c above the output threshold γ_T by gradually changing from a low-order MRC scheme to a higher-order MRC scheme. For the sake of convenience and clarity, we adopt

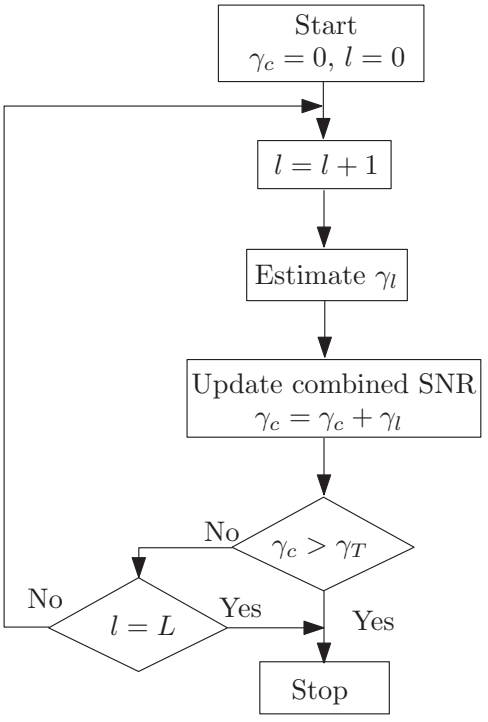

Figure 5.2 Flow chart for OT-MRC mode of operation.

a discrete-time implementation in the following presentation. More specifically, short guard periods are periodically, usually at the rate of channel coherent time, inserted into the transmitted signal. During these guard periods, the receiver reaches the appropriate diversity combining decisions for the subsequent data burst.

In each guard period, starting from the single-branch case, the OT-MRC combiner successively estimates additional diversity paths, activates MRC branches and applies MRC to the estimated paths in order to raise the combined SNR above the threshold γ_T. The flow chart in Fig. 5.2 illustrates the mode of operation of OT-MRC. In particular, after the guard interval starts, the combiner checks the SNR of the first available diversity path, denoted by γ_1. If it is above the threshold γ_T, then the combiner simply uses this path for data reception, i.e. $\gamma_c = \gamma_1$. This is exactly the same as the no-diversity case. If $\gamma_1 < \gamma_T$, the combiner estimates a second diversity path, whose SNR is denoted by γ_2, activates another MRC branch, and applies MRC to these two paths. If the resulting combined SNR $\gamma_c = \gamma_1 + \gamma_2$ is above γ_T, then the combiner just acts as a dual-branch MRC. Otherwise (i.e. $\gamma_1 + \gamma_2 < \gamma_T$), a third path is estimated and another MRC branch is activated. This process stops whenever the combined SNR γ_c exceeds the threshold γ_T. Note that an L-branch MRC receiver will be used only in the worst case when the combined SNR γ_c is still below γ_T after the activation of $L - 1$ MRC branches.

Based on the OT-MRC mode of operation, we can see that the receiver does not always utilize all the L available diversity paths. If the MRC-combined SNR after the activation of the first l MRC branches is above the threshold, the receiver does not need to estimate the remaining $L-l$ diversity paths. Correspondingly, only l MRC branches need to be active during the data reception. These features constitute the main power saving of OT-MRC over the traditional MRC combiner, where all L diversity paths always have to be estimated and all L MRC branches are always active during data reception. This comes, of course, at the cost of a certain performance loss, which will be accurately quantified in the following section.

5.2.1 Statistics of output SNR

To analyze the performance of OT-MRC, we need a statistical characterization of the combiner output SNR. In this subsection, we derive the cumulative distribution function (CDF), the probability density function (PDF), and the moment generating function (MGF) of the combiner output SNR with OT-MRC.

Based on the mode of operation of OT-MRC, we note that the events that l diversity paths (or equivalently, an l-branch MRC) are used for data reception, $l = 1, 2, \cdots, L$, are mutually exclusive. Applying the total probability theorem, we can write the CDF of the combined SNR, $F_{\gamma_c}^{\mathrm{MRC}}(\cdot)$, in a summation form as

$$\begin{aligned} F_{\gamma_c}(x) &= \Pr[\gamma_c < x] \\ &= \sum_{l=1}^{L} \Pr\left[\gamma_c = \sum_{j=1}^{l} \gamma_j \ \& \ \gamma_c < x\right], \end{aligned} \tag{5.1}$$

where $\gamma_c = \sum_{j=1}^{l} \gamma_j$ corresponds to the event that an l-branch MRC scheme is used for data reception. We observe that with OT-MRC (i) a single branch receiver is used when the SNR of the first diversity path is above the threshold (i.e. $\gamma_1 \geq \gamma_T$), (ii) an l-branch MRC (with $2 \leq l \leq L-1$) is used when the combined SNR of an $l-1$-branch MRC is below the threshold whereas the combined SNR of an l-branch MRC is above the threshold (i.e. $\sum_{j=1}^{l-1} \gamma_j < \gamma_T$ and $\sum_{j=1}^{l} \gamma_j \geq \gamma_T$), and (iii) an L-branch MRC is used when the combined SNR of an $L-1$-branch MRC is below the threshold (i.e. $\sum_{j=1}^{L-1} \gamma_j < \gamma_T$). Mathematically speaking, we then have

$$\Pr\left[\gamma_c = \sum_{j=1}^{l} \gamma_j\right] = \begin{cases} \Pr[\gamma_1 \geq \gamma_T], & l = 1; \\ \Pr[\sum_{j=1}^{l-1} \gamma_j < \gamma_T \ \& \ \sum_{j=1}^{l} \gamma_j \geq \gamma_T], & 2 \leq l \leq L-1; \\ \Pr[\sum_{j=1}^{L-1} \gamma_j < \gamma_T], & l = L. \end{cases} \tag{5.2}$$

Using (5.2) in (5.1), we can rewrite the CDF of the combined SNR with OT-MRC after some manipulations as

$$\begin{aligned} F_{\gamma_c}(x) &= \Pr[\gamma_T \le \gamma_1 \ \&\ \gamma_1 < x] \\ &\quad + \sum_{l=2}^{L-1} \Pr\left[\sum_{j=1}^{l-1} \gamma_j < \gamma_T \le \sum_{j=1}^{l} \gamma_j \ \&\ \sum_{j=1}^{l} \gamma_j < x\right] \\ &\quad + \Pr\left[\sum_{j=1}^{L-1} \gamma_j < \gamma_T \ \&\ \sum_{j=1}^{L} \gamma_j < x\right] \\ &= \begin{cases} \Pr[\gamma_T \le \gamma_1 < x] \\ \quad + \sum_{l=2}^{L-1} \Pr\left[\sum_{j=1}^{l-1} \gamma_j < \gamma_T \le \sum_{j=1}^{l} \gamma_j < x\right] \\ \quad + \Pr\left[\sum_{j=1}^{L-1} \gamma_j < \gamma_T \ \&\ \sum_{j=1}^{L} \gamma_j < x\right], & \gamma_T < x; \\ \Pr\left[\sum_{j=1}^{L} \gamma_j < x\right], & \gamma_T \ge x. \end{cases} \end{aligned} \tag{5.3}$$

Under the assumption of i.i.d. fading paths, we can rewrite (5.3) in terms of the single-branch CDF, $F_\gamma(\cdot)$, and the PDF of an l-branch MRC output SNR (i.e. $\sum_{j=1}^{l} \gamma_j$), $p_{\gamma_c}^{l-MRC}(\cdot)$, as

$$F_{\gamma_c}(x) = \begin{cases} F_\gamma(x) - F_\gamma(\gamma_T) \\ \quad + \sum_{l=2}^{L-1} \int_0^{\gamma_T} p_{\gamma_c}^{(l-1)-MRC}(y)(F_\gamma(x-y) - F_\gamma(\gamma_T - y))\mathrm{d}y \\ \quad + \int_0^{\gamma_T} p_{\gamma_c}^{(L-1)-MRC}(y) F_\gamma(x-y)\mathrm{d}y, & \gamma_T < x; \\ \int_0^{x} p_{\gamma_c}^{L-MRC}(y)\mathrm{d}y, & \gamma_T \ge x. \end{cases} \tag{5.4}$$

Differentiating $F_{\gamma_c}(x)$ in (5.4) with respect to x, we obtain a generic formula for the PDF of the combined SNR as

$$p_{\gamma_c}(x) = \begin{cases} p_\gamma(x) + \sum_{l=2}^{L} \int_0^{\gamma_T} p_{\gamma_c}^{(l-1)-MRC}(y) F_\gamma(x-y)\mathrm{d}y, & \gamma_T < x; \\ p_{\gamma_c}^{L-MRC}(x), & \gamma_T \ge x, \end{cases} \tag{5.5}$$

where $p_\gamma(\cdot)$ is the single branch SNR PDF. Applying the CDF and PDF of an l-branch MRC output SNR summarized in Table 5.1, we can obtain the CDF and PDF of the combined SNR γ_c for various fading models of interest.

As an example, for the Rayleigh fading case, the CDF of the combined SNR with OT-MRC is given, after integration and some simplifications, by the following closed-form expression

$$F_{\gamma_c}(x) = \begin{cases} 1 - Ae^{-\frac{x}{\bar{\gamma}}}, & \gamma_T < x; \\ 1 - \sum_{l=1}^{L} \frac{1}{(l-1)!} \left(\frac{x}{\bar{\gamma}}\right)^{l-1} e^{-\frac{x}{\bar{\gamma}}}, & \gamma_T \ge x, \end{cases} \tag{5.6}$$

Table 5.1 Closed-form expressions of $p_{\gamma_c}^{l-MRC}(x)$ and $F_{\gamma_c}^{l-MRC}(x)$ for the three popular fading models.

Model	$p_{\gamma_c}^{l-MRC}(x)$	$F_{\gamma_c}^{l-MRC}(x)$
Rayleigh	$\frac{1}{(l-1)!}\frac{x^{l-1}}{\overline{\gamma}^l}e^{-\frac{x}{\overline{\gamma}}}$	$1-e^{-\frac{x}{\overline{\gamma}}}\sum_{i=0}^{l-1}\frac{1}{i!}\left(\frac{x}{\overline{\gamma}}\right)^i$
Rician	$\frac{K+1}{\overline{\gamma}}e^{-lK-\frac{(K+1)}{\overline{\gamma}}x}$ $\left(\frac{K+1}{lK\overline{\gamma}}x\right)^{\frac{l-1}{2}} I_{l-1}\left(2\sqrt{\frac{lK(K+1)}{\overline{\gamma}}x}\right)$	$1-Q_l\left(\sqrt{2lK},\sqrt{\frac{2(K+1)}{\overline{\gamma}}x}\right)$
Nakagami	$\left(\frac{m}{\overline{\gamma}}\right)^{lm}\frac{x^{lm-1}}{\Gamma(lm)}e^{-\frac{m}{\overline{\gamma}}x}$	$1-\frac{\Gamma(lm,\frac{m}{\overline{\gamma}}x)}{\Gamma(lm)}$

where

$$A=\sum_{l=1}^{L}\frac{1}{(l-1)!}\left(\frac{\gamma_T}{\overline{\gamma}}\right)^{l-1}. \tag{5.7}$$

Similarly, the PDF of the combined SNR with OT-MRC is obtained as

$$p_{\gamma_c}(x)=\begin{cases}\frac{A}{\overline{\gamma}}e^{-\frac{x}{\overline{\gamma}}}, & \gamma_T<x;\\ \frac{1}{(L-1)!}\frac{x^{L-1}}{\overline{\gamma}^L}e^{-\frac{x}{\overline{\gamma}}}, & \gamma_T\geq x.\end{cases} \tag{5.8}$$

With the statistics of the combined SNR of OT-MRC derived, we can accurately evaluate the performance of OT-MRC. Specifically, the average error rate of OT-MRC can be calculated by averaging the conditional error rate of an interested modulation scheme, $P_E(\gamma_c)$, over the PDF of the combined SNR γ_c, $f_{\gamma_c}(x)$, given in (5.5). For the important special case of BPSK over Rayleigh fading, we can show, after proper substitution and manipulations, that the average BER with OT-MRC is given by the following closed-form expression

$$\begin{aligned}\overline{P}_b&=\int_0^\infty Q(\sqrt{2x})p_{\gamma_c}(x)\mathrm{d}x \\ &=\frac{1}{2}-\sqrt{\frac{\overline{\gamma}}{1+\overline{\gamma}}}\sum_{l=0}^{L-1}\frac{1}{l!}\left\{\left(\frac{\gamma_T}{\overline{\gamma}}\right)^l Q\left(\sqrt{2\frac{1+\overline{\gamma}}{\overline{\gamma}}\gamma_T}\right)\right. \\ &\quad\left.+\frac{1}{2\sqrt{\pi}}\left(\frac{1}{1+\overline{\gamma}}\right)^l\left[\Gamma\left(l+\frac{1}{2}\right)-\Gamma\left(l+\frac{1}{2},\frac{1+\overline{\gamma}}{\overline{\gamma}}\gamma_T\right)\right]\right\},\end{aligned} \tag{5.9}$$

where $Q(\cdot)$ is the Gaussian Q-function.

In Fig. 5.3(b), we plot the average bit error rate of BPSK with OT-MRC in a Rayleigh fading environment (given in (5.9)) as a function of the SNR threshold γ_T. For reference purposes, the error rate of no diversity and conventional MRC cases are also plotted. As we can see, when the threshold γ_T is small, OT-MRC gives roughly the same performance as the no-diversity case. Conversely, when the threshold γ_T increases, the error rate of OT-MRC decreases and becomes the same as that of the conventional MRC eventually. This is because as γ_T

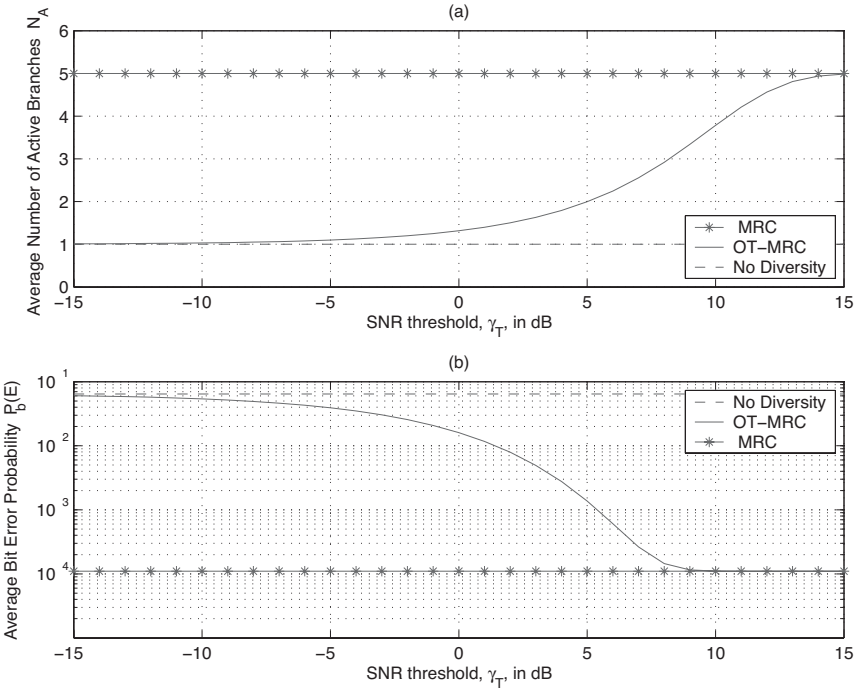

Figure 5.3 Performance of OT-MRC in a Rayleigh fading environment: (a) average bit error rate of BPSK as function of average SNR per path; (b) outage probability as function of outage threshold with $\overline{\gamma} = 10$ dB ($L = 3$ and $\gamma_T = 6$ dB) [5]. © 2005 IEEE.

increases, more paths need to be used to raise the combined SNR above γ_T and this of course leads to a better performance.

5.2.2 Power saving analysis

We now quantify the power savings of OT-MRC scheme by calculating the average number of path estimations during guard period, or equivalently, the average number of active MRC branches during data reception.

Note that with OT-MRC, $l = 1, 2, \cdots, L$, MRC branches may be active during data reception. Since they are mutually exclusive events, we can write the average number of active MRC branches, denoted by N_A, into a finite summation form as

$$N_A = \sum_{l=1}^{L} l \ \Pr\left[\gamma_c = \sum_{j=1}^{l} \gamma_j\right], \tag{5.10}$$

where $\Pr[\gamma_c = \sum_{j=1}^{l} \gamma_j]$ is the probability that an l-branch MRC is used for the subsequent data reception, which was given in (5.2). With the help of the assumption of i.i.d. fading paths, (5.2) can be rewritten in terms of the common

SNR CDF per branch $F_\gamma(\cdot)$ and the combined SNR CDF of an i-branch MRC $F_{\gamma_c}^{l-MRC}(\cdot)$ as

$$\Pr\left[\gamma_c = \sum_{j=1}^{l} \gamma_j\right] = \begin{cases} 1 - F_\gamma(\gamma_T), & l = 1; \\ F_{\gamma_c}^{(l-1)-MRC}(\gamma_T) - F_{\gamma_c}^{l-MRC}(\gamma_T), & 2 \le l \le L-1; \\ F_{\gamma_c}^{(L-1)-MRC}(\gamma_T), & l = L, \end{cases} \quad (5.11)$$

Substituting (5.11) into (5.10), the average number of active MRC branches with OT-MRC can be finally obtained after some simplifications as

$$N_A = 1 + \sum_{l=1}^{L-1} F_{\gamma_c}^{l-MRC}(\gamma_T). \quad (5.12)$$

Note that (5.12) also gives the average number of path estimations needed by OT-MRC during the guard period.

For the Rayleigh fading environment, using an appropriate expression for $F^{(l)}(\cdot)$ from Table 5.1, we obtain the average number of active MRC branches needed with OT-MRC for the Rayleigh fading case as

$$N_A = 1 + \sum_{l=1}^{L-1} \left[1 - e^{-\frac{\gamma_T}{\overline{\gamma}}} \sum_{i=0}^{l-1} \frac{1}{i!} \left(\frac{\gamma_T}{\overline{\gamma}}\right)^i\right]. \quad (5.13)$$

Figure 5.3(a) shows the average number of active MRC branches with OT-MRC in Rayleigh fading environment with $L = 5$. We can see that as the SNR threshold γ_T increases, the average number of active MRC branches increases from 1 to 5, just as expected. When the threshold γ_T is small, a single-branch SNR will be larger than γ_T. As the threshold γ_T increases, it becomes more difficult to raise the combined SNR above γ_T. Note that for conventional MRC, all 5 branches are always active. So with a moderate choice of γ_T, OT-MRC can provide considerable power saving over conventional MRC by maintaining fewer active branches on average. Hence, Fig. 5.3 gives a clear view of the trade-off of power consumption versus performance for OT-MRC. The choice of the SNR threshold γ_T is of critical importance in this trade-off. By looking at Fig. 5.3(a) and 5.3(b) simultaneously, we can see that if γ_T is set, for example, to 10 dB in this scenario, OT-MRC gives the same error performance as the conventional MRC but it just needs less than 4 active MRC branches on average. Therefore, we can conclude that OT-MRC can achieve the optimal MRC performance while offering a notable amount of power savings.

5.3 Minimum selection GSC

Minimum selection GSC (MS-GSC) was first proposed in [2] as a power-saving implementation of the GSC scheme. With MS-GSC, the receiver combines the least number of best diversity paths such that the combiner output SNR is above a certain threshold. Both the simulation study in [2] and the preliminary

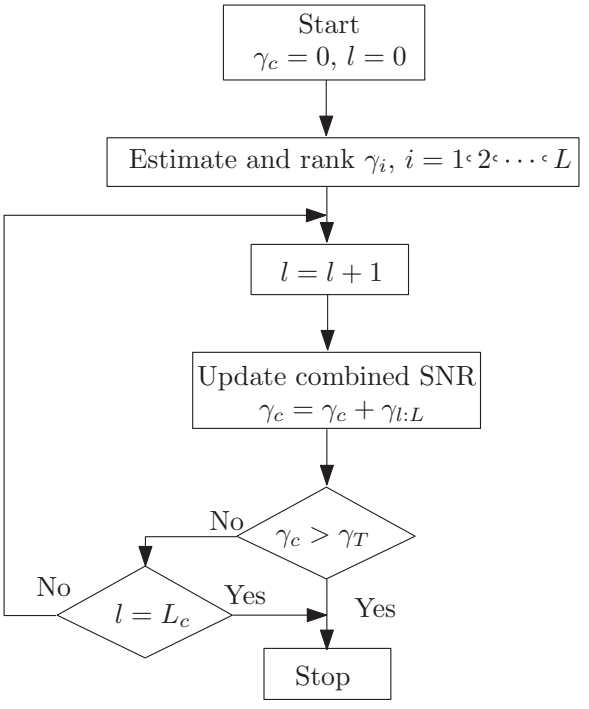

Figure 5.4 Flow chart for MS-GSC mode of operation.

theoretical analysis in [3] show that MS-GSC can save a considerable amount of processing power by keeping fewer MRC branches active on average. In what follows, we present the mode of operation of MS-GSC and derive the statistics of the combined SNR, which involves the new results of order statistics from the previous chapter. The statistical results are then applied to the exact performance analysis of MS-GSC over fading channels.

5.3.1 Mode of operation

As is usually the case in practice, we assume a discrete-time implementation approach where combining decisions are made during a short guard period before the transmission of data burst. With MS-GSC, the receiver combines the least number of best branches such that the SNR of combined signal, denoted by γ_c, is greater than a preselected output threshold, γ_T. The flow chart in Fig. 5.4 explains the mode of operation of MS-GSC, where $\gamma_{l:L}$ denotes the SNR of the lth strongest path. In particular, after the guard period starts, the receiver first estimates and ranks the SNR of all diversity paths. Then, starting from the best path, i.e. the path whose SNR is equal to $\gamma_{1:L}$, the receiver tries to increase the combined SNR γ_c above the threshold γ_T by combining an increasing number of diversity paths. More specifically, if $\gamma_{1:L} \geq \gamma_T$, then only the strongest diversity path will be used, i.e. $\gamma_c = \gamma_{1:L}$. In this case, the receiver acts as an L-branch

selection combiner. If $\gamma_{1:L} < \gamma_T$, then the receiver will activate another MRC-branch, find the second strongest path and apply MRC to the two strongest paths. If the output SNR, now equal to $\gamma_{1:L} + \gamma_{2:L}$, is greater than γ_T, only two-branch MRC will be used for data reception, i.e. $\gamma_c = \gamma_{1:L} + \gamma_{2:L}$. Similarly, if the output SNR of $i-1$-branch MRC $\sum_{j=1}^{i-1} \gamma_{j:L}$ is less than γ_T and the output SNR of i-branch MRC $\sum_{j=1}^{i} \gamma_{j:L}$ is greater than γ_T, then i strongest paths will be combined for the succeeding data burst reception. This process is continued until either the combined SNR is above γ_T or all L_c MRC branches are activated. In the latter case, the receiver will act as a traditional L/L_c GSC combiner, i.e. the L_c strongest paths are combined in an MRC fashion.

The mode of operation of MS-GSC can be mathematically summarized as

$$\begin{aligned}
\gamma_c = \gamma_{1:L} \quad &\text{iff} \quad \gamma_{1:L} \geq \gamma_T; \\
\gamma_c = \gamma_{1:L} + \gamma_{2:L} \quad &\text{iff} \quad \gamma_{1:L} < \gamma_T \ \& \ \gamma_{1:L} + \gamma_{2:L} \geq \gamma_T; \\
&\vdots \\
\gamma_c = \sum_{j=1}^{i} \gamma_{j:L} \quad &\text{iff} \quad \sum_{j=1}^{i-1} \gamma_{j:L} < \gamma_T \ \& \ \sum_{j=1}^{i} \gamma_{j:L} \geq \gamma_T; \\
&\vdots \\
\gamma_c = \sum_{j=1}^{L_c} \gamma_{j:L} \quad &\text{iff} \quad \sum_{j=1}^{L_c-1} \gamma_{j:L} < \gamma_T.
\end{aligned} \tag{5.14}$$

5.3.2 Statistics of output SNR

With the help of the order statistics results from the previous chapter, we now derive the statistical characterization of the combined SNR with MS-GSC. From the mode of operation of MS-GSC, we can see that the events $\gamma_c = \sum_{j=1}^{i} \gamma_{(j)}$ are mutually exclusive. Applying the total probability theorem, we can write the CDF of γ_c as

$$\begin{aligned}
F_{\gamma_c}(x) &= \Pr[\gamma_c < x] \\
&= \sum_{i=1}^{L_c} \Pr[\gamma_c = \sum_{j=1}^{i} \gamma_{j:L} \ \& \ \gamma_c < x].
\end{aligned} \tag{5.15}$$

Applying the mode of operation of MS-GSC as summarized in (5.14), we have

$$\begin{aligned}
F_{\gamma_c}(x) = &\Pr[\gamma_{1:L} \geq \gamma_T \ \& \ \gamma_c = \gamma_{1:L} < x] \\
&+ \sum_{i=2}^{L_c-1} \Pr[\sum_{j=1}^{i-1} \gamma_{j:L} < \gamma_T \ \& \ \gamma_c = \sum_{j=1}^{i} \gamma_{j:L} \geq \gamma_T \ \& \ \gamma_c < x] \\
&+ \Pr[\sum_{j=1}^{L_c-1} \gamma_{j:L} < \gamma_T \ \& \ \gamma_c = \sum_{j=1}^{L_c} \gamma_{j:L} < x].
\end{aligned} \tag{5.16}$$

Note that only when $\gamma_c = \sum_{j=1}^{L_c} \gamma_{(j)}$ can the combined SNR be smaller than γ_T. We can rewrite the CDF of γ_c as

$$F_{\gamma_c}(x) = \begin{cases} F_{\Gamma_1}(x) - F_{\Gamma_1}(\gamma_T) \\ \quad + \sum_{i=2}^{L_c} F_{\gamma_c}^{(i)}(x) + F_{\Gamma_{L_c}}(\gamma_T), & x \geq \gamma_T; \\ F_{\Gamma_{L_c}}(x), & 0 \leq x < \gamma_T, \end{cases} \tag{5.17}$$

where $F_{\Gamma_i}(\cdot)$ is the CDF of the sum of the first i largest path SNRs and $F_{\gamma_c}^{(i)}(x)$ denotes the probability $\Pr[\sum_{j=1}^{i-1} \gamma_{(j)} < \gamma_T \ \& \ \gamma_T \leq \sum_{j=1}^{i} \gamma_{(j)} < x]$. The statistics of the sum of the first i largest path SNRs has been extensively studied in the previous chapter during the discussion of the conventional GSC scheme. Specifically, the closed-form expression of $F_{\Gamma_i}(\cdot)$ for i.i.d. Rayleigh fading case is given by [13, eq. (9.332)]

$$\begin{aligned} F_{\Gamma_i}(x) = \frac{L!}{(L-i)!i!} \Bigg\{ & 1 - e^{-\frac{x}{\overline{\gamma}}} \sum_{k=0}^{i-1} \frac{1}{k!} \left(\frac{x}{\overline{\gamma}}\right)^k \\ & + \sum_{l=1}^{L-i} (-1)^{i+l-1} \frac{(L-i)!}{(L-i-l)!l!} \left(\frac{i}{l}\right)^{i-1} \\ & \times \left[\left(1 + \frac{l}{i}\right)^{-1} \left[1 - e^{-\left(1+\frac{l}{i}\right)\frac{x}{\overline{\gamma}}}\right] \right. \\ & \left. - \sum_{m=0}^{i-2} \left(-\frac{l}{i}\right)^m \left(1 - e^{-\frac{x}{\overline{\gamma}}} \sum_{k=0}^{m} \frac{1}{k!} \left(\frac{x}{\overline{\gamma}}\right)^k \right) \right] \Bigg\}. \end{aligned} \tag{5.18}$$

Let Γ_{i-1} denote the sum of the first $i-1$ largest SNRs, i.e. $\Gamma_{i-1} = \sum_{j=1}^{i-1} \gamma_{j:L}$. Then, the probability $F_{\gamma_c}^{(i)}(x)$ can be rewritten as

$$F_{\gamma_c}^{(i)}(x) = \Pr[\Gamma_{i-1} < \gamma_T \ \& \ \gamma_T \leq \gamma_{i:L} + \Gamma_{i-1} < x], \tag{5.19}$$

which can be calculated using the joint PDF of $\gamma_{i:L}$ and Γ_{i-1}. $p_{\gamma_{i:L},\Gamma_{i-1}}(\cdot,\cdot)$. Specifically, with the help of Fig. 5.5, $F_{\gamma_c}^{(i)}(x)$ can be calculated as

$$F_{\gamma_c}^{(i)}(x) = \begin{cases} \int_{\frac{i-1}{i}\gamma_T}^{\frac{i-1}{i}x} \int_{\gamma_T - y}^{\frac{y}{i-1}} p_{\gamma_{i:L},\Gamma_{i-1}}(z,y)\mathrm{d}z\mathrm{d}y \\ \quad + \int_{\frac{i-1}{i}x}^{\gamma_T} \int_{\gamma_T - y}^{x-y} p_{\gamma_{i:L},\Gamma_{i-1}}(z,y)\mathrm{d}z\mathrm{d}y, & \gamma_T \leq x < \frac{i}{i-1}\gamma_T; \\ F_{\Gamma_{i-1}}(\gamma_T) - F_{\Gamma_i}(\gamma_T), & \frac{i}{i-1}\gamma_T \leq x. \end{cases} \tag{5.20}$$

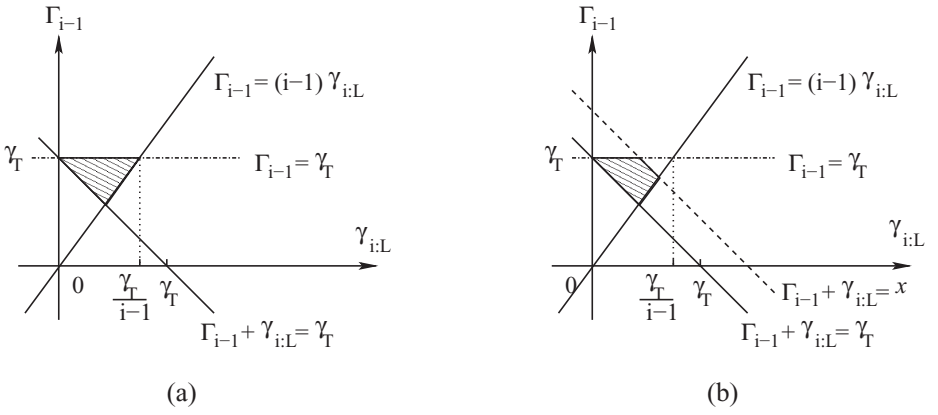

Figure 5.5 The integration region of the joint PDF of Γ_{i-1} and $\gamma_{i:L}$ for calculating (a) $F_{\gamma_c}^{(i)}(x)$, $x \geq i\gamma_T/(i-1)$ and $\Pr[N=i]$; (b) $F_{\gamma_c}^{(i)}(x)$, $\gamma_T \leq x < i\gamma_T/(i-1)$ [4]. © 2006 IEEE.

After substituting (5.20) into (5.17), we obtain the generic expression of the CDF of the combined SNR γ_c with MS-GSC as

$$F_{\gamma_c}(x) = \begin{cases} F_{\Gamma_{L_c}}(x), & 0 \leq x < \gamma_T; \\ F_{\Gamma_1}(x) - F_{\Gamma_1}(\gamma_T) + F_{\Gamma_{L_c}}(\gamma_T) & \\ \quad + \sum_{i=2}^{L_c} \left(\int_{\frac{i-1}{i}\gamma_T}^{\frac{i-1}{i}x} \int_{\gamma_T - y}^{\frac{y}{i-1}} p_{\gamma_{i:L},\Gamma_{i-1}}(z,y)dzdy \right. & \\ \quad \left. + \int_{\frac{i-1}{i}x}^{\gamma_T} \int_{\gamma_T - y}^{x-y} p_{\gamma_{i:L},\Gamma_{i-1}}(z,y)dzdy \right), & \gamma_T \leq x < \frac{L_c}{L_c-1}\gamma_T; \\ \vdots & \\ F_{\Gamma_1}(x) - F_{\Gamma_1}(\gamma_T) + F_{\Gamma_l}(\gamma_T) & \\ \quad + \sum_{i=2}^{l} \left(\int_{\frac{i-1}{i}\gamma_T}^{\frac{i-1}{i}x} \int_{\gamma_T - y}^{\frac{y}{i-1}} p_{\gamma_{i:L},\Gamma_{i-1}}(z,y)\mathrm{d}z\mathrm{d}y \right. & \\ \quad \left. + \int_{\frac{i-1}{i}x}^{\gamma_T} \int_{\gamma_T - y}^{x-y} p_{\gamma_{i:L},\Gamma_{i-1}}(z,y)\mathrm{d}z\mathrm{d}y \right), & \frac{l+1}{l}\gamma_T \leq x < \frac{l}{l-1}\gamma_T; \\ \vdots & \\ F_{\Gamma_1}(x), & 2\gamma_T < x. \end{cases} \tag{5.21}$$

The generic expression for the PDF of the combined SNR with MS-GSC can be obtained by differentiating (5.21) with respect to x and noting that

$$\frac{\mathrm{d}}{\mathrm{d}x} F_{\gamma_c}^{(i)}(x) = \int_{\frac{i-1}{i}x}^{\gamma_T} p_{\gamma_{i:L},\Gamma_{i-1}}(x-y,y)\mathrm{d}y, \ \gamma_T \leq x < \frac{i}{i-1}\gamma_T, \tag{5.22}$$

as

$$p_{\gamma_c}(x) = \begin{cases} p_{\Gamma_1}(x) + \sum_{i=2}^{L_c} \int_{\frac{i-1}{i}x}^{\gamma_T} p_{\gamma_{i:L},\Gamma_{i-1}}(x-y,y)dy & \\ \quad \times (\mathcal{U}(x-\gamma_T) - \mathcal{U}(x - \frac{i}{i-1}\gamma_T)), & x \geq \gamma_T; \\ p_{\Gamma_{L_c}}(x), & 0 \leq x < \gamma_T, \end{cases} \tag{5.23}$$

where $\mathcal{U}(\cdot)$ is the unit step function. It follows that the generic expression of the MGF of the combined SNR with MS-GSC is given by

$$\mathcal{M}_{\gamma_c}(s) = \int_0^{\gamma_T} p_{\Gamma_{L_c}}(x)e^{sx}\mathrm{d}x + \int_{\gamma_T}^{\infty} p_{\Gamma_1}(x)e^{sx}\mathrm{d}x + \sum_{i=1}^{L_c}\int_{\gamma_T}^{\frac{i}{i-1}\gamma_T}\left[\int_{\frac{i-1}{i}x}^{\gamma_T} p_{\gamma_{i:L},\Gamma_{i-1}}(x-y,y)\mathrm{d}y\right]e^{sx}\mathrm{d}x. \quad (5.24)$$

The joint PDF of $p_{\gamma_{i:L},\Gamma_{i-1}}(\cdot,\cdot)$ has been extensively studied in a previous chapter. Specifically, for i.i.d. Rayleigh fading environments, its closed-form expression was given in (3.31) and is reproduced here for convenience

$$p_{\gamma_{l:L},y_l}(x,y) = \sum_{j=0}^{L-l}\frac{(-1)^j L!}{(L-l-j)!(l-1)!(l-2)!j!\overline{\gamma}^l}[y-(l-1)x]^{(l-2)}e^{-\frac{y+(j+1)x}{\overline{\gamma}}}, \quad x\geq 0,\ y\geq (l-1)x. \quad (5.25)$$

After proper substitution and integration, we can obtain the statistics of the combined SNR with MS-GSC in closed form. For example, we can show that the summand in (5.23) is given, after successive integration by parts, by

$$\begin{aligned}\int_{\frac{i-1}{i}x}^{\gamma_T} p_{\gamma_{i:L},\Gamma_{i-1}}(x-y,y)\mathrm{d}y = {} & \frac{L!}{(L-i)!(i-1)!i!\overline{\gamma}}e^{-\frac{x}{\overline{\gamma}}}\left(\frac{i\gamma_T-(i-1)x}{\overline{\gamma}}\right)^{i-1} \\ & + \sum_{j=1}^{L-i}\frac{L!(-1)^{j-i+1}}{(L-i-j)!i!j!\overline{\gamma}}\left(\frac{i}{j}\right)^{i-1}e^{-\frac{(i+j)x}{i\overline{\gamma}}} \\ & \times\left[1-e^{-\frac{j((i-1)x-i\gamma_T)}{i\overline{\gamma}}}\sum_{k=0}^{i-2}\frac{1}{k!}\left(\frac{j((i-1)x-i\gamma_T)}{i\overline{\gamma}}\right)^k\right], \\ & \gamma_T \leq x < \frac{i}{i-1}\gamma_T. \end{aligned} \quad (5.26)$$

Note that the PDF of the sum of the first i order statistics $p_{\Gamma_i}(\cdot)$ is given by [13, eq. (9.325)]

$$\begin{aligned} p_{\Gamma_i}(x) = {} & \frac{L!}{(L-i)!i!}e^{-\frac{x}{\overline{\gamma}}}\left[\frac{x^{i-1}}{\overline{\gamma}^i(i-1)!}\right. \\ & + \frac{1}{\overline{\gamma}}\sum_{l=1}^{L-i}(-1)^{i+l-1}\frac{(L-i)!}{(L-i-l)!l!}\left(\frac{i}{l}\right)^{i-1} \\ & \left.\times\left(e^{-\frac{lx}{i\overline{\gamma}}}-\sum_{m=0}^{i-2}\frac{1}{m!}\left(-\frac{lx}{i\overline{\gamma}}\right)^m\right)\right]. \end{aligned} \quad (5.27)$$

Therefore, the PDF of the combined SNR γ_c with MS-GSC over i.i.d. Rayleigh fading paths can be shown, by specializing (5.23) with (5.26) and (5.27), to be

given in the following closed-form expression

$$p_{\gamma_c}(x) = \begin{cases} \frac{L}{\overline{\gamma}}\left(1-e^{-\frac{x}{\overline{\gamma}}}\right)^{L-1} e^{-\frac{x}{\overline{\gamma}}} \\ \quad + \sum_{i=2}^{L_c}\left\{\frac{L!}{(L-i)!(i-1)!i!\overline{\gamma}} e^{-\frac{x}{\overline{\gamma}}}\left(\frac{i\gamma_T-(i-1)x}{\overline{\gamma}}\right)^{i-1}\right. \\ \quad + \sum_{j=1}^{L-i}\frac{L!(-1)^{j-i+1}}{(L-i-j)!i!j!\overline{\gamma}}\left(\frac{i}{j}\right)^{i-1}\exp\left(-\frac{(i+j)x}{i\overline{\gamma}}\right) \\ \quad \left.\times\left[1-e^{-\frac{j((i-1)x-i\gamma_T)}{i\overline{\gamma}}}\sum_{k=0}^{i-2}\frac{1}{k!}\left(\frac{j((i-1)x-i\gamma_T)}{i\overline{\gamma}}\right)^k\right]\right\} \\ \quad \times(\mathcal{U}(x-\gamma_T)-\mathcal{U}(x-\tfrac{i}{i-1}\gamma_T)), & x\geq\gamma_T; \\ \frac{L!}{(L-L_c)!L_c!}e^{-\frac{x}{\overline{\gamma}}}\left[\frac{x^{L_c-1}}{\overline{\gamma}^{L_c}(L_c-1)!}\right. \\ \quad + \frac{1}{\overline{\gamma}}\sum_{l=1}^{L-L_c}(-1)^{L_c+l-1}\frac{(L-L_c)!}{(L-L_c-l)!l!}\left(\frac{L_c}{l}\right)^{L_c-1} \\ \quad \left.\times\left(e^{-\frac{lx}{L_c\overline{\gamma}}}-\sum_{m=0}^{L_c-2}\frac{1}{m!}\left(-\frac{lx}{L_c\overline{\gamma}}\right)^m\right)\right], & 0\leq x<\gamma_T. \end{cases} \tag{5.28}$$

Furthermore, after substituting the closed-form expression for the Rayleigh PDF of γ_c given in (5.28) into (5.24) and carrying out the integration with the help of the definition of incomplete Gamma function [14, sec. 8.35], we obtain the closed-form expression for the MGF of γ_c as

$$\begin{aligned} \mathcal{M}_{\gamma_c}(s) &= L\sum_{j=0}^{L-1}\binom{L-1}{j}(-1)^j\frac{e^{-\left(\frac{1+j}{\overline{\gamma}}-s\right)\gamma_T}}{1+j-\overline{\gamma}s} \\ &+\sum_{i=2}^{l}\binom{L}{i}\left[\sum_{m=0}^{i-1}\frac{(1-i)^m}{(i-1-m)!}\left(\frac{i\gamma_T}{\overline{\gamma}}\right)^{i-1-m}\mathcal{G}_{i,0}(s)\right. \\ &+\sum_{j=1}^{L-i}\binom{L-i}{j}(-1)^{j-i+1}\left(\frac{i}{j}\right)^{i-1}\left(\frac{e^{-\left(\frac{1+j/i}{\overline{\gamma}}-s\right)\gamma_T}-e^{-\left(\frac{1+j/i}{\overline{\gamma}}-s\right)\frac{i}{i-1}\gamma_T}}{1+j/i-\overline{\gamma}s}\right. \\ &\left.\left.-\sum_{k=0}^{i-2}\sum_{m=0}^{k}\frac{\left(\frac{i-1}{i}j\right)^m\left(-j\frac{\gamma_T}{\overline{\gamma}}\right)^{k-m}\mathcal{G}_{i,j}(s)}{(k-m)!}\right)\right]+\binom{L}{l}\left[\mathcal{F}_l(s)+\sum_{i=1}^{L-l}\binom{L-l}{i}\right. \\ &\left.\times(-1)^{l+i-1}\left(\frac{l}{i}\right)^{l-1}\left(\frac{1-e^{-\left(\frac{1+i/l}{\overline{\gamma}}-s\right)\gamma_T}}{1+i/l-\overline{\gamma}s}-\sum_{m=0}^{l-2}\left(-\frac{i}{l}\right)^m\mathcal{F}_{m+1}(s)\right)\right], \end{aligned} \tag{5.29}$$

where

$$\mathcal{G}_{i,j}(s) = e^{j\frac{\gamma_T}{\overline{\gamma}}}\frac{\Gamma(m+1,\left(\frac{1+j}{\overline{\gamma}}-s\right)\gamma_T)-\Gamma(m+1,\left(\frac{1+j}{\overline{\gamma}}-s\right)\left(\frac{i}{i-1}\right)\gamma_T)}{m!(1+j-\overline{\gamma}s)^{m+1}}, \tag{5.30}$$

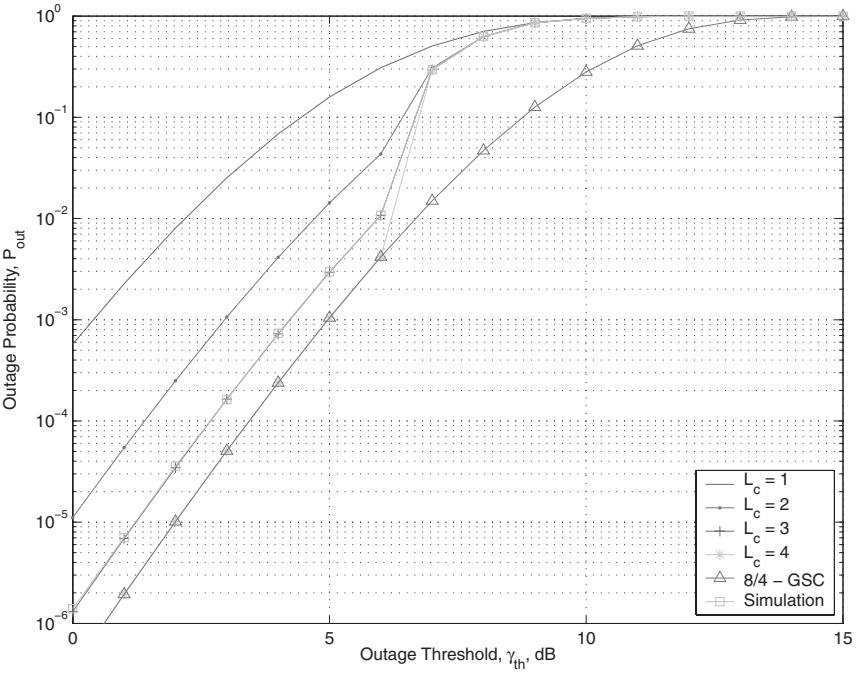

Figure 5.6 Outage probability, or equivalently CDF of the combined SNR, with MS-GSC over i.i.d. Rayleigh fading paths ($L = 8$, $\overline{\gamma} = 3$ dB, and $\gamma_T = 6$ dB) [4]. ©2006 IEEE

$$\mathcal{F}_l(s) = \frac{\Gamma(l) - \Gamma(l, (1/\overline{\gamma} - s)\,\gamma_T)}{(l-1)!(1-\overline{\gamma}s)^l}, \tag{5.31}$$

and $\Gamma(\cdot)$ and $\Gamma(\cdot,\cdot)$ are the complete and the incomplete gamma functions, respectively. It can be shown that when $\gamma_T = \infty$, (5.29) reduces to the MGF of the original GSC over i.i.d. Rayleigh fading paths, as given in [13, eq. (9.430)]. These closed-form results can be readily applied to the error rate analysis of MS-GSC over Rayleigh fading environment.

Figure 5.6 plots the outage probability of MS-GSC over eight i.i.d. Rayleigh fading paths for different number of MRC branches. The outage probability of conventional 8/4-GSC is also plotted for comparison. As we can see, the outage performance improves as the number of MRC branches increases, especially when γ_{th} is smaller than γ_T. In fact, comparing the outage performance of an MS-GSC of $L_c = 4$ case with that of conventional GSC, we can see that they have the same outage performance if $\gamma_{\text{th}} \leq \gamma_T$. Intuitively, this is correct because the combined SNR with MS-GSC can only be smaller than γ_T if the combined SNR of the corresponding conventional MRC is smaller than γ_T. When $\gamma_{\text{th}} > \gamma_T$, the outage performance of MS-GSC degrades rapidly in comparison with the original GSC scheme because the MS-GSC combiner only tries to increase the combined SNR above γ_T. We can conclude from this figure that the SNR threshold γ_T for

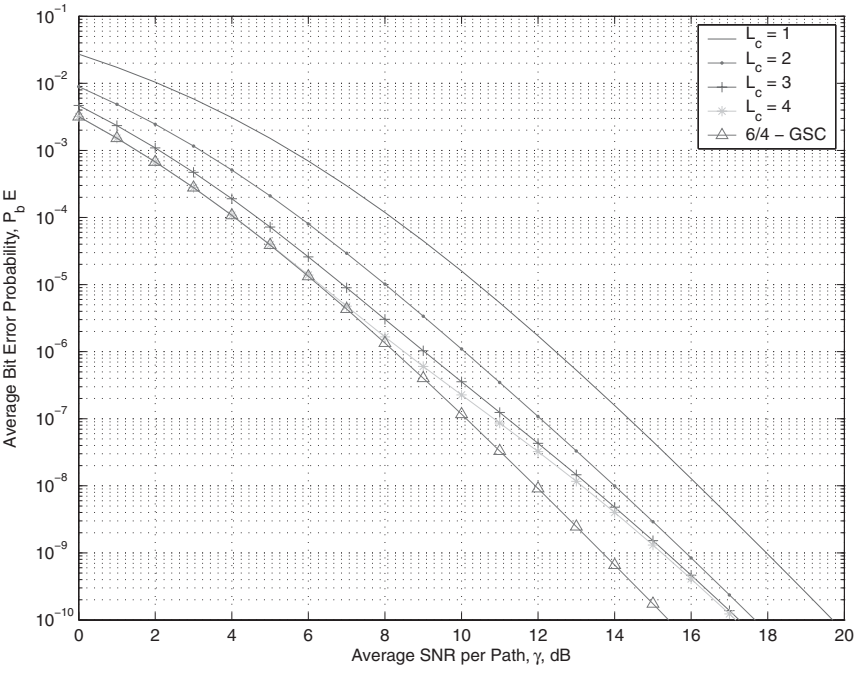

Figure 5.7 Average bit error rate of BPSK with MS-GSC over i.i.d. Rayleigh fading paths ($L = 6$ and $\gamma_T = 10$ dB) [4]. © 2006 IEEE.

MS-GSC should be chosen to be larger than or equal to the outage threshold γ_{th} in practice. As a validation of the analytical result, simulation results for the outage probability of MS-GSC for $L_c = 3$ case are also presented. Note that these simulation results match perfectly our analytical results.

Figure 5.7 shows the average error rate of BPSK with MS-GSC over six i.i.d. Rayleigh fading paths for different number of MRC branches. The error rate of the conventional 6/4-GSC is also plotted for reference. As we can see, the error performance improves as L_c increases, especially in the low average SNR region. Comparing the error rate of the MS-GSC for $L_c = 4$ case and that of conventional GSC, we observe that they have the same error performance in the low average SNR region, but the performance of MS-GSC is not as good in the medium to large SNR region. This BER behavior of MS-GSC can be explained by the following. When the average SNR is small compared to the output threshold, the receiver will always combine the L_c best paths because combining fewer paths will not result in a combined SNR above the required output threshold. As a result, the combiner is actually working as a conventional GSC. On the other hand, when the average SNR is large compared to the output threshold, the receiver will most likely combine the best path because it usually suffices to increase the combined SNR above the output threshold. As a result, the combiner is actually working as a selection combiner (SC).

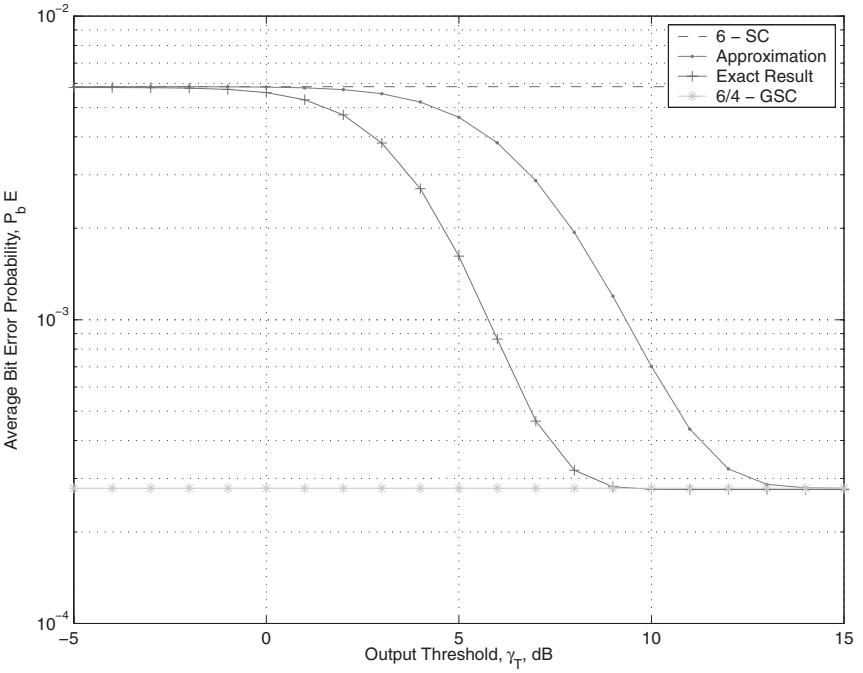

Figure 5.8 Average bit error rate of BPSK with MS-GSC over i.i.d. Rayleigh fading paths as function of output threshold γ_T ($L = 6$, $L_c = 4$, and $\overline{\gamma} = 3$ dB) [4]. © 2006 IEEE.

This interpretation is further verified in Fig. 5.8 where we plot the average error rate of BPSK with 6/4-MS-GSC as a function of the output threshold γ_T. As we can see, the error rate of MS-GSC decreases from the error rate of six-branch SC to that of conventional 6/4-GSC as the output threshold increases from –5 dB to 15 dB. In Fig. 5.8, we also compare the approximate error rate result for MS-GSC in [3] with the exact result. It is observed that the approximation in [3] gives considerable larger error rate values.

5.3.3 Complexity savings

Note that unlike the traditional GSC scheme, where the receiver always needs to find the L_c best paths, MS-GSC needs only to find enough best paths such that the combined SNR is above the threshold γ_T. This feature of MS-GSC constitutes the major complexity savings over conventional GSC. However, the MS-GSC receiver needs to introduce a threshold check at the combiner output. As the threshold checks are much easier to perform than path SNR ordering, MS-GSC requires less computing power than the original GSC for path selection. In addition, the receiver with MS-GSC needs to keep fewer MRC branches active on average during the data reception stage. As such, the valuable processing power of the receiver is saved with MS-GSC. As a quantification of the power savings

with MS-GSC, we derive the average number of active MRC branches with MS-GSC in this section. A distribution of the number of active MRC branches with MS-GSC has been obtained in [3]. Based on the new results on order statistics presented in the previous chapter, we offer a more compact solution for the distribution of the number of active MRC branches and its average.

The number of active MRC branches with MS-GSC, denoted by n, takes values from 1 to L_c. From the mode of operation of MS-GSC, we have that $n = 1$ if and only if $\gamma_{1:L} > \gamma_T$, $n = i$, $2 \le i \le L_c - 1$ if and only if $\sum_{j=1}^{i-1} \gamma_{j:L} < \gamma_T$ and $\sum_{j=1}^{i} \gamma_{j:L} \ge \gamma_T$, and $n = L_c$ if $\sum_{j=1}^{L_c-1} \gamma_{j:L} < \gamma_T$. Therefore, the probability mass function (PMF) of n can be written as

$$\Pr[n=i] = \begin{cases} \Pr[\gamma_{1:L} > \gamma_T], & i = 1; \\ \Pr[\sum_{j=1}^{i-1} \gamma_{j:L} < \gamma_T \ \& \ \sum_{j=1}^{i} \gamma_{j:L} \ge \gamma_T], & 2 \le i \le L_c - 1; \\ \Pr[\sum_{j=1}^{L_c-1} \gamma_{j:L} < \gamma_T], & i = L_c. \end{cases} \quad (5.32)$$

Note that the probability $\Pr[\sum_{j=1}^{i-1} \gamma_{j:L} < \gamma_T \ \& \ \sum_{j=1}^{i} \gamma_{j:L} \ge \gamma_T]$ is equivalent to $\Pr[\Gamma_{i-1} < \gamma_T \ \& \ \Gamma_{i-1} + \gamma_{i:L} \ge \gamma_T]$. Therefore, this probability can be calculated by integrating the joint PDF of Γ_{i-1} and $\gamma_{i:L}$ over the shaded region shown in Fig. 5.5(a). Since the region of integration is exactly the difference of the regions $\Gamma_{i-1} < \gamma_T$ and $\Gamma_{i-1} + \gamma_{i:L} < \gamma_T$, we can instead calculate this probability by using the CDFs of Γ_{i-1} and $\Gamma_{i-1} + \gamma_{i:L}$ as the following

$$\begin{aligned} \Pr[\Gamma_{i-1} < \gamma_T \ \& \ \Gamma_{i-1} + \gamma_{i:L} \ge \gamma_T] &= F_{\Gamma_{i-1}}(\gamma_T) - F_{\Gamma_{i-1}+\gamma_{i:L}}(\gamma_T) \\ &= F_{\Gamma_{i-1}}(\gamma_T) - F_{\Gamma_i}(\gamma_T), \end{aligned} \quad (5.33)$$

where $F_{\Gamma_i}(\cdot) = F_{\sum_{j=1}^{i} \gamma(j)}(\cdot)$, $i = 1, 2, \cdots, L_c - 1$, is the CDF of the sum of the first i order statistics of L random variables. Consequently, the PMF of n can be shown to be given by

$$\Pr[N=i] = \begin{cases} 1 - F_{\Gamma_1}(\gamma_T), & i = 1; \\ F_{\Gamma_{i-1}}(\gamma_T) - F_{\Gamma_i}(\gamma_T), & 2 \le i \le L_c - 1; \\ F_{\Gamma_{L_c-1}}(\gamma_T), & i = L_c. \end{cases} \quad (5.34)$$

The average number of combined paths with MS-GSC can then be easily obtained as

$$\begin{aligned} N_A &= \sum_{i=1}^{L_c} i \Pr[N=i] \\ &= 1 + \sum_{i=1}^{L_c-1} F_{\Gamma_i}(\gamma_T). \end{aligned} \quad (5.35)$$

Note that the closed-form expression of $F_{\Gamma_i}(\cdot)$ for i.i.d. Rayleigh fading was given in (5.18). As such, both the PMF of N and its average $\overline{N}$ can be calculated with closed-form results.

In Figs. 5.9 and 5.10, we study the performance versus power consumption trade-off involved in MS-GSC. Figure 5.9 shows the average error rate of

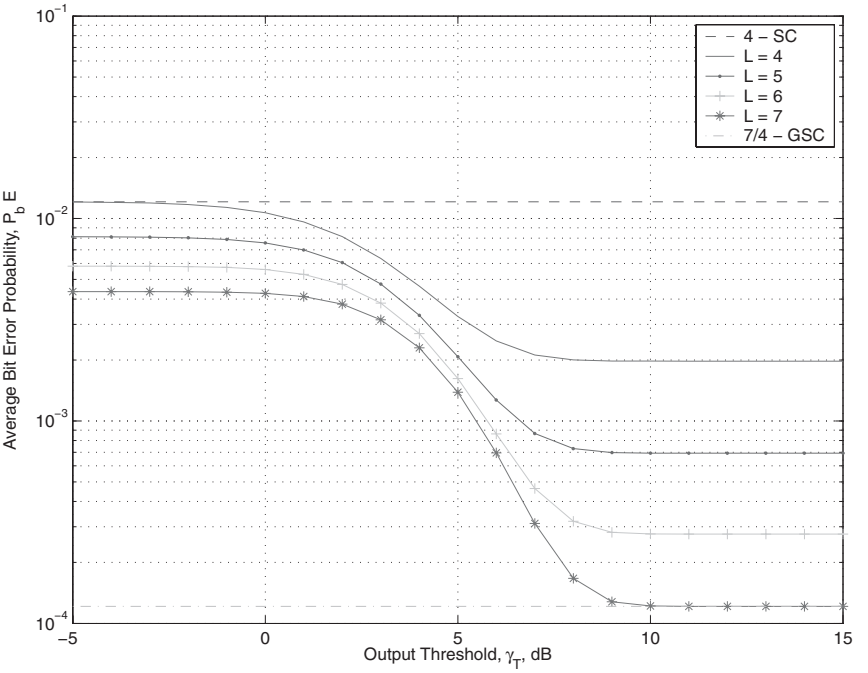

Figure 5.9 Average bit error rate of BPSK with MS-GSC over i.i.d. Rayleigh fading paths as function of output threshold γ_T ($L_c = 4$ and $\overline{\gamma} = 3$ dB) [4]. © 2006 IEEE.

MS-GSC as function of the output threshold with four MRC branches and different number of diversity paths. As expected, the performance of MS-GSC improves as the number of available diversity paths L increases. In addition, the error rate of MS-GSC decrease from that of the L-branch SC to that of the $L/4$-GSC scheme as γ_T increases. Figure 5.10 shows the corresponding average number of active MRC branches with MS-GSC as the function of the output threshold. As we can see, the average number of active MRC branches decreases as the number of available diversity paths increase, but increases as the output threshold increases since it becomes more difficult to raise the combined SNR above the output threshold. Considering both Figs. 5.9 and 5.10, we can see that if the output threshold γ_T is set to 10 dB, MS-GSC has the same error rate performance as the conventional GSC while requiring fewer active branches on average. In particular, for the $L = 6$ and $L_c = 4$ case, MS-GSC needs on average 3.3 active MRC branches, which translates to a power saving of 17.5% compared to conventional GSC.

5.4 Output-threshold GSC

The OT-MRC scheme saves the receiver processing power by estimating and combining a minimum number of paths. It still requires the same hardware complexity as conventional MRC. On the other hand, the MS-GSC scheme can

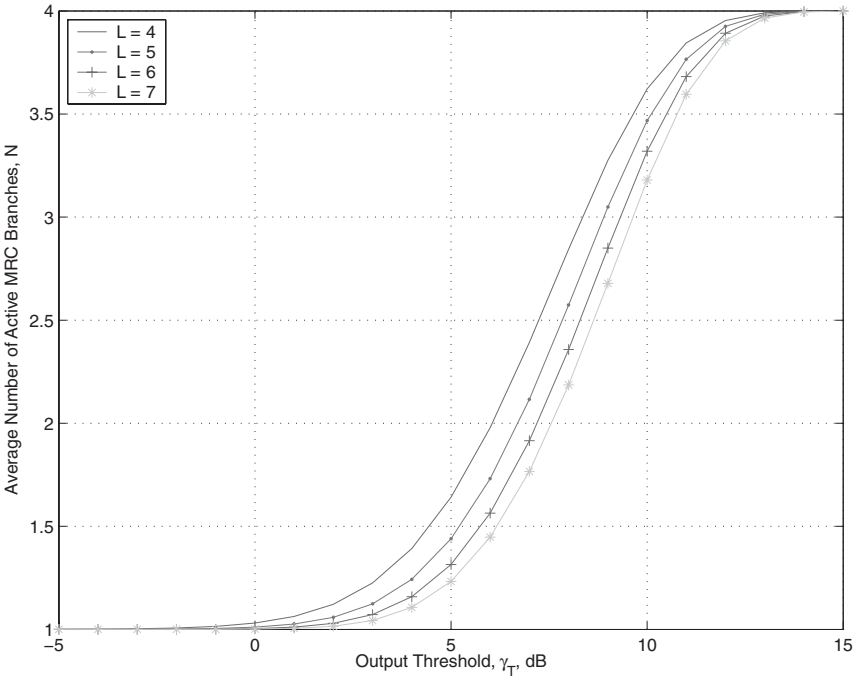

Figure 5.10 Average number of active MRC branches with MS-GSC as a function of output threshold γ_T ($L_c = 4$ and $\overline{\gamma} = 3$ dB) [4]. © 2006 IEEE.

reduce the receiver hardware complexity with the GSC principle and the number of combining paths through minimum best selection. However, the MS-GSC receiver always needs to estimate all L available diversity paths. In this section, we present another power-saving variant of GSC [5], which essentially combines the desired properties of both OT-MRC and MS-GSC schemes. The resulting output-threshold GSC (OT-GSC) scheme is shown to provide considerable processing power saving compared with conventional GSC while maintaining the same diversity benefit.

The OT-GSC scheme estimates and combines additional diversity paths only if necessary. When the number of estimated paths is larger than the number of available MRC branches, the receiver applies the best selection to reduce the hardware complexity. The flow chart in Fig. 5.11 illustrates the mode of operation of OT-GSC. In particular, the operation of OT-GSC combiner can be divided into two stages: an MRC stage followed by a GSC stage.

MRC stage. During the MRC stage, the combiner acts as an L_c-branch OT-MRC combiner. In particular, the combiner tries to improve the combined SNR Γ above the threshold γ_T by gradually changing its configuration from a single-branch MRC to an L_c-branch MRC. If all L_c branches of the MRC combiner have been activated but the combined SNR is still below γ_T, then the receiver operation enters the GSC stage.

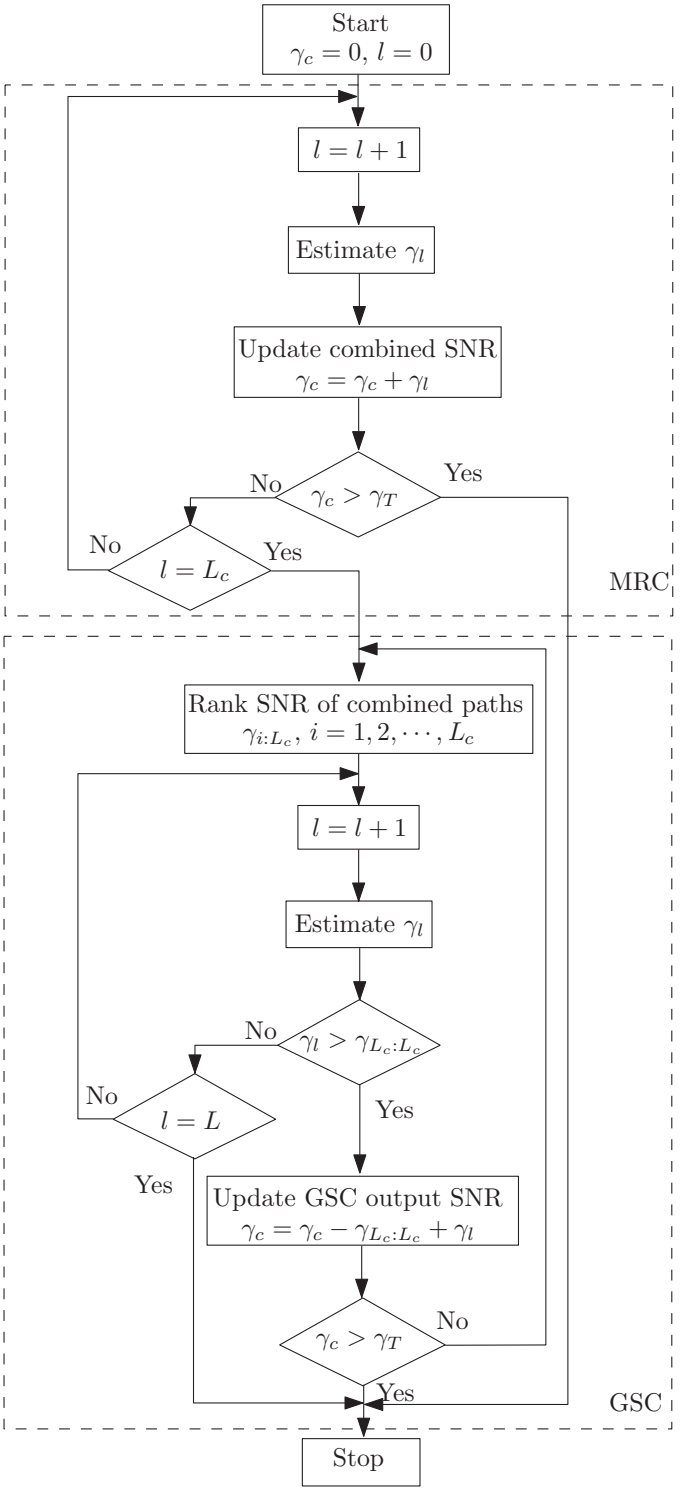

Figure 5.11 Flow chart for the OT-GSC mode of operation.

GSC stage. During the GSC stage, the combiner tries to improve the combined SNR Γ above the SNR threshold γ_T by gradually changing its configuration from an $L_c + 1/L_c$ GSC to an L/L_c GSC, where l/L_c GSC denotes a combiner that combines in an MRC fashion the L_c strongest paths out of the l available paths. In particular, knowing that the combined SNR after MRC combining of the first L_c diversity paths is still below γ_T, the combiner checks the SNR of $L_c + 1/L_c$ GSC output. As such, the combiner first estimates another diversity path and then checks if its SNR is greater than the minimum SNR of the L_c used paths. If it is greater, the newly estimated path is used as an MRC input in place of the path which has minimum SNR. If the resulting combined SNR is above γ_T, the combiner stops the branch update. On the other hand, if either the SNR of the newly estimated path is less than the minimum SNR of the currently used paths or if the resulting combined SNR is still below the threshold after path replacement, then the combiner looks into the combined SNR of $L_c + 2/L_c$ GSC by estimating another diversity path. This process is continued until either the combined SNR Γ is above γ_T or all L available diversity paths have been checked. Note again that only in the worst case will the receiver use an L/L_c GSC combiner for reception.

From the operation of OT-GSC, we can see that unlike conventional GSC, where all L diversity paths need to be estimated and ranked in every guard period and all L_c MRC branches need to be active all the time, the receiver with the OT-GSC scheme uses the available resources adaptively. In particular, both path estimation and MRC branch activation are performed only if necessary. These features of OT-GSC constitute the major power saving of this new GSC scheme over conventional GSC.

5.4.1 Complexity analysis

In this section, we accurately quantify the power savings of OT-GSC by deriving closed-form expressions for both average number of path estimations and average number of active MRC branches.

Average number of path estimations

Based on the mode of operation of the OT-GSC scheme, the number of path estimations performed during a guard period varies from 1 to L. Therefore, conditional on the number of path estimations in a guard period, we can write the average number of path estimations, denoted by N_E, in the following summation form

$$N_E = \sum_{l=1}^{L} \pi_l \; l, \tag{5.36}$$

where π_l is the probability that exactly l diversity paths are estimated during a guard period and it is equal to the probability that either an l-branch MRC for $l \leq L_c$ or an l/L_c-GSC for $l > L_c$ is used for the subsequent data reception. As

a single branch receiver is used if the SNR of the first diversity path is above γ_T while an l-branch MRC receiver is used if the combined SNR of an $l-1$-branch MRC is below γ_T whereas the combined SNR of an l-branch MRC is above γ_T, we have under the i.i.d. fading paths assumption:

$$\pi_l = \begin{cases} 1 - F_\gamma(\gamma_T), & l = 1; \\ F_{\gamma_c}^{(l-1)-MRC}(\gamma_T) - F_{\gamma_c}^{l-MRC}(\gamma_T), & 1 < l \leq L_c, \end{cases} \tag{5.37}$$

where $F_{\gamma_c}^{l-MRC}(\cdot)$ is the CDF of the combined SNR with l-branch MRC combiner, the closed-form expression of which for three popular fading channel model of interest are given in Table 5.1. On the other hand, for $L_c < l \leq L-1$, an l/L_c-branch GSC is used if the combined SNR of an $(l-1)/L_c$-branch GSC is below γ_T whereas the combined SNR of an l/L_c-branch GSC is above γ_T. In addition, if the combined SNR of an $(L-1)/L_c$-branch GSC is below γ_T, then an L/L_c-branch GSC is used. Based on these observations and under the i.i.d. fading path assumption, it can be shown that

$$\pi_l = \begin{cases} F_{\gamma_c}^{(l-1)/L_c-GSC}(\gamma_T) - F_{\gamma_c}^{l/L_c-GSC}(\gamma_T), & L_c < l < L; \\ F_{\gamma_c}^{(L-1)/L_c-GSC}(\gamma_T), & l = L, \end{cases} \tag{5.38}$$

where $F_{\gamma_c}^{l/L_c-GSC}(\cdot)$ is the CDF of the combined SNR with l/L_c branch GSC, i.e. the CDF of the sum of the L_c largest path SNR out of l estimated ones. Substituting (5.37) and (5.38) into (5.36), it can be shown after some manipulations and simplifications, that the average number of path estimations is given by

$$N_E = 1 + \sum_{l=1}^{L_c} F_{\gamma_c}^{l-MRC}(\gamma_T) + \sum_{l=L_c+1}^{L-1} F_{\gamma_c}^{l/L_c-GSC}(\gamma_T). \tag{5.39}$$

For the i.i.d. Rayleigh fading case, substituting $F_{\gamma_c}^{l-MRC}(\cdot)$ from Table 5.1 (for the Rayleigh case) and $F_{\gamma_c}^{l/L_c-GSC}(\cdot)$ as given in (5.18) into (5.39) leads to the following closed-form expression for N_E in i.i.d. Rayleigh fading

$$\begin{aligned} N_E = 1 &+ \sum_{l=1}^{L_c} \left[1 - e^{-\frac{\gamma_T}{\overline{\gamma}}} \sum_{i=0}^{l-1} \frac{1}{i!} \left(\frac{\gamma_T}{\overline{\gamma}} \right)^i \right] \\ &+ \sum_{l=L_c+1}^{L-1} \binom{l}{L_c} \left\{ 1 - e^{-\frac{\gamma_T}{\overline{\gamma}}} \sum_{i=0}^{L_c-1} \frac{1}{i!} \left(\frac{\gamma_T}{\overline{\gamma}} \right)^i \right. \\ &+ \sum_{i=1}^{l-L_c} (-1)^{L_c+i-1} \binom{l-L_c}{i} \left(\frac{L_c}{i} \right)^{L_c-1} \\ &\times \left[\left(1 + \frac{i}{L_c} \right)^{-1} \left[1 - e^{\left(1+\frac{i}{L_c}\right)\frac{\gamma_T}{\overline{\gamma}}} \right] \right. \\ &\left. \left. - \sum_{m=0}^{L_c-2} \left(-\frac{i}{L_c} \right)^m \left(1 - e^{-\frac{\gamma_T}{\overline{\gamma}}} \sum_{k=0}^{m} \frac{1}{k!} \left(\frac{\gamma_T}{\overline{\gamma}} \right)^k \right) \right] \right\}. \end{aligned} \tag{5.40}$$

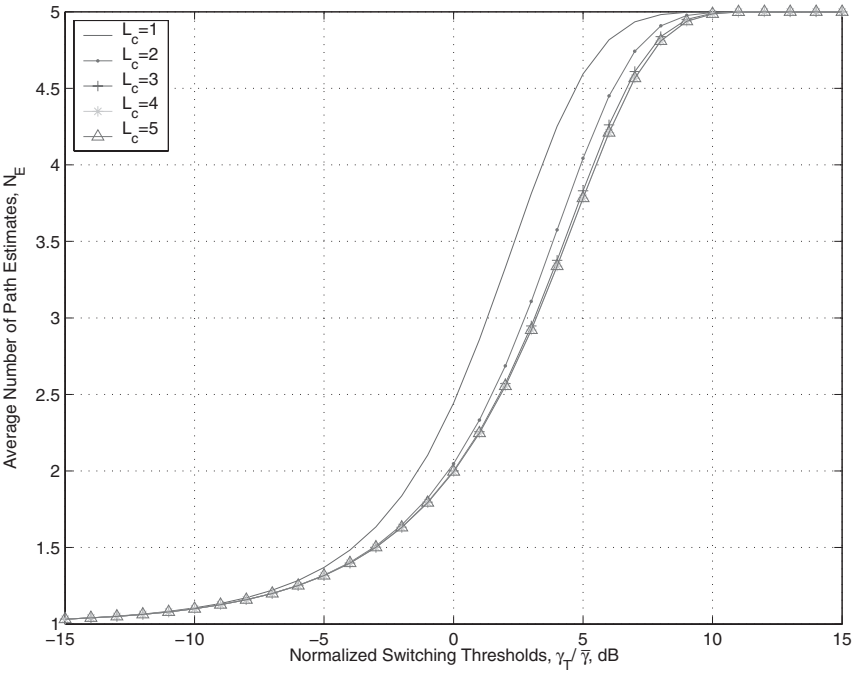

Figure 5.12 Average number of path estimations with OT-GSC as a function of the normalized SNR threshold, $\gamma_T/\overline{\gamma}$ ($L = 5$) [5]. © 2005 IEEE.

In Fig. 5.12, we show the average number of path estimations with OT-GSC in a guard period (given in (5.40)) as a function of the normalized SNR threshold, $\gamma_T/\overline{\gamma}$. Note that the average number of path estimations N_E increases from 1 to L as the threshold increases, just as expected, since it becomes more difficult to raise the combined SNR above the threshold. Note also that N_E decreases as the number of available MRC branches L_c increases, but the difference becomes negligible after L_c becomes greater than 2.

Average number of active MRC branches

With OT-GSC, if the combined SNR exceeds the SNR threshold during the MRC stage, fewer than L_c MRC branches might be active during the subsequent data burst reception. As a result, a considerable amount of receiver processing power will be saved. Conditional on the number of active MRC branches during the data burst reception, we can write the average number of active MRC branches, denoted by N_A, in the following summation form

$$N_A = \sum_{l=1}^{L_c} \pi_l \; l, \tag{5.41}$$

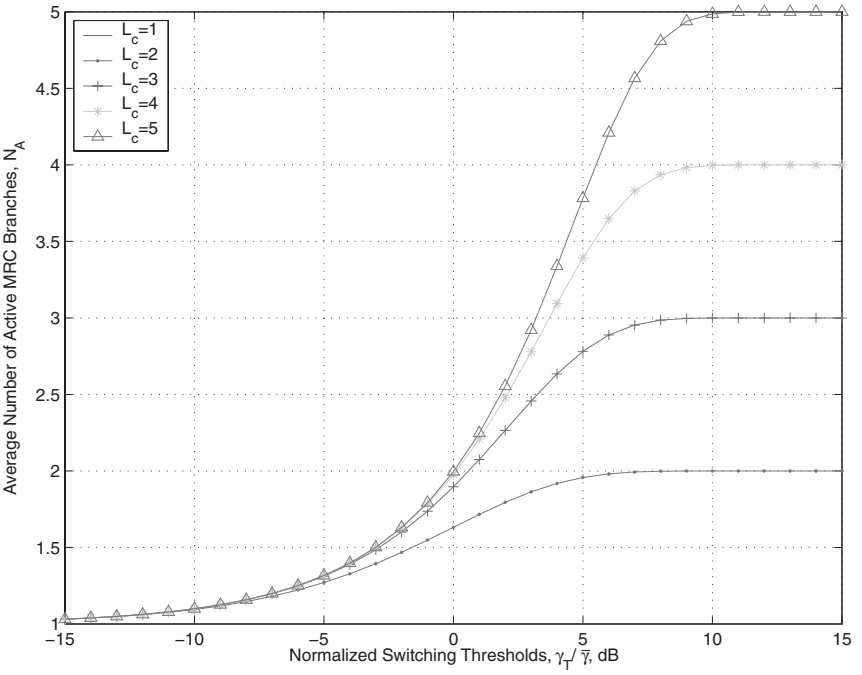

Figure 5.13 Average number of active MRC branches with OT-GSC as a function of the normalized SNR threshold, $\gamma_T/\overline{\gamma}$ ($L = 5$) [3]. © 2004 IEEE.

where π_l is the probability that exactly l MRC branches are active during a data burst reception. For $l < L_c$, this is equal to the probability that an l-branch MRC is used during data reception. Based on the results of the previous subsection and noting that once the operation of the combiner reaches the GSC stage, all L_c MRC branches need to be active, it can be shown that N_A is given by

$$N_A = 1 + \sum_{l=1}^{L_c-1} F_{\gamma_c}^{l-MRC}(\gamma_T). \tag{5.42}$$

For the i.i.d. Rayleigh fading case, after substituting the Rayleigh case of $F_{\gamma_c}^{l-MRC}(\cdot)$ from Table 5.1 in (5.42), we have the closed-form expression for N_A given by

$$N_A = 1 + \sum_{l=1}^{L_c-1} \left[1 - e^{-\frac{\gamma_T}{\overline{\gamma}}} \sum_{i=0}^{l-1} \frac{1}{i!} \left(\frac{\gamma_T}{\overline{\gamma}} \right)^i \right]. \tag{5.43}$$

In Fig. 5.13, we show the average number of active MRC branches during data reception (given in (5.43)) as a function of the normalized SNR threshold, $\gamma_T/\overline{\gamma}$. Note that the average number of active MRC branches N_A increases

from 1 to L_c as the normalized SNR threshold increases, just as expected by intuition.

5.4.2 Statistics of output SNR

We now derive the statistics of the combined SNR with OT-GSC, which will facilitate its performance analysis over fading channels. We again focus on the i.i.d. Rayleigh fading environment. Note that the events that L_e, $L_e = 1, 2, ..., L$, diversity branches are examined are mutually exclusive. Applying the total probability theorem, we can write the CDF of the combined SNR γ_c in a summation form as

$$F_{\gamma_c}(x) = \Pr[\gamma_c < x] = \sum_{k=1}^{L} \Pr[\gamma_c < x, L_e = k], \tag{5.44}$$

where $\Pr[\gamma_c < x, L_e = k]$ is the joint probability of the events that $\gamma_c < x$ and the receiver has examined exactly k paths. Based on the mode of operation of OT-GSC, we note that when $L_e \leq L_c$, the OT-GSC operation terminates at the MRC stage. Moreover, it can be observed that L_e paths are estimated, $L_e \leq L_c$, if and only if the MRC-combined SNR of the first $L_e - 1$ branches is less than the output-threshold γ_T but the combined SNR of the first L_e branches is above γ_T. Therefore, $\Pr[\gamma_c < x, L_e = k]$, $k \leq L_c$, can be shown to be given by

$$\Pr[\gamma_c < x, L_e = k] = \begin{cases} \Pr[\gamma_T \leq \gamma_c = \gamma_1 < x], & k = 1 \\ \Pr[\gamma_T \leq \gamma_c = \sum_{j=1}^{k} \gamma_j < x, \sum_{j=1}^{k-1} \gamma_j < \gamma_T], & 2 \leq k \leq L_c. \end{cases} \tag{5.45}$$

When $L_e > L_c$, the OT-GSC operation terminates at the GSC stage. In particular, for $L_c + 1 \leq L_e \leq L - 1$, an L_e/L_c-GSC is used when the combined SNR of the L_e/L_c-GSC is above the output-threshold γ_T whereas the output SNR of the $(L_e - 1)/L_c$-GSC is less than γ_T. Finally, $L_e = L$ if and only if the combined SNR of the $(L - 1)/L_c$-GSC is below the output threshold. Mathematically speaking, we have, for $k > L_c$

$$\Pr[\gamma_c < x, L_e = k] = \begin{cases} \Pr[\gamma_T \leq \gamma_c = \sum_{j=1}^{L_c} \gamma_{j:k} < x, \sum_{j=1}^{L_c} \gamma_{j:k-1} < \gamma_T], & k \leq L - 1 \\ \Pr[\gamma_c = \sum_{j=1}^{L_c} \gamma_{j:L} < x, \sum_{j=1}^{L_c} \gamma_{j:L-1} < \gamma_T], & k = L, \end{cases} \tag{5.46}$$

where $\gamma_{j:k}$ denotes the jth largest SNR among k estimated path SNRs. Substituting (5.45) and (5.46) into (5.44), we can rewrite the CDF of the combined

SNR with OT-GSC as

$$F_{\gamma_c}(x) = \begin{cases} \Pr[\sum_{j=1}^{L_c} \gamma_{j:L} < \gamma_T] \\ \quad \underbrace{+ \Pr[\gamma_T \le \gamma_1 < x] + \sum_{k=2}^{L_c} \Pr[\gamma_T \le \sum_{j=1}^{k} \gamma_j < x, \sum_{j=1}^{k-1} \gamma_j < \gamma_T]}_{F_1(x)} \\ \quad + \underbrace{\sum_{k=L_c+1}^{L} \Pr[\gamma_T \le \sum_{j=1}^{L_c} \gamma_{j:k} < x, \sum_{j=1}^{L_c} \gamma_{j:k-1} < \gamma_T]}_{F_2(x)}, & x \ge \gamma_T \\ \Pr[\sum_{j=1}^{L_c} \gamma_{j:L} < x], & x < \gamma_T . \end{cases} \tag{5.47}$$

Note that the probability $\Pr[\sum_{j=1}^{L_c} \gamma_{j:L} < x]$ is equal to the CDF of the combined SNR of L/L_c-GSC evaluated at x, i.e. $F_{\gamma_c}^{l/L_c-GSC}(x)$. For i.i.d. Rayleigh fading channels, the closed-form expression of $F_{\gamma_c}^{l/L_c-GSC}(x)$ is given in (5.18). The term $F_1(x)$ defined in (5.47) can be rewritten in terms of the single-branch SNR CDF $F_\gamma(\cdot)$ and the PDF of an l-branch MRC output SNR $f_{\gamma_c}^{l-MRC}(\cdot)$ as

$$F_1(x) = F_\gamma(x) - F_\gamma(\gamma_T) + \sum_{k=2}^{L_c} \int_0^{\gamma_T} f_{\gamma_c}^{k-MRC}(y)\big(F_\gamma(x-y) - F_\gamma(\gamma_T - y)\big)\mathrm{d}y \tag{5.48}$$

For Rayleigh fading, after proper substitution from Table 5.1, carrying out the integrations and some manipulation, $F_1(x)$ can be shown to be given by

$$F_1(x) = \sum_{k=1}^{L_c} \frac{{\gamma_T}^{k-1}}{(k-1)!\overline{\gamma}^{k-1}} \big[e^{-\frac{\gamma_T}{\overline{\gamma}}} - e^{-\frac{x}{\overline{\gamma}}}\big]. \tag{5.49}$$

To derive $F_2(x)$, we first note that $\sum_{j=1}^{L_c} \gamma_{j:k-1}$ can be written as $\sum_{j=1}^{L_c} \gamma_{j:k-1} = \Gamma_{L_c-1/k-1} + \gamma_{L_c:k-1}$, where $\gamma_{L_c:k-1}$ is the L_cth largest SNR among $k-1$ estimated path SNRs and $\Gamma_{L_c-1/k-1} = \sum_{j=1}^{L_c-1} \gamma_{j:k-1}$, i.e. $\Gamma_{L_c-1/k-1}$ is the sum of the largest $L_c - 1$ branch SNRs. Based on the mode of operation of OT-GSC, the weakest path is replaced at the GSC stage if and only if the instantaneous SNR of the newly examined branch γ_k is larger than $\gamma_{L_c:k-1}$. Also note that in this case $\Gamma_{L_c-1/k-1}$ remains unchanged, we can write the summand of $F_2(x)$ as

$$\begin{aligned} &\Pr[\gamma_T \le \sum_{j=1}^{L_c} \gamma_{j:k} < x, \sum_{j=1}^{L_c} \gamma_{j:k-1} < \gamma_T] \\ &\qquad = \Pr[\gamma_T \le \Gamma_{L_c-1/k-1} + \gamma_k < x, \Gamma_{L_c-1/k-1} + \gamma_{L_c:k-1} < \gamma_T]. \end{aligned} \tag{5.50}$$

Because all branch SNRs are i.i.d. random variables, γ_k is independent of both $\Gamma_{L_c-1/k-1}$ and $\gamma_{L_c:k-1}$. As such, we can compute the probability in (5.50) with the joint PDF of $\Gamma_{L_c-1/k-1}$ and $\gamma_{L_c:k-1}$, denoted by $p_{\gamma_{L_c:k-1},\Gamma_{L_c-1/k-1}}(y,z)$, and

the CDF for γ_k, $F_\gamma(\cdot)$. In particular, $F_2(x)$ can be written as

$$F_2(x) = \sum_{k=L_c+1}^{L} \int_0^{\frac{\gamma_T}{L_c}} \int_{(L_c-1)y}^{\gamma_T - y} p_{\gamma_{L_c:k-1},\Gamma_{L_c-1:k-1}}(y,z) \times (F_\gamma(x-z) - F_\gamma(\gamma_T - z))\mathrm{d}z\mathrm{d}y. \tag{5.51}$$

For i.i.d. Rayleigh fading channels, it can be shown in that the joint PDF $p_{\gamma_{L_c:L},\Gamma_{L_c-1/L}}(y,z)$ was given in (5.25). After substituting (5.25) into (5.51), carrying out the integration and appropriate simplifications, we obtain the closed-form expression of $F_2(x)$ as

$$\begin{aligned} F_2(x) =& [e^{-\frac{\gamma_T}{\overline{\gamma}}} - e^{-\frac{x}{\overline{\gamma}}}] \sum_{k=L_c+1}^{L} \sum_{j=0}^{k-1-L_c} A(k-1,j) \\ & \times \left[B(L_c,j) + (-\frac{\overline{\gamma} L_c}{j+1})^{L_c} e^{-\frac{(j+1)\gamma_T}{\overline{\gamma} L_c}} \right], \end{aligned} \tag{5.52}$$

where

$$A(k,j) = \frac{(-1)^j k!}{L_c(k-L_c-j)!(L_c-1)!j!\overline{\gamma}^{L_c}}, \tag{5.53}$$

and

$$B(L_c,j) = \sum_{i=0}^{L_c-1} \frac{(-1)^i {\gamma_T}^{L_c-1-i}}{(L_c-1-i)!(\frac{j+1}{\overline{\gamma} L_c})^{i+1}}. \tag{5.54}$$

Finally, after substituting (5.49), (5.52) and (5.18) into (5.47), we arrive at the closed-form expression of the CDF of OT-GSC output SNR, or equivalently, the outage probability of OT-GSC, over i.i.d. Rayleigh fading channels.

Starting from the CDF of γ_c with OT-GSC, we can routinely obtain its PDF and MGF. In particular, after differentiation and some manipulations, the PDF of γ_c with OT-GSC for i.i.d. Rayleigh fading channels is given by

$$p_{\gamma_c}(x) = \begin{cases} \frac{1}{\overline{\gamma}} e^{-\frac{x}{\overline{\gamma}}} \left\{ \sum_{k=1}^{L_c} \frac{{\gamma_T}^{k-1}}{(k-1)!\overline{\gamma}^{k-1}} + \sum_{k=L_c+1}^{L} \sum_{j=0}^{k-1-L_c} A(k-1,j) \right. & \\ \left. \times \left[B(L_c,j) + (-\frac{\overline{\gamma} L_c}{j+1})^{L_c} e^{-\frac{(j+1)\gamma_T}{\overline{\gamma} L_c}} \right] \right\}, & x \geq \gamma_T \\ \binom{L}{L_c} \left[\frac{x^{L_c-1} e^{-x/\overline{\gamma}}}{\overline{\gamma}^{L_c}(L_c-1)!} + \frac{1}{\overline{\gamma}} \sum_{l=1}^{L-L_c} (-1)^{L_c+l-1} \binom{L-L_c}{l} \right. & \\ \left. \times \left(\frac{L_c}{l} \right)^{L_c-1} e^{-x/\overline{\gamma}} \left(e^{-lx/L_c\overline{\gamma}} - \sum_{m=0}^{L_c-2} \frac{1}{m!} (\frac{-lx}{L_c\overline{\gamma}})^m \right) \right], & x < \gamma_T \end{cases} \tag{5.55}$$

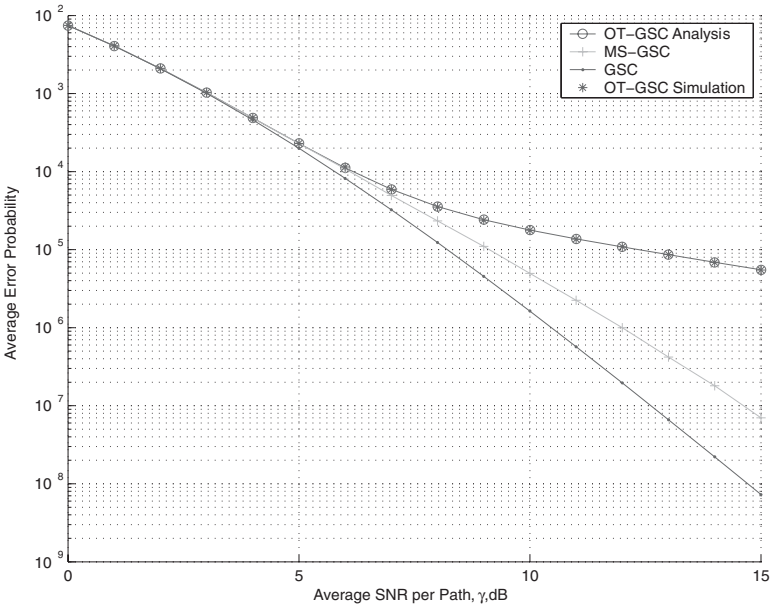

Figure 5.14 Average error rate of BPSK with OT-GSC, MS-GSC and GSC over $L = 5$ i.i.d. Rayleigh fading channels as function of the average SNR per branch($L_c = 3$ and $\gamma_T = 8$ dB) [15]. © 2007 IEEE.

where $A(k, j)$ and $B(L_c, j)$ are defined in (5.53) and (5.54), respectively. It follows that the MGF of γ_c can be obtained as

$$\begin{aligned} M_{\gamma_c}(t) = & \binom{L}{L_c}\Bigg\{\frac{1-\Gamma(L_c,(1-t\overline{\gamma})\gamma_T/\overline{\gamma})}{(1-t\overline{\gamma})^{L_c}} + \sum_{l=1}^{L-L_c}(-1)^{L_c+l-1}\binom{L-L_c}{l} \\ & \times \left(\frac{L_c}{l}\right)^{L_c-1}\left[I(l,t) - \sum_{m=0}^{L_c-2}\left(\frac{-l}{L_c}\right)^m \times \frac{(1-\Gamma(m+1,(1-t\overline{\gamma})\gamma_T/\overline{\gamma}))}{(1-t\overline{\gamma})^{m+1}}\right]\Bigg\} \\ & + \frac{e^{-\frac{(1-\overline{\gamma}t)\gamma_T}{\overline{\gamma}}}}{1-\overline{\gamma}t}\Bigg\{\sum_{k=1}^{L_c}\frac{{\gamma_T}^{k-1}}{(k-1)!\overline{\gamma}^{k-1}} + \sum_{k=L_c+1}^{L}\sum_{j=0}^{k-1-L_c}A(k-1,j) \\ & \times \left[B(L_c,j) + (-\frac{\overline{\gamma}L_c}{j+1})^{L_c}e^{-\frac{(j+1)\gamma_T}{\overline{\gamma}L_c}}\right]\Bigg\}, \end{aligned} \tag{5.56}$$

where

$$I(l,t) = \frac{1}{\overline{\gamma}t - \frac{L_c+l}{L_c}}\left[\exp\left(\frac{\gamma_T(tL_c\overline{\gamma} - L_c - l)}{L_c\overline{\gamma}}\right) - 1\right]. \tag{5.57}$$

These closed-form results can be readily applied to the performance analysis of OT-GSC over fading channels.

Figure 5.14 compares the average error rate of BPSK with OT-GSC, MS-GSC and GSC as a function of average SNR per branch with the output-threshold

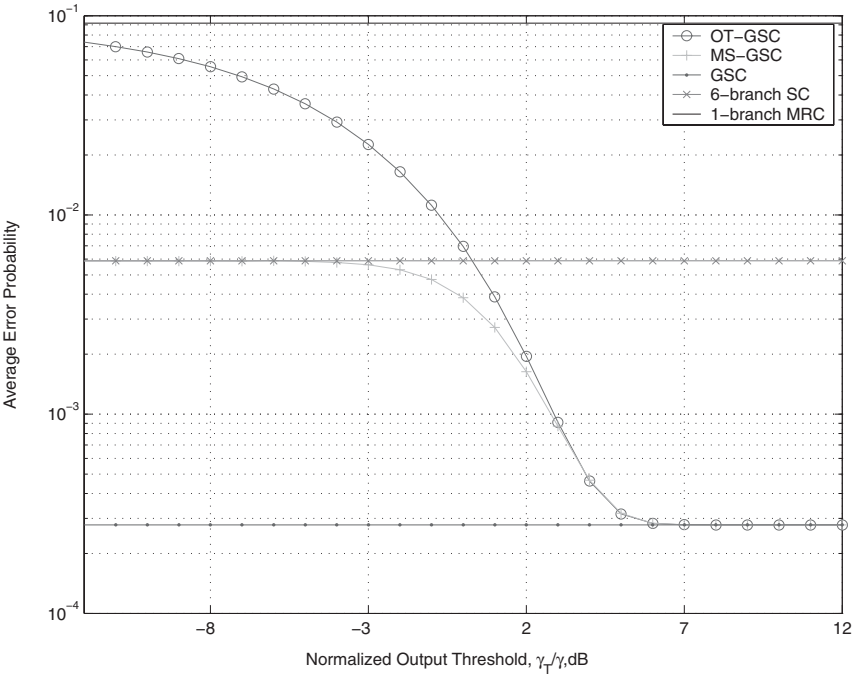

Figure 5.15 Average error rate of BPSK with OT-GSC, MS-GSC and GSC over $L = 6$ i.i.d. Rayleigh fading channels as function of the normalized output-threshold $\gamma_T/\overline{\gamma}$ ($L_c = 3$ and $\overline{\gamma} = 3$ dB) [15]. © 2007 IEEE.

γ_T for both OT-GSC and MS-GSC set to be 8 dB. As a verification of our analytic result, simulation results for the average error rate of OT-GSC are also presented. Note that these simulation results match the analytic results perfectly. We can also see, when the channel condition is poor, i.e. $\overline{\gamma}$ is small compared to γ_T, these schemes have the same error performance. This behavior can be explained as follows. When the average branch SNR is small compared to the output threshold, the receiver with OT-GSC and MS-GSC will usually estimate all available branches and combine the best L_c ones because applying MRC/GSC to a subset of available branches will not be able to raise the combined SNR over γ_T. Therefore, both MS-GSC and OT-GSC are actually working in the same way as a conventional GSC. As $\overline{\gamma}$ becomes larger, i.e. the channel condition is improving, OT-GSC has a higher error probability than both GSC and MS-GSC. This can be explained by noting that in this case, it is more likely that the instantaneous SNR of the first branch is greater than γ_T and, as such, OT-GSC reduces to a single-branch receiver while MS-GSC tends to work as a selection combiner.

In Fig. 5.15, we plot the average error rate of BPSK with OT-GSC, MS-GSC and GSC schemes as function of the normalized output threshold $\gamma_T/\overline{\gamma}$. As we can see, the error rate of OT-GSC decreases from that of a single-branch MRC to

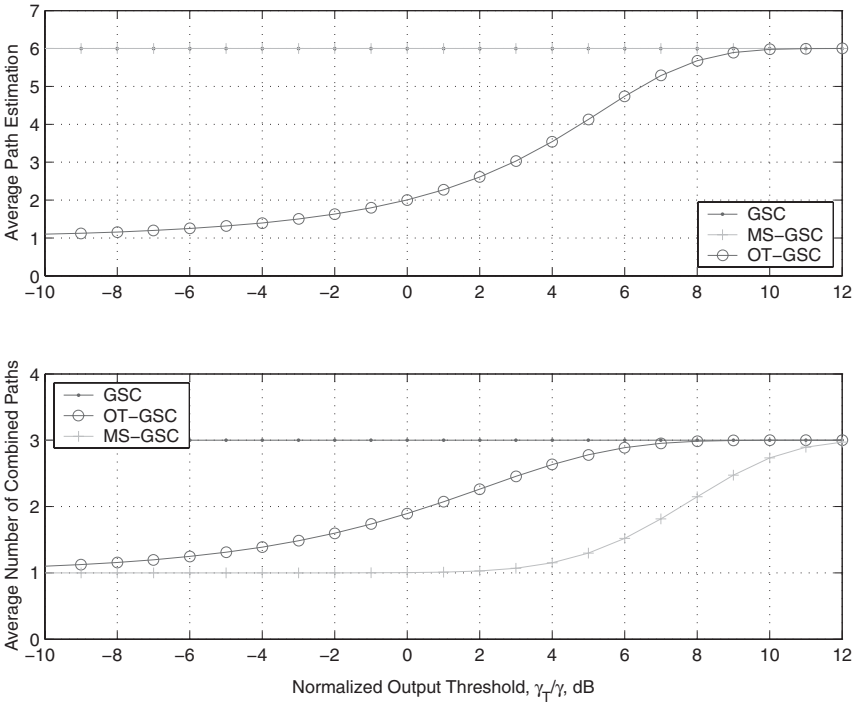

Figure 5.16 Average number of path estimations and combined paths with OT-GSC, MS-GSC and GSC over $L = 6$ i.i.d. Rayleigh fading channels as function of normalized output-threshold $\gamma_T/\overline{\gamma}$ ($L_c = 3$ and $\overline{\gamma} = 3$ dB) [15]. © 2007 IEEE.

that of a conventional 6/3 GSC when the normalized output threshold increases from –12 dB to 12 dB, whereas that of MS-GSC degrades from a 6-branch SC. To better illustrate the new trade-off of complexity versus performance offered by OT-GSC, we present in Fig. 5.16 the average number of path estimations and combined paths with OT-GSC, MS-GSC and GSC schemes based on the analytical results given in previous sections. It can be seen that while both GSC and MS-GSC always require L path estimations, OT-GSC requires much fewer path estimations, especially when the normalized SNR is small. Considering Figs. 5.15 and 5.16 together, we can observe that the OT-GSC scheme can offer the same performance as GSC with a fewer number of combined paths and path estimations. In comparison with MS-GSC, OT-GSC still saves certain amount of path estimations while combining more paths to achieve the same error performance.

5.5 Adaptive transmit diversity

The idea of adaptive diversity combining can also apply to transmit diversity scenarios. The main advantage of transmit diversity is that diversity gain offered by multiple antenna at the base station can be explored for the downlink

transmission even with single-antenna receivers. In general, transmit diversity systems can be classified into open-loop and closed-loop depending on whether or not the channel state information feedback is required. The most popular open-loop schemes are those based on orthogonal space-time block code (STBC) [16–20], which can achieve full diversity gain with simple linear processing at the receiver, and as such receive considerable research and industrial interest. On the other hand, OSTBC will suffer a rate loss when the number of transmit antennae is greater. Moreover, the more the transmit antennae are used, the larger the SNR loss occurring due to the power spreading over multiple antennae.

A viable solution to these issues is antenna selection at the transmitter side [21–26]. It has been shown that while requiring a certain amount of closed-loop feedback, these antenna selection schemes incur much less of a rate/power loss compared to conventional STBC-based transmit diversity systems. Nevertheless, these antenna selection schemes still require the estimation of wireless channels corresponding to every transmit antenna. The receiver needs to feed back the index of all selected channels. In this section, we illustrate how the idea of adaptive combining can be applied to the transmit diversity systems by considering a new class of closed-loop transmit diversity system [10, 27, 28]. Specifically, a subset of the available transmit antennae is used for data transmission with STBC. The transmitter will replace the antenna leads to the lowest-path SNR with an unused transmit antenna if the output SNR of the space-time decoder is below a certain threshold. The resulting OSTBC system with transmit antenna replacement offers performance comparable to the corresponding selection-based transmit diversity systems with reduced feedback load.

5.5.1 Mode of operation

The system model of transmit diversity with antenna replacement is illustrated in Fig. 5.17. The transmitter is equipped with a total of $N + L$ antennae, where N antennae are used for orthogonal space-time transmission and L antennae are used for replacement. The receiver compares the output SNR of the space-time decoder with a fixed SNR threshold, denoted by γ_T. If the output SNR $\sum_{i=1}^{N} \gamma_i$ is larger than or equal to γ_T, no antenna replacement is necessary and the receiver informs the transmitter to keep using the current antennae. On the other hand, if $\sum_{i=1}^{N} \gamma_i$ is smaller than the threshold γ_T, the receiver asks the transmitter to replace the L antennae leading to the weakest received signal with the L remaining antennae. Therefore, the receiver needs to feedback either one bit of information to indicate no need for antenna replacement or $1 + \log_2({}_N C_L)$, where ${}_N C_L = \frac{N!}{(N-L)!L!}$ bits of information inform the transmitter that the index of transmitting antennae needs to be replaced. It is not difficult to show that the average feedback load of the proposed scheme is

$$N_A = 1 \cdot \Pr\left[\sum_{i=1}^{N} \gamma_i \geq \gamma_T\right] + (1 + \log_2({}_N \mathrm{C}_L)) \cdot \Pr\left[\sum_{i=1}^{N} \gamma_i < \gamma_T\right]. \quad (5.58)$$

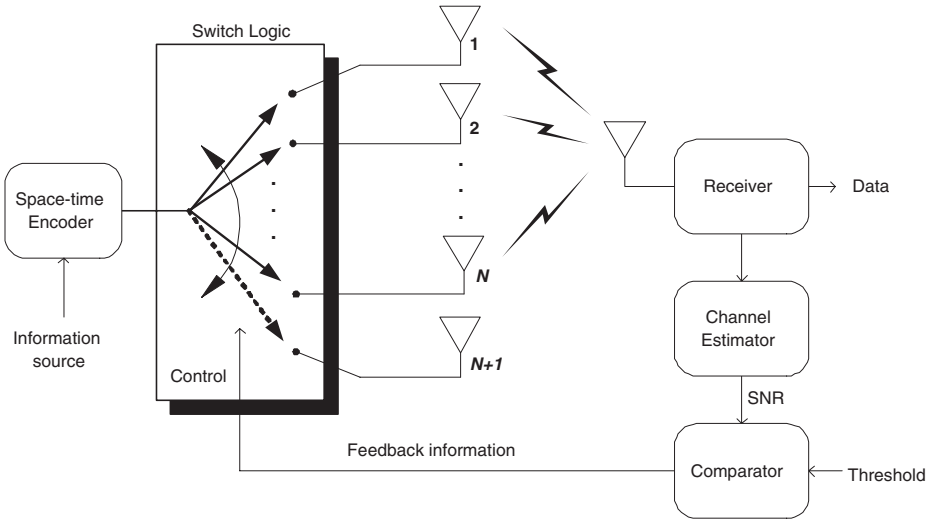

Figure 5.17 System model of transmit diversity systems [10].

For the i.i.d. Rayleigh fading scenario, it can be shown that the average feedback load specializes to

$$N_A = 1 + \log_2({}_N\mathrm{C}_L)\left(1 - e^{-\frac{\gamma_T}{\bar{\gamma}}}\sum_{i=0}^{N-1}\frac{1}{i!}\left(\frac{\gamma_T}{\bar{\gamma}}\right)^i\right). \tag{5.59}$$

It can be seen that the proposed system has the maximum feedback load when the number of switching antennae $L \approx N/2$. In Fig. 5.18, we plot the average feedback load of the proposed system as a function of γ_T for different values of L and fixed average SNR, $\bar{\gamma} = 15$ dB, while keeping the total number of transmit antennas $(N + L)$ fixed to 6. As we can see, for $L < N$ cases, the feedback load increases from 1 bit to $\log_2({}_N C_L) + 1$ bits when the threshold γ_T increases, as expected. When $N = L = 3$, the systems need only one bit of feedback information to indicate whether all transmit antennae should be replaced or not. We note that different threshold values will lead to different trade-offs of error performance and feedback load. To illustrate this, we also plot the average error rate of the proposed system on the same figure. As we can see, the error performance improves and eventually saturates to a constant value as the threshold γ_T increases. Based on this figure, we can that see if we select the threshold properly, the proposed scheme can achieve its best possible error performance with very low feedback load. Note that the proposed scheme also enjoys low hardware complexity in terms of pilot channels and RF chains.

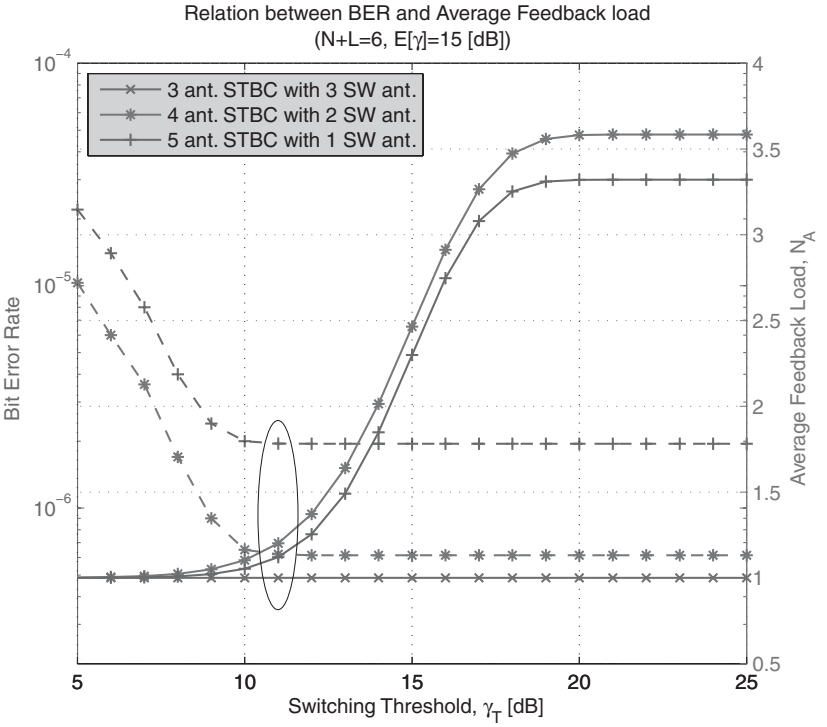

Figure 5.18 Comparison of average feedback load of the proposed systems with $N + L = 6$ transmit antennae over i.i.d. Rayleigh fading channels.

5.5.2 Statistics of received SNR

We now derive the statistics of the received SNR of the antenna replacement scheme. We first consider the case of $L = N$. In this case, all transmit antennae will be replaced when the output SNR $\sum_{i=1}^{N} \gamma_i$ is smaller than the threshold γ_T. The proposed scheme operates in a similar way to the traditional SSC scheme, while the output SNR of each branch is equal to $\sum_{j=1}^{N} \gamma_j$. Therefore, we can write the CDF of the combined SNR as

$$F_{\gamma_c}(x) = \begin{cases} \Pr[\gamma_T \leq \sum_{j=1}^{N} \gamma_j < x] + \Pr\left[\sum_{j=1}^{N} \gamma_j < \gamma_T \ \& \ \sum_{j=1}^{N} \gamma_j < x\right], & x \geq \gamma_T, \\ \Pr\left[\sum_{j=1}^{N} \gamma_j < \gamma_T \ \ \& \ \ \sum_{j=1}^{N} \gamma_j < x\right], & 0 \leq x < \gamma_T. \end{cases} \tag{5.60}$$

Following the similar analytical approach for SSC, we can then obtain the closed-form expression of the PDF of γ_c under the i.i.d. Rayleigh fading assumption

as

$$p_{\gamma_c}(x) = \begin{cases} \left(2 - e^{-\frac{\gamma_T}{\overline{\gamma}}} \sum_{k=0}^{L-1} \frac{1}{k!} \left(\frac{\gamma_T}{\overline{\gamma}}\right)^k\right) \frac{x^{L-1}}{(L-1)!\overline{\gamma}^L} e^{-\frac{x}{\overline{\gamma}}}, & x \geq \gamma_T, \\ \left(1 - e^{-\frac{\gamma_T}{\overline{\gamma}}} \sum_{k=0}^{L-1} \frac{1}{k!} \left(\frac{\gamma_T}{\overline{\gamma}}\right)^k\right) \frac{x^{L-1}}{(L-1)!\overline{\gamma}^L} e^{-\frac{x}{\overline{\gamma}}}, & 0 \leq x < \gamma_T. \end{cases} \tag{5.61}$$

We now consider the case $1 \leq L < N$. Let $\gamma_{i:N}$ denote the ith largest SNR with $\gamma_{1:N} > \gamma_{2:N} > ... > \gamma_{N:N}$. Based on the mode of operation of the proposed scheme, the combined SNR γ_c is given by

$$\gamma_c = \begin{cases} \sum_{i=1}^{N} \gamma_i, & \sum_{i=1}^{N} \gamma_i \geq \gamma_T, \\ \sum_{i=1}^{N-L} \gamma_{i:N} + \sum_{j=1}^{L} \gamma_j, & \sum_{i=1}^{N} \gamma_i < \gamma_T. \end{cases} \tag{5.62}$$

Let Γ_j denote the sum of the largest j SNRs among the N ones, i.e. $\Gamma_j = \sum_{i=1}^{j} \gamma_{i:N}$. We can write the CDF of γ_c as

$$F_{\gamma_c}(x) = \begin{cases} \Pr[\gamma_T \leq \Gamma_N < x] \\ \quad + \Pr\left[\Gamma_N < \gamma_T \ \ \& \ \ \Gamma_{N-L} + \sum_{j=1}^{L} \gamma_j < x\right], & x \geq \gamma_T, \\ \Pr\left[\Gamma_N < \gamma_T \ \ \& \ \ \Gamma_{N-L} + \sum_{j=1}^{L} \gamma_j < x\right], & 0 \leq x < \gamma_T. \end{cases} \tag{5.63}$$

Applying the Bayesian rule and the i.i.d. fading channel assumption, we can rewrite the joint probability in (5.63) as

$$\begin{aligned} &\Pr\left[\Gamma_N < \gamma_T \ \& \ \Gamma_{N-L} + \sum_{j=1}^{L} \gamma_j < x\right] \\ &= \Pr\left[\Gamma_{N-L} + \sum_{j=1}^{L} \gamma_j < x \middle| \Gamma_N < \gamma_T\right] \Pr[\Gamma_N < \gamma_T] \\ &= \Pr[\gamma_s < x] \Pr[\Gamma_N < \gamma_T], \end{aligned} \tag{5.64}$$

where we define a new random variable $\gamma_s \equiv \sum_{j=1}^{L} \gamma_j + (\Gamma_{N-L} | \Gamma_N < \gamma_T)$. The PDF of the combined SNR can be obtained by taking the derivative of (5.63) and is given by

$$p_{\gamma_c}(x) = \begin{cases} p_{\Gamma_N}(x) + \Pr[\ \Gamma_N < \gamma_T] p_{\gamma_s}(x), & x \geq \gamma_T, \\ \Pr[\ \Gamma_N < \gamma_T] p_{\gamma_s}(x), & 0 \leq x < \gamma_T, \end{cases} \tag{5.65}$$

where $p_{\gamma_s}(x)$ denotes the PDF of the γ_s. Since γ_s is the sum of the two random variables $\sum_{j=1}^{L} \gamma_j$ and $(\Gamma_{N-L} | \Gamma_N < \gamma_T)$, we can calculate $p_{\gamma_s}(x)$ in the

convolution form as

$$p_{\gamma_s}(x) = \int_0^x p_{\sum_{j=1}^{L}\gamma_j}(x-z)p_{\Gamma_{N-L}|\Gamma_N<\gamma_T}(z)\mathrm{d}z. \tag{5.66}$$

Noting that the PDF $p_{\sum_{j=1}^{L}\gamma_j}(x-z)$ is readily available in closed form, we focus on the following derivation of the conditional PDF $p_{\Gamma_{N-L}|\Gamma_N<\gamma_T}(x)$.

We start with the CDF of $\Gamma_{N-L}|\Gamma_N<\gamma_T$, which can be written as

$$F_{\Gamma_{N-L}|\Gamma_N<\gamma_T}(x) = \frac{1}{\Pr[\Gamma_N<\gamma_T]}\Pr[\Gamma_{N-L}<x, \Gamma_N<\gamma_T], \tag{5.67}$$

where the joint probability can be calculated as

$$\begin{aligned}\Pr[\Gamma_{N-L}<x, \Gamma_N<\gamma_T] &= \Pr[\Gamma_{N-L}<x, \Gamma_{N-L}+\gamma_{N-L+1:N}+z_l<\gamma_T] \\ &= \int_0^x \int_0^{\gamma_T-y} \int_0^{\gamma_T-y-\gamma} p_{\Gamma_{N-L},\gamma_{N-L-1:N},z_l}(y,\gamma,z)\mathrm{d}z\mathrm{d}\gamma\mathrm{d}y.\end{aligned} \tag{5.68}$$

In (5.69), z_l denotes the sum of the $L-1$ smallest SNRs among total N ones, i.e. $z_l = \sum_{i=N-L+2}^{N}\gamma_{i:N}$ and $p_{\Gamma_{N-L},\gamma_{N-L-1:N},z_l}(y,\gamma,z)$ denotes the joint PDF of Γ_{N-L}, $\gamma_{N-L-1:N}$ and z_l, which has been investigated in a previous chapter. For an i.i.d. Rayleigh fading environment, the three-dimensional PDF is available in closed form. Consequently, the conditional PDF $p_{\Gamma_{N-L}|\Gamma_N<\gamma_T}(x)$ can be written as

$$\begin{aligned}p_{\Gamma_{N-L}|\Gamma_N<\gamma_T}(x) &= \frac{d}{dx}\frac{\Pr[\Gamma_{N-L}<x, \Gamma_N<\gamma_T]}{\Pr[\Gamma_N<\gamma_T]} \\ &= \frac{1}{\Pr[\Gamma_N<\gamma_T]}\int_0^{\min[\gamma_T-x, \frac{x}{N-L}]}\int_0^{\min[\gamma_T-x-\gamma,(L-1)\gamma]} \\ &\quad \times p_{\Gamma_{N-L},\gamma_{N-L-1:N},z_l}(y,\gamma,z)\mathrm{d}z\mathrm{d}\gamma,\ 0\le x<\gamma_T.\end{aligned} \tag{5.69}$$

Finally, after substituting (5.69) into (5.66) and then into (5.65), we have the integral closed form for the PDF of the combined SNR, γ_c, given by

$$p_{\gamma_c}(x) = \begin{cases} p_{\Gamma_N}(x) + \int_0^{\gamma_T} p_{\sum_{l=N+1}^{N+L}\gamma_l}(x-y)\int_0^{\min[\gamma_T-y, \frac{y}{N-L}]}\int_0^{\min[\gamma_T-y-\gamma,(L-1)\gamma]} \\ \quad p_{\Gamma_{N-L},\gamma_{N-L-1:N},z_l}(y,\gamma,z)\mathrm{d}z\mathrm{d}\gamma\mathrm{d}y, & x\ge\gamma_T, \\ \int_0^{x} p_{\sum_{l=N+1}^{N+L}\gamma_l}(x-y)\int_0^{\min[\gamma_T-y, \frac{y}{N-L}]}\int_0^{\min[\gamma_T-y-\gamma,(L-1)\gamma]} \\ \quad \times p_{\Gamma_{N-L},\gamma_{N-L-1:N},z_l}(y,\gamma,z)\mathrm{d}z\mathrm{d}\gamma\mathrm{d}y, & 0\le x<\gamma_T. \end{cases} \tag{5.70}$$

To verify the validity of this new analytical result, we compare the PDF in (5.70) with the Monte Carlo simulation result in Fig. 5.19. It is clear that there is an excellent match between the analytical result and the Monte Carlo simulation. Using the PDF of the combined SNR obtained, we can study the outage

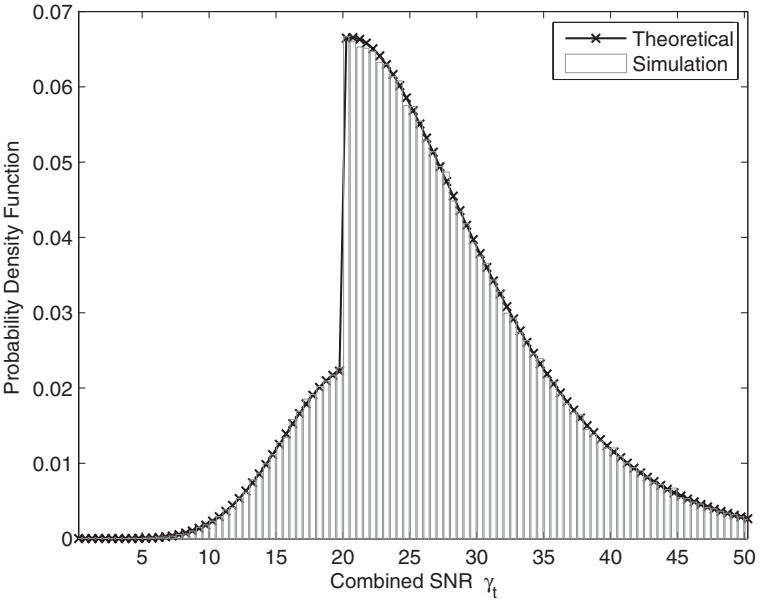

Figure 5.19 Comparison of the analytical results for the PDF of the combined SNR and the Monte Carlo simulation.

probability and the average bit error rate performance of the proposed scheme over i.i.d. Rayleigh fading.

Figure 5.20 plots the outage probability of the proposed diversity system with the fixed threshold, $\gamma_T = 2$ dB. We vary the number of antennae for replacement while keeping four transmit antennae for orthogonal STBC transmission and one antenna for reception. Note that the $L = 0$ case corresponds to traditional open-loop transmit diversity. We note that when $L < N$, the outage performance of the proposed diversity improves with increasing number of switching antennae L, especially when the outage threshold is smaller than the switching threshold. However, if $L = N$, the outage performance actually degrades considerably for the smaller value of the switching threshold.

Figure 5.21 shows the average BER of the proposed diversity system with fixed switching threshold $\gamma_T = 16$ dB. Again, we vary the number of antennae for replacement from 0 to $N = 4$. It is interesting to see from this figure that as the number of antennae used for switching increases, the error performance of the proposed scheme improves. When $L = N$, however, the error performance also degrades significantly, while still slightly better than no antenna for the replacement case.

In Fig. 5.22, we investigate the average BER performance of different transmit configurations while fixing the total number of antennae at the transmitter $N + L$ to 6. The total transmitting power is also fixed irrespective of the number of

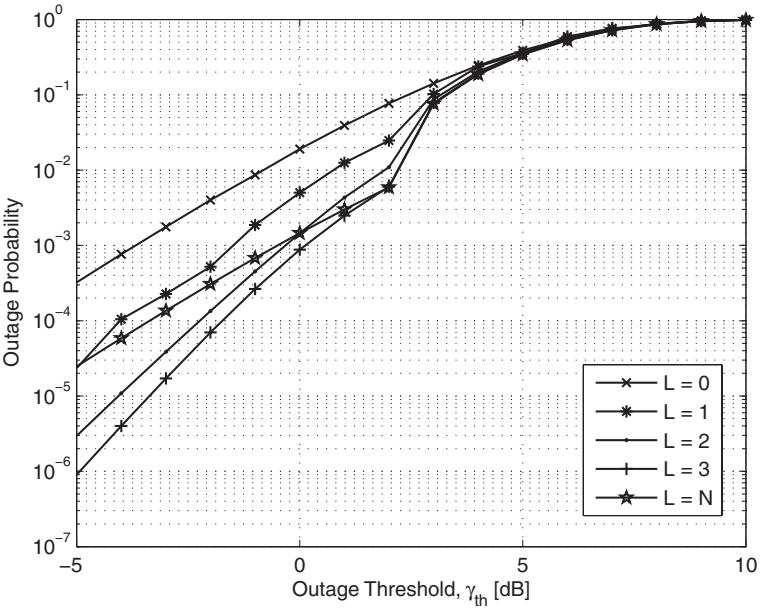

Figure 5.20 Comparison of the outage probability of N-fold MRC for $N = 4$ and the proposed systems with $L = 1, 2, 3$ and $N = 4$.

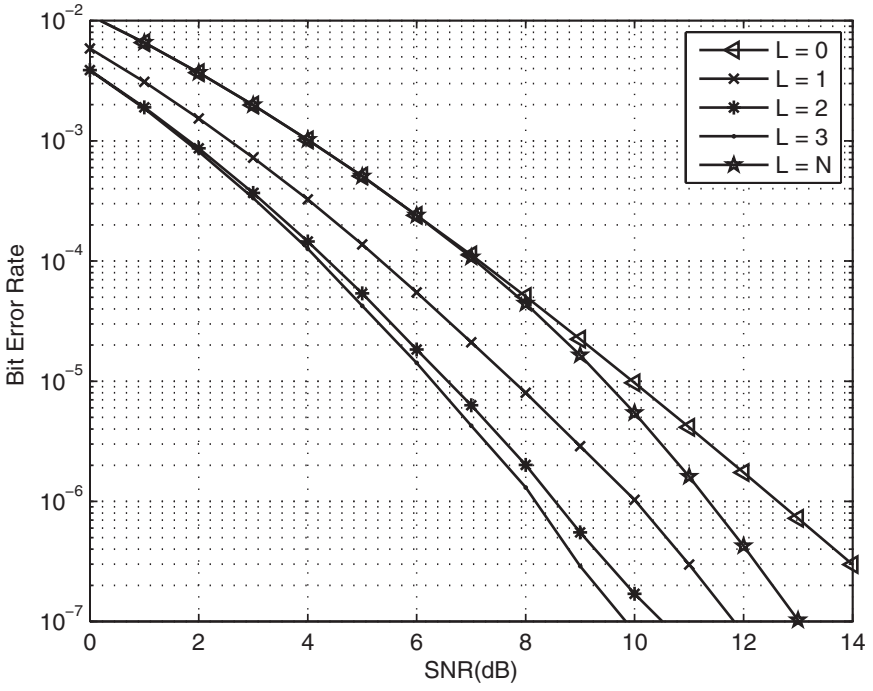

Figure 5.21 Average BER of BPSK of the proposed systems with threshold $\gamma_T = 16$ (dB) and N-fold MRC over i.i.d. Rayleigh fading channels.

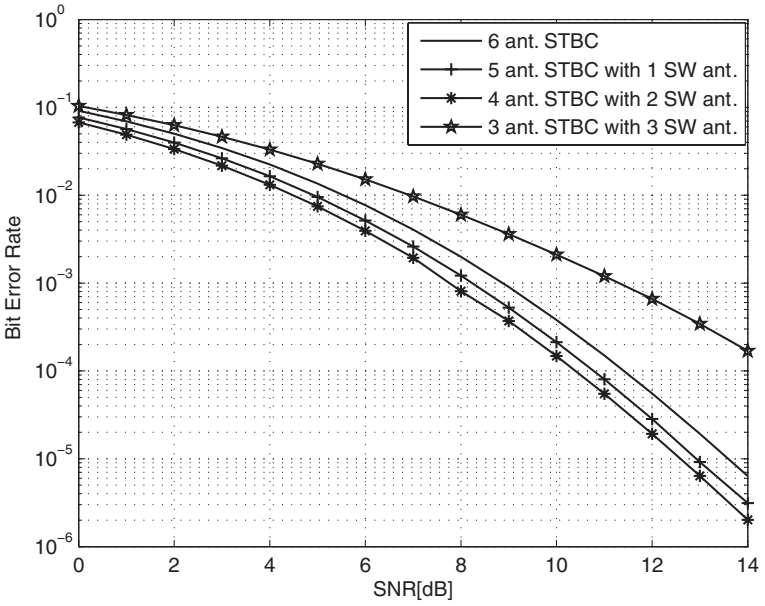

Figure 5.22 Average BER of BPSK of the proposed systems with $N + L = 6$ transmit antennae and OSTBC over i.i.d. Rayleigh fading channels.

antennae used for orthogonal STBC transmission. As we can see, as L increases and as long as $L < N$, the proposed transmit diversity system offers improved performance in the case that all six antennas are used for ST transmission. In particular, the configuration with four transmitting antennae and two switching antennae offers about 1 dB gain more than the 6-antenna orthogonal STBC system and more than a half dB gain over the configuration with five transmitting antennae and one switching antenna.

5.6 RAKE finger management over the soft handoff region

Another application of the concept of adaptive combining is the figure management for a RAKE receiver operating in the handover region. RAKE receivers are commonly used in wideband wireless systems, such as WCDMA and UWB systems, to mitigate the effect of fading. RAKE receivers also facilitate the soft handover (SHO) in the handover region. Specifically, the mobile receiver can combine resolvable paths from both the serving base station (BS) and the target BS, which can greatly reduce the probability of dropped connections when the mobile receiver is at the cell boundary [29, sect. 9.5.1]. On the other hand, serving the mobile user with more than one BS will incur a significant amount

of system overhead, usually termed SHO overhead. Note that user data signals need to be sent to and from all involved BSs to enjoy the diversity benefit.

In this section, we apply the concept of adaptive combining to develop several low-complexity finger management schemes and investigate their performance and complexity [11, 30]. The main idea is to minimize the SHO overhead by letting the receiver scan the additional resolvable paths from the target BS only if the received signal based solely on the serving BS is of unsatisfactory quality. We will show that the proposed schemes can reduce the unnecessary path estimations and the SHO overhead compared to the conventional GSC scheme [31,32] which always uses the best resolved paths from both BSs.

5.6.1 Finger management schemes

We consider the mobile unit which is equipped with an L_c finger RAKE receiver and is capable of despreading signals from different BSs using different fingers, and thus facilitating the SHO process. Without loss of generality, we assume that there are L resolvable paths from the serving BS and L_a paths from the target BS. We focus on the receiver operation when the mobile unit is moving from the coverage area of its serving BS to that of a target BS. As the mobile unit enters the SHO region, the RAKE receiver relies at first on the L resolvable paths gathered from the serving BS and as such starts with L_c/L-GSC. If we let $\Gamma_{i:j}$ be the sum of the i largest SNRs among j ones, i.e. $\Gamma_{i:j} = \sum_{k=1}^{i} \gamma_{k:j}$ where $\gamma_{k:j}$ is the kth-order statistics, then the total received SNR after GSC is given by $\Gamma_{L_c:L}$. At the beginning of every time slot, the receiver compares the received SNR, $\Gamma_{L_c:L}$, with a certain target SNR, denoted by γ_T. If $\Gamma_{L_c:L}$ is greater than or equal to γ_T, the mobile continues to rely solely on its current serving BS and SHO is not initiated.

On the other hand, whenever $\Gamma_{L_c:L}$ falls below γ_T, the mobile will initiate SHO by estimating and combining resolvable paths from the target BS using the available figures. We consider two finger update strategies in this work, i.e. full GSC [11] or block change [30]. With full GSC, the RAKE receiver reassigns its L_c fingers to the L_c strongest paths among the total $L + L_a$ available resolvable paths from both the serving and the target BSs (i.e. the RAKE receiver uses $(L + L_a)/L_c$-GSC). Now the total received SNR is given by $\Gamma_{L_c/L+L_a}$. Based on the above mode of operation, we can see that the final combined SNR, denoted by γ_c, with full GSC scheme, is given mathematically by

$$\gamma_c = \begin{cases} \Gamma_{L_c/L+L_a}, & 0 \le \Gamma_{L_c/L} < \gamma_T; \\ \Gamma_{L_c/L}, & \Gamma_{L_c/L} \ge \gamma_T. \end{cases} \tag{5.71}$$

With the block change scheme, the RAKE receiver compares the sums of two groups of path SNRs: the sum of the L_s smallest paths among the L_c currently used paths from the serving BS (i.e. $\sum_{i=L_c-L_s+1}^{L_c} \gamma_{i:L}$) and the sum of the L_s strongest paths from the target BS (i.e. $\sum_{i=1}^{L_s} \gamma_{i:L_a}$). Then, the receiver replaces

the L_s smallest paths which are currently used with the best group. Note that no replacement occurs if the sum of the L_s strongest additional paths from the target BS is less than the sum of the L_s weakest paths among the L_c strongest paths from the serving BS. For simplicity, if we let

$$Y = \sum_{i=1}^{L_c - L_s} \gamma_{i:L}, \qquad Z = \sum_{i=L_c - L_s + 1}^{L_c} \gamma_{i:L},$$
$$\text{and} \quad W = \sum_{i=1}^{L_s} \gamma_{i:L_a},$$

then, based on the above mode of operation, the final combined SNR, γ_c, with block change is then given by

$$\gamma_c = \begin{cases} Y + \max\{Z, W\}, & 0 \le Y + Z < \gamma_T; \\ Y + Z, & Y + Z \ge \gamma_T. \end{cases} \tag{5.72}$$

Note that the block change scheme only needs to compare the sum of two groups of L_s path SNRs and, as such, avoids reordering all the paths, which is essential for the full GSC scheme. Therefore, a further reduction in SNR comparisons and SHO overhead can be obtained. In the following analysis, we focus on the block change scheme and compare its performance with the full GSC scheme whenever appropriate.

5.6.2 Statistics of output SNR

Based on the mode of operation of the block change scheme summarized in (5.72), the CDF of the combined SNR γ_c, $F_{\gamma_c}(x)$, can be written as

$$\begin{aligned} F_{\gamma_c}(x) &= \begin{cases} \Pr\left[Y + \max\{Z, W\} < x\right], & 0 \le x < \gamma_T; \\ \Pr\left[\gamma_T \le Y + Z < x\right] \\ \quad + \Pr[Y + \max\{Z, W\} < x, \\ \quad\quad Y + Z < \gamma_T], & x \ge \gamma_T \end{cases} \\ &= \begin{cases} \Pr\left[Z \ge W, Y + Z < x\right] \\ \quad + \Pr\left[Z < W, Y + W < x\right], & 0 \le x < \gamma_T; \\ \Pr\left[\gamma_T \le Y + Z < x\right] \\ \quad + \Pr[Z \ge W, Y + Z < \gamma_T] \\ \quad + \Pr[Z < W, Y + W < x, \\ \quad\quad Y + Z < \gamma_T], & x \ge \gamma_T. \end{cases} \end{aligned} \tag{5.73}$$

In (5.73), $\Pr\left[\gamma_T \le Y + Z < x\right]$ can be calculated easily using the CDF of the combined SNR of L/L_c-GSC. Noting that W is independent of Y and Z, we can

calculate the other joint probabilities in (5.73) as

$$\Pr[Z \geq W, Y + Z < x] \tag{5.74}$$
$$= \int_0^x \int_0^{x-y} \int_w^{x-y} p_{Y,Z}(y,z) p_W(w) \mathrm{d}z\mathrm{d}w\mathrm{d}y,$$
$$\Pr[Z < W, Y + W < x] \tag{5.75}$$
$$= \int_0^x \int_0^{x-y} \int_0^{w} p_{Y,Z}(y,z) p_W(w) \mathrm{d}z\mathrm{d}w\mathrm{d}y,$$
$$\Pr[Z \geq W, Y + Z < \gamma_T] \tag{5.76}$$
$$= \int_0^{\gamma_T} \int_0^{\gamma_T - y} \int_w^{\gamma_T - y} p_{Y,Z}(y,z) p_W(w) \mathrm{d}z\mathrm{d}w\mathrm{d}y,$$
$$\Pr[Z < W, Y + W < x, Y + Z < \gamma_T] \tag{5.77}$$
$$= \int_0^{\gamma_T} \int_0^{x-y} \int_0^{\min\{w, \gamma_T - y\}} p_{Y,Z}(y,z) p_W(w) \mathrm{d}z\mathrm{d}w\mathrm{d}y.$$

It is easy to see that $p_W(w)$ is simply the PDF of the combined SNR with L_a/L_s-GSC. The joint PDF of Y and Z, $p_{Y,Z}(y,z)$ is the joint PDF of two partial sums of ordered random variables. Based on the result of the previous chapters, $p_{Y,Z}(y,z)$ can be calculated as

$$p_{Y,Z}(y,z) = \int_0^{\frac{z}{L_s}} \int_{\frac{z}{L_s}}^{\frac{y}{L_c - L_s}} p_{A,\gamma_{L_c - L_s:L}, B, \gamma_{L_c:L}}(y - \alpha, \alpha, z - \beta, \beta) \mathrm{d}\alpha\mathrm{d}\beta,$$
$$y > \frac{L_c - L_s}{L_s} z, \tag{5.78}$$

where $p_{A,\gamma_{l:L},B,\gamma_{k:L}}(a,\alpha,b,\beta)$ is the joint PDF of four random variables defined as the following

$$\underbrace{\overbrace{\gamma_{1:L}, \cdots, \gamma_{L_c - L_s - 1:L}}^{A = \sum_{i=1}^{L_c - L_s - 1} \gamma_{i:L}}, \gamma_{L_c - L_s:L}}_{Y = \sum_{i=1}^{L_c - L_s} \gamma_{i:L}}, \underbrace{\overbrace{\gamma_{L_c - L_s + 1:L}, \cdots, \gamma_{L_c - 1:L}}^{B = \sum_{i=L_c - L_s + 1}^{L_c - 1} \gamma_{i:L}}, \gamma_{L_c:L}}_{Z = \sum_{i=L_c - L_s + 1}^{L_c} \gamma_{i:L}}, \gamma_{L_c + 1:L}, \cdots, \gamma_{L:L}. \tag{5.79}$$

For i.i.d. Rayleigh fading channels, we can obtain the closed-form expression for the joint PDF, $p_{A,\gamma_{l:L},B,\gamma_{k:L}}(a,\alpha,b,\beta)$, as

$$p_{A,\gamma_{l:L},B,\gamma_{k:L}}(a,\alpha,b,\beta) \tag{5.80}$$
$$= \frac{L! e^{-(a+\alpha+b+\beta)/\overline{\gamma}} (1 - e^{-\beta/\overline{\gamma}})^{L-k} [a - (l-1)\alpha]^{l-2}}{(L-k)!(k-l-1)!(k-l-2)!(l-1)!(l-2)!\overline{\gamma}^k}$$
$$\times \sum_{j=0}^{k-l-1} \binom{k-l-1}{j} (-1)^j [b - \beta(k-l-j-1) - \alpha j]^{k-l-2}$$
$$\times \mathcal{U}(\alpha)\mathcal{U}(\alpha - \beta)\mathcal{U}(a - (l-1)\alpha)$$
$$\times \mathcal{U}(b - \beta(k-l-j-1) - \alpha j),$$
$$0 < (k-l-1)\beta < b < (k-l-1)\alpha.$$

Note that the joint PDF of Y and Z (5.78) involves only finite integrations of elementary functions and, as such, can be easily calculated with mathematical software, such as Mathematica. Also note that even though (5.78) is valid only when $l \geq 2$ and $k \geq l+2$, all other cases can be obtained easily by following similar steps used for (5.80).

Finally, considering (5.78) together with (5.74)–(5.77), the CDF of γ_t, $F_{\gamma_c}(x)$, in (5.73) can be obtained. Differentiating (5.73) with respect to x, we can obtain, after some manipulations, the following generic expression for the PDF of the combined SNR, γ_c, as

$$p_{\gamma_c}(x) = \begin{cases} \int_0^x \Big(p_{Y,Z}(y, x-y) F_W(x-y) \\ + p_W(x-y) \int_0^{x-y} p_{Y,Z}(y,z) \mathrm{d}z \Big) \mathrm{d}y, \quad 0 \leq x < \gamma_T; \\ p_{Y+Z}(x) \\ + \int_0^{\gamma_T} \Big(p_W(x-y) \int_0^{\gamma_T - y} p_{Y,Z}(y,z) \mathrm{d}z \Big) \mathrm{d}y, \ x \geq \gamma_T, \end{cases} \tag{5.81}$$

where $p_{Y,Z}(\cdot,\cdot)$ is defined in (5.78), $p_{Y+Z}(\cdot)$ is the PDF of the combined SNR with L/L_c-GSC, $p_W(\cdot)$ and $F_W(\cdot)$ are the PDF and CDF of the combined SNR with L_a/L_s-GSC, respectively, for both of which the closed-form expression for i.i.d. Rayleigh fading environment is available (see (5.27) and (5.18)).

With the statistics of the combined SNR derived, we can evaluate the performance of the block change scheme and compare it with that of the full GSC scheme through numerical example. In Fig. 5.23, we consider the effect of the switching threshold on the performance by plotting the average BER of BPSK versus the average SNR per path, $\overline{\gamma}$, of the block change scheme proposed and the full GSC scheme in [11] for various values of γ_T over i.i.d. Rayleigh fading channels when $L = 5, L_a = 5, L_c = 3$, and $L_s = 2$. From this figure, it is clear that the higher the threshold, the better the performance, as we expect intuitively. Note that when $\overline{\gamma}$ becomes larger, the combined SNR is typically large enough in a way that the receiver does not need to rely on the additional paths from the target BS. Hence, we can observe that in good channel conditions (i.e. $\overline{\gamma}$ is relatively large compared to γ_T), both schemes become insensitive to variations in γ_T. Also note that when the switching threshold is small, both schemes have almost the same performance since the additional paths are not necessary. On the other hand, in the case of large threshold values, the full GSC scheme shows better performance, as with the full GSC scheme, instead of comparing and replacing blocks, the L_c largest paths are selected among the $L + L_a$ ones.

In Fig. 5.24, we vary the block size, L_s, with two values of γ_T. We can see that for the low threshold, the variations of the block size do not affect the performance since in this case no replacement is needed. However, when the threshold is set high, we can observe the performance difference according to the value of L_s. For our chosen set of parameters, the best performance which

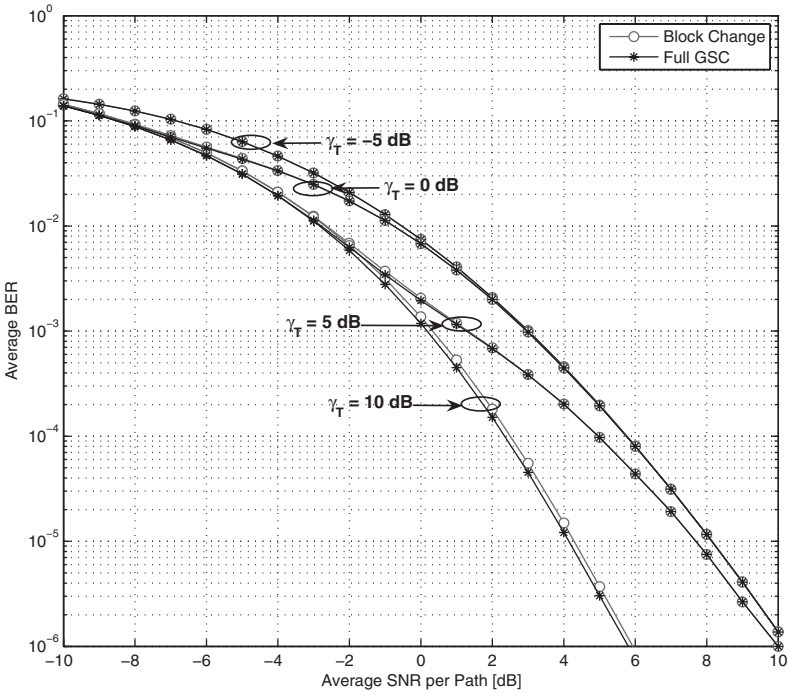

Figure 5.23 Average BER of BPSK versus the average SNR per path, $\overline{\gamma}$, of the Block Change and the full GSC schemes for various values of γ_T over i.i.d. Rayleigh fading channels when $L = 5, L_a = 5, L_c = 3$, and $L_s = 2$ [30]. © 2008 IEEE.

is very close to that of the full GSC scheme can be acquired when $L_s = 2$. This is because if $L_s = 1$, we have little benefit from the additional paths, while if $L_s = 3$, we have more chances to lose the better paths during the replacement process.

5.6.3 Complexity analysis

As shown in the previous section, because the paths with the strongest SNR values are selected whenever SHO is initiated, the full GSC scheme always provides a better performance than the block change scheme. However, the block change scheme enjoys a lower complexity, as it avoids the need for a full reordering process of all available paths from the serving and the target BSs. In this section, we investigate this complexity trade-off issue by quantifying the average number of path estimations, the average number of SNR comparisons, and the SHO overhead.

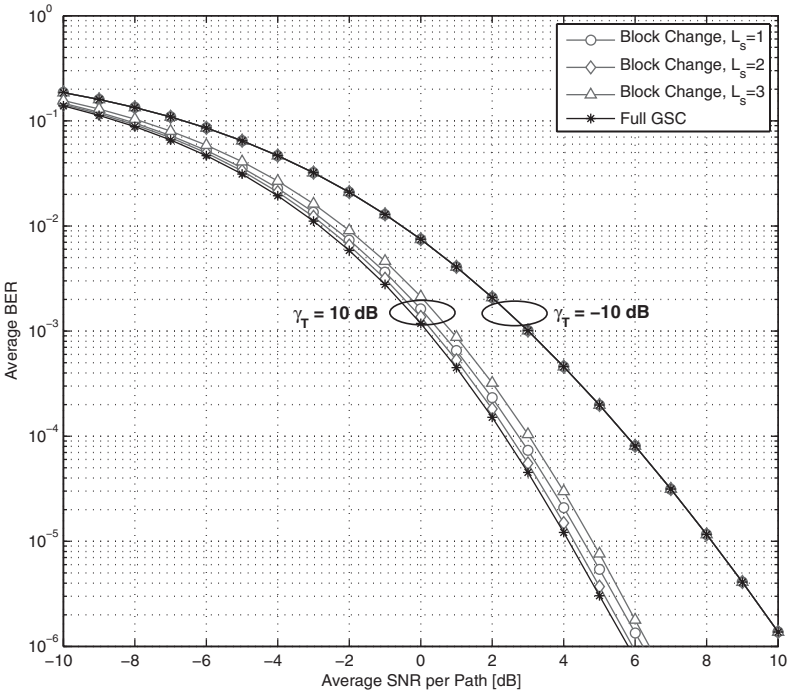

Figure 5.24 Average BER of BPSK versus the average SNR per path, $\overline{\gamma}$, of the Block Change and the full GSC schemes for various values of L_s and γ_T over i.i.d. Rayleigh fading channels when $L = 5, L_a = 5$ and $L_c = 3$ [30]. © 2008 IEEE.

With the proposed scheme, the RAKE receiver estimates the L paths in the case of $\Gamma_{L_c/L} \geq \gamma_T$ or $L + L_a$ in the case of $\Gamma_{L_c/L} < \gamma_T$. Hence, the average number of path estimations of the block change scheme is the same as that of the full GSC scheme [11, eq. (25)].

As another complexity measure, we calculate the average number of required SNR comparisons. Noting that the average number of SNR comparisons for j/i-GSC, denoted by $C_{j/i-GSC}$, can be obtained as[1]

$$C_{j/i-GSC} = \sum_{k=1}^{\min[i,j-i]} (j-k), \tag{5.82}$$

[1] With the traditional sorting approach, we need $k-1$ comparisons to find the kth largest/smallest one after the previous $k-1$ largest/smallest ones have been found. We follow this traditional approach in order to perform an accurate complexity comparison while noting that with a quick sorting algorithm for n paths, we just need $O(\log(n))$ complexity.

we can express the average number of SNR comparisons for the full GSC scheme and the block change scheme as

$$C_{Full} = \Pr\left[\Gamma_{L_c/L} \geq \gamma_T\right] C_{L/L_c-GSC} + \Pr\left[\Gamma_{L_c/L} < \gamma_T\right] C_{(L+L_a)/L_c-GSC} \tag{5.83}$$

and

$$C_{Block} = C_{L/L_c-GSC} + \Pr\left[\Gamma_{L_c/L} < \gamma_T\right] \times \left(C_{L_c/L_s-GSC} + C_{L_a/L_s-GSC} + 1\right), \tag{5.84}$$

respectively.

Since the SHO is attempted whenever $\Gamma_{L_c/L}$ is below γ_T, the probability of the SHO attempt is same as the outage probability of L_c/L-GSC evaluated at γ_T, i.e. $F_{\Gamma_{L_c/L}}(\gamma_T)$. The SHO overhead, denoted by β, is commonly used to quantify the SHO activity in a network and is defined as [33, eq. (9.2)]

$$\beta = \sum_{n=1}^{N} nF_n - 1, \tag{5.85}$$

where N is the number of active BSs and F_n is the average probability that the mobile unit uses n-way SHO. Based on the mode of operation of the block change scheme, we can express its SHO overhead, β, as

$$\beta = \begin{cases} F_{Y+Z}(\gamma_T) \Pr\left[Z < W | Y + Z < \gamma_T\right], & L_s < L_c; \\ 0, & L_s = L_c. \end{cases} \tag{5.86}$$

Note that $F_{Y+Z}(\gamma_T)$ is the CDF of L_c/L-GSC output SNR evaluated at γ_T. Since W is independent to Z and Y, we can calculate the conditional probability, $\Pr[Z < W|Y + Z < \gamma_T]$, in (5.86) as

$$\Pr\left[Z < W | Y + Z < \gamma_T\right] = \int_0^\infty F_{Z|Y+Z<\gamma_T}(x) p_W(x) \mathrm{d}x, \tag{5.87}$$

where the conditional CDF in (5.87) can be obtained as

$$F_{Z|Y+Z<\gamma_T}(x) = \frac{\Pr\left[Z < x, Y + Z < \gamma_T\right]}{\Pr\left[Y + Z < \gamma_T\right]} = \frac{1}{F_{Y+Z}(\gamma_T)} \times \begin{cases} \int_0^x \int_{(L_c-L_s)z/L_s}^{\gamma_T - z} f_{Y,Z}(y,z) \mathrm{d}y \mathrm{d}z, & 0 \leq x < \frac{L_s}{L_c}\gamma_T; \\ \int_0^{L_s\gamma_T/L_c} \int_{(L_c-L_s)z/L_s}^{\gamma_T - z} f_{Y,Z}(y,z) \mathrm{d}y \mathrm{d}z, & x \geq \frac{L_s}{L_c}\gamma_T, \end{cases} \tag{5.88}$$

After successive substitutions from (5.88) to (5.86), we can finally obtain the analytical expression of the SHO overhead.

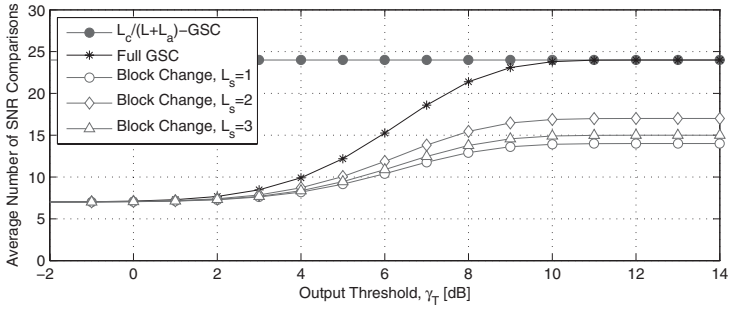

(a) Average Number of SNR Comparisons

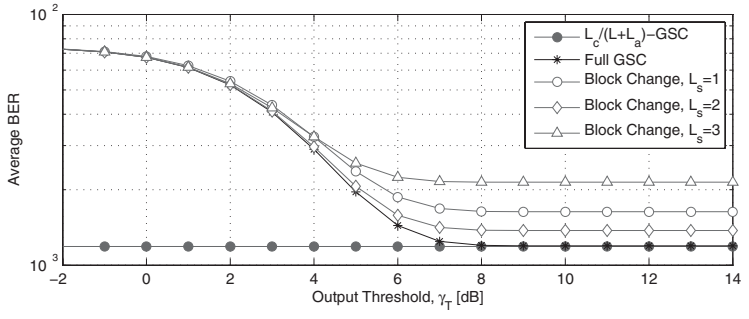

(b) Average BER

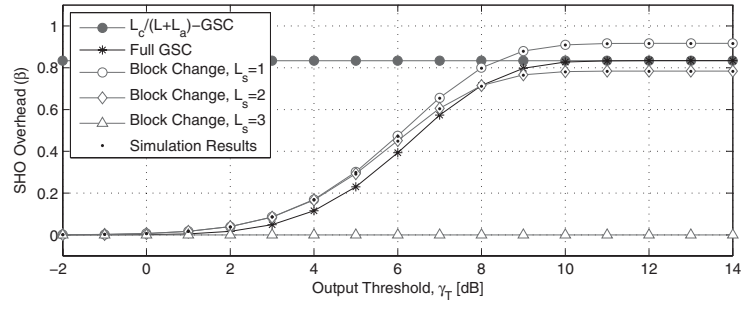

(c) SHO Overhead

Figure 5.25 Complexity trade-off versus the output threshold, γ_T, of the block change and the full GSC schemes, and conventional GSC for various values of L_s over i.i.d. Rayleigh fading channels with $L = 5, L_a = 5, L_c = 3$, and $\overline{\gamma} = 0$ dB [30]. © 2008 IEEE.

In Fig. 5.25, we plot (a) the average number of SNR comparisons, (b) the average BER, and (c) the SHO overhead versus the output threshold, γ_T, of the block change and the full GSC schemes for various values of L_s over i.i.d. Rayleigh fading channels when $L = 5, L_a = 5, L_c = 3$, and $\overline{\gamma} = 0$ dB. For comparison purposes, we also plot those for conventional $(L + L_a)/L_c$-GSC. Note that

the full GSC scheme is acting as $(L + L_a)/L_c$-GSC when the output threshold becomes large. Hence, we can observe from all the subfigures that the full GSC scheme converges to GSC as γ_T increases.

Recall that the block change scheme has the same path estimation load as the full GSC scheme. However, from Fig. 5.25(a), we can see that the block change scheme leads to a great reduction of the SNR comparison load compared to the full GSC scheme. For example, let us consider the case that $\gamma_T > 8$ dB and $L_s = 2$. In this case, the reduction of the SNR comparison load is maximized compared to the full GSC scheme. However, from Fig. 5.25(b), we can observe in the same SNR region a very slight performance loss of the block change scheme compared to the full GSC as well as the conventional GSC schemes.

For the SHO overhead, simulation results are also presented in Fig. 5.25(c) to verify our analysis. It is clear from this figure that the receiver has a higher chance to use 2-way SHO as L_s decreases. This is because as L_s decreases, the probability that the sum of the L_s smallest paths among the L_c currently used paths from the serving BS is less than the sum of the L_s strongest paths from the target BS is increasing and as such, we have a higher chance to replace groups. From this figure together with Fig. 5.25(b), we can quantify the trade-off between the SHO overhead and the performance. Again, let us consider the case that $\gamma_T > 8$ dB and $L_s = 2$. In this case, note the reduction of SHO overhead at the expense of a slight performance loss in comparison to the full GSC scheme. If we increase the number of fingers, i.e. $L_c = 4$, we can observe more reductions in complexity with a slight performance loss.

5.7 Joint adaptive modulation and diversity combining

Adaptive modulation has been widely utilized to achieve efficient and reliable communications over time-varying wireless fading channels. The basic idea of adaptive modulation, as summarized in a previous chapter, is to match the modulation parameters with the instantaneous fading channel conditions such that the transmission rate is maximized while satisfying a certain instantaneous error rate requirement [34–36]. For the constant-power variable-rate uncoded M-ary QAM scheme studied in [35], the value range of the instantaneous SNR is divided into $N + 1$ regions with properly selected threshold γ_{T_n}, $n = 0, 1, \cdots, N$. The modulation scheme 2^n-QAM is used during the data reception if received SNR γ is in the nth region, where $\gamma_{T_n} \leq \gamma < \gamma_{T_{n+1}}$. More thorough treatment on adaptive transmission can be found in [37].

We can naturally observe that both adaptive modulation and adaptive diversity combining schemes utilize some predetermined threshold in their operation. Based on this observation, we look into some joint design of adaptive modulation and diversity combining in this section. With the resulting joint adaptive

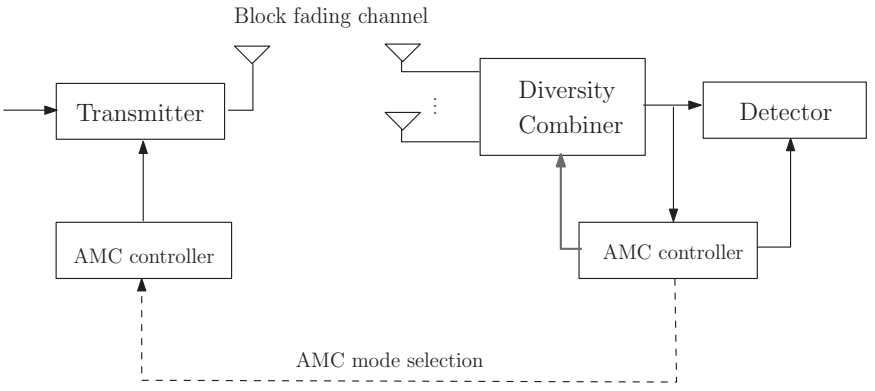

Figure 5.26 System model of joint adaptive modulation and diversity combining.

modulation and diversity combining (AMDC) schemes, the receiver jointly determines the most appropriate modulation mode and diversity combiner structure based on the current channel conditions and the desired BER requirements. In the meantime, the receiver simultaneously uses the thresholds set for the adaptive modulation mode selection to guide the operation of the adaptive combining schemes. The system model of the proposed joint design is illustrated in Fig. 5.26. The proposed AMDC systems can efficiently explore the bandwidth and power resource by transmitting at higher data rate and/or combining the least number of diversity paths under favorable channel conditions. On the other hand, the AMDC system also responds to channel degradation with an increase in the number of combined paths and/or a reduction in the data rate.

While our proposed ideas are applicable to many output threshold based adaptive combining schemes [2–6, 38], for the sake of clarity, we focus on MS-GSC with $L_c = L$, i.e. the receiver implements the same number of MRC branches as the number of available diversity paths [4]. Depending on the primary objective of the joint design, we can arrive at an AMDC scheme with a high processing power efficiency (termed power-efficient AMDC), an AMDC scheme with a high bandwidth efficiency (termed bandwidth-efficient AMDC), and an AMDC scheme with a high bandwidth efficiency and improved power efficiency at the cost of a higher error rate than the bandwidth-efficient AMDC scheme (termed bandwidth-efficient and power-greedy AMDC) [12], all of which satisfy the desired BER requirement. For all the three AMDC schemes under consideration, we quantify through accurate analysis their processing power consumption (quantified in terms of average number of combined diversity paths), spectral efficiency (quantified in terms of average number of transmitted bits/s/Hz), and performance (quantified in terms of average BER). In addition, some selected numerical examples are presented to illustrate the mathematical formalism.

5.7.1 Power-efficient AMDC scheme

The primary objective of the power-efficient AMDC scheme is to minimize the processing power consumption of the diversity combiner, i.e. to minimize the average number of combined/active diversity paths during the data burst reception. Once this primary objective is met, this scheme tries to afford the largest possible spectral efficiency while meeting the required target BER. Based on these objectives, the diversity combiner will perform just enough combining operations such that at least the lowest adaptive modulation mode, e.g. BPSK, will exhibit an instantaneous BER smaller than the predetermined target value. In particular, the receiver tries to increase the output SNR γ_c above the threshold for BPSK, denoted by γ_{T_1}, by performing MS-GSC diversity. After estimating and ranking the L available diversity paths, the combiner first checks if the SNR of the strongest path is greater than γ_{T_1}. If so, the combiner uses the output signal from just the strongest path. If not, the combiner checks the combined SNR of the first two strongest paths. If the combined SNR is still less than γ_{T_1}, then the combiner checks the combined SNR of the first three strongest paths. This process is continued until either (i) the combined SNRs become greater than γ_{T_1}, or (ii) all L available paths have been combined. In the first case, the receiver starts to determine the modulation mode to be selected by checking in which interval the resulting output SNR falls. In particular, the receiver sequentially compares the output SNR with respect to the thresholds, γ_{T_2}, γ_{T_3}, $\cdots$, γ_{T_N}. Whenever the receiver finds that the output SNR is smaller than $\gamma_{T_{n+1}}$ but greater than γ_{T_n}, it selects the modulation mode n for the subsequent data burst and feeds back that particular modulation mode to the transmitter. If the combined SNR of all L available branches is still below γ_{T_1}, the receiver may ask the transmitter to either (i) transmit using the lowest modulation mode in violation of the target instantaneous BER requirement (option 1), or (ii) buffer the data and wait until the next guard period for more favorable channel conditions (option 2).

While this mode of operation is different than that of the power-efficient multiple thresholds minimum selection combining (MT-MSC) scheme, which was described and simulated in [39], it can be shown easily that these two schemes are actually equivalent from an output SNR and performance standpoint. As such, an alternative presentation/implementation of our proposed power-efficient AMDC scheme can be found in the flow chart illustrating the mode of operation of the power efficient MT-MSC given in [39, fig. 1].

Statistics of output SNR

Based on the mode of operation described above, we can see that the received SNR, γ_c, of the power-efficient AMDC system is the same as the combined SNR of MS-GSC scheme with γ_{T_1} as the output threshold. In other words, the CDF of the received SNR, $F_{\gamma_c}(\cdot)$, of the power-efficient AMDC based on MS-GSC is

given by

$$F_{\gamma_c}(\gamma) = \begin{cases} F_{\gamma_c}^{MSC(\gamma_{T_1})}(\gamma), & \text{for option 1;} \\ \begin{cases} F_{\gamma_c}^{MSC(\gamma_{T_1})}(\gamma), & \gamma > \gamma_{T_1}; \\ F_{\gamma_c}^{MSC(\gamma_{T_1})}(\gamma_{T_1}), & 0 < \gamma \leq \gamma_{T_1} \end{cases} & \text{for option 2,} \end{cases} \tag{5.89}$$

where $F_{\gamma_c}^{MSC(\gamma_{T_1})}(\cdot)$ denotes the CDF of the combined SNR with L-branch MS-GSC and using γ_{T_1} as an output threshold. The generic expression of $F_{\gamma_c}^{MSC(\gamma_{T_1})}(\cdot)$ was given in (5.21) with γ_T changed to γ_{T_1} and $L_c = L$, which is available in closed-form for the i.i.d. Rayleigh fading environment in [4, eq. (30)].

Correspondingly, the PDF of the received SNR, $p_{\gamma_c}(\cdot)$, is given by

$$p_{\gamma_c}(\gamma) = \begin{cases} p_{\gamma_c}^{MSC(\gamma_{T_1})}(\gamma), & \text{for option 1;} \\ p_{\gamma_c}^{MSC(\gamma_{T_1})}(\gamma)\mathcal{U}(\gamma - \gamma_{T_1}) + p_{\gamma_c}^{MSC(\gamma_{T_1})}(\gamma_{T_1})\delta(\gamma), & \text{for option 2,} \end{cases} \tag{5.90}$$

where $\delta(\cdot)$ is the Delta function and $p_{\gamma_c}^{MSC(\gamma_{T_1})}(\cdot)$ denotes the PDF of the combined SNR with L-branch MS-GSC and using γ_{T_1} as an output threshold, which is available in closed form for the i.i.d. Rayleigh fading environment in (5.23) with γ_T changed to γ_{T_1} and $L_c = L$.

Performance and processing power analysis

The power consumption for diversity combining can be quantified in terms of the average number of combined paths [4]. It can be shown that the average number of combined paths with the power-efficient AMDC is given for option 1 by

$$\overline{N}_C = 1 + \sum_{i=1}^{L-1} F_{\Gamma_i}(\gamma_{T_1}),$$

and for option 2 by

$$\overline{N}_C = 1 + \sum_{i=1}^{L-1} F_{\Gamma_i}(\gamma_{T_1}) - L F_{\gamma_c}^{L-MRC}(\gamma_{T_1}),$$

where $F_{\Gamma_i}(\cdot)$ is the CDF of the combined SNR with L/i-GSC scheme (which is given in closed-form for i.i.d. Rayleigh fading in (5.18)) and $F_{\gamma_c}^{L-MRC}(\cdot)$ is the CDF of the combined SNR with L-branch MRC scheme (which is given in closed-form for i.i.d. Rayleigh fading in Table 5.1).

The average spectral efficiency of an adaptive modulation system can be calculated as [35, eq. (33)]

$$\eta = \sum_{n=1}^{N} n \; P_n,$$

where n is the number of bits carried by a symbol of modulation mode, P_n is the probability that the nth constellation is used. For the power-efficient AMDC system based on MS-GSC, it can be shown that P_n is given by

$$P_n = \begin{cases} \begin{cases} F_{\gamma_c}^{MSC(\gamma_{T_1})}(\gamma_{T_{n+1}}) - F_{\gamma_c}^{MSC(\gamma_{T_1})}(\gamma_{T_n}), & n \geq 2; \\ F_{\gamma_c}^{MSC(\gamma_{T_1})}(\gamma_{T_2}), & n = 1 \end{cases} & \text{for option 1;} \\ F_{\gamma_c}^{MSC(\gamma_{T_1})}(\gamma_{T_{n+1}}) - F_{\gamma_c}^{MSC(\gamma_{T_1})}(\gamma_{T_n}), & \text{for option 2.} \end{cases} \tag{5.91}$$

Therefore, the average spectral efficiency of the MS-GSC-based AMDC system is given by

$$\eta = \begin{cases} N - \sum_{n=2}^{N} F_{\gamma_c}^{MSC(\gamma_{T_1})}(\gamma_{T_n}), & \text{for option 1;} \\ N - \sum_{n=1}^{N} F_{\gamma_c}^{MSC(\gamma_{T_1})}(\gamma_{T_n}), & \text{for option 2.} \end{cases} \tag{5.92}$$

The average BER for adaptive modulation system can be calculated as [35, eq. (35)]

$$< BER >= \frac{1}{\eta} \sum_{n=1}^{N} n \, \overline{BER}_n, \tag{5.93}$$

where $\overline{BER}_n$ is the average error rate for constellation n, and which is given by

$$\overline{BER}_n = \int_{\gamma_{T_n}}^{\gamma_{T_{n+1}}} BER_n(\gamma) p_{\gamma_c}^{MSC(\gamma_{T_1})}(\gamma) \mathrm{d}\gamma, \tag{5.94}$$

where $BER_n(\gamma)$ is the conditional BER of the constellation n over the AWGN channel given that the SNR is equal to γ, an approximate expression of which was given in (2.59). Therefore, the average BER of the power-efficient AMDC based on MS-GSC can be calculated as

$$< BER >= \begin{cases} \frac{1}{\eta} \left(\int_0^{\gamma_{T_2}} BER_1(\gamma) \; p_{\gamma_c}^{MSC(\gamma_{T_1})}(\gamma) \; \mathrm{d}\gamma \right. \\ \left. + \sum_{n=2}^{N} n \int_{\gamma_{T_n}}^{\gamma_{T_{n+1}}} BER_n(\gamma) \; p_{\gamma_c}^{MSC(\gamma_{T_1})}(\gamma) \; \mathrm{d}\gamma \right), & \text{for option 1;} \\ \frac{1}{\eta} \sum_{n=1}^{N} n \int_{\gamma_{T_n}}^{\gamma_{T_{n+1}}} BER_n(\gamma) \; p_{\gamma_c}^{MSC(\gamma_{T_1})}(\gamma) \; \mathrm{d}\gamma, & \text{for option 2.} \end{cases} \tag{5.95}$$

5.7.2 Bandwidth-efficient AMDC scheme

The primary objective of the bandwidth-efficient AMDC scheme is to maximize the spectral efficiency. As such, the receiver with this scheme performs the necessary combining operations so that the highest achievable modulation mode can be used while satisfying the instantaneous BER requirement. More specifically, the receiver tries first to increase the output SNR γ_c above the threshold of highest modulation mode 2^N-QAM, i.e. γ_{T_N} , by employing an MS-GSC type of diversity. After estimating and ranking all the available diversity paths, the

combiner sequentially checks the SNR of the strongest path, the combined SNR of the two strongest paths, the combined SNR of the three strongest paths, etc. Whenever the combined SNR is larger than γ_{T_N}, the receiver stops checking and informs the transmitter to use 2^N-QAM as the modulation mode for the subsequent data reception. If the combined SNR of all the available paths is still below γ_{T_N}, the receiver selects the modulation mode corresponding to the SNR interval in which the combined SNR falls into. In particular, the receiver sequentially compares the output SNR with the thresholds, $\gamma_{T_{N-1}}$, $\gamma_{T_{N-2}}$, $\cdots$, γ_{T_1}. Whenever the receiver finds that the output SNR is smaller than $\gamma_{T_{n+1}}$ but greater than γ_{T_n}, it selects the modulation mode n for the subsequent data burst and feeds back this selected mode to the transmitter. If, in the worst case, the combined SNR of all the available paths ends up being below γ_{T_1}, the receiver has the same two termination options as for the power-efficient scheme (i.e. to transmit using the lowest modulation mode (option 1) or to wait until the next guard period (option 2)).

Statistics of output SNR

Based on the mode of operation described above, we can see that the received SNR, γ_c, of the bandwidth-efficient AMDC system is the same as the combined SNR of MS-GSC diversity with γ_{T_N} as the output threshold. Therefore, the CDF of the received SNR of this bandwidth-efficient AMDC scheme based on MS-GSC is given by

$$F_{\gamma_c}(\gamma) = \begin{cases} F_{\gamma_c}^{MSC(\gamma_{T_N})}(\gamma), & \text{for option 1;} \\ \begin{cases} F_{\gamma_c}^{MSC(\gamma_{T_N})}(\gamma), & \gamma > \gamma_{T_1}; \\ F_{\gamma_c}^{MSC(\gamma_{T_N})}(\gamma_{T_1}), & 0 < \gamma \leq \gamma_{T_1} \end{cases} & \text{for option 2,} \end{cases} \tag{5.96}$$

where $F_{\gamma_c}^{MSC(\gamma_{T_N})}(\cdot)$ denotes the CDF of the combined SNR with L-branch MS-GSC and γ_{T_N} as an output threshold. Correspondingly, the PDF of the received SNR is given by

$$p_{\gamma_c}(\gamma) = \begin{cases} p_{\gamma_c}^{MSC(\gamma_{T_N})}(\gamma), & \text{for option 1;} \\ p_{\gamma_c}^{MSC(\gamma_{T_N})}(\gamma)\mathcal{U}(\gamma - \gamma_{T_1}) + p_{\gamma_c}^{MSC(\gamma_{T_N})}(\gamma_{T_1})\delta(\gamma), & \text{for option 2,} \end{cases} \tag{5.97}$$

where $p_{\gamma_c}^{MSC(\gamma_{T_N})}(\cdot)$ denotes the PDF of the combined SNR with L-branch MS-GSC and γ_{T_N} as output threshold.

Performance and processing power analysis

With the statistics of the received SNR, as given in previous subsection, we can now study the processing power and the performance of the bandwidth-efficient AMDC scheme as we did for the power-efficient AMDC system. For conciseness, we just list the analytical results in the following.

- Average number of combined branches

$$\overline{N}_C = \begin{cases} 1 + \sum_{i=1}^{L-1} F_{\Gamma_i}(\gamma_{T_N}), & \text{for option 1;} \\ 1 + \sum_{i=1}^{L-1} F_{\Gamma_i}(\gamma_{T_N}) - LF{\gamma_c}^{L-MRC}(\gamma_{T_1}), & \text{for option 2.} \end{cases} \tag{5.98}$$

- Average spectral efficiency

$$\eta = \begin{cases} N - \sum_{n=2}^{N} F_{\gamma_c}^{MSC(\gamma_{T_N})}(\gamma_{T_n}), & \text{for option 1;} \\ N - \sum_{n=1}^{N} F_{\gamma_c}^{MSC(\gamma_{T_N})}(\gamma_{T_n}), & \text{for option 2.} \end{cases} \tag{5.99}$$

- Average BER

$$< BER >= \begin{cases} \frac{1}{\eta}\left(\int_0^{\gamma_{T_2}} BER_1(\gamma)\ p_{\gamma_c}^{MSC(\gamma_{T_N})}(\gamma)\ \mathrm{d}\gamma \right. \\ \left. + \sum_{n=2}^{N} n \int_{\gamma_{T_n}}^{\gamma_{T_{n+1}}} BER_n(\gamma)\ p_{\gamma_c}^{MSC(\gamma_{T_N})}(\gamma)\ \mathrm{d}\gamma \right), & \text{for option 1;} \\ \frac{1}{\eta} \sum_{n=1}^{N} n \int_{\gamma_{T_n}}^{\gamma_{T_{n+1}}} BER_n(\gamma)\ p_{\gamma_c}^{MSC(\gamma_{T_N})}(\gamma)\ \mathrm{d}\gamma, & \text{for option 2.} \end{cases} \tag{5.100}$$

5.7.3 Bandwidth-efficient and power-greedy AMDC scheme

The bandwidth-efficient and power-greedy AMDC scheme can be viewed as a modified bandwidth-efficient scheme with better power efficiency at the cost of a slightly higher error rate. Basically, the receiver combines the least number of diversity branches such that the highest achievable modulation mode can be used while satisfying the instantaneous BER requirement. During this process, the receiver ensures that combining additional branches does not make a higher modulation mode feasible.

More specifically, the receiver tries first to increase the output SNR γ_c above the threshold of 2^N-QAM, i.e. γ_{T_N}, by using the MS-GSC diversity combining scheme. After estimating and ranking all the available diversity paths, the combiner sequentially checks the SNR of the strongest path, the combined SNR of the two strongest paths, the combined SNR of the three strongest paths, etc. Whenever the combined SNR is larger than γ_{T_N}, the receiver selects 2^N-QAM as the modulation mode and uses current combiner structure for data reception during the subsequent data burst. If the combined SNR of all available branches is still below γ_{T_N}, the receiver determines the highest achievable modulation mode by checking in which interval the combined SNR of these branches falls. The receiver sequentially compares the output SNR with respect to the

thresholds, $\gamma_{T_{N-1}}$, $\gamma_{T_{N-2}}$, $\cdots$, γ_{T_1}. Whenever the receiver finds that the output SNR is smaller than $\gamma_{T_{n+1}}$ but greater than γ_{T_n}, it selects the modulation mode n for the subsequent data burst as it is the highest achievable one. Before the data transmission, the receiver selects the minimum combiner structure (i.e. with the minimum number of active branches) such that the output SNR is still greater than γ_{T_n}. Basically, the receiver sequentially turns off the weakest branches until a further branch turnoff will lead to an output SNR below γ_{T_n}. If, in the worst case, the combined SNR of all the available branches is below γ_{T_1}, the receiver has the same two terminating options as for the two previously presented schemes.

While this mode of operation is different than the mode of operation of the bandwidth-efficient MT-MSC scheme, which was described and simulated in [40], it can be shown easily that these two schemes are actually equivalent from an output SNR and performance standpoint. As such, an alternative presentation/implementation of our proposed bandwidth-efficient and power-greedy AMDC scheme can be found in the flow chart illustrating the mode of operation of the bandwidth-efficient MT-MSC given in [40, fig. 1].

Statistics of output SNR

Based on its mode of operation described above, we can see that the output SNR, γ_c, of the bandwidth-efficient and power-greedy AMDC scheme is the same as the combined SNR of MS-GSC with γ_{T_N} as the output threshold only for $\gamma_c > \gamma_{T_N}$ case, i.e.

$$F_{\gamma_c}(x) = F_{\gamma_c}^{MSC(\gamma_{T_N})}(x),\ x > \gamma_{T_N}. \tag{5.101}$$

For the case of $\gamma_{T_1} \le \Gamma < \gamma_{T_N}$, the statistics are more complicated to calculate. Note that $\gamma_{T_n} \le \gamma_c < \gamma_{T_{n+1}}$ if and only if $\gamma_{T_n} \le \sum_{i=1}^{L} \gamma_i < \gamma_{T_{n+1}}$. It can be shown that the CDF of the received SNR γ_c over the range of $[\gamma_{T_n}, \gamma_{T_{n+1}}]$ is mathematically given by

$$\begin{aligned} F_{\gamma_c}(x) = F_{\gamma_c}^{L-MRC}(\gamma_{T_n}) &+ \Pr\left[\gamma_{T_n} \le \gamma_{1:L} < x \,\&\, \sum_{k=1}^{L} \gamma_k < \gamma_{T_{n+1}}\right] \\ &+ \sum_{l=2}^{L} \Pr\left[\sum_{j=1}^{l-1} \gamma_{j:L} < \gamma_{T_n} \le \sum_{j=1}^{l} \gamma_{j:L} < x \,\&\, \sum_{k=1}^{L} \gamma_k < \gamma_{T_{n+1}}\right], \end{aligned} \tag{5.102}$$

where $F_{\gamma_c}^{L-MRC}(\cdot)$ denotes the CDF of the combined SNR with L-branch MRC and $\gamma_{j:L}$ denotes the jth largest path SNR among the L available ones. Let y_l denote the sum of the $l-1$ largest ordered path SNRs, i.e. $y_l = \sum_{j=1}^{l-1} \gamma_{j:L}$, and let z_l denote the sum of the $L-l$ smallest ordered path SNRs,

i.e. $z_l = \sum_{j=l+1}^{L} \gamma_{j:L}$. The CDF can be rewritten as

$$\begin{aligned} F_{\gamma_c}(x) = {} & F^{(L)}(\gamma_{T_n}) + \Pr\left[\gamma_{T_n} \le \gamma_{1:L} < x \,\&\, \gamma_{1:L} + z_1 < \gamma_{T_{n+1}}\right] \\ & + \sum_{l=2}^{L-1} \Pr\left[y_l < \gamma_{T_n} \le y_l + \gamma_{l:L} < x \,\&\, y_l + \gamma_{l:L} + z_l < \gamma_{T_{n+1}}\right] \\ & + \Pr\left[y_L < \gamma_{T_n} \le y_L + \gamma_{L:L} < x\right], \end{aligned} \tag{5.103}$$

which can be calculated in terms of the joint PDFs of y_l, $\gamma_{l:L}$ and z_l as

$$\begin{aligned} F_{\gamma_c}(x) = {} & F_{\gamma_c}^{L-MRC}(\gamma_{T_n}) + \int_{\gamma_{T_n}}^{x} \int_{0}^{\gamma_{T_{n+1}}-\gamma} p_{\gamma_{1:L},z_1}(\gamma, z)\mathrm{d}z\mathrm{d}\gamma \\ & + \sum_{l=2}^{L-1} \int_{0}^{\gamma_{T_n}} \int_{\gamma_{T_n}-y}^{\min[y/(l-1),x-y]} \int_{0}^{\gamma_{T_{n+1}}-y-\gamma} p_{y_l,\gamma_{l:L},z_l}(y,\gamma,z)\mathrm{d}z\mathrm{d}\gamma\mathrm{d}y \\ & + \int_{0}^{\gamma_{T_n}} \int_{\gamma_{T_n}-y}^{\min[y/(L-1),x-y]} p_{y_L,\gamma_{L:L}}(y,\gamma)\mathrm{d}\gamma\mathrm{d}y, \ \gamma_{T_n} \le x < \gamma_{T_{n+1}}. \end{aligned} \tag{5.104}$$

For the case of $\gamma_c < \gamma_{T_1}$, it can be shown that the CDF of γ_c for the MS-GSC-based AMDC scheme is given by

$$F_{\gamma_c}(x) = \begin{cases} F_{\gamma_c}^{L-MRC}(x), & \text{for option 1;} \\ F_{\gamma_c}^{L-MRC}(\gamma_{T_1}), & \text{for option 2,} \end{cases} \quad 0 < x < \gamma_{T_1}. \tag{5.105}$$

Thus, we have obtained the generic expression of the CDF of the combined SNR for the whole SNR value range. After differentiating $F_{\gamma_c}(x)$ with respect to x, we obtain a generic formula for the PDF of the output SNR, γ_c, as

$$p_{\gamma_c}(x) = \begin{cases} p_{\gamma_c}^{MSC(\gamma_{T_N})}(x), & x > \gamma_{T_N}; \\ \int_{0}^{\gamma_{T_{n+1}}-x} p_{\gamma_{1:L},z_1}(x,z)\mathrm{d}z \\ \quad + \sum_{l=2}^{L-1} \left(\int_{\frac{l-1}{l}x}^{\gamma_{T_n}} \int_{0}^{\gamma_{T_{n+1}}-x} p_{y_l,\gamma_{l:L},z_l}(y, x-y, z)\mathrm{d}z\mathrm{d}y \right. \\ \quad \left. \times \left(\mathcal{U}(x-\gamma_{T_n}) - \mathcal{U}(x - \frac{l}{l-1}\gamma_{T_n})\right)\right) \\ \quad + \int_{\frac{L-1}{L}x}^{\gamma_{T_n}} p_{y_L,\gamma_{L:L}}(y, x-y)\mathrm{d}y \\ \quad \times (\mathcal{U}(x-\gamma_{T_n}) - \mathcal{U}(x - \frac{L}{L-1}\gamma_{T_n})), & \gamma_{T_n} \le x < \gamma_{T_{n+1}}; \\ \begin{cases} p_{\gamma_c}^{L-MRC}(x), & \text{for option 1;} \\ \delta(x) p_{\gamma_c}^{L-MRC}(\gamma_{T_1}), & \text{for option 2,} \end{cases} & 0 < x < \gamma_{T_1}. \end{cases} \tag{5.106}$$

Note that the CDF and the PDF of the combined SNR are given in terms of the joint PDFs of y_l, $\gamma_{l:L}$, and z_l, which was studied extensively in the previous chapter. Specifically, it has been shown that these joint PDFs are available in closed form for the i.i.d. Rayleigh fading case. Specifically, it has been shown

that $F_{y_l,\gamma_{l:L},z_l}(y,\gamma,z)$ is given by

$$\begin{aligned} p_{y_l,\gamma_{l:L},z_l}(y,\gamma,z) &= p_{\gamma_{l:L}}(\gamma) \times p_{z_l|\gamma_{l:L}=\gamma}(z) \times p_{y_l|\gamma_{l:L}=\gamma,z_l=z}(y) \\ &= \frac{L!}{(L-l)!(l-1)!\overline{\gamma}^L} \frac{[y-(l-1)\gamma]^{l-2}}{(l-2)!(L-l-1)!} e^{-\frac{y+\gamma+z}{\overline{\gamma}}} \mathcal{U}(y-(l-1)\gamma) \\ &\quad \times \sum_{i=0}^{L-l} \binom{L-l}{i} (-1)^i (z-i\gamma)^{L-l-1} \mathcal{U}(z-i\gamma) \\ &\quad \gamma > 0, y > (l-1)\gamma, z < (L-l)\gamma, \end{aligned} \tag{5.107}$$

where $\mathcal{U}(\cdot)$ is the unit step function. The joint PDFs $p_{\gamma_{1:L},z_1}(\gamma,z)$ and $p_{y_L,\gamma_{L:L}}(y,\gamma)$ can be obtained as marginals of the joint PDF given in (5.107).

Performance and processing power analysis

We now study the performance and processing power of the bandwidth-efficient and power-greedy AMDC schemes based on the statistics of the received SNR that we just derived. Note that the bandwidth-efficient and power-greedy AMDC scheme always uses the highest achievable modulation mode, and as such it will have the same average spectral efficiency as the bandwidth-efficient AMDC scheme, which was analyzed in a previous section. In the following we focus on the average number of combined branches and on the average BER.

Let $P_{l,n}$ denote the probability that mode n is used with l combined branches. We can calculate the average number of combined branches with the bandwidth-efficient and power-greedy AMDC scheme by averaging over all possible values of l and n as

$$\overline{N}_c = \begin{cases} \sum_{l=1}^{L} \sum_{n=1}^{N} l\ P_{l,n} + L F_{\gamma_c}^{L-MRC}(\gamma_{T_1}), & \text{for option 1;} \\ \sum_{l=1}^{L} \sum_{n=1}^{N} l\ P_{l,n}, & \text{for option 2.} \end{cases} \tag{5.108}$$

Based on the mode of operation of the bandwidth-efficient and power-greedy schemes, it can be shown that $P_{l,n}$ can be calculated for $n = N$ as

$$P_{l,N} = \begin{cases} 1 - F_{\gamma_c}^{L/1-GSC}(\gamma_{T_N}), & l = 1 \\ F_{\gamma_c}^{L/(l-1)-GSC}(\gamma_{T_N}) - F_{\gamma_c}^{L/l-GSC}(\gamma_{T_N}), & 1 < l \le L, \end{cases} \tag{5.109}$$

and for $n < N$ as

$$P_{l,n} = \begin{cases} \Pr\left[\gamma_{T_n} \le \gamma_{1:L}\ \&\ \sum_{k=1}^{L} \gamma_{k:L} < \gamma_{T_{n+1}}\right], & l = 1 \\ \Pr\left[\sum_{j=1}^{l-1} \gamma_{j:L} < \gamma_{T_n} \le \sum_{j=1}^{l} \gamma_{j:L}\ \&\ \sum_{k=1}^{L} \gamma_{k:L} < \gamma_{T_{n+1}}\right], & 1 < l < L \\ \Pr\left[\sum_{j=1}^{L-1} \gamma_{j:L} < \gamma_{T_n} \le \sum_{j=1}^{L} \gamma_{j:L} < \gamma_{T_{n+1}}\right], & l = L, \end{cases} \tag{5.110}$$

which can be calculated using the joint PDFs of y_l, $\gamma_{l:L}$ and z_l as

$$P_{l,n} = \begin{cases} \int_{\gamma_{T_n}}^{\gamma_{T_{n+1}}} \int_{0}^{\gamma_{T_{n+1}}-\gamma} p_{\gamma_{1:L},z_1}(\gamma,z)\mathrm{d}z\mathrm{d}\gamma, & l=1; \\ \int_{(l-1)\gamma_{T_n}/l}^{(l-1)\gamma_{T_{n+1}}/l} \int_{\gamma_{T_n}-y}^{y/(l-1)} \int_{0}^{\gamma_{T_{n+1}}-y-\gamma} p_{y_l,\gamma_{l:L},z_l}(y,\gamma,z)\mathrm{d}z\mathrm{d}\gamma\mathrm{d}y \\ \quad + \int_{(l-1)\gamma_{T_{n+1}}/l}^{\gamma_{T_n}} \int_{\gamma_{T_n}-y}^{\gamma_{T_{n+1}}-y} \int_{0}^{\gamma_{T_{n+1}}-y-\gamma} p_{y_l,\gamma_{l:L},z_l}(y,\gamma,z)\mathrm{d}z\mathrm{d}\gamma\mathrm{d}y, & 1<l<L; \\ \int_{(L-1)\gamma_{T_{n+1}}/L}^{(L-1)\gamma_{T_{n+1}}/L} \int_{\gamma_{T_n}-y}^{y/(L-1)} p_{y_L,\gamma_{L:L}}(y,\gamma)\mathrm{d}\gamma\mathrm{d}y \\ \quad + \int_{(L-1)\gamma_{T_{n+1}}/L}^{\gamma_{T_n}} \int_{\gamma_{T_n}-y}^{\gamma_{T_{n+1}}-y} p_{y_L,\gamma_{L:L}}(y,\gamma)\mathrm{d}\gamma\mathrm{d}y, & l=L. \end{cases} \tag{5.111}$$

Following the same approach as for the power-efficient AMDC while applying the PDF of the received SNR given in (5.106), the average BER of a bandwidth-efficient and power-greedy AMDC scheme based on MS-GSC can be calculated as

$$< BER >= \begin{cases} \dfrac{\int_{0}^{\gamma_{T_2}} BER_1(\gamma)\ p_{\gamma_c}(\gamma)\ \mathrm{d}\gamma + \sum_{n=2}^{N} n \int_{\gamma_{T_n}}^{\gamma_{T_{n+1}}} BER_n(\gamma)\ p_{\gamma_c}(\gamma)\ \mathrm{d}\gamma}{N - \sum_{n=2}^{N} F_{\gamma_c}^{MSC(\gamma_{T_N})}(\gamma_{T_n})}, & \text{for option 1;} \\ \dfrac{\sum_{n=1}^{N} n \int_{\gamma_{T_n}}^{\gamma_{T_{n+1}}} BER_n(\gamma)\ p_{\gamma_c}(\gamma)\ \mathrm{d}\gamma}{N - \sum_{n=1}^{N} F_{\gamma_c}^{MSC(\gamma_{T_N})}(\gamma_{T_n})}, & \text{for option 2.} \end{cases} \tag{5.112}$$

5.7.4 Numerical examples

We now illustrate the mathematical formalism that we developed in the previous sections through several numerical examples. In particular, we compare the processing power consumption, spectral efficiency, and BER performance of three AMDC schemes. In the following numerical examples, we set the number of available diversity branches $L = 5$, the number of adaptive modulation mode $N = 4$, and the SNR thresholds are set to satisfy the instantaneous BER requirement of $\mathrm{BER}_0 = 10^{-3}$.

Note that the greater the average number of combined branches during data burst reception, the larger the average receiver processing power consumption. We investigate the power efficiency of the three AMDC schemes under

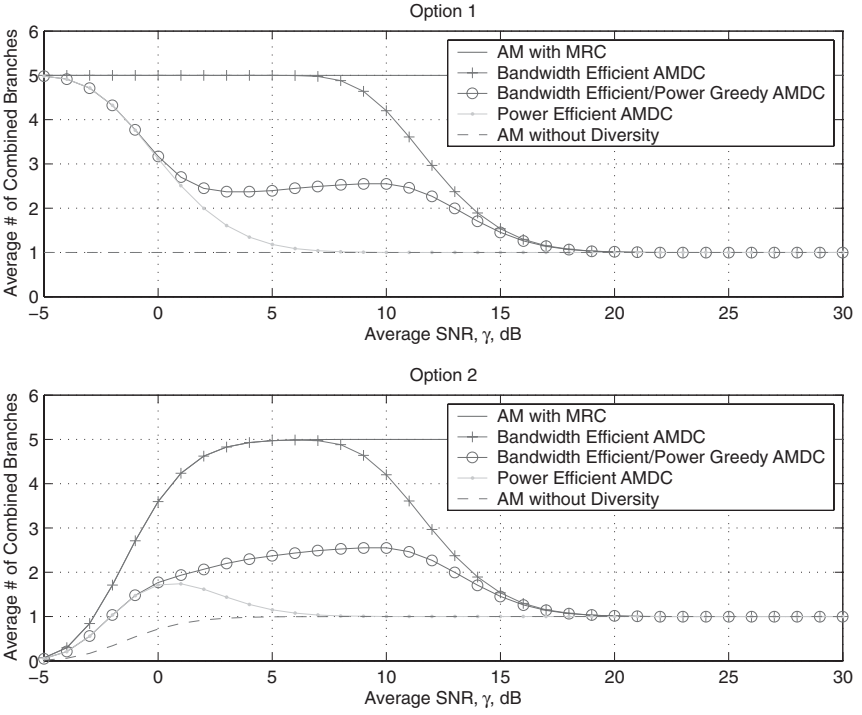

Figure 5.27 Average number of combined branches of three AMDC schemes with two options as a function of the average path SNR $\overline{\gamma}$ ($L = 5$, $N = 4$ and $\text{BER}_0 = 10^{-3}$) [12]. © 2007 IEEE.

consideration in Fig. 5.27 by plotting the average number of combined branches of these AMDC schemes with two options as a function of the average path SNR $\overline{\gamma}$. For reference purposes, the average number of combined branches of adaptive modulation without diversity and with L-branch MRC cases are also plotted. We observe that on average, the power-efficient AMDC scheme always combines the least number of diversity branches for any value of $\overline{\gamma}$, whereas the bandwidth-efficient AMDC scheme combines the most among the three schemes, but still less than the adaptive modulation with L-branch MRC case. We also notice that when the average path SNR is very small, the three AMDC schemes with option 1 (i.e. transmitting using the lowest modulation mode in the worst case when the combined SNR of all L available paths ends up being below γ_{T_1}) consumes more processing power than with option 2 (i.e. buffering the data and waiting until the next guard period for a more favorable channel when the combined SNR of all L available paths ends up being below γ_{T_1}) by combining more diversity branches.

The average spectral efficiency of three AMDC schemes with two options are plotted as a function of the average path SNR $\overline{\gamma}$ in Fig. 5.28. The average spectral efficiency curves of adaptive modulation without diversity and with L-branch MRC cases are also included. We can see that the bandwidth-efficient AMDC and

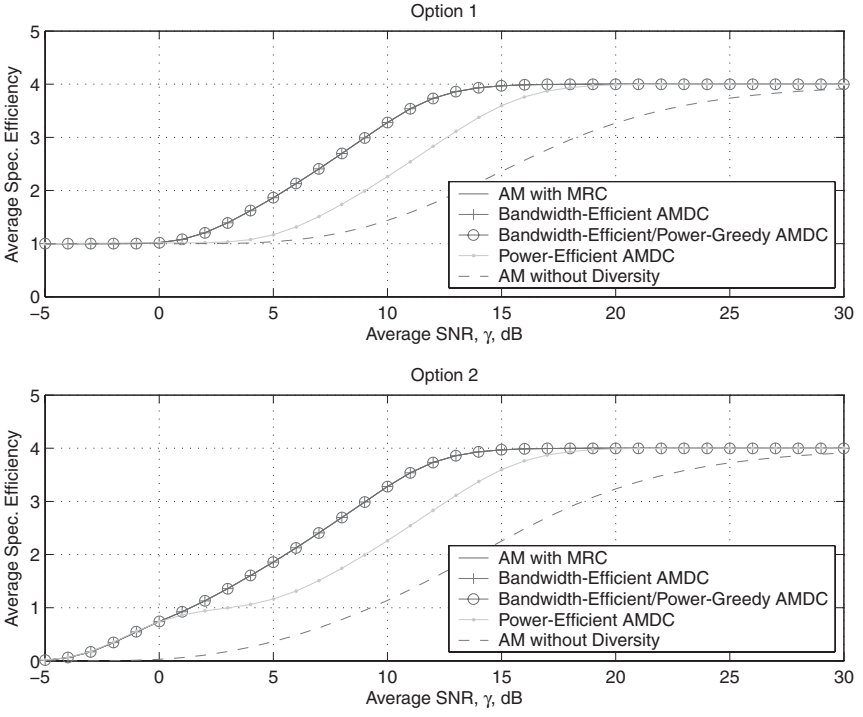

Figure 5.28 Average spectral efficiency of three AMDC schemes with two options as a function of the average path SNR $\overline{\gamma}$ ($L = 5$, $N = 4$ and $\text{BER}_0 = 10^{-3}$) [12]. © 2007 IEEE.

the bandwidth-efficient/power-greedy AMDC schemes have the same spectral efficiency as adaptive modulation with L-branch MRC, which is much greater than that of the power-efficient AMDC scheme over the medium value range of $\overline{\gamma}$. Thus by observing Figs. 5.27 and 5.28, there is a trade-off of spectral efficiency and power consumption between power-efficient and bandwidth-efficient AMDC schemes. We also observe that when the average SNR is very small, three AMDC schemes with option 1 exhibit higher spectral efficiency than with option 2, at the expense that the target BER is not met with option 1.[2]

Finally, we examine the BER performance of three AMDC schemes in Fig. 5.29. This figure confirms that when the average SNR is very small, the average BER of the three AMDC schemes with option 1 become larger than the target $\text{BER}_0 = 10^{-3}$ in violation of the instantaneous BER requirement. We can also see that the bandwidth-efficient/power-greedy AMDC scheme has the poorest error performance among the three AMDC schemes, but still satisfies

[2] Note that the average spectral efficiency is viewed as a valid performance measure only if the BER requirement is satisfied, then the results for option 1 are valid only for an average SNR greater than 1 dB.

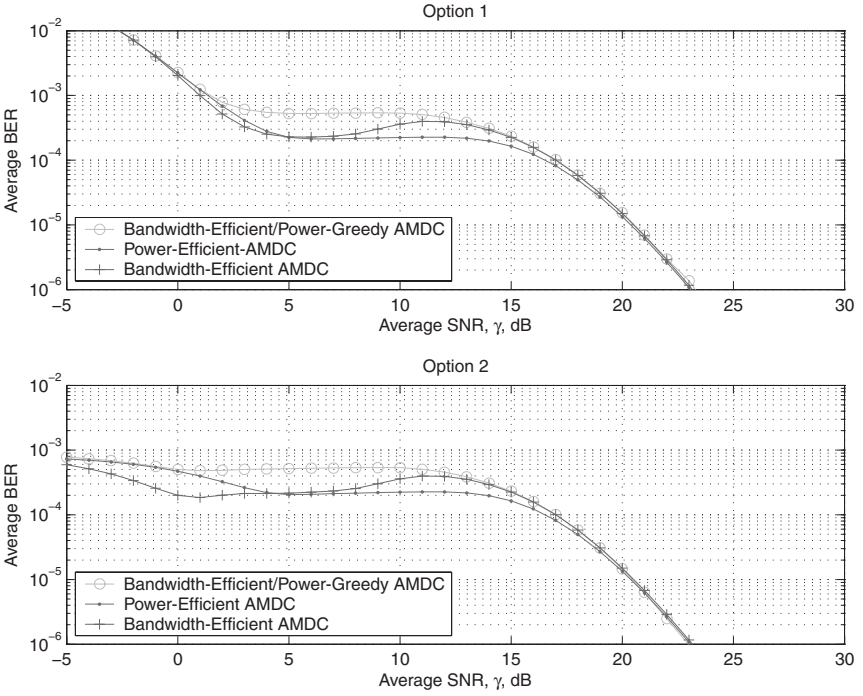

Figure 5.29 Average BER of three AMDC schemes with two options as a function of the average path SNR $\overline{\gamma}$ ($L = 5$, $N = 4$ and $\text{BER}_0 = 10^{-3}$) [12]. © 2007 IEEE.

the BER requirement except over the low-SNR range with option 1. Comparing the error performance of the power-efficient AMDC and bandwidth-efficient AMDC, we find that over the low-SNR range, the bandwidth-efficient scheme slightly outperforms the power-efficient scheme, whereas for the medium to high SNR range, the power-efficient scheme performs better. This is because when the SNR is low, the bandwidth-efficient scheme needs to combine more diversity branches and when the SNR is higher, the power-efficient scheme tends to settle on the lower adaptive modulation mode, which has better error protection.

Considering the three figures together, we can draw the following conclusions.

- There is a trade-off of power consumption versus spectral efficiency between the power-efficient AMDC scheme and the bandwidth-efficient AMDC scheme, which have comparable BER performance.
- The bandwidth-efficient/power-greedy AMDC scheme offers better power-efficiency than the bandwidth-efficient AMDC scheme at the cost of slightly poorer BER performance and with the same spectral efficiency.
- Option 1 for the worst case scenario leads to a better spectral efficiency at the expense of higher power consumption and in violation of the BER requirement, whereas option 2 avoids the extra power consumption and BER requirement violation but causes a certain amount of transmission delay.

5.8 Summary

In this chapter, we investigated the idea of adaptive combining through its applications in various scenarios, including traditional reception diversity systems, transmit diversity systems, RAKE receiver over soft handover region, and joint design with adaptive modulation. In most cases, the joint distribution functions of partial sums of ordered random variables were of critical importance in the performance and complexity analysis of the resulting systems. Through the accurate trade-off analysis through selected numerical examples, we were able to confirm that adaptive combining can bring significant complexity and processing power savings to the wireless systems operating over fading channel, as a minimum or no loss in performance. As such, adaptive combining has huge application potential in future wireless systems.

5.9 Bibliography notes

Minimum estimation and combining GSC (MEC-GSC) [6] extends the idea of MS-GSC by introducing a switching and examining combining (SEC) stage. Lioumpas *et al.* [41] propose an adaptive GSC scheme, which essentially applies the adaptive combining principle to NT-GSC scheme. Bouida *et al.* combine adaptive combining based on MS-GSC with transmit power control in [42]. The joint design of adaptive modulation with OT-MRC scheme is presented in [43]. Lee and Ko extend the joint AMDC scheme to a multi-channel environment in [44]. Discrete transmit power control is considered together with joint AMDC scheme in [45].

References

[1] W. C. Jakes, *Microwave Mobile Communication*, 2nd ed. Piscataway, NJ: IEEE Press, 1994.

[2] S. W. Kim, D. S. Ha and J. H. Reed, "Minimum selection GSC and adaptive low-power RAKE combining scheme," in *Proc. of IEEE Int. Symp. on Circuits and Systems. (ISCAS'03)*, Bangkok, Thailand, vol. 4, May 2003, pp. 357–360.

[3] P. Gupta, N. Bansal and R. K. Mallik, "Analysis of minimum selection H-S/MRC in Rayleigh fading," *IEEE Trans. Commun.*, vol. COM-53, no. 5, pp. 780–784, May 2005. See also the conference version in *Proc. of IEEE Int. Conf. on Commun. (ICC'05)*.

[4] H.-C. Yang, "New results on ordered statistics and analysis of minimum-selection generalized selection combining (GSC)," *IEEE Trans. Wireless Commun.*, vol. TWC-5, no. 7, July 2006. See also the conference version in *Proc. of IEEE Int. Conf. on Commun. (ICC'05)*.

[5] H.-C. Yang and M.-S. Alouini, "MRC and GSC diversity combining with an output threshold," *IEEE Trans. Veh. Technol.*, vol. TVT-54, no. 3, pp. 1081–1090, May 2005.

[6] M.-S. Alouini and H.-C. Yang, "Minimum estimation and combining generalized selection combining (MEC-GSC)," *IEEE Trans. Wireless Commun.*, vol. 6, no. 7, pp. 526–532, February 2007.

[7] M. K. Simon and M.-S. Alouini, "Performance analysis of generalized selection combining with threshold test per branch (T-GSC)," *IEEE Trans. Veh. Technol.*, vol. VT-51, no. 5, pp. 1018–1029, September 2002.

[8] A. Annamalai, G. Deora and C. Tellambura, "Unified analysis of generalized selection diversity with normalized threshold test per branch," in *Proc. of IEEE Wireless Commun. and Networking Conf. (WCNC'03)*, New Orleans, Louisiana, vol. 2, March 2003, pp. 752–756.

[9] X. Zhang and N. C. Beaulieu, "SER and outage of thresholdbased hybrid selection/maximal-ratio combining over generalized fading channels," *IEEE Trans. Commun.*, vol. 52, no. 12, pp. 2143–2153, December 2004.

[10] S. Choi, H.-C. Yang and Y.-C. Ko, "Performance analysis of transmit diversity systems with antenna replacement," *IEEE Trans. Veh. Technol.*, vol. 57, no. 4, pp. 2588–2595, July 2008.

[11] S. Choi, M.-S. Alouini, K. A. Qaraqe and H.-C. Yang, "Soft handover overhead reduction by RAKE reception with finger reassignment," *IEEE Trans. on Commun.*, vol. 56, no. 2, pp. 213–221, February 2008.

[12] H.-C. Yang, N. Belhaj and M.-S. Alouini, "Performance analysis of joint adaptive modulation and diversity combining over fading channels," *IEEE Trans. on Commun.*, vol. COM-55, no. 3, pp. 520–528, March 2007.

[13] M. K. Simon and M.-S. Alouini, *Digital Communications over Generalized Fading Channels*, 2nd ed. New York, NY: John Wiley & Sons, 2004.

[14] I. S. Gradshteyn and I. M. Ryzhik, *Table of Integrals, Series, and Products*, 5th ed. San Diego, CA: Academic Press, 1994.

[15] H.-C. Yang and L. Yang, "Exact error rate analysis of output-threshold generalized selection combining (OT-GSC)," *IEEE Trans. Wireless Commun.*, vol. 6, no. 9, pp. 3159–3162, September 2007.

[16] V. Tarokh, N. Seshadri and A. R. Calderbank, "Spacetime codes for high data rate wireless communication: performance criterion and code construction," *IEEE Trans. Inf. Theory*, vol. 44, no. 2, pp. 744–765, March 1998.

[17] G. J. Foschini and M. J. Gans, "On limits of wireless communications in a fading environment when using multiple antennas," *Wirel. Pers. Commun.*, vol. 6, no. 3, pp. 311–335, March 1998.

[18] S. M. Alamouti, "A simple transmit diversity technique for wireless communications," *IEEE J. Sel. Areas Commun.*, vol. 16, no. 8, pp. 1451–1458, October 1998.

[19] D. Gesbert, M. Shafi, D. S. Shiu, P. Smith and A. Naguib, "From theory to practice: an overview of MIMO spacetime coded wireless systems," *IEEE J. Sel. Areas Commun.*, vol. 21, no. 3, pp. 281–302, April 2003.

[20] A. J. Paulraj, D. A. Gore, R. U. Nabar and H. Blcskei, "an overview of MIMO communications. A key to gigabit wireless," *Proc. IEEE*, vol. 92, no. 2, pp. 198–218, February 2004.

[21] S. Thoen, L. V. der Perre, B. Gyselinckx and M. Engels, "Performance analysis of combined transmit-SC/receive-MRC," *IEEE Trans. Commun.*, vol. 49, no. 1, p. 5–8, January 2001.

[22] Z. Chen, "Asymptotic performance of transmit antenna selection with maximal-ratio combining for generalized selection criterion," *IEEE Commun. Lett.*, vol. 8, no. 4, pp. 247–249, April 2004.

[23] A. F. Molisch, M. Z. Win and J. H. Winters, "Reduced-complexity transmit/receive-diversity systems," *IEEE Trans. Signal Processing*, vol. 51, no. 11, pp. 2729–2738, November 2003.

[24] A. Ghrayeb and T. M. Duman, "Performance analysis of MIMO systems with antenna selection over quasi-static fading channels," *IEEE Trans. Veh. Technol.*, vol. 52, no. 2, pp. 281–288, March 2003.

[25] D. A. Gore and A. J. Paulraj, "MIMO antenna subset selection with space-time coding," *IEEE Trans. Signal Processing*, vol. 50, no. 10, pp. 2580–2588, October 2002.

[26] D. J. Love and R. W. Heath, "Diversity performance of precoded orthogonal space-time block codes using limited feedback," *IEEE Commun. Lett.*, vol. 8, no. 5, pp. 305–307, May 2004.

[27] S. Choi, Y.-C. Ko and E. J. Powers, "Optimization of switched MIMO systems over Rayleigh fading channels," *IEEE Trans. Veh. Technol.*, vol. 56, no. 1, pp. 103–114, January 2007.

[28] K.-H. Park, Y.-C. Ko and H.-C. Yang, "Performance analysis of transmit diversity systems with multiple antenna replacement," *IEICE Trans. on Commun.*, vol. E91-B, no. 10, pp. 3281–3287, October 2008.

[29] G. L. Stüber, *Principles of Mobile Communications*, 2nd ed. Norwell, MA: Kluwer Academic Publishers, 2000.

[30] S. Choi, M.-S. Alouini, K. A. Qaraqe and H.-C. Yang, "Fingers replacement method for RAKE receivers in the soft handover region," *IEEE Trans. on Wireless Commun.*, vol. 7, no. 4, pp. 1152–1156, April 2008.

[31] M. Z. Win and J. H. Winters, "Analysis of hybrid selection/maximal-ratio combining in Rayleigh fading," *IEEE Trans. Commun.*, vol. COM-47, no. 12, pp. 1773–1776, December 1999. See also *Proce. IEEE Int. Conf. Commun. (ICC'99)*, pp. 6-10, Vancouver, British Columbia, Canada, June 1999.

[32] M.-S. Alouini and M. K. Simon, "An MGF-based performance analysis of generalized selective combining over Rayleigh fading channels," *IEEE Trans. Commun.*, vol. COM-48, no. 3, pp. 401–415, March 2000.

[33] H. Holma and A. Toskala, *WCDMA for UMTS, revised ed.* New York, NY: John Wiley & Sons, 2001.

[34] A. J. Goldsmith and S.-G. Chua, "Adaptive coded modulation for fading channels," *IEEE Trans. Commun.*, vol. COM-46, no. 5, pp. 595–602, May 1998.

[35] M.-S. Alouini and A. J. Goldsmith, "Adaptive modulation over Nakagami fading channels," *Kluwer J. Wireless Commun.*, vol. 13, nos. 1–2, pp. 119–143, 2000.

[36] K. J. Hole, H. Holm, and G. E. Oien, "Adaptive multidimentional coded modulation over flat fading channels," *IEEE J. Select. Areas Commun.*, vol. SAC-18, no. 7, pp. 1153–1158, July 2000.

[37] A. Goldsmith, *Wireless Communications.* New York, NY: Cambridge University Press, 2005.

[38] R. K. Mallik, P. Gupta and Q. T. Zhang, "Minimum selection GSC in independent Rayleigh fading," *IEEE Trans. Veh. Technol.*, vol. TVT-54, no. 3, pp. 1013–1021, May 2005.

[39] N. Belhaj, N. Hamdi, M.-S. Alouini and A. Bouallegue, "Low-power minimum estimation and combining with adaptive modulation," in *Proc. of the Eighth IEEE International Symposium on Signal Processing and its Applications (ISSPA'2005)*, Sydney, Australia, August 2005.

[40] ——, "Adaptive modulation and combining for bandwidth efficient communication over fading channels," in *Proc. of the IEEE Personal Indoor Mobile Radio Conference (PIMRC'2005)*, Berlin, Germany, September 2005.

[41] A. S. Lioumpas, G. K. Karagiannidis and T. A. Tsiftsis, "Adaptive generalized selection combining (A-GSC) receivers," *IEEE Trans. on Wireless Commun.*, vol. TWC-7, no. 12, pp. 5214–5219, December 2008.

[42] Z. Bouida, N. Belhaj, M.-S. Alouini and K. A. Qaraqe, "Minimum selection GSC with downlink power control," *IEEE Trans. on Wireless Commun.*, vol. TWC-7, no. 7, pp. 2492–2501, July 2008.

[43] Y.-C. Ko, H.-C. Yang, S.-S. Eom and M.-S. Alouini, "Adaptive modulation and diversity combining based on output-threshold MRC," *IEEE Trans. Wireless Commun.*, vol. TWC-6, no. 10, pp. 3728–3737, October 2007.

[44] S.-D. Lee and Y.-C. Ko, "Exact performance analysis of hybrid adaptive modulation schemes in multi-channel system," *IEEE Trans. Wireless Commun.*, vol. TWC-8, no. 6, pp. 3206–3215, June 2009.

[45] A. Gjendemsjø, H.-C. Yang, G. E. Øien and M.-S. Alouini, "Joint adaptive modulation and diversity combining with downlink power control," *IEEE Trans. Veh. Technol.*, vol. VT-57, no. 4, pp. 2145–2152, July 2008.

6 Multiuser scheduling

6.1 Introduction

Multiple antenna techniques can provide significant diversity benefit to wireless systems. In certain practical scenarios, however, it might be challenging to implement multiple antennas at the wireless terminals. In such a case, we can still extract the diversity benefit by exploring the different fading channels corresponding to multiple users. Since users are separately located, different user channel will most likely experience independent fading [1, 2]. At any given time instant, it is highly probable that at least one user channel will have a favorable channel condition. The overall system performance will improve if the channel access is always granted to the users with the best instantaneous channel quality, usually the one with the highest SNR, resulting in the so-called multiuser diversity gain.

Both multiple antenna diversity and multiuser diversity try to improve the performance of wireless systems over fading channels. Their approaches, however, are conceptually different. Antenna diversity targets at eliminating deep SNR fades by combining multiple diversity paths together, whereas multiuser diversity rides the SNR peaks of different users channels. As such, multiuser diversity exploits multipath fading rather than reducing it. In certain cases, fading might need to be intentionally introduced with some random beamforming approach [3]. Multiuser diversity enjoys several inherent advantages, including simpler receiver structures, as a single antenna per receiver is sufficient, and naturally independent fading channels, as users are usually geographically separated. On the other hand, multiuser diversity may require additional system resources to collect user channel state information, especially for non-reciprocal channels. Furthermore, multiuser diversity may lead to unfairness across users in the short term, even though it can guarantee long-term fairness through channel normalization and/or utilizing historical throughput information.

In this chapter, we will analyze the performance of different multiuser diversity strategies and discuss their associate implementation complexity whenever appropriate. We first review the basics of multiuser scheduling, including the capacity benefit, fairness issue, and feedback load reduction. We then analyze the single user scheduling schemes for the perspective of channel access statistics, such as channel access rate and access duration of an arbitrary user. After

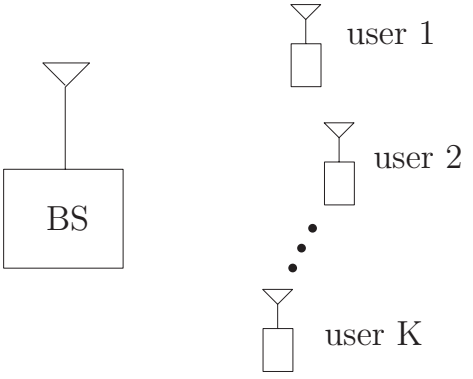

Figure 6.1 Sample multiuser system.

that, the study is extended to the multiuser scheduling scenario. We present three different schemes and analyze their performance and efficiency. The chapter concludes with a discussion about the power reallocation for parallel multiuser scheduling. We focus mainly on those schemes that have low complexity and, as such, can be readily applied to practical multiuser wireless systems.

6.2 Multiuser diversity

We consider a generic cell with one base station and K active single-antenna users, as illustrated in Fig. 6.1. For the sake of clarity, we assume that the base station has only one antenna and the system operates in the time division multiple access (TDMA) fashion in this chapter (the extension to the multiple-antenna base station will be considered in the next chapter). During each TDMA time slot, the system will schedule the user with the best channel condition to transmit. With the assumption of a frequency flat-fading channel model, the quality of user channels can be characterized solely by the instantaneous received SNR, denoted by γ_k. As such, the user with the largest instantaneous received SNR will be selected for data transmission during the a particular time slot [1,2]. Mathematically speaking, user k^* where

$$k^* = \arg\max_k \{\gamma_k\}, \tag{6.1}$$

will be scheduled for transmission.[1] It follows that the received SNR of the scheduled user is the largest one of K user SNRs, which are inherently independent as users are randomly distributed in the coverage area. The CDF of the received

[1] Note that we employ the absolute SNR value-based scheduling strategy here, which may lead to fairness issues. An alternative normalized SNR-based scheduling will be considered in the following sections.

SNR over the time slot is given by [4]

$$F_{\gamma_{k^*}}(x) = \prod_{k=1}^{K} F_{\gamma_k}(x). \tag{6.2}$$

If users experience identical fading, which may be possible with a proper power control mechanism, the PDF of the received SNR at the scheduled user becomes

$$p_{\gamma_{k^*}}(x) = K p_{\gamma}(x)[F_{\gamma}(x)]^{K-1}, \tag{6.3}$$

which is the PDF of combiner output SNR with K branch selection combining. Therefore, multiuser diversity can achieve the same diversity gain as selection based antenna reception diversity. With the statistics of the received SNR at the scheduled user, we can evaluate the performance gain offered by multiuser diversity transmission [5]. In what follows, we use the system ergodic capacity as the performance metric to evaluate different scheduling strategies. Mathematically, the system ergodic capacity can be calculated by averaging the instantaneous capacity over the distribution of the received SNR as

$$C_{\text{sys}} = \int_0^{\infty} \log_2(1+\gamma) p_{\gamma_{k^*}}(\gamma) \mathrm{d}\gamma.$$

For i.i.d. Rayleigh fading, after appropriate substitution and carrying out integration, the capacity with multiuser diversity transmission specializes to

$$C_{\text{sys}} = K \log_2(e) \sum_{k=0}^{K-1} (-1)^k \frac{(K-1)!}{(k+1)!(K-k-2)!} e^{(k+1)/\overline{\gamma}} E_1\left(\frac{k+1}{\overline{\gamma}}\right), \tag{6.4}$$

where $E_1(\cdot)$ is the exponential integral function of the first order [6], defined by

$$E_1(x) = \int_1^{\infty} \frac{e^{-xt}}{t} \mathrm{d}t, x \geq 0, \tag{6.5}$$

which is related to the exponential-integral function $E_i(x)$ by $E_1(x) = -E_i(-x)$.

The multiuser diversity gain can also be demonstrated with the asymptotic behavior of the γ_{k^*} when K approaches infinity. For i.i.d. Rayleigh fading scenario, it can be shown that γ_{k^*}, which is the largest one of K random variables, has the limiting distribution of the Gumbel type. More specifically, the limiting CDF of γ_{k^*} as K approaches infinity is given by

$$\lim_{K \to +\infty} F_{\gamma_{1:K} - b_K}(x) = \exp\left(-e^{-x}\right), \tag{6.6}$$

where b_K is the solution of the equation $F_{\gamma}(l_K) = 1 - b/K$, which is equal to $\log K$ for the Rayleigh fading case. It follows that the SNR of the selected user increases at the same rate with $\log K$ as K approaches infinity [3].

6.2.1 Addressing fairness

In a practical environment, the average channel gain corresponding to different users differs with the experienced path loss and shadowing process. If the power

control mechanism is not available or not perfect, then the users experience favorable average fading conditions that might be scheduled much more frequently, which leads to unfairness to other users. In this scenario, we can improve fairness among users by taking into account the historical throughput information of each user during the user selection stage [3]. The basic principle is that users receiving more channel access should be weighted less during the competition for channel access during upcoming time slots. A popular strategy that implements this principle is the so-called proportional fair scheduling, which was shown to be able to achieve long-term fairness [3]. With proportional fair scheduling, the selected users over the ith time slot, denoted by $k^*(i)$, should have the maximum normalized instantaneous capacity, i.e.

$$k^*(i) = \arg\max_k \left\{ \frac{C_k(i)}{R_k(i)} \right\}, \tag{6.7}$$

where $C_k(i)$ is the instantaneous rate of user k over slot i, given by

$$C_k(i) = \log_2(1 + \gamma_k(i)), \tag{6.8}$$

and $R_k(i)$ denotes the historical throughput of user k for up to the $i-1$th time slots, which can be updated with the following relationship

$$R_k(s) = R_k(s-1), k \neq k^*, \tag{6.9}$$

$$R_{k^*}(s) = R_{k^*}(s-1) + C_{k^*}(s-1). \tag{6.10}$$

Alternatively, we can schedule users based on their normalized SNR rather than the absolute SNR. Specifically, as users will have different average received SNR, denoted by $\overline{\gamma}_k$, we can improve the fairness among users by scheduling users based on their normalized SNRs, given by $\tilde{\gamma}_k = \frac{\gamma_k}{\overline{\gamma}_k}$ [5]. User $k^*$where

$$k^* = \arg\max_k \left\{ \frac{\gamma_k}{\overline{\gamma}_k} \right\}, \tag{6.11}$$

will be scheduled for transmission during a particular time slot. It is easy to show that the PDF of the normalized SNR $\tilde{\gamma}_k$ under the Rayleigh fading channel model is commonly given by

$$p_{\tilde{\gamma}_k}(x) = e^{-x}. \tag{6.12}$$

To derive the PDF of the scheduled user's SNR γ_k^* based on the normalized SNR based user selection, we first consider its CDF, which can be shown to be given

by

$$\begin{aligned} F_{\gamma_{k^*}}(\gamma) &= \Pr[\gamma_{k^*} < \gamma] \\ &= \sum_{i=1}^{K} \Pr[\gamma_{k^*} < \gamma; \gamma_{k^*} = \gamma_i] \\ &= \sum_{i=1}^{K} \int_0^{\frac{\gamma}{\overline{\gamma}_i}} p_{\tilde{\gamma}_k}(x) \prod_{k=1, k\neq i}^{K} F_{\tilde{\gamma}_k}(x) \mathrm{d}x. \end{aligned} \tag{6.13}$$

After taking derivatives with respect to γ, the PDF of the received SNR at the scheduled user is obtained, after some manipulations, as

$$p_{\gamma_{k^*}}(\gamma) = \sum_{i=1}^{K} \frac{1}{\overline{\gamma}_i} p_{\tilde{\gamma}_i}(\frac{\gamma}{\overline{\gamma}_i}) \prod_{k=1, k\neq i}^{K} F_{\tilde{\gamma}_k}(\frac{\gamma}{\overline{\gamma}_i}). \tag{6.14}$$

For the Rayleigh fading model, after proper substitution and carrying out integration, the system capacity with normalized SNR-based scheduling is given by

$$C_{\text{sys}} = \log_2(e) \sum_{i=1}^{K} \sum_{k=0}^{K-1} \frac{(-1)^k}{1+k} \binom{K-1}{k} e^{(k+1)/\overline{\gamma}_i} E_1\left(\frac{k+1}{\overline{\gamma}_i}\right). \tag{6.15}$$

6.2.2 Feedback load reduction

The availability of users' instantaneous channel state information is essential to the implementation of multiuser diversity transmission. For the downlink scenario, the base station needs to collect the channel SNRs corresponding to all users in order to select the best user for data transmission. This will translate into a huge amount of channel probing and/or channel quality feedback, which consume additional system resource. It is of great practical importance if we can reduce the feedback load while maintaining nearly the same multiuser diversity gain. In this context, the selective multiuser diversity scheduling scheme has been demonstrated to be an effective solution among several other approaches [5].

The basic idea of selective multiuser diversity is to allow only those users whose channel qualities are good enough, i.e. with received SNR above a certain threshold γ_T, to feed back their channel state information. Note that with multiuser diversity scheduling, the base station will select a single user for transmission. As such, only users with a good enough channel will have the chance to be selected. Furthermore, the base station only requires the quality of scheduled users for capacity-achieving rate adaptation. Intuitively, we can expect the selective multiuser diversity approach can achieve the same diversity gain as conventional multiuser diversity if at least only one user feeds back. On the other hand, selective multiuser scheduling may lead to scheduling outage when no user feeds back. It is not difficult to show that the probability of scheduling outage

under the assumption of i.i.d. faded user channels is

$$P_{\text{out}} = \prod_{i=1}^{K} F_{\gamma_i}(\gamma_T), \tag{6.16}$$

where $F_{\gamma_i}(\cdot)$ denotes the CDF of received SNR at the ith user.

An easy solution to avoid the scheduling outage is to randomly probe and select a user for data transmission when there is no user feedback. With minor modification, we can show that the SNR of the final scheduled user is given by

$$\gamma_{k^*} = \begin{cases} \max_k\{\gamma_k\}, & \text{if no outage;} \\ \text{rand}_k\{\gamma_k\}, & \text{if outage.} \end{cases} \tag{6.17}$$

It follows that the CDF of the received SNR γ_k^* over i.i.d. fading channels can be shown to be

$$F_{\gamma_{k^*}}(x) = \begin{cases} \displaystyle\sum_{k=1}^{K} \frac{K!}{k!(K-k)!}[F_\gamma(\gamma_T)]^{K-k} \\ \quad \times [F_\gamma(x) - F_\gamma(\gamma_T)]^k, & x \geq \gamma_T; \\ [F_\gamma(\gamma_T)]^{K-1} F_\gamma(x), & x < \gamma_T. \end{cases} \tag{6.18}$$

The PDF of γ_k^* can be routinely obtained after taking the derivative with respect to x as

$$p_{\gamma_{k^*}}(x) = \begin{cases} \displaystyle\sum_{k=1}^{K} \frac{K!}{(k-1)!(K-k)!}[F_\gamma(\gamma_T)]^{K-k} \\ \quad \times [F_\gamma(x) - F_\gamma(\gamma_T)]^{k-1} p_\gamma(x), & x \geq \gamma_T; \\ [F_\gamma(\gamma_T)]^{K-1} p_\gamma(x), & x < \gamma_T, \end{cases} \tag{6.19}$$

which can be readily utilized to evaluate the system capacity. The average feedback load (AFL) in terms of the average number of SNR feedback per scheduling time slot can be determined as

$$\begin{aligned} \overline{N} &= \sum_{k=1}^{K} k \Pr[k \text{ users feedback}] \\ &= \sum_{k=1}^{K} \frac{K!}{(K-k)!(k-1)!}[F_\gamma(\gamma_T)]^{K-k}[1 - F_\gamma(\gamma_T)]^k. \end{aligned} \tag{6.20}$$

When the user channels are independent but not identically distributed, we can utilize normalized SNR during feedback thresholding as well as the user selection process. In particular, user k will feed back if its normalized SNR $\tilde{\gamma}_k = \gamma_k/\overline{\gamma}_k$ is greater than a particular threshold $\tilde{\gamma}_T$. It follows that the probability of scheduling outage is given by

$$P_{\text{out}} = [F_{\tilde{\gamma}}(\tilde{\gamma}_T)]^K, \tag{6.21}$$

where $F_{\tilde{\gamma}}(\cdot)$ is the common CDF of the normalized SNR. The average feedback load in terms of the average number of SNR feedback per scheduling time slot

can be determined as

$$\overline{N} = \sum_{k=1}^{K} \frac{K!}{(K-k)!(k-1)!} [F_{\tilde{\gamma}}(\tilde{\gamma}_T)]^{K-k} [1 - F_{\tilde{\gamma}}(\tilde{\gamma}_T)]^k. \tag{6.22}$$

The statistics of the received SNR at the scheduled user can also be obtained, and this is left as an exercise for the readers.

6.3 Performance analysis of multiuser selection diversity

In general, the viability of these multiuser scheduling schemes in practical systems largely depends on the number of active users and the channel changing rate [1]. While having more users increases the multiuser diversity gain, the average length of time that each individual user is picked to communicate decreases. On the other hand, if the channel varies too quickly, an accurate estimate of the channel strength would be difficult. However, the channel fading must be fast enough so that the average time that any user accesses the channel is not too long to ensure a certain fairness among all users. Clearly, a key measure to evaluate the viability of the multiuser scheduling algorithms is to determine the average channel access time based on the fading rate and the number of users. In this section, we study the average access time (AAT) and the average access rate (AAR) of individual users in a multiuser environment subject to the ergodic Rayleigh fading [7]. From a practical perspective, the AAT can be used for setting the time-slot length, as if the time slot is longer compared to the AAT, the scheduler basically cannot track the channel variation fast enough and the scheduling gain will be seriously reduced. On the other hand, if the time slot is too short compared to the AAT, there will be too much unnecessary feedback. We also introduce another quantity, which is average waiting time (AWT), to indicate how long on average a user has to wait for the next access. The AWT is important for the time-out timer consideration in the upper-layer protocols.

6.3.1 Absolute SNR-based scheduling

With absolute SNR-based scheduling, the scheduler selects user i in a time slot if and only if the instantaneous SNR of the user i is larger than that of all other users, i.e.

$$\gamma_i \geq \gamma_j, j = 1, ..., L; j \neq i. \tag{6.23}$$

Equivalently, we can write

$$\gamma_i \geq \gamma_*, \tag{6.24}$$

where γ_* is the maximum SNR among all other users, i.e.

$$\gamma_* = \max_{j=1,...,L, j\neq i} (\gamma_j). \tag{6.25}$$

Therefore, the AAR of user i is precisely the average number of times the process $r = \sqrt{\gamma_i/\gamma_*} = \alpha_i/\alpha_*$ crosses level 1 per unit time, where α_i is the amplitude of the complex channel gain for user i and α_* is the largest amplitude of all other users. It follows that the AAR of user i can be evaluated as the average level crossing rate (LCR) [8, eq. (2.90)] of the process r at level 1, which is given by

$$N_i = \int_0^\infty \dot{r} p_{r,\dot{r}}(1,\dot{r}) \mathrm{d}\dot{r}, \tag{6.26}$$

where $\dot{r}$ is the time derivative of the process r and $p_{r,\dot{r}}(1,\dot{r})$ is the joint PDF of r and $\dot{r}$, which was given by [9, eq. (9); 10, eq. (15)]

$$\begin{aligned} p_{r,\dot{r}}(1,\dot{r}) = \int_0^\infty \int_{-\infty}^\infty \alpha_*^2 p_{\alpha_i}(\alpha_* r) p_{\dot{\alpha}_i}(\dot{r}\alpha_* + \dot{\alpha}_* r) \\ \times p_{\alpha_*,\dot{\alpha}_*}(\alpha_*, \dot{\alpha}_*) \mathrm{d}\dot{\alpha}_* \mathrm{d}\alpha_*. \end{aligned} \tag{6.27}$$

For Rayleigh fading user channels, the PDF of the channel amplitude α_i is given by

$$p_{\alpha_i}(\alpha) = \frac{2\alpha}{\Omega_i} \exp\left(-\frac{\alpha^2}{\Omega_i}\right), \quad \alpha \geq 0, \tag{6.28}$$

where Ω_i is the short-term average channel power gain of the ith user, and the time derivative of signal amplitude process $\dot{\alpha}_i$ follows normal distribution with zero mean and is independent of the signal amplitude α_i, with PDF given by [11, eq. (1.3–34)]

$$p_{\dot{\alpha}_i}(\dot{\alpha}) = \frac{1}{\sqrt{2\pi}\sigma_i} \exp\left(-\frac{\dot{\alpha}^2}{2\sigma_i^2}\right), \tag{6.29}$$

where $\sigma_i^2 = \Omega_i \pi^2 f_i^2$ for isotropic scattering and f_i is the maximum Doppler frequency shift of the ith user, and finally, the joint PDF of α_* and $\dot{\alpha}_*$ is given by [12]

$$\begin{aligned} p_{\alpha_*,\dot{\alpha}_*}(x,\dot{x}) &= \sum_{j=1,j\neq i}^{L} \frac{1}{\sqrt{2\pi}\sigma_j} \exp\left(-\frac{\dot{x}^2}{2\sigma_j^2}\right) \frac{2x}{\Omega_j} \exp\left(-\frac{x^2}{\Omega_j}\right) \\ &\quad \times \prod_{k=1,k\neq i,j}^{L} \left[1 - \exp\left(-\frac{x^2}{\Omega_k}\right)\right] \\ &= \sum_{j=1,j\neq i}^{L} \sum_{\tau \in T_{ij}^L} \mathrm{sign}(\tau) \frac{1}{\sqrt{2\pi}\sigma_j} \exp\left(-\frac{\dot{x}^2}{2\sigma_j^2}\right) \frac{2x}{\Omega_j} \exp\left(-\frac{x^2}{\Omega_j} - \tau x^2\right), \end{aligned} \tag{6.30}$$

where T_{ij}^L is the set obtained by expanding the product $\prod_{k=1,k\neq i,j}^{L} \left[1 - \exp\left(-\frac{x^2}{\Omega_k}\right)\right]$ then taking the natural logarithm of each term [13, 14], and $\mathrm{sign}(\tau)$ is the corresponding sign of each term in the expansion. After proper substitution and carrying out integrations, we can obtain the

analytical expression of AAR for user i as

$$N_i = \sum_{j=1, j\neq i}^{L} \sum_{\tau \in T_{ij}^L} \text{sign}(\tau) \frac{\pi}{\sqrt{2}} \frac{\sqrt{\Omega_i f_i^2 + \Omega_j f_j^2}}{\Omega_i \Omega_j} \left(\frac{1}{\Omega_i} + \frac{1}{\Omega_j} + \tau \right)^{-3/2}. \quad (6.31)$$

The AAT of user i, denote by T_i, is defined as the average time duration of user i's channel access. It can be shown that the AAT of user i can be calculated as

$$T_i = \frac{P_i}{N_i} \quad (6.32)$$

where P_i denotes the probability that user i accesses the channel at any time instant or, equivalently, the average access probability (AAP) of user i. The probability P_i can be calculated as

$$P_i = \Pr[\alpha_i \geq \alpha_*] = \int_0^\infty p_{\alpha_i}(x) \int_0^x p_{\alpha_*}(y) \mathrm{d}y \mathrm{d}x. \quad (6.33)$$

For the Rayleigh fading case under consideration, we can show after proper substitution and manipulation that the access probability is given by

$$\begin{aligned} P_i &= \int_0^\infty \frac{2x}{\Omega_i} \exp\left(-\frac{x^2}{\Omega_i}\right) \prod_{k=1, k\neq i}^{L} \left[1 - \exp\left(-\frac{x^2}{\Omega_k}\right)\right] \mathrm{d}x \quad (6.34) \\ &= \sum_{\tau' \in T_i^L} \text{sign}(\tau') \frac{1}{1 + \tau' \Omega_i}. \end{aligned}$$

Similarly, the AWT of user i, which characterizes the average time duration a user has to wait for the next access, can be calculated as

$$W_i = \frac{1 - P_i}{N_i} = \frac{1}{N_i} - T_i. \quad (6.35)$$

6.3.2 Normalized SNR-based scheduling

With normalized SNR-based scheduling, the base station schedules the user with the largest normalized SNR, or equavalently, the user with largest normalized channel amplitude, defined as $\beta_k = \alpha_k / \sqrt{\Omega_k}$. The AAR and AAT of user i in this case can be calculated using the up-crossing rate of the process

$$r = \beta_i / \beta_*, \quad (6.36)$$

where

$$\beta_* = \max_{j=1,\cdots,L, j\neq i} (\beta_j), \quad (6.37)$$

at the level 1. The rate can be similarly calculated as the absolute SNR-based case but using the PDFs of βs and $\dot{\beta}$s. As a result of normalization, the PDF of

β_k becomes

$$p_{\beta_k}(x) = 2x\exp(-x^2), \tag{6.38}$$

the PDF of its time derivative $\dot{\beta}_k$ is

$$p_{\dot{\beta}_k}(\dot{x}) = \frac{1}{\sqrt{2\pi}\sigma_k}\exp\left(-\frac{\dot{x}^2}{2\sigma_k^2}\right), \tag{6.39}$$

where $\sigma_k^2 = \pi^2 f_k^2$, and the joint PDF of β_* and $\dot{\beta}_*$ becomes

$$p_{\beta_*,\dot{\beta}_*}(x,\dot{x}) = \sum_{j=1,j\neq i}^{L} \frac{2x}{\sqrt{2\pi}\sigma_j}\exp\left(-\frac{\dot{x}^2}{2\sigma_j^2} - x^2\right)[1-\exp(-x^2)]^{L-2}. \tag{6.40}$$

Following the exact same steps as in the absolute SNR-based scheduling case, we get the AAR of user i, N_i, as

$$N_i = \sum_{j=1,j\neq i}^{L} \frac{\pi}{\sqrt{2}}\sqrt{f_i^2+f_j^2}\sum_{n=0}^{L-2}\binom{L-2}{n}(-1)^n(n+2)^{-3/2}. \tag{6.41}$$

With normalized SNR-based scheduling, the access probability of user i becomes $1/L$. It follows that the AAT of user i is given by

$$T_i = \frac{1}{N_i L}. \tag{6.42}$$

After proper substitution and some rearrangement, we can rewrite T_i as

$$T_i = \frac{\text{const}}{\sum_{j=1,j\neq i}^{L}\sqrt{f_i^2+f_j^2}}, \tag{6.43}$$

where const denotes some constant. We see that if the network has a fast-moving user k among many other stationary users, we have

$$T_i = \begin{cases} \frac{\text{const}}{(L-1)f_k}, & i = k; \\ \frac{\text{const}}{f_k}, & i \neq k, \end{cases} \tag{6.44}$$

which implies that the AAT of the fast-moving user is roughly $1/(L-1)$ times that of other stationary users.

6.4 Multiuser parallel scheduling

In some wireless networks, we might need to schedule multiple users at the same time. This applies to, for example, the TDMA systems where multiple time slots within channel coherence time T_c are to be allocated to users, or the FDMA systems where multiple frequency subchannels with one channel coherence bandwidth B_c are to be allocated. Parallel orthogonal channel access is also feasible in wideband CDMA systems or ultra-wideband (UWB) systems. In

this scenario, we need efficient scheduling algorithms to carry out the user selection. While there exist some optimization-based approaches in the literature, they often require the solution of a multi-dimensional nonlinear optimization problem, which make them impractical in a real-world environment [15]. In this section, we present several low-complexity schemes and investigate their performance and complexity.

Note that all the user selection schemes can be implemented based on both the absolute SNRs or the normalized SNRs of user channels. In this section, for the sake of clarity, we focus on the absolute SNR-based approach with the assumption that with proper power control algorithm, the received SNRs at different users experience independent and identical fading. The generalization to non-identical fading is straightforward. In the following discussion, we also assume the multiuser channels are orthogonal, in either time, frequency, or code domain, and their mutual interference and external interference are ignored.

6.4.1 Generalized selection multiuser scheduling (GSMuS)

GSMuS [16] was originated from the conventional GSC diversity systems. With this scheme, the system schedules a fixed number of the best users among all K active users in each scheduling interval. Specifically, the scheduler ranks the instantaneous SNRs of all K users in the descending order, denoted by $\gamma_{1:K} \geq \gamma_{2:K} \geq \cdots \geq \gamma_{K:K}$, where $\gamma_{k:K}$ is the kth largest user SNR. The scheduler will then choose the K_s users with the largest SNRs for simultaneous transmission in the next available time slots. We can immediately see that similar to the conventional multiuser diversity scheme, GSMuS requires the channel information feedback from all users. The analysis of GSMuS scheme is simpler than that for GSC diversity systems as we only need the marginal statistics of the first K_s largest SNR, instead of their sum. Specifically, when user channels experience i.i.d. fading, the PDF of the kth largest user SNR can be easily obtained from the classical order statistical result as

$$p_{\gamma_{k:K}}(x) = \frac{K!}{(K-k)!(k-1)!}[P_\gamma(x)]^{K-k}[1-P_\gamma(x)]^{k-1}p_\gamma(x), \tag{6.45}$$

where $P_\gamma(x)$ and $p_\gamma(x)$ are the common CDF and PDF of user SNRs, available for popular fading channel models.

For the general independent and non-identical distributed (i.n.d.) fading channel case, the MGF of the kth largest user SNR, denoted by $\mathcal{M}_{\gamma_{k:K}}(s)$, can be obtained as [17, eq. (6)]

$$\mathcal{M}_{\gamma_{k:K}}(s) = \sum_{\substack{n_1,\cdots,n_{k-1} \\ n_1<n_2<\cdots<n_{k-1}}} \sum_{n_k} \int_0^\infty e^{-sx} p_{n_k}(x) \left[\prod_{l=1}^{k-1}[1-F_{n_l}(x)]\right]\left[\prod_{l'=k+1}^{K} F_{n_{l'}}(x)\right] \mathrm{d}x, \tag{6.46}$$

where $n_i \in \{1, 2, \cdots, K\}$, $i = 1, \cdots, K_s$, are the index of the ith best user, $f_{n_k}(x)$ is the PDF of the kth best user SNR, and $F_{n_l}(x)$ is the CDF of the lth largest user SNR. Note that summation $\sum_{\substack{n_1, \cdots, n_{k-1} \\ n_1 < n_2 < \cdots < n_{k-1}}}$ is carrying over all possible index sets of the largest $k-1$ user SNRs out of the total K users, $\sum_{n_k}$ over the possible indexes of the kth selected user and there are total $\frac{K!}{(K-k)!(k-1)!}$ terms in the double summations. It follows that the PDF of the Kth largest user SNR is given by

$$p_{\gamma_{k:K}}(s) = \sum_{\substack{n_1, \cdots, n_{k-1} \\ n_1 < n_2 < \cdots < n_{k-1}}} \sum_{n_k} p_{n_k}(x) \left[\prod_{l=1}^{k-1} [1 - F_{n_l}(x)] \right] \left[\prod_{l'=k+1}^{K} F_{n_l'}(x) \right], \quad (6.47)$$

which reduces to (6.45) with the i.i.d. assumption.

With the above PDFs of the scheduled users' SNR, we can readily evaluate the throughput and error rate performance of GSMuS scheme. We can also calculate the channel access statistics of an arbitrary user, including the AAR and the AAT defined in the previous section [16]. In particular, the AAR of user k can be calculated as the up-crossing rate at level 1 of the process $r_k = \alpha_k / \alpha_*$, where α_k is the channel amplitude of user k and $\alpha_* = \alpha_{K_s:K-1}$ is the K_sth largest channel amplitude among the other $K-1$ users (excluding user k). Note that with GSMuS, user k will be selected whenever its channel amplitude becomes one of the K_s largest among all users. Applying the result of LCR, the AAR of user k can given by

$$N_k = \int_0^\infty \dot{r} p_{r_k, \dot{r}_k}(1, \dot{r}) \mathrm{d}\dot{r}, \quad (6.48)$$

where $\dot{r}_k$ is the time derivative of the process r_k and $f_{r_k, \dot{r}_k}(1, \dot{r})$ is the joint PDF of r_k and $\dot{r}_k$, which can be calculated in terms of the PDF of α_k, $\dot{\alpha}_k$, and the joint PDF of α_* and $\dot{\alpha}_* = \dot{\alpha}_{K_s:K-1}$ as in (6.27). Assuming that the $\alpha_{K_s:K-1}$ and $\dot{\alpha}_{K_s:K-1}$ are independent, it can be shown that the joint PDF of $f_{\alpha_*, \dot{\alpha}_*}(x, \dot{x})$ is given by

$$p_{\alpha_*, \dot{\alpha}_*}(x, \dot{x}) = \sum_{\substack{n_1, \cdots, n_{K_s-1} \\ n_1 < n_2 < \cdots < n_{K_s-1}}} \sum_{n_{K_s}} p_{\alpha_{n_{K_s}}}(x) \left[\prod_{l=1}^{K_s-1} [1 - F_{\alpha_{n_l}}(x)] \right] \times \left[\prod_{l'=K_s+1}^{K} F_{\alpha_{n_l'}}(x) \right] p_{\dot{\alpha}_{n_{K_s}}}(\dot{x}), \quad (6.49)$$

where $n_i \in \{1, \cdots, k-1, k+1, \cdots, K\}$ $(n_i \neq k)$, $i = 1, \cdots, K_s$, are the index of the ith best user SNR among $K-1$ users. Note that the summation $\sum_{\substack{n_1, \cdots, n_{K_s-1} \\ n_1 < n_2 < \cdots < n_{K_s-1}}}$ is carried over all possible index sets of the largest $K_s - 1$ branch SNRs and $\sum_{n_{K_s}}$ over the possible indexes of the K_sth user, out of the total $K-1$ users, except for the kth user. For the i.n.d. Rayleigh fading user channel scenario, after proper substitutions and carrying out the integration, the

AAR of user k can be shown to be given by

$$N_k = \sum_{\substack{n_1,\cdots,n_{K_s-1} \\ n_1<n_2<\cdots<n_{K_s-1}}} \sum_{n_{K_s}} \sum_{\tau\in T_{1\cdots K_s}^{K-1}} \operatorname{sign}(\tau)\frac{\pi}{\sqrt{2}} \times \frac{\sqrt{\Omega_k f_k^2 + \Omega_{n_{K_s}} f_{n_{K_s}}^2}}{\Omega_k \Omega_{n_{K_s}}} \left(\frac{1}{\Omega_k} + \sum_{l=1}^{K_s} \frac{1}{\Omega_{n_l}} + \tau\right)^{-3/2}, \tag{6.50}$$

where $T_{1\cdots K_s}^{K-1}$ denote the set obtained by expanding the product $\prod_{l'=K_s+1}^{K-1}\left[1-\exp\left(-\frac{x^2}{\Omega_{n_{l'}}}\right)\right]$ then taking the natural logarithm of each term [13, 14], and $\operatorname{sign}(\tau)$ is the corresponding sign of each term in the expansion.

Based on the above notation, the AAP of user k can be calculated as its channel amplitude α_k becomes larger than the K_sth largest channel amplitude among the other $K-1$ users $\alpha_* = \alpha_{K_s:K-1}$. Mathematically speaking, we have

$$P_k = \int_0^\infty p_{\alpha_k}(x) \int_0^x p_{\alpha_{K_s:K-1}}(y)\mathrm{d}y\mathrm{d}x. \tag{6.51}$$

After substituting (6.28) and (6.47) and carrying out integration and manipulation, we can obtain the closed-form expression of the AAP of user k for Rayleigh fading case as

$$P_k = \sum_{\substack{n_1,\cdots,n_{K_s-1} \\ n_1<n_2<\cdots<n_{K_s-1}}} \sum_{n_{K_s}} \sum_{\tau'\in T_{1\cdots K_s}^{K-1}} \operatorname{sign}(\tau')\frac{\Omega_k}{\Omega_{n_{K_s}}(1+(\tau'+\sum_{l=1}^{K_s-1}\frac{1}{\Omega_{n_l}})\Omega_k)}. \tag{6.52}$$

The AAT of user k then can be readily calculated as the ratio of the AAP over AAR, i.e. $T_k = P_k/N_k$.

6.4.2 On–off based scheduling (OOBS)

The OOBS scheme is inspired by the AT-GSC diversity combining scheme [18] and the on–off type of schemes discussed in [5, 19]. The difference with the AT-GSC scheme is that the OOBS scheme will process the selected users in parallel without combining them together [20]. The mode of operation of the OOBS scheme can be summarized as follows. At the beginning of each scheduling time interval, the BS sends a pilot signal to all users. These users will estimate the received SNR γ_i using the received signal and compare it to a preselected threshold SNR, denoted by γ_T. A user will feed back its SNR information to the BS only if its SNR are above the threshold γ_T. Only these acceptable users are then scheduled by the BS for the subsequent transmission time slot. If no user has an acceptable SNR, the BS simply waits a time period, in the order of the channel coherence time, before starting a new round of scheduling. Note that with the

GSMuS scheme, the BS needs always to collect the SNR feedbacks from all K users to determine the K_s best users for scheduling.

We can see that the OOBS scheme will lead to a random time-varying feedback load and the number of scheduled user is also randomly varying. As only the users with acceptable channel condition, i.e. the users with SNR greater than the SNR threshold γ_T, will feed back their channel SNRs, the AFL of the OOBS scheme over i.i.d. fading environment is the same as that of the SMuS scheme discussed in the previous section, which is given by

$$\begin{aligned} \text{AFL} &= \sum_{k=0}^{K} k \binom{K}{k} \left[1 - F_\gamma\left(\gamma_T\right)\right]^k \left[F_\gamma\left(\gamma_T\right)\right]^{K-k} \\ &= K\left[1 - F_\gamma\left(\gamma_T\right)\right]. \end{aligned} \tag{6.53}$$

For the i.i.d. Rayleigh fading case, (6.53) specializes to, after substituting in the common CDF of Rayleigh faded received SNR,

$$\overline{N} = K \exp\left(-\frac{\gamma_T}{\bar{\gamma}}\right). \tag{6.54}$$

Therefore, the OOBS scheme requires, on average, fewer feedbacks than the GSMuS scheme. Note that the average number of scheduled user with the OOBS scheme is equal to the number of acceptable users. In a practical system, the number of users that can be scheduled for simultaneous transmission may be limited by other constraints.

We now evaluate the performance of the OOBS scheme over an i.i.d. fading environment in terms of the more practical performance measures of average spectrum efficiency (ASE). Based on the mode of operation of the OOBS scheme, the received SNR of scheduled users has a truncated PDF from above at γ_T. It can be shown that the PDF of the received SNR of a scheduled user is given by

$$p_{\gamma_s}\left(\gamma\right) = \begin{cases} \frac{p_\gamma\left(\gamma\right)}{1 - F_\gamma\left(\gamma_T\right)} & \gamma \geq \gamma_T; \\ 0 & \text{otherwise}, \end{cases} \tag{6.55}$$

where $p_\gamma(\cdot)$ and $F_\gamma(\cdot)$ are the common PDF and CDF of user SNRs. For i.i.d. the Rayleigh fading special case, (6.55) specializes to

$$p_{\gamma_s}\left(\gamma\right) = \begin{cases} \frac{1}{\bar{\gamma}} \exp\left(-\frac{\gamma - \gamma_T}{\bar{\gamma}}\right), & \gamma \geq \gamma_T; \\ 0 & \text{otherwise}, \end{cases} \tag{6.56}$$

where $\overline{\gamma}$ are the common average SNR for all users.

We assume the constant-power variable-rate adaptive M-QAM scheme discussed in earlier chapters. The threshold values γ_{T_n} for different constellation sizes and instantaneous BER requirements were summarized in Table 2.1. The

ASE of a scheduled user with the OOBS scheme can be calculated as [21, eq. (33)]

$$\mathrm{ASE}_u = \sum_{n=1}^{N} R_n P_n, \tag{6.57}$$

where $\{R_n\}_{n=1}^{N}$ are the spectral efficiencies of N available constellation sizes and P_n is the probability of using the nth constellation, which can be obtained as

$$P_n = \int_{\gamma_{T_n}}^{\gamma_{T_{n+1}}} p_{\gamma_s}(\gamma)\,\mathrm{d}\gamma. \tag{6.58}$$

The ASE of all scheduled users can then be determined by multiplying the average number of scheduled users to the ASE of a single scheduled user, as

$$\mathrm{ASE}_t = [K(1 - P_{\gamma_s}(\gamma_T))] \sum_{n=1}^{N} R_n \int_{\gamma_{T_n}}^{\gamma_{T_{n+1}}} p_{\gamma_s}(\gamma)\,\mathrm{d}\gamma. \tag{6.59}$$

Inserting (6.55) into (6.59), we have

$$\mathrm{ASE}_t = K \sum_{n=1}^{N} R_n \int_{\gamma_{T_n}}^{\gamma_{T_{n+1}}} p_{\gamma}(\gamma)\,U(\gamma - \gamma_T)\,\mathrm{d}\gamma. \tag{6.60}$$

For the i.i.d. Rayleigh fading assumption, inserting (6.56) into (6.60) and carrying out integration, we can write

$$\mathrm{ASE}_t = K \sum_{n=1}^{N} R_n P_n', \tag{6.61}$$

where

$$P_n' = \begin{cases} \exp\left(-\frac{\max(\gamma_T, \gamma_{T_n})}{\bar{\gamma}}\right) - \exp\left(-\frac{\gamma_{T_{n+1}}}{\bar{\gamma}}\right) & \text{if} \quad \gamma_{T_{n+1}} \geq \gamma_T; \\ 0 & \text{if} \quad \gamma_{T_{n+1}} < \gamma_T. \end{cases} \tag{6.62}$$

If the SNR threshold $\gamma_T = \gamma_{T_q}$ where $q \in \{1, 2, 3, \ldots, N\}$, then $\{R_n\}_{n=1}^{q-1} = 0$ and (6.61) simplifies to

$$\mathrm{ASE}_t = K \left[\sum_{n=q}^{N-1} R_n \left\{ \exp\left(-\frac{\gamma_{T_n}}{\bar{\gamma}}\right) - \exp\left(-\frac{\gamma_{T_{n+1}}}{\bar{\gamma}}\right) \right\} + R_N \exp\left(-\frac{\gamma_{T_N}}{\bar{\gamma}}\right) \right]. \tag{6.63}$$

6.4.3 Switched-based scheduling (SBS)

The SBS scheme is inspired by the switching-based diversity combining schemes [22, 23]. With the SBS scheme, the BS schedules a predetermined fixed total number of acceptable users, denoted by K_s, and if necessary, the best unacceptable users in a GSC fashion [20]. More specifically, at the beginning of each

scheduling period, the BS sends a pilot signal sequentially to each user in order to request a channel state information from each user in a sequential manner. After receiving the pilot signal from the BS, each user estimates its SNR γ_i and feeds it back to the BS. The BS will compare each received SNR with the preselected SNR threshold γ_T. If the user SNR γ_i is greater than γ_T, then the user channel is considered acceptable and the user will be scheduled for transmission. This process of estimation, feedback, and comparison is repeated until the BS finds K_s acceptable users, after which the data transmission will start without further probing. If the BS only finds $K_a < K_s$ acceptable users after probing all K user channels, the BS will rank the $K - K_a$ users with unacceptable channels and schedules the best $K_s - K_a$ unacceptable users along the already selected K_a acceptable users. As the SBS scheme may not always select the best users for transmission, its performance will be worse than the GSC-based GSMuS scheduling scheme, especially when the threshold is relative small in comparison with average SNR. On the other hand, the SBS scheme can approach the performance of the GSMuS scheme as γ_T increases. Note that that when γ_T goes to infinity, the SBS scheme becomes equivalent to the GSMuS scheme. The advantage of the SBS scheme is a lower feedback load. The GSMuS scheme needs always full K feedbacks during each scheduling period. The feedback with the SBS scheme varies between K_s and K.

In the following, we derive the analytical expressions of the AFL and the ASE with the SBS scheme over i.i.d. fading environment. This study allows for a thorough trade-off study between SBS and GSMuS schemes.

To calculate the AFL, we consider two mutually exclusive cases depending on whether there are K_s acceptable users or not. If there are less than K_s acceptable users among the total K users, the SBS scheme needs to request SNR feedbacks from all K users. As a result, the number of feedback becomes K and the number of unacceptable users is random and takes values from $(K - K_s + 1)$ to K and follows a binomial distribution. Since the diversity paths are assumed to be i.i.d. faded, the probability that there are less than K_s acceptable users can be easily written as

$$P_B = \sum_{l=K-K_s+1}^{K} \binom{K}{l} \left[F_\gamma\left(\gamma_T\right)\right]^l \left[1 - F_\gamma\left(\gamma_T\right)\right]^{K-l}. \tag{6.64}$$

When there are at least K_s acceptable users among the total K users, the SBS scheme will terminate the process of SNR feedback as soon as K_s acceptable users are found. In this case, the number of feedbacks takes values from K_s to K and follows a negative binomial (or Pascal) distribution, with the probability of K feedbacks given by

$$P_k = \binom{k-1}{k-K_s} \left[1 - F_\gamma\left(\gamma_T\right)\right]^{K_s} \left[F_\gamma\left(\gamma_T\right)\right]^{k-K_s}, \; k = K_s, \ldots, K. \tag{6.65}$$

Finally, by combining these two mutually exclusive cases, we can obtain the overall average amount of feedback during the guard period as

$$\begin{aligned}\mathrm{AFL} &= \sum_{k=K_s}^{K} k\, P_k + KP_B \\ &= \sum_{k=K_s}^{K} k\binom{k-1}{k-K_s}\left[1-F_\gamma\left(\gamma_T\right)\right]^{K_s}\left[F_\gamma\left(\gamma_T\right)\right]^{k-K_s} \\ &\quad + K\sum_{l=K-K_s+1}^{K}\binom{K}{l}\left[F_\gamma\left(\gamma_T\right)\right]^{l}\left[1-F_\gamma\left(\gamma_T\right)\right]^{K-l}. \end{aligned} \tag{6.66}$$

For the i.i.d. Rayleigh fading case, after replacing $F_\gamma\left(\gamma\right)$ with $1-\exp\left(-\frac{\gamma}{\bar{\gamma}}\right)$, we obtain the following closed-form expression for AFL

$$\begin{aligned}\mathrm{AFL} &= \sum_{k=K_s}^{K} k\binom{k-1}{k-K_s}\left[\exp\left(-\frac{\gamma_T}{\bar{\gamma}}\right)\right]^{K_s}\left[1-\exp\left(-\frac{\gamma_T}{\bar{\gamma}}\right)\right]^{k-K_s} \\ &\quad + K\sum_{l=K-K_s+1}^{K}\binom{K}{l}\left[1-\exp\left(-\frac{\gamma_T}{\bar{\gamma}}\right)\right]^{l}\left[\exp\left(-\frac{\gamma_T}{\bar{\gamma}}\right)\right]^{K-l}. \end{aligned} \tag{6.67}$$

To calculate the ASE, we now derive the statistics of the received SNR of a scheduled user. Considering the cases that the number of acceptable users K_a is greater or equal to K_s and that K_a is smaller than K_s separately, we can write the PDF of the received SNR of a scheduled user with the SBS scheme as

$$p_{\gamma_s}\left(\gamma\right) = \Pr\left[K_a \geq K_s\right] p_{\gamma_{s_1}}\left(\gamma\right) + \Pr\left[K_a < K_s\right] p_{\gamma_{s_2}}\left(\gamma\right), \tag{6.68}$$

where $p_{\gamma_{s_1}}\left(\gamma\right)$ is the PDF of a scheduled user when $K_a \geq K_s$, the probability of which is given by

$$\Pr\left[K_a \geq K_s\right] = \sum_{K_a=K_s}^{K}\binom{K}{K_a}\left[1-F_\gamma\left(\gamma_T\right)\right]^{K_a}\left[F_\gamma\left(\gamma_T\right)\right]^{K-K_a}, \tag{6.69}$$

and $p_{\gamma_{s_2}}\left(\gamma\right)$ is the PDF of a scheduled user in case of $K_a < K_s$, the probability of which is equal to

$$\Pr\left[K_a < K_s\right] = \sum_{K_a=0}^{K_s-1}\binom{K}{K_a}\left[1-F_\gamma\left(\gamma_T\right)\right]^{K_a}\left[F_\gamma\left(\gamma_T\right)\right]^{K-K_a}. \tag{6.70}$$

In the case of $K_a \geq K_s$, i.e. all scheduled users have acceptable SNR, the PDF of the received SNR at a scheduled user is the truncated version of standard fading distribution from below at γ_T, which is given by [22, eq. (5)]

$$p_{\gamma_{s_1}}\left(\gamma\right) = \frac{p_\gamma\left(\gamma\right)}{1-F_\gamma\left(\gamma_T\right)} U\left(\gamma-\gamma_T\right), \tag{6.71}$$

where $U\left(x\right)$ is the unit step function. For the case of $K_a < K_s$, we first note that with the SBS scheme, $K_a < K_s$ holds if and only if the K_sth largest user

SNR is below the threshold and, as such, some unacceptable users are scheduled. Therefore, the PDF of a scheduled user's SNR is the PDF of any one of the K_s best user SNRs, given the fact that the K_sth best user SNR is below threshold. Since the scheduled user has equal probability to be the first to the K_s best user, the PDF of a scheduled user can be written as

$$p_{\gamma_{s_2}}(\gamma) = \frac{1}{K_s}\left(\sum_{i=1}^{K_s-1} p_{\gamma_{i:K}|\gamma_{K_s:K}<\gamma_T}(\gamma) + \frac{p_{\gamma_{K_s:K}}(\gamma)}{F_{\gamma_{K_s:K}}(\gamma_T)}\left(1-U(\gamma-\gamma_T)\right)\right), \tag{6.72}$$

where $p_{\gamma_{i:K}|\gamma_{K_s:K<\gamma_T}}(\gamma)$ is the conditional PDF of the ith ($i < K_s$) best user SNR given the K_sth best user SNR is below the threshold γ_T, which can be calculated using the joint PDF of $\gamma_{i:K}$ and $\gamma_{K_s:K}$ as

$$p_{\gamma_{i:K}|\gamma_{K_s:K}<\gamma_T}(x) = \frac{1}{\int_0^{\gamma_T} p_{\gamma_{K_s:K}}(\gamma)d\gamma}\int_0^{\min(\gamma_T,x)} p_{\gamma_{i:K},\gamma_{K_s:K}}(x,y)\,\mathrm{d}y, \tag{6.73}$$

where $p_{\gamma_{i:K}}(\gamma)$ is the PDF of the ith largest user SNR and $p_{\gamma_{i:K},\gamma_{K_s:K}}(x,y)$ is the joint PDF of the $i$thand K_sth largest user SNRs, both of which have been discussed in earlier chapters but reproduced here for the reader's convenience.

$$\begin{aligned} p_{\gamma_{i:K},\gamma_{K_s:K}}(x,y) = {} & \frac{K!}{(K-K_s)!(K_s-i-1)!\,(i-1)!} \\ & \times [F_\gamma(y)]^{K-K_s}\,[F_\gamma(x)-F_\gamma(y)]^{K_S-i-1} \\ & \times [1-F_\gamma(x)]^{i-1}\,p_\gamma(x)p_\gamma(y), \\ & x>y \ \text{ and } \ 1\le i<K_s\le K \end{aligned} \tag{6.74}$$

$$p_{\gamma_{j:K}}(\gamma) = \binom{K}{j} j\cdot p_\gamma(\gamma)\,[1-F_\gamma(\gamma)]^{j-1}\,[F_\gamma(\gamma)]^{K-j}. \tag{6.75}$$

Note that the second term in the parenthesis of (6.72) corresponding to the case of $i = K_s$, i.e. the PDF of the K_sth largest user SNR given that it is smaller than the threshold.

Finally, after proper substitution, the PDF of the received SNR at a scheduled user with the SBS scheme can be obtained as

$$\begin{aligned} p_{\gamma_s}(\gamma) = {} & \Pr[K_a<K_s]\,\frac{1}{K_s}\left(\sum_{i=1}^{K_s-1} p_{\gamma_{i:K_s}|\gamma_{K_s:K}<\gamma_T}(\gamma)\right. \\ & \left.+\frac{p_{\gamma_{K_s:K}}(\gamma)}{F_{\gamma_{K_s:K}}(\gamma_T)}\left(1-U(\gamma-\gamma_T)\right)\right) \\ & +\Pr[K_a\ge K_s]\,\frac{p_\gamma(\gamma)}{1-F_\gamma(\gamma_T)}U(\gamma-\gamma_T), \end{aligned} \tag{6.76}$$

which can be utilized to evalulate the ASE of the SBS scheme. Specifically, the ASE of a scheduled user can be calculated, after applying (6.76) to the definition

in (6.57) as

$$\mathrm{ASE}_u = \sum_{n=1}^{N} R_n \int_{\gamma_{T_n}}^{\gamma_{T_{n+1}}} p_{\gamma_s}(\gamma)\,\mathrm{d}\gamma. \tag{6.77}$$

Note that SBS scheme always schedules K_s users. Therefore, the total system ASE can be simply calculated by adding a factor of K_s, i.e. $\mathrm{ASE}_t = K_s \mathrm{ASE}_u$.

6.4.4 Numerical examples

In this subsection, we discuss the trade-off involved in the three multiuser parallel scheduling schemes presented in previous sections through selected numerical examples. Note that the number of scheduled users with the OOBS scheme is random varying, whereas both GSMuS and SBS schemes schedule a fixed number of K_s users. To allow a fair comparison between these scheduling schemes, we must define an appropriate basis for this comparison. In particular, we select the feedback threshold γ_T for the OOBS scheme such that the average number of scheduled users with the OOBS scheme is equal to K_s. For the i.i.d. Rayleigh fading scenario of interest, starting from (6.53), the threshold values satisfying this constraint can be calculated by solving the following equation for γ_T^*

$$K_s = K \exp\left(-\frac{\gamma_T^*}{\bar{\gamma}}\right), \tag{6.78}$$

which leads to

$$\gamma_T^* = \bar{\gamma} \ln\left(\frac{K}{K_s}\right). \tag{6.79}$$

Note that γ_T^* is the equivalent SNR threshold of the OOBS scheme and is varying with $\bar{\gamma}$.

In Fig. 6.2, we present the AFL of the OOBS scheme, the SBS scheme, and the GSMuS scheme over i.i.d. Rayleigh fading conditions with $K = 5$ and $K_s = 3$. Specifically, we plot the AFL of three schemes with different threshold values as the function of the average SNR $\bar{\gamma}$. We first note that the AFL of the SBS scheme is decreasing from K and eventually converging to K_s as $\bar{\gamma}$ increases while that of the GSC-based scheme is always equal to K. We can also see that the AFL of the SBS scheme increases as γ_T increases for a fixed $\bar{\gamma}$. On the other hand, for fixed γ_T, the AFL of the OOBS scheme is increasing from 0 to K, which is that of the GSC-based scheme, as $\bar{\gamma}$ increases. For fixed $\bar{\gamma}$, the AFL of the OOBS scheme is decreasing as γ_T increases because the feedback load is the same as the number of scheduled users in the OOBS scheme and the number of scheduled users is decreasing as γ_T increases. Finally, with the equivalent threshold γ_T^*, the AFL of the OOBS scheme remains constant and varies with $\bar{\gamma}$.

Figure 6.3 presents the ASE of the OOBS scheme, the SBS scheme, and the GSMuS scheme with adaptive coded M-QAM modulation as a function of average

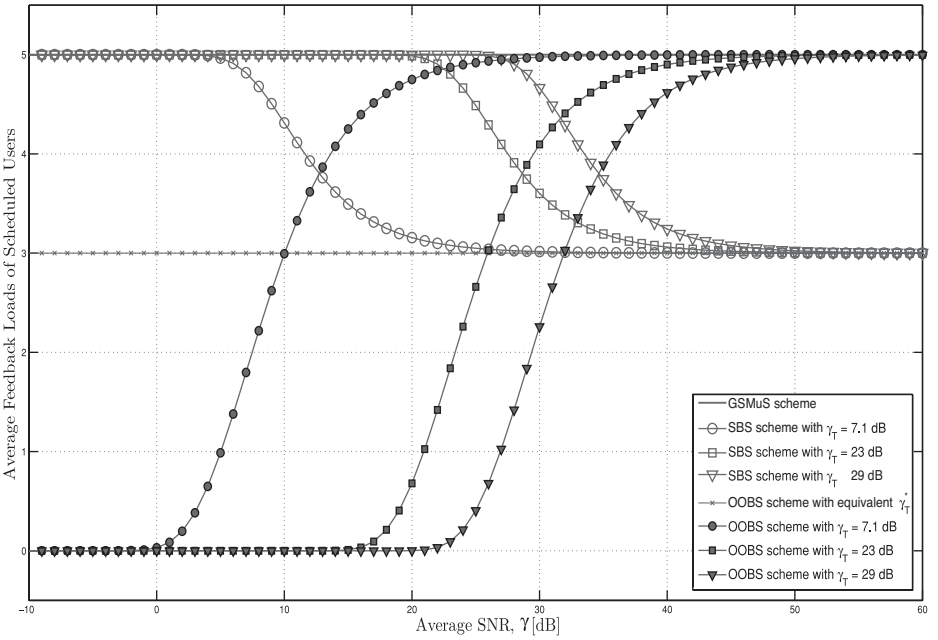

Figure 6.2 Average feedback loads for the (i) OOBS scheme, (ii) SBS scheme, and (iii) GSMuS scheme ($K = 5$ and $K_s = 3$) [20]. © 2009 IEEE.

SNR $\bar{\gamma}$ over the i.i.d. Rayleigh fading condition with $K = 5$ and $K_s = 3$. We can see that, with the fixed γ_T, the ASE of the OOBS scheme is increasing and eventually converging to $K \cdot R_N$ as $\bar{\gamma}$ increases because with fixed γ_T, (i) as $\bar{\gamma}$ increases the number of scheduled users increases and eventually converges to K, (ii) the total data rate depends on the number of scheduled users and each data rate depends on its SNR. We also notice that the ASE of the OOBS scheme with small γ_T is converging faster than that with large γ_T. When the channel condition is good, the ASE of the OOBS scheme is much larger than that of the GSMuS scheme because the number of scheduled users with the OOBS scheme is converging to K while the number of scheduled users with the GSMuS scheme is always K_s. By applying the equivalent threshold γ_T^* in the OOBS scheme, when the channel condition is poor, the OOBS scheme has almost the same ASE as the GSMuS scheme and the ASE of the OOBS scheme is slightly higher than that of the GSMuS scheme from 5 to 35 dB. For high average SNR (above 35 dB), the ASE of the OOBS scheme is re-converging to that of the GSMuS scheme, $K_s \cdot R_N$. Comparing the ASE between the SBS scheme and the GSMuS scheme, we can see that for the fixed γ_T, when the channel condition is poor, the SBS scheme has almost the same ASE as the GSMuS scheme and as $\bar{\gamma}$ increases, the GSMuS scheme has a slightly better ASE and eventually these two schemes have the same ASE again.

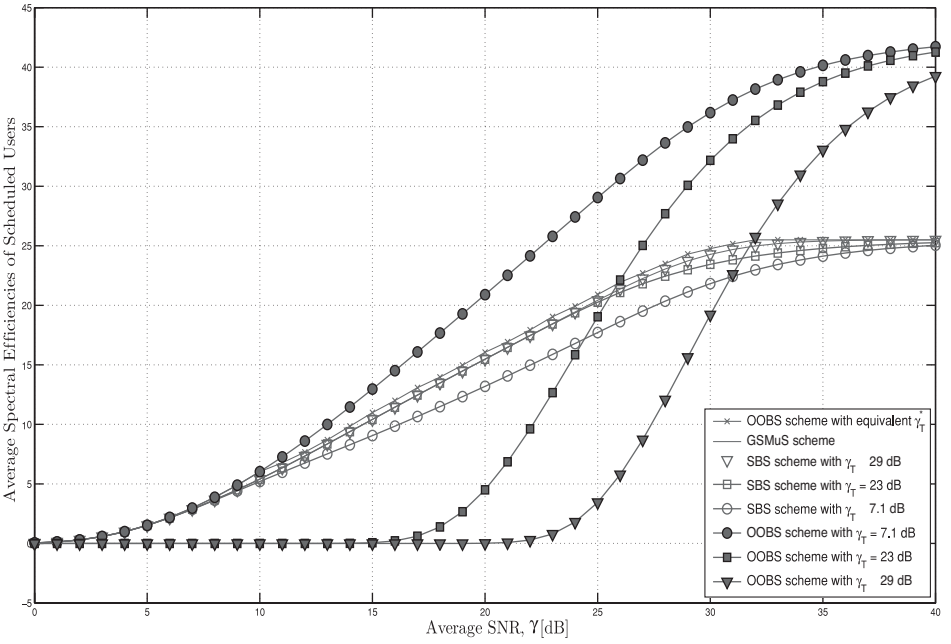

Figure 6.3 Average spectral efficiencies of adaptive coded M-QAM modulation for the (i) OOBS scheme, (ii) SBS scheme, and (iii) GSC-based scheduling scheme over i.i.d. Rayleigh fading conditions with $K = 5$ and $K_s = 3$ [20]. © 2009 IEEE.

6.5 Power allocation for SBS

So far, we assume that the transmit powers are uniformly allocated to the scheduled users, irrespective of their instantaneous channel conditions. The performance of the multiuser parallel user scheduling scheme studied in a previous section can be further improved with power allocation among scheduled users. Power allocation for GSMuD scheme was investigated by Ma *et al.* in [24]. Specifically, optimal power allocation strategies based on one- or two-dimensional water-filling solution are derived and demonstrated to achieve a better sum-rate performance than equal power allocation. In this section, we focus on the transmit power allocation for selected users with the SBS scheme [25].

Based on the mode of operation of the SBS scheme, when there are not enough acceptable users, at least one user will have an SNR smaller than the SNR threshold, which will limit the performance of the SBS scheme. One way to reduce or eliminate the number of scheduled unacceptable users is to redistribute the transmission power to different scheduled users while satisfying the total transmitting power constraint. Note that because of the discrete nature of adaptive modulation, such power redistribution among scheduled users may not affect the achieved ASE of those acceptable users, as the same modulation mode can be used for all values of the received SNRs in the same interval. With the above

motivation in mind, we propose in this section several threshold-based power allocation algorithms for the SBS multiuser parallel scheduling scheme.

6.5.1 Power reallocation algorithms

The main purpose of the power reallocation algorithms for the SBS-based scheduling scheme is to increase the number of the scheduled acceptable users without consuming any additional down-link transmit power. This is achieved by re-allocating the excess transmit power extracted from the scheduled acceptable users to those scheduled unacceptable users. Based on this general principle, we present three specific power allocation algorithms. For later reference, $\gamma_i^{'}$ denotes the SNR of the scheduled user after power allocation. K_a denotes the number of acceptable users before power allocation, and γ_T denotes the preselected SNR threshold.

Algorithm 1: ranking maintained power reallocation
This algorithm maintains the SNR ranking information of scheduled acceptable users when extracting power from acceptable users. The algorithm extracts only the required transmitting power from the acceptable users and allocates it to the unacceptable users sequentially from the strongest user to the weakest user. The operation of Algorithm 1 is summarized as follows. After SBS-based user scheduling, the system calculates the required additional transmission power for the unacceptable users in dB scale as $\gamma_{\text{req}} = \sum_{i=K_a+1}^{K_s} (\gamma_T - \gamma_i)$. Then, the system tries to extract the same amount of excess power from K_a acceptable users while ensuring the acceptance of user SNR, as

(i) If $\left(\gamma_i - \frac{\gamma_{\text{req}}}{K_a}\right) \geq \gamma_T$, then we reduce the transmitting power for user i in the amount of γ_{req}/K_a. Then the resulting received SNR of user i becomes $\gamma_i^{'} = \gamma_i - (\gamma_{req}/K_a)$.
(ii) If $(\gamma_i - (\gamma_{req}/K_a)) < \gamma_{TP}$, then we reduce the transmitting power for user i in the amount of $(\gamma_i - \gamma_{TP})$. As such, the modified SNR of the acceptable user is $\gamma_i^{'} = \gamma_T$.

The total excess transmission power from the acceptable users is

$$\gamma_{\text{excess}} = \sum_{i=1}^{K_a} \left(\gamma_i - \gamma_i^{'}\right), \tag{6.80}$$

which will be less or equal to γ_{req}. The system will then allocate γ_{excess} to the unacceptable users. More specifically, if $\gamma_{\text{excess}} = \gamma_{\text{req}}$, the received SNRs of all scheduled unacceptable users will be increased to γ_T and as such become acceptable with power reallocation. If $\gamma_{\text{excess}} < \gamma_{\text{req}}$, i.e. when case (ii) above occurs for at least one acceptable user, then γ_{excess} is sequentially allocated to the unacceptable users, starting from that with the strongest SNR. With this approach,

the number of remaining unacceptable users will be the smallest after the power reallocation process.

Algorithm 2: rate maintained power reallocation
This algorithm extracts transmit power from scheduled acceptable users while ensuring that their supported transmission rates remain unchanged. Similar to Algorithm 1, the extracted power is allocated to unacceptable users sequentially starting from the strongest user. Specifically, excess SNR of the ith acceptable user is calculated as $\gamma_{\text{excess},i} = \gamma_i - \gamma_{T_j}$, where γ_{T_j} is the lower threshold for modulation mode that ith user's SNR can support, i.e. $\gamma_{T_j} \leq \gamma_i \leq \gamma_{T_{j+1}}$. The total excess transmission power from all acceptable users becomes

$$\gamma_{\text{excess}} = \sum_{i=1}^{K_a} \gamma_{\text{excess,i}}, \tag{6.81}$$

which will be reallocated to the users, such that the number of scheduled unacceptable users is minimized. In particular, these excess transmission powers are then allocated to the unacceptable users in a similar fashion as in Algorithm 1. The only difference is that in this case, some excess power may remain after power allocation to all unacceptable users, in which case, the system equally allocates it to all the scheduled users. Note that Algorithm 2 has lower complexity in comparison with Algorithm 1 as the system does not need to calculate γ_{req}.

Algorithm 3: equal SNR power reallocation
With Algorithm 3, the received SNR of all acceptable users after power reallocation will be the same. Specifically, the transmission power will be redistributed among the scheduled users with the best channel conditions such that their received SNRs are equal and above the threshold γ_T. The mode of operation of Algorithm 3 is as follows. When some unacceptable users are scheduled, i.e. $K_a < K_s$, the base station will first determine the number of acceptable users after power reallocation, denoted by K'_a. In particular, if $\sum_{k=1}^{i} \gamma_{k:K} \geq i\gamma_T$ but $\sum_{k=1}^{i+1} \gamma_{k:K} < (i+1)\gamma_T$, then we conclude that $K'_a = i$ and the received SNR of all K'_a acceptable users after power reallocation is equal to $\frac{1}{i}\sum_{k=1}^{i} \gamma_{k:K}$. Note that if $K_a \leq K'_a < K_s$, then there will still remain $K_s - K'_a$ unacceptable users after power reallocation, whose SNR will not be changed with power reallocation. This algorithm has the lowest implementation complexity among the three proposed algorithms.

6.5.2 Performance analysis

In this section, we analyze the performance of the third power allocation algorithm for SBS scheduling through accurate analysis based on order statistics.

We first calculate the average numbers of scheduled acceptable users before and after power reallocation based on Algorithm 3. The average number of scheduled acceptable users before power reallocation can be calculated as

$$\overline{K}_a = \sum_{i=1}^{K_s-1} i \Pr[i \text{ acceptable users in total}] + K_s \Pr[\text{at least } K_s \text{ acceptable users}]. \tag{6.82}$$

Using the joint PDF and marginal PDF of ordered statistics, the probabilities involved can be calculated as

$$\Pr[i \text{ acceptable users in total}] = \int_{\gamma_T}^{\infty} \int_{0}^{\gamma_T} p_{\gamma_{i:K},\gamma_{i+1:K}}(x,y)\mathrm{d}y\mathrm{d}x \tag{6.83}$$

and

$$\Pr[\text{at least } K_s \text{ acceptable users}] = \int_{\gamma_T}^{\infty} p_{\gamma_{K_s:K}}(z)\mathrm{d}z, \tag{6.84}$$

where $p_{\gamma_{i:K},\gamma_{i+1:K}}(x,y)$ is the joint PDF of the ith largest and the $i+1$ largest received SNRs, which is given by

$$\begin{aligned} p_{\gamma_{i:K},\gamma_{j:K}}(x,y) &= \frac{K!}{(K-j)!\,(j-i-1)!\,(i-1)!} \\ &\times [F_\gamma(y)]^{K-j} [F_\gamma(x) - F_\gamma(y)]^{j-i-1} [1 - F_\gamma(x)]^{i-1} \\ &\times p_\gamma(x) p_\gamma(y), \\ &\qquad x > y \;\; \& \;\; 1 \le i < j \le K, \end{aligned} \tag{6.85}$$

and $p_{\gamma_{K_s:K}}(z)$ is the PDF of the K_sth largest received SNR, given by

$$p_{\gamma_{(K_s:K)}}(\gamma) = \binom{K}{K_s} K_s \cdot p_\gamma(\gamma) [1 - F_\gamma(\gamma)]^{K_s-1} [F_\gamma(\gamma)]^{K-K_s}. \tag{6.86}$$

Based on the mode of operation of Algorithm 3, the average number of scheduled acceptable users after power reallocation can be calculated as

$$\begin{aligned} \overline{K}'_a = &\sum_{i=1}^{K_s-1} i \Pr\left[\sum_{k=1}^{i} \gamma_{k:K} \ge i\gamma_T \,\&\, \sum_{k=1}^{i+1} \gamma_{k:K} < (i+1)\gamma_T\right] \\ &+ K_s \Pr\left[\sum_{k=1}^{K_s} \gamma_{k:K} \ge K_s \gamma_T\right]. \end{aligned} \tag{6.87}$$

In this case, the probabilities involved in the about summation can be calculated using the joint PDF of $\sum_{k=1}^{i} \gamma_{i:K}$ and $\gamma_{i+1:K}$ and the marginal PDF of $\sum_{k=1}^{K_s} \gamma_{i:K}$,

respectively, as

$$\Pr\left[\sum_{k=1}^{i}\gamma_{k:K} \geq i\gamma_T \,\&\, \sum_{k=1}^{i+1}\gamma_{k:K} < (i+1)\gamma_T\right] \tag{6.88}$$
$$= \int_0^{\gamma_T}\int_{i\gamma_T}^{(i+1)\gamma_T - x} p_{\sum_{k=1}^{i}\gamma_{k:K},\gamma_{i+1:K}}(x,y)\mathrm{d}y\mathrm{d}x,$$

and

$$\Pr\left[\sum_{k=1}^{K_s}\gamma_{k:K} \geq K_s\gamma_T\right] = \int_{K_s\gamma_T}^{\infty} p_{\sum_{k=1}^{K_s}\gamma_{k:K}}(z)\mathrm{d}z. \tag{6.89}$$

These joint statistics of the partial sums of order statistics have been investigated in a previous chapter. For example, the joint PDF of $\sum_{i=1}^{j}\gamma_{i:K}$ and $\gamma_{j+1:K}$ can be shown to be given by

$$p_{\gamma_{j+1:K},\sum_{i=1}^{j}\gamma_{i:K}}(x,y) = \frac{K!}{(K-j-1)!(j)!}[F_\gamma(x)]^{K-j-1}[1-F_\gamma(x)]^j$$
$$\times\, p_\gamma(x)p_{\sum_{i=1}^{j}\gamma_i^+}(y),$$
$$x \geq 0,\ y \geq jx, \tag{6.90}$$

where $p_{\sum_{i=1}^{j}\gamma_i^+}(\gamma)$ denote the PDF of the sum of j i.i.d. random variables γ_i^+, whose PDF is a truncated version of the PDF of γ_i on the left at x.

6.5.3 Numerical examples

The average number of the scheduled acceptable users, the ASE, and the average BER with our three proposed power allocation algorithms are investigated using Monte Carlo computer simulations. In our simulation, we assume the SBS scheme the coded adaptive modulation of [26] with $N = 8$ modes and i.i.d. Rayleigh fading conditions.

Figure 6.4 presents the average number of scheduled acceptable users with our proposed power allocation algorithms over i.i.d. Rayleigh fading conditions with $K = 5$, $K_s = 3$, and $\gamma_T = 7.1$ dB. As we can see, after power allocation with our proposed power allocation algorithms, the average number of scheduled acceptable users increases significantly for all three algorithms. Among the three algorithms, the third has the best performance among our proposed algorithms and the second has a better performance than the first.

Figure 6.5 presents the ASE of SBS with our proposed power allocation algorithms over i.i.d. Rayleigh fading conditions with $K = 5$, $K_s = 3$, and $\gamma_T = 7.1$ dB. Based on their mode of operation, when the average SNR is close to the SNR threshold for power allocation, Algorithm 2 acts like Algorithm 1 and in

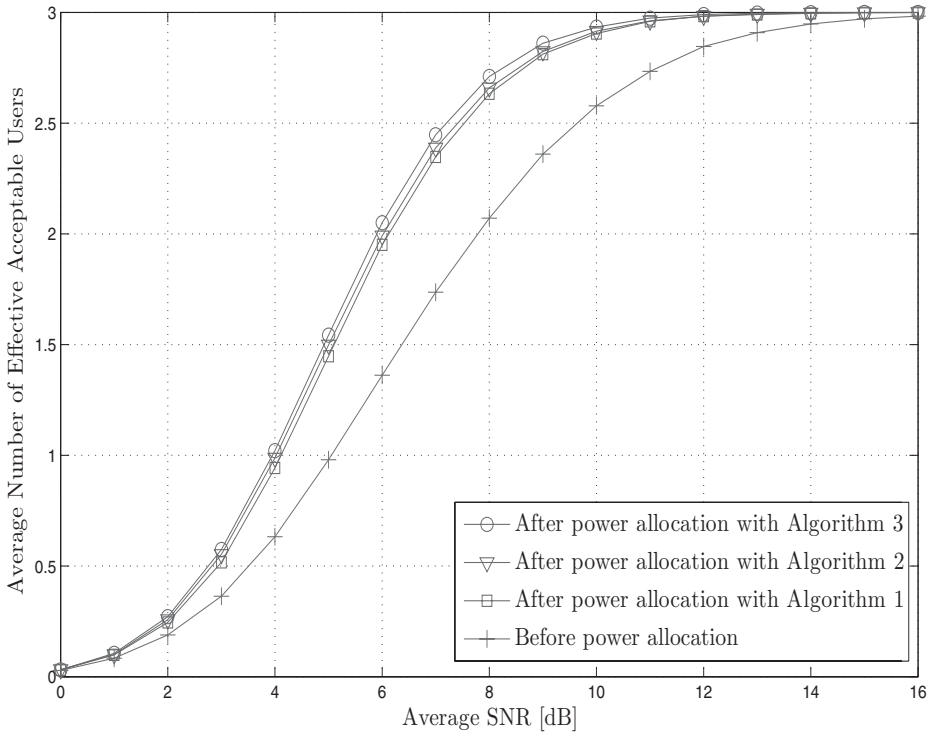

Figure 6.4 Average number of effective acceptable users with SBS over i.i.d. Rayleigh fading conditions with $K = 5$, $K_s = 3$, and $\gamma_T = 7.1$ dB [25]. © 2009 IEEE.

the region of average SNR, $\overline{\gamma}$, higher than the SNR threshold, Algorithm 2 acts like Algorithm 3. As expected, after power allocation with Algorithm 2, the ASE was increased because the acceptable users still have the same ASE and the ASE of the power allocated to unacceptable users was increased. On the other hand, contrary to our original expectations, after power allocation with Algorithms 1 and 3, the ASE was also increased. This can be explained by the fact that based on the statistical property of the scheduled users with SBS, at least one of the acceptable users has very large SNR compared with others among the scheduled users and then after power allocation, most of the acceptable users can still maintain their SNR regions after power allocation. The ASE with Algorithm 1 was increased only when the average SNR is close to the SNR threshold for power allocation because in the region of high $\overline{\gamma}$, the required SNR is decreasing and the number of acceptable users is increasing and for that reason, most of the acceptable users can maintain their SNR regions. The ASE with Algorithm 1 was increasing only in the region of low $\overline{\gamma}$. Based on the mode of operation of SBS, all the scheduled users with SBS may have acceptable SNRs in the region of high $\overline{\gamma}$. Therefore, based on the mode of operation of Algorithm 1, the system

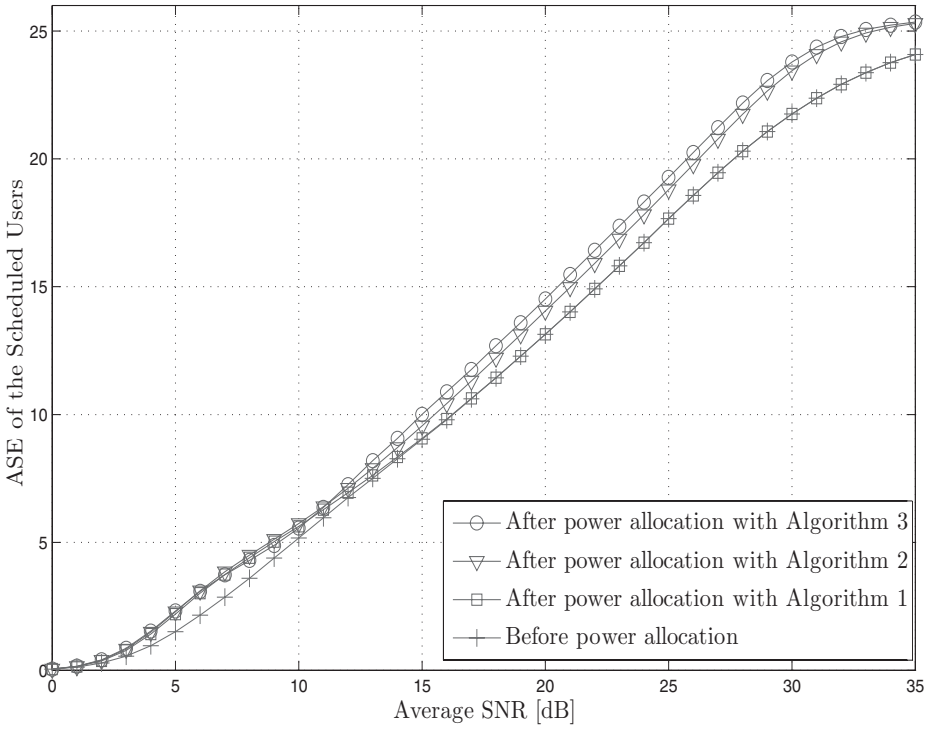

Figure 6.5 ASE [bits/s/Hz] with SBS over i.i.d. Rayleigh fading conditions with $K = 5$, $K_s = 3$, and $\gamma_T = 7.1$ dB [25]. © 2009 IEEE.

did not need the power allocation process in the region of high $\overline{\gamma}$. The ASE with Algorithm 2 was increasing when $\overline{\gamma}$ is slightly lower than the SNR threshold and finally approaching to the ASE prior to the application of the power allocation. Similar to Algorithm 2, the ASE with Algorithm 3 is also increasing when $\overline{\gamma}$ is slightly lower than the SNR threshold and finally it approaches to the ASE prior to the application of power allocation.

Figure 6.6 presents the average BER of SBS with our proposed power allocation algorithms over i.i.d. Rayleigh fading conditions with $K = 5$, $K_s = 3$, and $\gamma_T = 7.1$ dB. After power allocation with algorithm 1, the average BER performance is degraded only when the average SNR is close to the SNR threshold for power allocation because the excess SNRs are extracted from the acceptable users. In the region of high $\overline{\gamma}$, the extracted SNR from the acceptable users is decreased and then the average BER is approaching the average BER prior to the application of the power allocation. Similar to the ASE results, the average BER of Algorithm 2 acts like the ASE of Algorithm 2 when the average SNR is close to the SNR threshold for power allocation. Considering the three algorithms together, it is clear that Algorithm 3 provides the best performance and the least complexity among the three proposed algorithms.

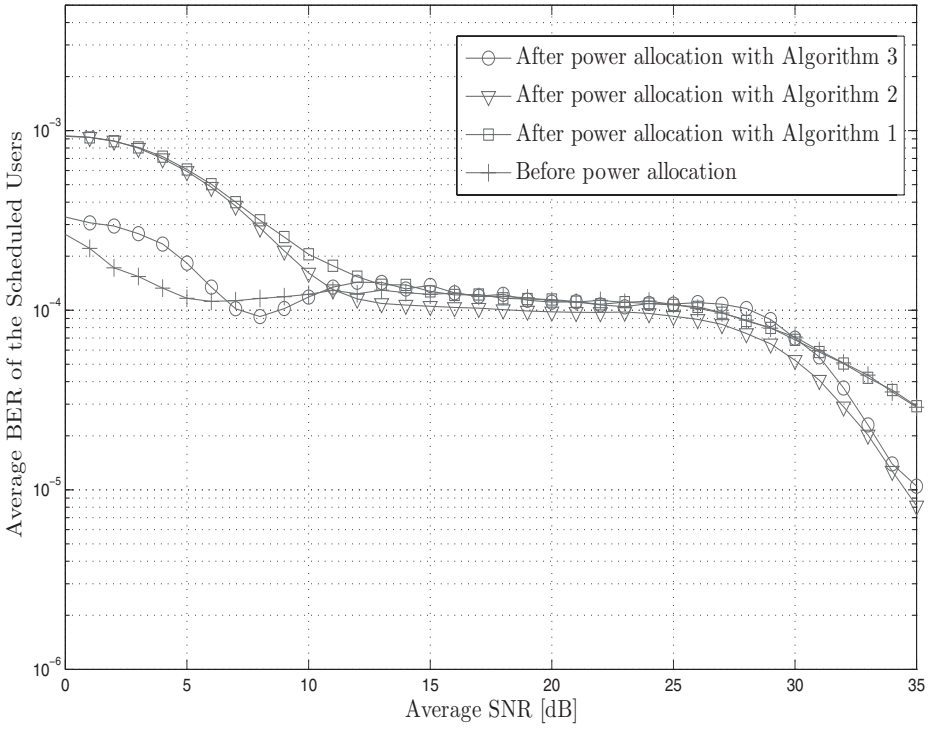

Figure 6.6 Average BER with SBS over i.i.d. Rayleigh fading conditions with $K = 5$, $K_s = 3$, and $\gamma_T = 7.1$ dB. © 2009 IEEE.

6.6 Summary

In this chapter, we addressed the design and analysis of user scheduling schemes for wireless communication systems. We focused on those schemes that have low implementation complexity. Both single-user scheduling and multiple user scheduling were considered. For single-user schemes, we quantified their performance, not only from the conventional capacity benefit perspective but also in terms of new metrics, such as channel access time and rate. The multiple user schemes assumed that users were competing for one of many channel resource units with common instantaneous quality to the same user. The performance and complexity of each scheme were accurately quantified. Finally, we presented and analyzed several practical power allocation strategies for one of the representative multiuser scheduling scheme.

6.7 Bibliography notes

A multiuser scheduling scheme based on switched diversity was studied in [27–29]. The performance of multiuser scheduling in a multi-antenna scenario with

different diversity combining scheme was analyzed in [30]. Feedback load reduction strategies for multiuser diversity systems were also considered in [31–34] among many others. Ma and Tepedelenlioglu quantified the effect of outdated feedback on the performance of multiuser diversity systems in [35]. The joint design of a multiuser scheduling scheme with adaptive diversity combining strategy is considered in [36, 37].

References

[1] R. Knopp and P. Humblet, "Information capacity and power control in single-cell multiuser communications," in *Proc. IEEE Int. Conf. Commun. (ICC95)*, Seattle, WA, vol. 1, pp. 331–335, June 1995.

[2] D. N. C. Tse,"Optimal power allocation over parallel Gaussian channels," in *Proc. Int. Symp. Inform. Theory (ISIT97)*, Ulm, Germany, p. 27, June 1997.

[3] P. Viswanath, D. Tse and R. Laroia,"Opportunistic beamforming using dumb antennas," *IEEE Trans. Inform. Theory*, vol. 48, pp. 1277–1294, June 2002.

[4] H. A. David, *Order Statistics*. New York, NY: John Wiley & Sons, Inc., 1981.

[5] D. Gesbert and M.-S. Alouini, "How much feedback is multi-user diversity really worth?" in *Proc. of IEEE Int. Conf. on Commun. (ICC'04)*, Paris, France, June 2004, pp. 234–238.

[6] M. Abramowitz and I. A. Stegun, *Handbook of Mathematical Functions with Formulas, Graphs, and Mathematical Tables*, 9th ed. New York, NY: Dover, 1970.

[7] L. Yang and M.-S. Alouini, "Performance analysis of multiuser selection diversity," *IEEE Trans. Veh. Technol.*, vol. 55, pp. 1003–1018, May 2006.

[8] G. L. Stüber, *Principles of Mobile Communication*, 2nd ed. Norwell, MA: Kluwer, 2000.

[9] G. W. Lank and L. S. Reed, "Average time to loss of lock for an automatic frequency control loop with two fading signals and a related probability density function," *IEEE Trans. Inf. Theory*, vol. IT-12, no. 1, pp. 73–75, January 1966.

[10] J.-P. M. G. Linnartz and R. Prasad, "Threshold crossing rate and average non-fade duration in a Rayleigh-fading channel with multiple interferers," *Archiv für Elektronik und Ubertragungstechnik Electonics and Communication*, vol. 43, no. 6, pp. 345–349, November/December 1989.

[11] W. C. Jakes, *Microwave Mobile Communications*. New York, NY: Wiley, 1974.

[12] X. Dong and N. C. Beaulieu, "Average level crossing rate and average fade duration of selection diversity," *IEEE Commun. Lett.*, vol. 5, no. 10, pp. 396–398, October 2001.

[13] T. Eng, N. Kong and L. B. Milstein, "Comparison of diversity combining techniques for Rayleigh-fading channels," *IEEE Trans. Commun.*, vol. 44, no. 9, pp. 1117–1129, September 1996.

[14] T. Eng, N. Kong and L. B. Milstein, "Correction to Comparison of diversity combining techniques for Rayleigh-fading channels," *IEEE Trans. Commun.*, vol. 46, no. 9, p. 1111, September 1998.

[15] R. Kwan and C. Leung, "Downlink scheduling optimization in CDMA networks," *IEEE Commun. Letters*, vol. 8, pp. 611–613, October 2004.

[16] Y. Ma, J. Jin and D. Zhang, "Throughput and channel access statistics of generalized selection multiuser scheduling," *IEEE Trans. Wireless Commun.*, vol. 7, no. 8, pp. 2975–2987, August 2008.

[17] Y. Ma and S. Pasupathy, "Efficient performance evaluation for generalized selection combining on generalized fading channels," *IEEE Trans. Wireless. Commun.*, vol. 3, no. 1, pp. 29–34, January 2004.

[18] M. K. Simon and M.-S. Alouini, "Performance analysis of generalized selection combining with threshold test per branch (T-GSC)," *IEEE Trans. Veh. Technol.*, vol. 51, no. 5, pp. 1018–1029, 2002.

[19] J. Hömäläinen and R. Wichman, "Capacities of physical layer scheduling strategies on a shared link," *Wireless Personal Communications*, vol. 39, no. 1, pp. 115–134, October 2006.

[20] S. Nam, M.-S. Alouini, H.-C. Yang and K. A. Qaraqe, "Threshold-based parallel multiuser scheduling," *IEEE Trans. on Wireless Commun.*, vol. 8, no. 4, pp. 2150–2159, April 2009.

[21] M.-S. Alouini and A. J. Goldsmith, "Adaptive modulation over Nakagami fading channels," *Kluwer J. Wireless Commun.*, vol. 13, nos. 1–2, pp. 119–143, 2000.

[22] H.-C. Yang and M.-S. Alouini, "Generalized switch and examine combining (GSEC): a low-complexity combining scheme for diversity rich environments," *IEEE Trans. Commun.*, vol. COM-52, no. 10, pp. 1711–1721, October 2004.

[23] H.-C. Yang and L. Yang, "Tradeoff analysis of performance and complexity on GSECps diversity combining scheme," *IEEE Trans. on Wireless Commun.*, vol. TWC-7, no. 1, pp. 32–36, January 2008.

[24] Y. Ma, D. Zhang and R. Schober, "Capacity-maximizing multiuser scheduling for parallel channel access," *IEEE Signal Processing Letters*, vol. 14, pp. 441–444, July 2007.

[25] S. Nam, H.-C. Yang, M.-S. Alouini and K. A. Qaraqe, "Performance evaluation of threshold-based power allocation algorithms for down-link switched-based parallel scheduling," *IEEE Trans. on Wireless Commun.*, vol. 8, no. 4, pp. 1744–1753, April 2009.

[26] K. J. Hole, H. Holm and G. E. Oien, "Adaptive multidimentional coded modulation over flat fading channels," *IEEE J. Select. Areas Commun.*, vol. SAC-18, no. 7, pp. 1153–1158, July 2000.

[27] G. B. Holter, M.-S. Alouini, G. E. Øien and H.-C. Yang, "Multiuser switched diversity transmission," in *Proc. IEEE Vehicular Technology Conf. (VTC'04-Fall)*, Los Angeles, CA, 2004, pp. 2038–2043.

[28] Y. S. Al-Harthi, A. H. Tewfik and M.-S. Alouini, "Multiuser diversity with quantized feedback," *IEEE Trans. Wireless Commun.*, vol. 6, no. 1, pp. 330–337, January 2007.

[29] H. Nam and M.-S. Alouini, "Multiuser switched diversity scheduling systems with per-user threshold," *IEEE Trans. on Commun.*, vol. 58, no. 5, pp. 1321–1326, May 2010.

[30] C.-J. Chen and L.-C. Wang, "A unified capacity analysis for wireless systems with joint multiuser scheduling and antenna diversity in Nakagami fading channels," *IEEE Trans. Commun.*, vol. 54, no. 3, pp. 469–478, March 2006.

[31] T. Tang and R. W. Heath, "Opportunistic feedback for downlink multiuser diversity," *IEEE Commun. Lett.*, vol. 9, no. 10, pp. 948–950, October 2005.

[32] S. Sanayei and A. Nosratinia, "Opportunistic downlink transmission with limited feedback," *IEEE Trans. Inform. Theory*, vol. 53, no. 11, pp. 4363–4372, November 2007.

[33] Y. Xue and T. Kaiser, "Exploiting multiuser diversity with imperfect one-bit channel state feedback," *IEEE Trans. Veh. Technol.*, vol. 56, no. 1, pp. 183–193, January 2007.

[34] J. So and J. M. Cioffi, "Feedback reduction scheme for downlink multiuser diversity," *IEEE Trans. Wireless Commun.*, vol. 8, no. 2, pp. 668–672, February 2009.

[35] Q. Ma and C. Tepedelenlioglu, "Practical multiuser diversity with outdated channel feedback," *IEEE Trans. Veh. Technol.*, vol. 54, no. 4, pp. 1334–1345, July 2005.

[36] K.-H. Park, Y.-C. Ko and M.-S. Alouini, "Joint adaptive combining and multiuser downlink scheduling," *IEEE Trans. Veh. Technol.*, vol. 57, no. 5, pp. 2958–2968, September 2008.

[37] S. B. Halima, M.-S. Alouini and K. A. Qaraqe, "Joint MS-GSC combining and downlink multiuser diversity scheduling," *IEEE Trans. Wireless Commun.*, Vol. 8, no. 7, pp. 3536–3545, July 2009.

7 Multiuser MIMO systems

7.1 Introduction

Multiple-antenna transmission and reception (i.e. MIMO) techniques can considerably improve the performance and/or efficiency of wireless communication systems. First introduced in mid 1990s [1, 2], MIMO technique has been an area of active research and has found applications in various emerging wireless systems. Most of early MIMO designs focus on point-to-point link where both transmitter and receiver have multiple antennas and demonstrate the huge potential of MIMO techniques in terms of providing array gain, spatial diversity gain, spatial multiplexing gain and interference reduction capability, among many others [3–5]. Meanwhile, most mobile receivers will possess less antennas than the base stations in the near future due to their size/cost constraints. In such scenarios, the capacity of a point-to-point link between the base station and a mobile will be limited by the number of antennas at the mobile. On the other hand, if we consider the antennas of different receivers together, a virtual MIMO system is formed with huge capacity potential [6–10]. The design and analysis of efficient transmission strategy for resulting multiuser MIMO systems is the subject of this chapter.

A rich literature on MIMO wireless communications already exists. There has already been a rich literature on MIMO wireless communications. Several books have been published on this general subject (see for example [11,12]). This chapter complements existing literature on MIMO wireless communications by focusing on the different multiuser scheduling schemes for multiuser MIMO systems. In general, the downlink transmission from the base station to mobile receivers is more challenging in the multiuser MIMO system, as mobile users are randomly distributed and cannot perform joint detection. In this context, the key idea to fully exploit the potential spatial multiplexing gain, offered by multiple antennae at the base station and at different users, is to transmit simultaneously to multiple properly selected mobile receivers. We will examine several practical designs and evaluate their particular performance versus complexity trade-off through accurate statistical analysis. Note that most previous works on multiuser MIMO systems have relied on asymptotic analysis, which has limited applicability in real-world systems. Here, we address the exact sum-rate performance of different multiuser MIMO systems with user scheduling with the help of some order statistics results.

In this chapter, we first review the basics of MIMO wireless communications and introduce multiuser MIMO systems. After that, we consider the zero-forcing beamforming (ZFBF) transmission scheme for multiuser MIMO systems and analyze the resulting sum-rate performance with two different user scheduling schemes. We then move onto the random unitary beamforming (RUB) scheme. For the RUB transmission scheme, we first consider the case of the single antenna per mobile user case, for which we present and analyze several low-complexity user scheduling strategies and quantify their respective trade-off of sum-rate performance versus feedback load. For the multiple antennae per user case, we focus on the schemes where receivers apply linear combining to the received signal on different antennas.

7.2 Basics of MIMO wireless communications

In this section, we review some basic results of MIMO wireless systems and then introduce the multiuser MIMO system model that will be used in a later section.

7.2.1 MIMO channel capacity

Let us consider a point-to-point link where the transmitter has M_t antennae and the receiver has M_r antennae. We assume that the channel for the jth transmit antenna to the ith receiver antenna experiences frequency flat fading, with complex channel gain h_{ij}, usually modeled as i.i.d. zero-mean unit-variance complex Gaussian random variables. As such, the received signal on the ith receive antenna is given by

$$y_i = h_{i1}x_1 + h_{i2}x_2 + \cdots + h_{iM_t}x_{M_t} + n_i, \tag{7.1}$$

where x_j is the transmitted symbol from the jth transmit antenna and n_i is the independent Gaussian noise with zero mean and variance $\sigma^2 = N_0/2$. The discrete time MIMO channel model can be rewritten in matrix form as

$$\begin{bmatrix} y_1 \\ y_2 \\ \vdots \\ y_{M_r} \end{bmatrix} = \begin{bmatrix} h_{11} & h_{12} & \cdots & h_{1M_t} \\ h_{21} & h_{22} & \cdots & h_{2M_t} \\ \vdots & \vdots & \ddots & \vdots \\ h_{M_r 1} & h_{M_r 2} & \cdots & h_{M_r M_t} \end{bmatrix} \begin{bmatrix} x_1 \\ x_2 \\ \vdots \\ x_{M_t} \end{bmatrix} + \begin{bmatrix} n_1 \\ n_2 \\ \vdots \\ n_{M_r} \end{bmatrix}$$

or in matrix notation

$$\mathbf{y} = \mathbf{H}\mathbf{x} + \mathbf{n}. \tag{7.2}$$

The inherent spatial degree of freedom of the above MIMO system can be exploited for both spatial multiplexing gain and diversity gain.

The most convenient way to demonstrate the capacity benefit of a MIMO system is parallel decomposition [11, 13]. Specifically, the MIMO channel can be

decomposed into multiple parallel channels as follows. After applying singular value decomposition to $\mathbf{H}$, we have

$$\mathbf{H}_{M_r \times M_t} = \mathbf{U}_{M_r \times M_r} \mathbf{\Sigma}_{M_r \times M_t} \mathbf{V}_{M_t \times M_t}{}^H,$$

where $\mathbf{U}$ and $\mathbf{V}$ are unitary matrices and $\mathbf{\Sigma}$ is the diagonal matrix of the singular values σ_i of $\mathbf{H}$. It is not difficult to see that the matrix will have $R_{\mathbf{H}}$ nonzero singular values, where $R_{\mathbf{H}} \in [1, \min\{M_t, M_r\}]$. Therefore, the MIMO channel can be transformed into $R_{\mathbf{H}}$ parallel independent channels if the channel input is precoded by $\mathbf{V}$, i.e. $\mathbf{x} = V\tilde{\mathbf{x}}$, and the channel output is preprocessed by $\mathbf{U}$, i.e. $\tilde{\mathbf{y}} = U^H \mathbf{y}$. The ith channel will have input $\tilde{x}_i$, output $\tilde{y}_i$, and channel gain σ_i with additive noise. Effectively, the data rate can be increased by $R_{\mathbf{H}}$ times. Note that the transmitter needs to have the complete knowledge of $\mathbf{V}$ or equivalently $\mathbf{H}$.

Based on the parallel decomposition, the capacity of the MIMO wireless channel can be determined as the sum of individual decomposed channels with optimal transmit power allocation. Let P_i denote the power allocation to the ith decomposed channel, which satisfies a total power constraint of $\sum_i P_i \leq P_T$. The MIMO capacity with perfect CSIT can be calculated by solving the following optimization problem: maximizing over $\{P_i\}_{i=1}^{R_{\mathbf{H}}}$

$$\sum_{i=1}^{R_{\mathbf{H}}} B \log_2 \left(1 + \frac{\sigma_i^2 P_i}{\sigma^2}\right),$$

under the constraint $\sum_i P_i \leq P_T$. The maximum is achieved with the well-known water-filling solution, given by

$$P_i = \begin{cases} \frac{1}{\gamma_0} - \frac{1}{\gamma_i}, & \gamma_i \geq \gamma_0, \\ 0, & \gamma_i < \gamma_0, \end{cases} \tag{7.3}$$

where $\gamma_i = \sigma_i^2/\sigma^2$ and γ_0 is the cutoff value based on the total power constraint $\sum_{i:\gamma_i \geq \gamma_0} P_i = P_T$. The resulting instantaneous channel capacity is equal to

$$C = \sum_{i:\gamma_i \geq \gamma_0} B \log_2 \left(\frac{\gamma_i}{\gamma_0}\right). \tag{7.4}$$

As the result of multipath fading, h_{ij} varies over time. The ergodic capacity of the MIMO channel over fading channels can be obtained by averaging the instantaneous capacity over the fading distribution of channel matrix $\mathbf{H}$.

$$C_f = \mathbf{E}_{\mathbf{H}}[C(\mathbf{H})], \tag{7.5}$$

or equivalently, over the distribution of the singular values of $\mathbf{H}$, σ_i^2 as

$$C_f = \mathbf{E}_{\sigma_i^2} \left[\max_{P_i : \sum_i P_i \leq P} \sum_i B \log_2 (1 + P_i \gamma_i) \right]. \tag{7.6}$$

The expectation can be solved in some cases while noting that σ_i^2 is the ith largest eigenvalue of $\mathbf{H}\mathbf{H}^H$, which is of the Wishart type.

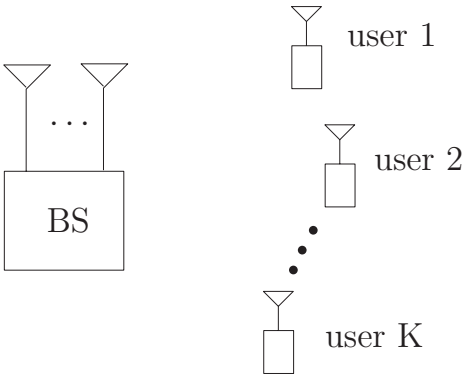

Figure 7.1 Multiuser MIMO system.

7.2.2 Multiuser MIMO systems

While MIMO techniques can bring huge capacity gains to wireless systems, it is in general difficult to implement the same number of antennae at the mobile receivers as at the base stations. Most mobile stations will still have only a single antennae due to their size and cost constraints. In such a scenario, we can still explore the potential spatial multiplexing gain offered by multiple antennae at the base station through the simultaneous transmission to multiple single-antenna receivers. The resulting multiuser MIMO system, as illustrated in Fig. 7.1, has received a significant amount of research interest. In particular, the dirty paper coding (DPC) technique [14] has been shown to be the optimal transmission scheme from the sum-capacity perspective for MIMO broadcast channels [6,8,15]. The sum-rate capacity of these channels with DPC scales at a rate of $M \log \log K$, where M is the number of transmit antennae and K is the total number of receive antennae at different users. On the other hand, DPC has prohibitively high computational complexity due to the associated successive encoding process and requires the complete channel state information at the transmitter (CSIT) side. Therefore, it is of great practical interest to design multiuser MIMO transmission schemes that can achieve high sum-rate capacity with low complexity and a minimum CSIT requirement.

The basic approach is to apply some linear precoding schemes, such as zero-forcing beamforming (ZFBF) [16, 17] or random unitary beamforming (RUB) [18–22], to the signals targeted at multiple selected users. With ZFBF, the precoding matrix is simply designed to be the pseudo-inverse of the channel matrix to the selected users. It has been shown that ZFBF is asymptotically optimal when the number of users approaches infinity [17]. With RUB, the precoding matrix consists of M random orthogonal beamforming vectors and users are selected based on their channel quality on different beamforming direction. RUB is also shown to be able to achieve the same sum-rate scaling law as DPC, even if each user just feeds back its largest beam signal to interference plus noise ratio (SINR) value and the index of the corresponding beam [20]. In the

following sections, we will present and analyze some practical user selection strategies for these linear precoding-based multiuser MIMO systems and focus specifically on their exact sum-rate performance evaluation. To establish a common context for the remaining discussion, we now present the signal model for the multiuser MIMO system under consideration.

We consider the downlink transmission of a single-cell wireless system. The base station is equipped with M antennae and as such can serve as many as M different selected users with a linear beamforming approach. The transmitted signal vector from M antennae over one symbol period can be written as

$$\mathbf{x} = \sum_{m=1}^{M} \mathbf{b}_m s_m, \tag{7.7}$$

where s_m is the information symbol, targeted to the mth selected user, and $\mathbf{b}_m$ is the beamforming vector for the mth selected user. The transmitted signal vector $\mathbf{x}$ has an average power constraint of $tr\{\mathbf{E}[\mathbf{x}\mathbf{x}^H]\} \leq P$, where P is the maximum average transmitting power, $\mathbf{E}[\cdot]$ denotes the statistical expectation and $(\cdot)^H$ the Hermitian transpose. We assume that there are a total of K active users in the cell, where $K \geq M$. Each user is equipped with a single antenna. We further assume that with a certain slow power control mechanism, the users experience homogeneous flat Rayleigh fading. In particular, the channel gain from the ith antenna to the kth mobile users, denoted by h_{ik}, is assumed to be an independent zero mean complex Gaussian random variable with unitary variance, i.e. $h_{ik} \sim \mathcal{C}N(0,1)$. As such, the instantaneous multiple-input single-output (MISO) channel from the base station to the kth mobile user can be characterized by a zero-mean complex Gaussian channel vector, denoted by $\mathbf{h}_k = \{h_{1k}, h_{2k}, \cdots, h_{Mk}\}^T$.

During each symbol period, the base station transmits simultaneously to a subset of M different chosen users using all M available beams. The received symbol of the ith chosen user, when the jth beam is assigned to it, can be written as

$$y_i = \mathbf{h}_i^T \mathbf{x} + n_i = \mathbf{h}_i^T \mathbf{b}_j s_j + \sum_{m=1, m\neq j}^{M} \mathbf{h}_i^T \mathbf{b}_m s_m + n_i, \tag{7.8}$$

where n_i are independent zero-mean additive Gaussian noise with unit variance. It is easy to see that the received signal will experience interuser interference as well as additive noise. The metric that will determine the quality of detection becomes the SINR, which is given for the ith user receiving on the jth beamforming direction, assuming uniform power allocation to different users, by

$$\gamma_{i,j} = \frac{\frac{P}{M}|\mathbf{h}_i^T \mathbf{b}_j|^2}{\frac{P}{M}\sum_{m=1, m\neq j}^{M} |\mathbf{h}_i^T \mathbf{n}_m|^2 + 1}, \; j = 1, 2, \cdots, M. \tag{7.9}$$

The interuser interference will be controlled through beamforming vector design and/or user selection, as will be detailed in the following subsections.

Finally, the total sum rate of the multiuser MIMO system with linear precoding is given, with the assumption of uniform power allocation among selected users, by

$$R = \mathbf{E}\left[\sum_{m=1}^{M} \log_2(1+\gamma_m^B)\right], \tag{7.10}$$

where γ_m^B is the received SINR on the mth beamforming direction.

7.3 ZFBF-based system with user selection

ZFBF is a practical multiuser transmission strategy for multiuser MIMO systems [16, 17]. By designing one user's beamforming vector to be orthogonal to other selected users' channel vectors, ZFBF can completely eliminate multiuser interference. A proper user selection scheme is essential for the ZFBF-based multiuser MIMO system to fully benefit from multiuser diversity gain [23]. The desired properties of selected user channels are (i) large channel power gain, and (ii) near orthogonal to one another. The optimum ZFBF user selection strategy involves the exhaustive search of all possible user subsets, which becomes prohibitive to implement when the number of users is large. Several low-complexity user selection strategies have been proposed and studied in the literature [17, 23–26]. Among them, two greedy search algorithms, the successive projection ZFBF (SUP-ZFBF) [17, 24] and the greedy weight clique ZFBF (GWC-ZFBF) [23], are attractive for simplicity of implementation and their ability to achieve the same scaling rate of double log as the DPC scheme. We will carry out accurate statistical analysis on these two schemes for the important two-transmit antenna special case. These analytical results will not only facilitate the trade-off study between them, but will also apply to the parameter optimization for each scheme.

7.3.1 Zeroforcing beamforming transmission

We consider the multiuser MIMO system as shown in Fig. 7.1. Specifically, the base station is equipped with two transmit antennae. There are in total K users in the system, where $K \geq 2$, and each user has one receive antenna. We assume a flat homogeneous Rayleigh fading channel model. The channel gain from the ith transmit antenna to the kth user h_{ki} is assumed to be i.i.d. zero-mean complex Gaussian random variable with unitary variance. As such, the instantaneous MISO channel from the base station to the kth mobile user can be characterized by a zero-mean complex Gaussian channel vector, denoted by $\mathbf{h}_k = [h_{k1} \;\; h_{k2}]^T, \;\; k = 1, 2, \cdots, K$. As such, the norm square of the kth user's channel vector $\|\mathbf{h}_k\|^2$ (termed channel power gain) is a Chi-square distributed

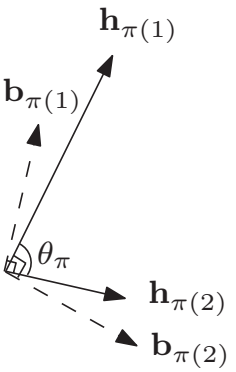

Figure 7.2 Zero-forcing beamforming for the two-user case [48].

random variable with four degrees of freedom, with PDF and CDF given by

$$p_{\|\mathbf{h}\|^2}(x) = xe^{-x},\ x \geq 0, \tag{7.11}$$

and

$$F_{\|\mathbf{h}\|^2}(x) = \gamma(2, x),\ x \geq 0, \tag{7.12}$$

respectively, where $\gamma(2, x) = \int_0^x te^{-t}\mathrm{d}t$ is the lower incomplete gamma function. We assume that the base station knows the downlink channel vector for every user either through a feedback mechanism or the reciprocity of the channel in time division duplexing (TDD) mode.

Let $\pi(1)$ and $\pi(2)$ denote the indexes of the selected users and $\mathbf{b}_{\pi(1)}$ and $\mathbf{b}_{\pi(2)}$ denote the beamforming vectors for the two selected users. As shown in Fig. 7.2, the beamforming vector of one user is chosen to be orthogonal to the channel vector of the other user, resulting in so-called zero-forcing beamforming. The transmitted signal vector from two antennae over one symbol period can then be written as

$$\mathbf{x} = \sum_{i=1}^{2} \sqrt{P_{\pi(i)}}\mathbf{b}_{\pi(i)}s_{\pi(i)}, \tag{7.13}$$

where $s_{\pi(i)}$ and $P_{\pi(i)}$ are the data symbol and transmit power scaling factor, respectively, for user $\pi(i)$. The power constraint imposed on the transmitted signal is $E[\|\mathbf{x}\|^2] \leq P$. Because of the orthogonality between beamforming vectors and channel vectors, the received symbol at user $\pi(i)$ is consequently given by

$$r_{\pi(i)} = \mathbf{h}_{\pi(i)}^T\mathbf{x} + n_{\pi(i)} = \sqrt{P_{\pi(i)}}\mathbf{h}_{\pi(i)}^T\mathbf{b}_{\pi(i)}s_{\pi(i)} + n_{\pi(i)}, \tag{7.14}$$

where $n_{\pi(i)}$ is the additive zero-mean Gaussian noise with variance N_0. Note that the interference for the two-user transmission is completely eliminated, whereas the effective channel power gain for user $\pi(i)$ becomes the norm square of the projection of its channel vector $\mathbf{h}_{\pi(i)}$ onto the corresponding beamforming vector $\mathbf{b}_{\pi(i)}$, which is termed projection power in this chapter. Let θ_π, as illustrated in

Fig. 7.2, denote the angle between $\mathbf{h}_{\pi(1)}$ and $\mathbf{h}_{\pi(2)}$. The effective power gain $\gamma_{\pi(i)}$ can be written as

$$\gamma_{\pi(i)} = \|\mathbf{h}_{\pi(i)}\|^2 |\sin(\theta_\pi)|^2. \tag{7.15}$$

Note that $|\sin(\theta_\pi)|^2$ can be viewed as a projection power loss factor due to ZFBF. Assuming the total transmit power P is equally divided between two selected users, then the instantaneous sum rate of the system is given by

$$R = \sum_{i=1}^{2} \log(1 + \frac{\rho}{2}\gamma_{\pi(i)}) \tag{7.16}$$

where $\rho = P/N_0$ denotes the total transmit SNR.

7.3.2 User selection strategies

The base station will select two users to serve simultaneously using either the SUP-ZFBF [17] or GWC-ZFBF [23] scheme. Basically, both schemes sequentially perform user selection from a user subset, which contains users whose channel vectors are near orthogonal to the channel vectors of already selected users. Here, two channel vectors are claimed to be near orthogonal if θ, the angle between the two channel vectors, satisfies $|\sin(\theta)|^2 \geq \lambda_d$, where $0 < \lambda_d < 1$ is a constant value. With GWC-ZFBF, the next selected user is the one with the largest channel power gain, whereas with SUP-ZFBF, the next user is the one with the largest projection power of its channel vector onto the complement space of the space spanned by the channel vectors of already selected users.

GWC-ZFBF

1. Order all K users based on their channel power gain $\|\mathbf{h}_k\|^2$ as $\|\mathbf{h}_{(1)}\|^2 > \|\mathbf{h}_{(2)}\|^2 > \cdots > \|\mathbf{h}_{(K)}\|^2$.
2. Select the one with the largest channel power gain as the first user, i.e. $\pi(1) = (1)$.
3. Examine sequentially the angle between $\mathbf{h}_{\pi(1)}$ and $\mathbf{h}_{(k)}$, $k = 2, 3, \ldots, K$ and select the first user whose channel vector is near orthogonal to $\mathbf{h}_{\pi(1)}$. Equivalently, the second selected user will be the one with the largest channel power gain among all users in the set

$$\mathcal{U} = \{i | |\sin(\theta_i)|^2 = 1 - \frac{|<\mathbf{h}_i, \mathbf{h}_{\pi(1)}>|^2}{\|\mathbf{h}_i\|^2 \|\mathbf{h}_{\pi(1)}\|^2} \geq \lambda_d\}, \tag{7.17}$$

where θ_i is the angle between $\mathbf{h}_i$ and $\mathbf{h}_{\pi(1)}$.

SUP-ZFBF

1. Select the user with the largest channel power gain as the first user.
2. Calculate and rank the projection power onto the complementary space of $\mathbf{h}_{\pi(1)}$ for all users in $\mathcal{U}$, which is defined in (7.17).

3. Select the user with the largest projection power as the second user, i.e.

$$\pi(2) = \max_{i \in \mathcal{U}} \{\|\mathbf{h}_i\|^2 |\sin(\theta_i)|^2\} \tag{7.18}$$

As SUP-ZFBF needs to calculate the projection power of all users in $\mathcal{U}$ while GWC-ZFBF stops searching when it encounters the first user that is near orthogonal to $\mathbf{h}_{\pi(1)}$, SUP-ZFBF exhibits higher computational complexity than GWC-ZFBF.

7.3.3 Sum-rate analysis

In this section, we analyze the ergodic sum rate of a ZFBF-based multiuser MIMO system with SUP-ZFBF and GWC-ZFBF schemes. For that purpose, we first derive the statistics of channel power gains of selected users $\|\mathbf{h}_{\pi(i)}\|^2$, $i = 1, 2$ and projection power loss factor $|\sin(\theta_\pi)|^2$.

Common analysis for both schemes

For both user selection schemes, the first selected user has the largest channel power gain among K users. Since the power gains of K users are i.i.d. random variables, the PDF of $\|\mathbf{h}_{\pi(1)}\|^2$ for both schemes is expressed as [27]

$$p_{\|\mathbf{h}_{\pi(1)}\|^2}(x) = K p_{\|\mathbf{h}\|^2}(x)(F_{\|\mathbf{h}\|^2}(x))^{K-1}. \tag{7.19}$$

If no user's channel vector is near orthogonal to the channel vector of the first selected user, i.e. $\mathcal{U} = \emptyset$, the base station transmits to the first selected user using traditional beamforming approach. In this case, the sum rate for both user selection schemes is expressed as

$$\mathbf{E}[R|\mathcal{U} = \emptyset] = \int_0^\infty \log(1 + \frac{\rho}{2}x) p_{\|\mathbf{h}_{\pi(1)}\|^2}(x)\mathrm{d}x. \tag{7.20}$$

It is shown in [17] that $|\sin(\theta)|^2$, where θ is the angle between a random channel vector and $\mathbf{h}_{\pi(1)}$, follows the standard uniform distribution over the interval $[0, 1]$. Therefore, after the selection of the first user, the probability that a remaining user belongs to $\mathcal{U}$ is $\Pr[|\sin(\theta)|^2 \geq \lambda_d] = 1 - \lambda_d$. It follows that

$$\Pr[\mathcal{U} = \emptyset] = \lambda_d^{K-1} \quad \text{and} \quad \Pr[\mathcal{U} \neq \emptyset] = 1 - \lambda_d^{K-1}. \tag{7.21}$$

where $\Pr[\mathcal{U} \neq \emptyset]$ is the probability of $\mathcal{U} \neq \emptyset$ and as such the second user can be selected. Considering these two mutually exclusive cases of $\mathcal{U} = \emptyset$ and $\mathcal{U} \neq \emptyset$, the ergodic sum rate of both schemes can be calculated as

$$\mathbf{E}[R] = \Pr[\mathcal{U} = \emptyset]\mathbf{E}[R|\mathcal{U} = \emptyset] + \Pr[\mathcal{U} \neq \emptyset]\mathbf{E}[R|\mathcal{U} \neq \emptyset]. \tag{7.22}$$

We now need to determine the average sum rate when $\mathcal{U}$ is not empty. This analysis requires the PDF of $\|\mathbf{h}_{\pi(2)}\|^2$ and $|\sin(\theta_\pi)|^2$, which will be derived separately for GWC-ZFBF and SUP-ZFBF in the following.

GWC-ZFBF specific analysis

With GWC-ZFBF, the second selected user is the one with the ith largest channel power gain, i.e. $\pi(2) = (i)$, if and only if user (i) belongs to $\mathcal{U}$ and none of the users from (2) to $(i-1)$ do. Therefore, the probability of $\pi(2) = (i)$, given that $\mathcal{U}$ is not empty, can be calculated as

$$\Pr\left[\pi(2) = (i) | \mathcal{U} \neq \emptyset\right] = \frac{(1-\lambda_d)}{1-\lambda_d^{K-1}} \lambda_d^{i-2}, \quad i = 2, 3, \ldots, K. \tag{7.23}$$

By applying the total probability theorem, the PDF of the channel power gain of the second selected user is obtained as

$$p_{\|\mathbf{h}_{\pi(2)}\|^2}(x|\mathcal{U} \neq \emptyset) = \sum_{i=2}^{K} \Pr\left[\pi(2) = (i) | \mathcal{U} \neq \emptyset\right] \cdot p_{\|\mathbf{h}_{(i)}\|^2}(x), \tag{7.24}$$

where $p_{\|\mathbf{h}_{(i)}\|^2}(\cdot)$ is the PDF of the ith largest channel power gain among K users, given by [27]

$$p_{\|\mathbf{h}_{(i)}\|^2}(x) = K \binom{K-1}{i-1} p_{\|\mathbf{h}\|^2}(x) \left(1 - F_{\|\mathbf{h}\|^2}(x)\right)^{i-1} F_{\|\mathbf{h}\|^2}^{K-i}(x). \tag{7.25}$$

After proper substitution and some mathematical manipulations, (7.24) can be rewritten as

$$p_{\|\mathbf{h}_{\pi(2)}\|^2}(x|\mathcal{U} \neq \emptyset) = \frac{K(1-\lambda_d)}{\lambda_d(1-\lambda_d^{K-1})} p_{\|\mathbf{h}\|^2}(x) \Big(\left(\lambda_d + (1-\lambda_d) F_{\|\mathbf{h}\|^2}(x)\right)^{K-1} - F_{\|\mathbf{h}\|^2}^{K-1}(x) \Big). \tag{7.26}$$

As the second user is always selected from set $\mathcal{U}$, the projection power loss factor, $|\sin(\theta_\pi)|^2$, follows a uniform distribution over the interval $[\lambda_d, 1]$. Therefore, the ergodic sum rate for the GWC-ZFBF scheme conditioned on $\mathcal{U} \neq \emptyset$ can be calculated, by averaging (7.16) over the distribution of $\|\mathbf{h}_{\pi(i)}\|^2$, $i = 1, 2$ and $|\sin(\theta_\pi)|^2$ as

$$\mathbf{E}[R|\mathcal{U} \neq \emptyset] = \sum_{i=1}^{2} \int_0^\infty \int_{\lambda_d}^1 \log(1 + \frac{\rho}{2} xy) \cdot p_{|\sin(\theta_\pi)|^2}(y|\mathcal{U} \neq \emptyset) \mathrm{d}y p_{\|\mathbf{h}_{\pi(i)}\|^2}(x|\mathcal{U} \neq \emptyset) \mathrm{d}x, \tag{7.27}$$

which can be further simplified to

$$\mathbf{E}[R|\mathcal{U} \neq \emptyset] = \sum_{i=1}^{2} \int_0^\infty \frac{g(x)}{1-\lambda_d} p_{\|\mathbf{h}_{\pi(i)}\|^2}(x|\mathcal{U} \neq \emptyset) \mathrm{d}x, \tag{7.28}$$

where

$$g(x) = \frac{2}{\rho x} [(1 + \frac{\rho x}{2}) \log(1 + \frac{\rho x}{2}) - (1 + \frac{\lambda_d \rho x}{2}) \log(1 + \frac{\lambda_d \rho x}{2})] - \frac{1}{\ln(2)}, \tag{7.29}$$

and $p_{\|\mathbf{h}_{\pi(i)}\|^2}(\cdot)$ for $i = 1$ and 2 are given in (7.19) and (7.26), respectively.

Finally, the final expression of sum-rate capacity of the multiuser MIMO system with GWC-ZEBF strategy can be obtained by substituting (7.20), (7.21),

and (7.28) into (7.22) as

$$\mathbf{E}[R] = \lambda_d^{K-1} \int_0^\infty \log(1+\frac{\rho}{2}x) p_{\|\mathbf{h}_{\pi(1)}\|^2}(x)\mathrm{d}x + \frac{1-\lambda_d^{K-1}}{1-\lambda_d} \sum_{i=1}^{2} \int_0^\infty g(x) p_{\|\mathbf{h}_{\pi(i)}\|^2}(x|\mathcal{U}\neq\emptyset)\mathrm{d}x. \tag{7.30}$$

SUP-ZFBF specific analysis

With SUP-ZFBF, the second selected user is the user in $\mathcal{U}$ that has the largest projection power onto the complementary space of the first selected user's channel vector. From (7.15), the second selected user's projection power is also its effective power gain. As such, the ergodic capacity of the second selected user can be obtained using the PDF of the largest projection power among all users in $\mathcal{U}$.

We first need to find the PDF of the channel power gain for a user in $\mathcal{U}$, which is denoted as $\|\tilde{\mathbf{h}}\|^2$. Noting that users in $\mathcal{U}$ cannot have the largest channel power gain, the PDF of $\|\tilde{\mathbf{h}}\|^2$ can be obtained as

$$\begin{aligned} p_{\|\tilde{\mathbf{h}}\|^2}(x) &= \frac{1}{K-1}\sum_{i=2}^{K} f_{\|\mathbf{h}_{(i)}\|^2}(x) \\ &= \frac{K}{K-1} p_{\|\mathbf{h}\|^2}(x)(1-F_{\|\mathbf{h}\|^2}^{K-1}(x)), \end{aligned} \tag{7.31}$$

where $p_{\|\mathbf{h}_{(i)}\|^2}(x)$ is the PDF of the ith largest channel power gain. Letting $\|\tilde{\mathbf{h}}_p\|^2$ represent the projection power of a user in $\mathcal{U}$, we have $\|\tilde{\mathbf{h}}_p\|^2 = \|\tilde{\mathbf{h}}\|^2 |\sin(\tilde{\theta})|^2$, where $\tilde{\theta}$ is the angle between channel vectors of that user and the first selected user. Since $|\sin(\tilde{\theta})|^2$ follows the uniform distribution over the interval $[\lambda_d, 1]$, the CDF of $\|\tilde{\mathbf{h}}_p\|^2$ can be obtained as

$$F_{\|\tilde{\mathbf{h}}_p\|^2}(z) = \Pr[\|\tilde{\mathbf{h}}\|^2 |\sin(\tilde{\theta})|^2 < z] = \frac{1}{1-\lambda_d}\int_{\lambda_d}^{1}\int_0^{\frac{z}{y}} p_{\|\tilde{\mathbf{h}}\|^2}(x)\mathrm{d}x\mathrm{d}y. \tag{7.32}$$

After taking the derivative with respect to z, the corresponding PDF is given by

$$p_{\|\tilde{\mathbf{h}}_p\|^2}(z) = \frac{1}{1-\lambda_d}\int_{\lambda_d}^{1}\frac{1}{y} p_{\|\tilde{\mathbf{h}}\|^2}(\frac{z}{y})\mathrm{d}y. \tag{7.33}$$

Denote the cardinality of the set $\mathcal{U}$, i.e. the number of users in $\mathcal{U}$, as $|\mathcal{U}|$. As the channel directions of users are independent, the distribution of $|\mathcal{U}|$ conditioned on $\mathcal{U}\neq\emptyset$ can be shown to be given by

$$\Pr[|\mathcal{U}| = k | \mathcal{U}\neq\emptyset] = \frac{1}{1-\lambda_d^{K-1}}\binom{K-1}{k}(1-\lambda_d)^k \lambda_d^{K-1-k}, \quad k = 1, \cdots, K-1. \tag{7.34}$$

When $|\mathcal{U}| = k$, the effective channel gain of the second selected user, $\gamma_{\pi(2)}$, is equal to the largest projection power among k users and its PDF is thus given

by

$$p_{\gamma_{\pi(2)}}(g\big||\mathcal{U}|=k)=kp_{\|\tilde{\mathbf{h}}_p\|^2}(g)F^{k-1}_{\|\tilde{\mathbf{h}}_p\|^2}(g). \tag{7.35}$$

Combining (7.34) and (7.35) and averaging over $|\mathcal{U}|$, the PDF of $\gamma_{\pi(2)}$ given that $\mathcal{U}\neq\emptyset$ can be obtained as

$$\begin{aligned} p_{\gamma_{\pi(2)}}(g|\mathcal{U}\neq\emptyset)&=\sum_{k=1}^{K-1}\Pr(|U|=k|\mathcal{U}\neq\emptyset)p_{\gamma_{\pi(2)}}(g||U|=k) \\ &=\frac{(K-1)(1-\lambda_d)\lambda_d^{K-2}}{1-\lambda_d^{K-1}}f_{\|\tilde{\mathbf{h}}_p\|^2}(g)\big(1+\frac{1-\lambda_d}{\lambda_d}F_{\|\tilde{\mathbf{h}}_p\|^2}(g)\big)^{K-2}. \end{aligned} \tag{7.36}$$

To derive the distribution of $|\sin(\theta_\pi)|^2$, we start with the joint PDF of a remaining user's channel power, $\|\tilde{\mathbf{h}}\|^2$, and its projection power loss factor, $|\sin(\tilde{\theta})|^2$,

$$p_{\|\tilde{\mathbf{h}}\|^2,|\sin(\tilde{\theta})|^2}(x,y)=\frac{1}{1-\lambda_d}p_{\|\tilde{\mathbf{h}}\|^2}(x),\quad x\geq 0,\lambda_d\leq y\leq 1. \tag{7.37}$$

With a change of variables, the joint PDF of projection power $\|\tilde{\mathbf{h}}_p\|^2$ and $|\sin(\tilde{\theta})|^2$ of a remaining user is obtained from (7.37) as

$$p_{\|\tilde{\mathbf{h}}_p\|^2,|\sin(\tilde{\theta})|^2}(z,y)=\frac{1}{(1-\lambda_d)y}p_{\|\tilde{\mathbf{h}}\|^2}(\frac{z}{y}),\ z\geq 0,\lambda_d\leq y\leq 1. \tag{7.38}$$

It follows that the conditional PDF of $|\sin(\tilde{\theta})|^2$ given that $\|\tilde{\mathbf{h}}_p\|^2=z$ is given by

$$p_{|\sin(\tilde{\theta})|^2}(y\big|\|\tilde{\mathbf{h}}_p\|^2=z)=\frac{1}{(1-\lambda_d)y}p_{\|\tilde{\mathbf{h}}\|^2}(\frac{z}{y})\big/p_{\|\tilde{\mathbf{h}}_p\|^2}(z),z\geq 0,\lambda_d\leq y\leq 1. \tag{7.39}$$

Since the projection power of the second selected user is given by (7.36), we can obtain the PDF of $|\sin(\theta_\pi)|^2$ conditioned on $\mathcal{U}\neq\emptyset$ by averaging (7.39) over (7.36) as

$$\begin{aligned} p_{|\sin(\theta_\pi)|^2}(y|\mathcal{U}\neq\emptyset)&=\int_0^\infty p_{|\sin(\tilde{\theta})|^2}(y\big|\|\tilde{\mathbf{h}}_p\|^2=z)p_{\gamma_{\pi(2)}}(z|\mathcal{U}\neq\emptyset)dz \\ &=\frac{(K-1)\lambda_d^{K-2}}{(1-\lambda_d^{K-1})y}\int_0^\infty p_{\|\tilde{\mathbf{h}}\|^2}(\frac{z}{y})\big(1+\frac{1-\lambda_d}{\lambda_d}F_{\|\tilde{\mathbf{h}}_p\|^2}(z)\big)^{K-2}\mathrm{d}z,\lambda_d\leq y\leq 1. \end{aligned} \tag{7.40}$$

Finally, $\mathbf{E}[R|\mathcal{U}\neq\emptyset]$ for the SUP-ZFBF scheme as

$$\begin{aligned} \mathbf{E}[R|\mathcal{U}\neq\emptyset]&=\int_0^\infty\log(1+\frac{\rho}{2}g)f_{\gamma_{\pi(2)}}(g|\mathcal{U}\neq\emptyset)\mathrm{d}g+ \\ &\int_0^\infty\int_{\lambda_d}^1\log(1+\frac{\rho}{2}xy)p_{\|\mathbf{h}_{\pi(1)}\|^2}(x)p_{|\sin(\theta_\pi)|^2}(y|\mathcal{U}\neq\emptyset)\mathrm{d}y\mathrm{d}x \end{aligned} \tag{7.41}$$

Consequently, the expression of ergodic sum rate of the multiuser MIMO system with SUP-ZEBF strategy can be obtained by substituting (7.20), (7.21) and (7.41) into (7.22).

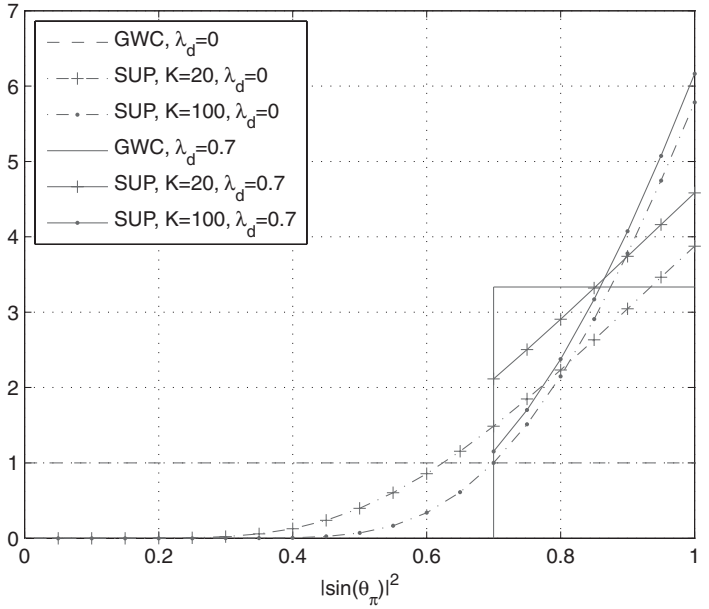

Figure 7.3 The probability density function of $|\sin(\theta_\pi)|^2$ for GWC-ZFBF and SUP-ZFBF ($\rho = 10$ dB) [48]. © 2009 IEEE.

7.3.4 Numerical examples

Figure 7.3 illustrates the PDF of projection power loss factor $|\sin(\theta_\pi)|^2$ for both GWC-ZFBF and SUP-ZFBF schemes with different λ_d and/or K values. As we can see, $|\sin(\theta_\pi)|^2$ with the GWC-ZFBF scheme always follows a uniform distribution over the interval $[\lambda_d, 1]$. On the other hand, $|\sin(\theta_\pi)|^2$ with the SUP-ZFBF scheme is not uniformly distributed. This is because its user selection is based on projection power, which is correlated to channel direction. We can also observe from Fig. 7.3 that the PDF of $|\sin(\theta_\pi)|^2$ with SUP-ZFBF is a monotonically increasing function and the mass of the PDF shifts to the right as K increases. We can conclude that SUP-ZFBF can explore more multiuser directional diversity gain than GWC-ZFBF by selecting "more orthogonal" users.

In Fig. 7.4, we plot the ergodic sum rate of both GWC-ZFBF and SUP-ZFBF schemes as a function of channel direction constraint λ_d. As we can see, while the ergodic sum rate with GWC-ZFBF is a unimodal function of λ_d, that of SUP-ZFBF remains roughly constant for the small to medium values of λ_d and decreases when λ_d becomes very close to 1. Note that when λ_d is small, the GWC-ZFBF may select fewer orthogonal users, which incurs larger projection power loss, whereas the SUP-ZFBF scheme tends to select "more orthogonal" users. On the other hand, when λ_d is very large, the number of candidate users for selection decreases, which leads to sum-rate performance degradation for both schemes. With the analytical sum-rate expression derived in this chapter,

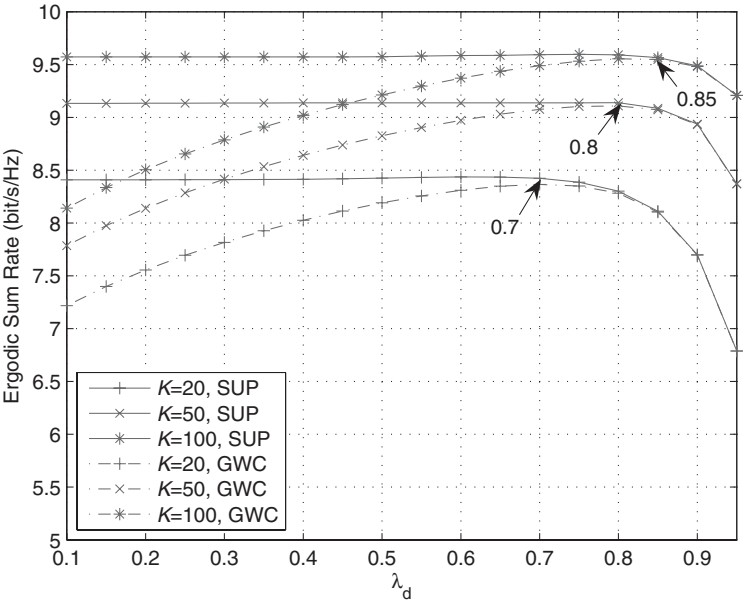

Figure 7.4 Effects of λ_d on the ergodic sum rate of GWC-ZFBF and SUP-ZFBF ($\rho = 10$ dB) [48]. © 2009 IEEE.

we can easily find the optimal value of λ_d by using one-dimensional optimization algorithms. We can also observe that the optimal value of λ_d increases with the number of users K, which indicates that when more users are in the system we should trade channel power diversity for directional diversity gain.

As an additional example, Fig. 7.5 plots the ergodic sum rate with both GWC-ZFBF and SUP-ZFBF schemes as a function of the number of users K. The sum-rate performance of the more complex scheme proposed in [26], dubbed the D-S scheme, is also plotted for comparison purposes. As shown in this figure, the performance of the GWC-ZFBF scheme with optimal λ_d values for different K approaches that of SUP-ZFBF, especially for a larger value of K. In addition, the performance gap between SUP-ZFBF and the D-S scheme is very small if λ_d for SUP-ZFBF is properly chosen. Note that both GWC-ZFBF and SUP-ZFBF enjoy much lower computational complexity than the D-S scheme.

7.4 RUB-based system with user selection

RUB is a low-complexity solution for exploring spatial multiplexing gain over multiuser MIMO broadcast channels [18–22]. With RUB, the base station generates M random orthogonal beams to communicate with as many as M selected users simultaneously. To explore multiuser diversity gain, each user will feed

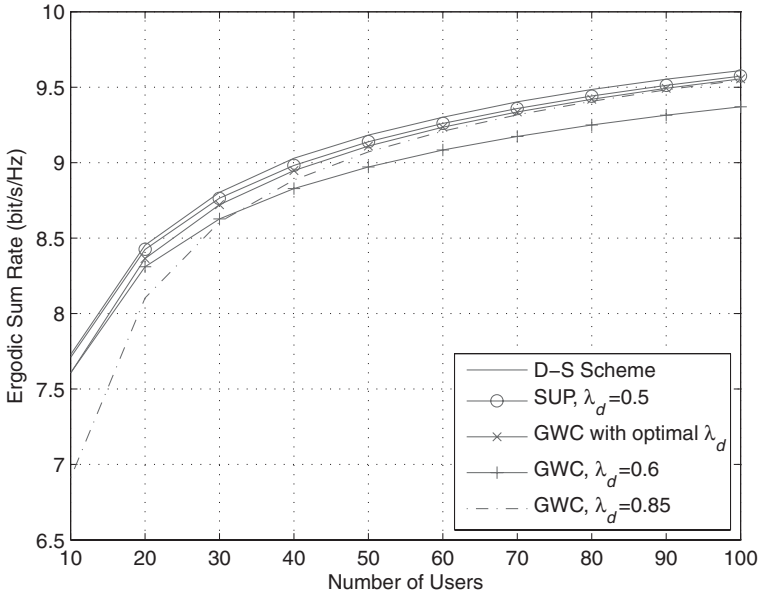

Figure 7.5 Ergodic sum rate of GWC-ZFBF and SUP-ZFBF schemes as the function of the number of users ($\rho = 10$ dB) [48]. © 2009 IEEE.

back some quality information, usually in terms of SINR, of each beam, based on which the base station carries out proper user selection. The major complexity saving of RUB over the ZFBF system is the lower feedback load, as users will no longer need to feed back their channel vectors. It has been proven in [20] that if each user just feeds back its maximum beam SINR and the index of the corresponding beam, RUB can achieve the same sum-rate scaling law as that of the DPC-based scheme (i.e. $M \log \log K$) when K approaches infinity. Note that the resulting feedback load is only a real number and an integer per user.

We attack the exact sum-rate analysis of RUB schemes over MIMO broadcast channels with an arbitrary number of users. We focus on the RUB schemes with low feedback load. In particular, we investigate the best beam SINR and index (BBSI)-based RUB scheme [20] and the best index (BBI)-based RUB [28,29], in which each user only feeds back the index of its best beam. The major difficulty in the sum-rate analysis for these schemes resides in the determination of the statistics of ordered beam SINRs for a particular user. Note that while the beam SINRs of different users can be assumed to be independent random variables [20], those corresponding to the same users are correlated to each other as they involve the same channel vector. As such, the SINR of the best beam of a user is the largest one among some correlated random variables. With the help of the order statistics results discussed in a previous chapter [30], we derive the accurate statistical characterization of ordered-beam SINRs for a user, in terms of the PDF

and the CDF, which are then applied to obtain the exact analytical expressions of the ergodic sum rate of different RUB schemes. These accurate analytical results greatly facilitate the investigation of the trade-off analysis on different RUB schemes in a practical scenario where the number of users is finite.

7.4.1 User selection strategies

We consider the downlink transmission of a single-cell wireless system. The M-antenna base station employs M random orthonormal beams, generated from an isotropic distribution [18], to serve M selected users simultaneously over the same frequency channel. Let $\mathcal{U} = \{\mathbf{u}_1, \mathbf{u}_2, \cdots, \mathbf{u}_M\}$ denote the set of beamforming vectors, assumed to be known to both the base station and the mobile users. The transmitted signal vector from M antennae over one symbol period can be written as

$$\mathbf{x} = \sum_{m=1}^{M} \mathbf{u}_m s_m, \tag{7.42}$$

where s_m is the information symbol, targeted to the mth selected user.

We assume that there are a total of K active users in the cell, where $K \geq M$. Each user is equipped with a single antenna. We further assume that with a certain slow power control mechanism, the users experience homogeneous Rayleigh fading. In particular, the channel gain from the ith antenna to the kth mobile users, denoted by h_{ik}, is assumed to be an independent zero-mean complex Gaussian random variable with unitary variance, i.e. $h_{ik} \sim \mathcal{C}N(0,1)$. Consequently, the SINR of user i while using the jth beam is given by

$$\gamma_{i,j} = \frac{\frac{P}{M}|\mathbf{h}_i^T \mathbf{u}_j|^2}{\frac{P}{M}\sum_{m=1,m\neq j}^{M}|\mathbf{h}_i^T \mathbf{u}_m|^2 + 1}, \; j = 1, 2, \cdots, M. \tag{7.43}$$

We assume that the users can accurately estimate their own channel vector and determine the instantaneous SINR corresponding to different beams using Eq. (7.43) with the knowledge of beamforming vector set $\mathcal{U}$.

Best-beam SINR and index strategy

With the BBSI strategy, each active user in the system feeds back its best beam index and the corresponding SINR value to the base station. For example, if the mth beam leads to the largest SINR for the kth user, i.e. $\gamma_{k,m} = \gamma_k^*$, then the kth user will feedback the beam index m and the corresponding SINR value $\gamma_{k,m}$. Note that with the BBSI strategy, each user needs to feed back a real number for the SINR value and a finite integer for the index of the best beam.

Based on the feedback information, the base station assigns a beam to the user with the largest SINR value among all users who feed back the index of that beam. Specifically, the base station ranks all K feedback best beam SINRs. If $\gamma_{k,m}$ is the largest among all K SINRs, then the base station selects the kth user for the mth beam. After that, the base station will rank the feedback SINRs

for the remaining beams. If now $\gamma_{n,l}$ is the largest, where $l \neq m$ and $n \neq k$, then the base station assigns the lth beam to the nth user. This process is continued until either all beams have been assigned to selected users or there are some unrequested beams remaining. In the latter case, the base station will randomly select users for the remaining beams.

Quantized best-beam SINR and index strategy
In practical systems, only a quantized value of the best beam SINR can be fed back, which leads to the quantized best beam SINR and index (QBBSI) strategy. Similar to the BBSI strategy, the users with the QBBSI strategy will first calculate the instantaneous SINRs for all M beams using its channel vector and determine the largest one after some comparison. Then, the users feed back the quantized SINR value of their best beam in the following fashion. In particular, the value range of SINR is divided into N intervals, with boundary values given as $0 = \alpha_0 < \alpha_1 < \alpha_2 < \cdots < \alpha_N = \infty$. If the SINR value of the best beam for the kth user, $\gamma_{k,1:M}$, is in the ith interval, $i = 1, 2, \cdots N$, i.e. $\alpha_{i-1} < \gamma_{k,1:M} < \alpha_i$, then the kth user will feedback the index of that interval, i, together with the index of its best beam. The base station allocates the beams to selected users based on the feedback information. Specifically, a beam will be assigned to a user who has the largest quantized SINR value, i.e. who feeds back the largest SINR interval index, among all the users requesting that beam. Note that a tie may exist in this case, which will be resolved using random selection. For those beams that no user requests for, the base station will assign them to randomly selected users. Based on the model of operation of QBBSI strategy, the amount of feedback per user is equal to $\log_2 MN$ bits.

Best-beam index strategy
With the best beam index (BBI) strategy, each user only feeds back the index of its best beam. After receiving the best beam information of all users, the base station allocates a beam to a randomly selected user among all users requesting that beam, i.e. all users who feed back the corresponding beam index. When no user requests one or several beams, the base station will assign that beam to a randomly selected user. Note that with the BBI strategy, each user only needs to feedback $\log_2(M)$ bits of information.

7.4.2 Asymptotic analysis for BBSI strategy

In this subsection, we investigate the asymptotic behavior of the beam SINR when the number of users in the system K approaches infinity. In particular, as K is large, we can ignore the cases that a user is the best user on two different beams and that a beam is not requested by any users. As a result, the SINR of a beam will be the largest of all user SINRs on that beam. Mathematically, we have $\gamma_j^B \cong \max\{\gamma_{1,j}, \gamma_{2,j}, \cdots, \gamma_{K,j}\} \doteq \gamma_{1:K,j}$. To investigate the asymptotic behavior of beam SINR $\gamma_{1:K,j}$, we first obtain the statistics of an unordered beam SINR

of a user $\gamma_{i,j}$, as defined in (7.43). We first rewrite $\gamma_{i,j}$ as

$$\gamma_{i,j} = \frac{|\mathbf{h}_i^T \mathbf{u}_j|^2}{\sum_{m=1,m\neq j}^{M} |\mathbf{h}_i^T \mathbf{u}_m|^2 + \rho}, \tag{7.44}$$

where $\rho = M/P$. Since $\mathbf{u}_j$s are orthonormal beamforming vectors, it can be shown that $|\mathbf{h}_i^T \mathbf{u}_j|^2$, $j = 1, 2, \cdots, M$, are i.i.d. Chi-square random variables with two degrees of freedom. It follows that the summation term in the denominator follows a chi-square distribution with $2M - 2$ degrees of freedom and is independent of the numerator. As such, the PDF of unordered SINR can be written as

$$p_{\gamma_{i,j}}(x) = \frac{e^{-\rho x}}{(1+x)^M} \left(\rho(1+x) + M - 1\right). \tag{7.45}$$

The CDF can be obtained after carrying out integration as

$$F_{\gamma_{i,j}}(x) = 1 - \frac{e^{-\rho x}}{(1+x)^{M-1}}. \tag{7.46}$$

Since the user channels are assumed to be independent, $\gamma_{i,j}$, $i = 1, 2, \cdots, K$ are i.i.d. random variables. As such, the CDF of their maximum $\max\{\gamma_{1,j}, \gamma_{2,j}, \cdots, \gamma_{K,j}\}$ is simply $(F_{\gamma_{i,j}}(x))^M$, which can be applied to calculate the approximate sum-rate performance of the BBSI strategy.

To obtain some insights into the nature of the sum-rate behavior as K approaches infinity, we examine the limiting distribution of $\gamma_{1:K,j}$ in what follows. It can be shown that

$$\begin{aligned} \lim_{x\to\infty} \frac{1 - F_{\gamma_{i,j}}(x)}{p_{\gamma_{i,j}}(x)} &= \lim_{x\to\infty} \left(\frac{1}{\rho} - \frac{(M-1)/\rho}{\rho(1+x) + M - 1} \right) \\ &= \frac{1}{\rho}. \end{aligned} \tag{7.47}$$

Therefore, the limiting distribution of $\gamma_{1:K,j}$ is of the Gumbel type. Solving the equation $1 - F_{\gamma_{i,j}}(b_K) = 1/K$ for b_K, we can show that b_K is approximately given by [20]

$$b_K = \frac{1}{\rho} \log K - \frac{M-1}{\rho} \log\log K. \tag{7.48}$$

The limiting CDF of $\gamma_{1:K,j}$ as K approaches infinity is then given by

$$\lim_{K\to+\infty} F_{\gamma_{1:K} - b_K}(x) = \exp\left(-e^{-x/a_K}\right). \tag{7.49}$$

We can conclude that $\gamma_{1:K,j}$ behaves like $\frac{1}{\rho}\log K$ when K approaches infinity.

7.4.3 Statistics of ordered-beam SINRs

We now derive the statistics of the ordered-beam SINRs for user i. Note that the beam SINRs for the same user, i.e. $\gamma_{i,j}$ in (7.43) with the same i but different j, are correlated random variables as they involve the same channel vector $\mathbf{h}_i$.

For notational conciseness, we use α_j to denote the norm square of the projection of user i's channel vector onto the jth beam direction, i.e. $\alpha_j = |\mathbf{h}_i^T \mathbf{u}_j|^2$, $j = 1, 2, \cdots, M$. The M beam SINRs for user i can be rewritten as

$$\gamma_{i,j} = \frac{\alpha_j}{\sum_{m=1, m\neq j}^{M} \alpha_m + \rho}, \ j = 1, 2, \cdots, M. \tag{7.50}$$

We are interested in the statistics of the ordered version of these M correlated random variables, i.e. $\gamma_{i,1:M} \geq \gamma_{i,2:M} \geq \cdots \geq \gamma_{i,M:M}$. We first note that all M beam SINRs for the ith user are calculated using the same set of projection powers $\{\alpha_j\}_{j=1}^{M}$ and, as such, they are correlated random variables. On the other hand, we also note from (7.50) that the interference terms for signal on a particular beam are always the project power of the channel vector on to the remaining $M-1$ beams. Therefore, we conclude that $\gamma_{i,j}$ is the largest beam SINR for user i if and only if α_j is the largest one among M projection norm squares for this user, i.e. $\alpha_j = \alpha_{1:M}$. Based on this observation, the largest SINR of user i, denoted by γ_i^*, can be written in terms of the ordered norm squares $\{\alpha_{m:M}\}_{m=1}^{M}$ as

$$\gamma_i^* = \frac{\alpha_{1:M}}{z_1 + \rho}, \tag{7.51}$$

where z_1 is the sum of the remaining $M-1$ norm squares, i.e. $z_1 = \sum_{m=1}^{M} \alpha_m - \alpha_{1:M}$. Consequently, the CDF of $\gamma_{i,1:M}$ can be calculated in terms of the joint PDF of $\alpha_{1:M}$ and z_1, denoted by $f_{\alpha_{1:M}, z_1}(y, z)$, as

$$F_{\gamma_{i,1:M}}(x) = \int_0^{\infty} \int_0^{x(\rho+z)} p_{\alpha_{1:M}, z_1}(y, z) \mathrm{d}y \mathrm{d}z. \tag{7.52}$$

It follows that the PDF of γ_i^* can be calculated using the joint PDF of $\alpha_{1:M}$ and z_1 as

$$p_{\gamma_i^*}(x) = \int_0^{\infty} (z+\rho) \cdot p_{\alpha_{1:M}, z_1}((z+\rho)x, z) \mathrm{d}z, \tag{7.53}$$

From (7.50), we can also conclude that $\gamma_{i,j}$ is the lth largest SINR for user i if and only if α_j is the lth largest one among all M norm squares, i.e. $\gamma_{i,l:M} = \gamma_{i,j}$ if and only if $\alpha_j = \alpha_{l:M}$. Consequently, $\gamma_{i,l:M}$ can be rewritten as

$$\gamma_{i,l:M} = \frac{\alpha_{l:M}}{(w_l + z_l) + \rho}, \tag{7.54}$$

where $w_l = \sum_{m=1}^{l-1} \alpha_{m:M}$ and $z_l = \sum_{m=l+1}^{M} \alpha_{m:M}$. It can be shown that the PDF of $\gamma_{i,l:M}$ can then be calculated in terms of the joint PDF of w_l, $\alpha_{l:M}$, and z_l, denoted by $f_{w_l, \alpha_{l:M}, z_l}(w, y, z)$, as

$$p_{\gamma_{i,l:M}}(x) = \int_0^{\infty} \int_0^{\frac{(M-l)w}{l-1}} (\rho + z + w) \cdot p_{w_l, \alpha_{l:M}, z_l}(w, x(\rho+z+w), z) \mathrm{d}z \mathrm{d}w, \tag{7.55}$$

where the integration limits is set using the fact $w/(l-1) > \alpha_{l:M} > z/(M-l)$.

The PDFs $f_{\alpha_{1:M}, z_1}(\cdot, \cdot)$ and $f_{w_l, \alpha_{l:M}, z_l}(\cdot, \cdot, \cdot)$ are joint PDFs of partial sums of ordered random variables, the general expressions of which have been obtained

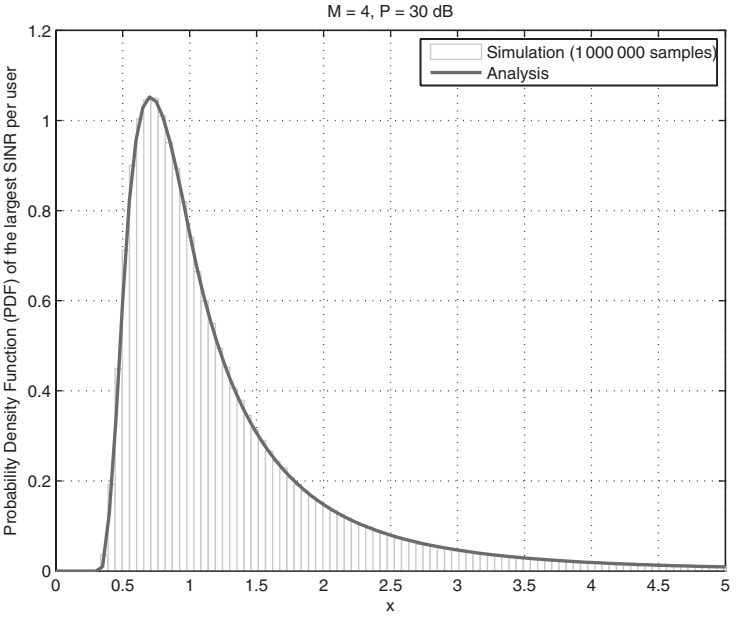

Figure 7.6 Simulation verification of the PDF expression given in (7.118). © 2008 IEEE.

in a previous chapter. As such, the statistical results of ordered SINR are quite general and independent of the distribution α_j. For the specific Rayleigh channel model under consideration, it can be shown, after proper substitution and carrying out integration, that we can obtain the following closed-form expression for the PDF of the largest beam SINR of a user as

$$p_{\gamma_i^*}(x) = \sum_{j=0}^{M-1} \frac{(-1)^j M!}{(M-j-1)!j!} \exp\left(-\frac{(1+j)\rho x}{jx-1}\right) \frac{(M+\rho-1+(\rho-jM+j)x)(1-jx)^{M-3}}{(1+x)^M}. \tag{7.56}$$

Figure 7.6 plots the PDF of the largest SINR for a particular user as given in (7.56) with $M = 4$ and $P = 30$ dB in comparison with the simulation results. As we can see, the analytical result matches the simulation result perfectly.

7.4.4 Sum-rate analysis

BBSI strategy

Based on the mode of operation of the BBSI strategy with ordered beam assignment, we can see that the SINR of the first beam is always the largest of all K best-beam SINRs, i.e. $\gamma_1^B = \gamma_{1:K}^*$, where $\gamma_{i:K}^*$ denotes the ith largest best-beam

SINRs among all K ones. Noting that the largest SINRs of different users are independent, the PDF of γ_1^B can be obtained easily as

$$p_{\gamma_1^B}(x) = KF_{\gamma_i^*}(x)^{K-1} p_{\gamma_i^*}(x), \tag{7.57}$$

where $F_{\gamma_i^*}(\cdot)$ and $p_{\gamma_i^*}(\cdot)$ are the CDF and PDF of the best beam SINR for a particular user, given in (7.52) and (7.53), respectively.

We now consider the SINR of the second beam. Based on the mode of operation of the BBSI strategy, the SINR of the second beam may be the ith largest one among all K best-beam SINRs, $i = 2, 3, \cdots, K$, if the previous $i-2$ largest ones are for the first beam. In particular, if, for example, the second and third largest best-beam SINRs are also for the first beam, then the SINR of the second beam will be equal to the fourth largest best-beam SINR. Since the user SINRs for different beams are i.i.d., each beam has the same probability to lead to the largest SINR for a particular user. It can be shown that the probability that the second beam is assigned to a user with the ith largest best-beam SINR among all K ones, i.e. $\gamma_2^B = \gamma_{i:K}^*, i = 2, 3, \cdots, K$, is given by

$$P_i^2 = \left(\frac{1}{M}\right)^{i-2} \left(1 - \frac{1}{M}\right), \tag{7.58}$$

where $1/M$ gives the probability that the best SINR of a user is for a particular beam. In the worst case, where all users request the same beam, the SINR of the second beam is equal to the SINR of a randomly chosen user.[1] Note that the SINR of a randomly assigned beam has the same probability to be the jth largest one, $j = 2, 3, \cdots, M$, among M beam SINRs. Correspondingly, the PDF of the SINR of a randomly assigned beam can be obtained as

$$p_{\gamma^R}(x) = \frac{1}{M-1} \sum_{j=2}^{M} p_{\gamma_{i,j:M}}(x), \tag{7.59}$$

where $f_{\gamma_{i,j:M}}(\cdot)$ is the PDF of the jth largest beam SINR for a user, given in (7.55). The probability that the second beam is assigned to a random user is equal to $(1/M)^{K-1}$. Consequently, the PDF of the SINR for the second beam γ_2^B can be shown to be given by

$$p_{\gamma_2^B}(x) = \sum_{i=2}^{K} P_i^2 p_{\gamma_{i:K}^*}(x) + \left(\frac{1}{M}\right)^{K-1} p_{\gamma^R}(x), \tag{7.60}$$

where $f_{\gamma_{i:K}^*}(x)$ is the PDF of the ith largest best beam SINR among all K ones, given by [27]

$$\begin{aligned} p_{\gamma_{i:K}^*}(x) = {} & \frac{K!}{(K-i)!(i-1)!} F_{\gamma_i^*}(x)^{(K-i)} \\ & \times [1 - F_{\gamma_i^*}(x)]^{i-1} p_{\gamma_i^*}(x). \end{aligned} \tag{7.61}$$

[1] This approach is to maintain the validity of (7.43). Alternatively, we may turn off those beams to reduce mutual interference.

Table 7.1 Sample scenario for the event that the mth beam is assigned to the user with the ith largest best-beam SINR among all K users, i.e. $\gamma_m^B = \gamma_{i:K}^*$.

Indexes of ordered best-beam SINRs	Associated beams	No. of users
1	First beam	1
2 to n_1+1	First beam	n_1
n_1+2	Second beam	1
n_1+3 to n_1+n_2+2	First two beams	n_2
$\vdots$	$\vdots$	$\vdots$
$\sum_{k=1}^{j-1} n_k + j$	jth beam	1
$\sum_{k=1}^{j-1} n_k + j + 1$ to $\sum_{k=1}^{j-1} n_k + n_j + j$	First j beams	n_j
$\vdots$	$\vdots$	$\vdots$
$\sum_{j=1}^{m-2} n_j + m$ to $\sum_{j=1}^{m-2} n_j + n_{m-1} + m - 1$	First $m-1$ beams	n_{m-1}
$i = \sum_{j=1}^{m-1} n_j + l$	mth beam	1

Similarly, the SINR of the third beam may be the ith largest best-beam SINRs among all K ones, $i = 3, 4, \cdots, K$, if one of the previous $i-2$ largest best-beam SINR is assigned to the second beam and the remaining $i-3$ largest ones are for the first and second beams. It can be shown that the probability that the third beam is assigned to a user with the ith largest best-beam SINRs among all K users, i.e. $\gamma_3^B = \gamma_{i:K}^*, i = 3, 4, \cdots, K$, is given by

$$P_i^3 = \sum_{j=0}^{i-3} \left(\frac{1}{M}\right)^j \left(1 - \frac{1}{M}\right) \left(\frac{2}{M}\right)^{i-3-j} \left(1 - \frac{2}{M}\right), \tag{7.62}$$

where $2/M$ gives the probability that the largest SINR for a particular user is for the first and second assigned beams. Note that in the worst case where all best-beam SINRs belong to the first and second beam, whose probability is $(2/M)^{K-1}$, the SINR of the third assigned beam is equal to the SINRs of a randomly chosen user, whose PDF was given in (7.59). Consequently, the PDF of the SINR for the third beam with BBSI strategy can be shown to be given by

$$p_{\gamma_3^B}(x) = \sum_{i=3}^{K} P_i^3 p_{\gamma_{i:K}^*}(x) + \left(\frac{2}{M}\right)^{K-1} p_{\gamma^R}(x). \tag{7.63}$$

In general, the SINR of the mth beam may be the ith largest best-beam SINRs, where $i = m, m+1, \cdots, K$. More specifically, $\gamma_m^B = \gamma_{i:K}^*$ when a scenario shown in Table 7.1 occurs, where n_j denotes the number of users whose best beam is one of the first j assigned beams. After determining the probability of the scenario in Table 7.1 for a particular vector $\{n_j\}_{j=1}^{m-1}$ and summing over all possible vectors $\{n_j\}_{j=1}^{m-1}$, while noting that $\{n_j\}_{j=1}^{m-1}$ needs to satisfy $n_j \in \{0, 1, \cdots, i-m\}$ and $\sum_{j=1}^{m-1} n_j = i - m$, we obtain the probability that the mth beam is assigned to the user with the ith largest best-beam SINR, i.e. $\gamma_m^B = \gamma_{i:K}^*, i = m, m+1, \cdots, K$

as

$$P_i^m = \sum_{\substack{\sum_{j=1}^{m-1} n_j = i-m \\ n_j \in \{0,1,\cdots,i-m\}}} \left[\prod_{j=1}^{m-1} \left(\frac{j}{M}\right)^{n_j} \left(1-\frac{j}{M}\right) \right] \quad i = m, m+1, \cdots, K. \tag{7.64}$$

Consequently, after noting that it is with a probability of $\left(\frac{m-1}{M}\right)^{K-1}$ that the mth beam is assigned to a random selected user, we can obtain the PDF of the SINR on the mth beam γ_m^B as

$$p_{\gamma_m^B}(x) = \sum_{i=m}^{K} P_i^m \; p_{\gamma_{i:K}^*}(x) + \left(\frac{m-1}{M}\right)^{K-1} p_{\gamma^R}(x). \tag{7.65}$$

Note that additional SINR feedback from the randomly selected users is required to achieve the data rate. When K is not too small, the extra feedback load can be neglected since the probability of beams not being requested is small.

Finally, after applying (7.57) and (7.65) in (7.10), the exact sum-rate expression for the BBSI strategy can be calculated as

$$\begin{aligned} R = & \int_0^\infty \log_2(1+x) K F_{\gamma_i^*}(x)^{K-1} p_{\gamma_i^*}(x) \mathrm{d}x \\ & + \sum_{m=2}^{M} \left(\sum_{i=m}^{K} P_i^m \int_0^\infty \log_2(1+x) \; p_{\gamma_{i:K}^*}(x) \mathrm{d}x \right. \\ & \left. + \left(\frac{m-1}{M}\right)^{K-1} \int_0^\infty \log_2(1+x) p_{\gamma^R}(x) \mathrm{d}x \right), \end{aligned} \tag{7.66}$$

where P_i^m and $p_{\gamma_{i:K}^*}(x)$ are given in (7.64) and (7.61), respectively.

Quantized best-beam SINR and index strategy

Let us consider one of the M available beams. It can be shown that the probability that exact j users among the total K users request this particular beam is equal to

$$\Pr[N_r = j] = \frac{K!}{(K-j)!j!} \left(\frac{1}{M}\right)^j \left(\frac{M-1}{M}\right)^{K-j}, \quad j = 0, 1, \cdots, K. \tag{7.67}$$

If $N_r = 0$, then that beam will be assigned to a randomly selected user whose best beam is a different one. In this case, the PDF of the SINR of this beam is the same as that given in (7.59). If $N_r = j > 0$, then that beam will be assigned to a user for whom this beam is the best one. It can be shown that the probability that the beam is assigned to a user with a best-beam SINR in the ith interval

to be given by

$$\Pr[\gamma^B \in (\alpha_{i-1}, \alpha_i) | N_r = j > 0] = F_{\gamma_{i,1:M}}(\alpha_i)^j - F_{\gamma_{i,1:M}}(\alpha_{i-1})^j, 1 \le i \le N, \tag{7.68}$$

where $F_{\gamma_{i,1:M}}(\cdot)$ is the CDF of the SINR of the best beam of a user, as given in (7.52). The corresponding SINR PDF of the beam when it is assigned to a user with best beam SINR in the ith interval can then be obtained as

$$p_{\gamma^B|\gamma^B \in (\alpha_{i-1},\alpha_i)}(x) = \frac{1}{F_{\gamma_{i,1:M}}(\alpha_i) - F_{\gamma_{i,1:M}}(\alpha_{i-1})} p_{\gamma_{i,1:M}}(x), \alpha_{i-1} \le x \le \alpha_i. \tag{7.69}$$

After successively removing the conditionings, the SINR PDF for the beam can be obtained as

$$\begin{aligned} p_{\gamma^B}(x) &= \sum_{j=1}^{K} \frac{K!}{(K-j)!j!} \left(\frac{1}{M}\right)^j \left(\frac{M-1}{M}\right)^{K-j} \\ &\times \sum_{i=1}^{N} \frac{F_{\gamma_{i,1:M}}(\alpha_i)^j - F_{\gamma_{i,1:M}}(\alpha_{i-1})^j}{F_{\gamma_{i,1:M}}(\alpha_i) - F_{\gamma_{i,1:M}}(\alpha_{i-1})} p_{\gamma_{i,1:M}}(x) \\ &\times (\mathcal{U}(x-\alpha_{i-1}) - \mathcal{U}(x-\alpha_i)) + \left(\frac{M-1}{M}\right)^K p_{\gamma^R}(x), \end{aligned} \tag{7.70}$$

where $p_{\gamma^R}(\cdot)$ was given in (7.59).

Finally, the sum rate of a RUB-based multiuser MIMO system with QBBSI-based user selection can be calculated as

$$\begin{aligned} R^{QBBSI} &= M \int_0^\infty \log_2(1+x) p_{\gamma_m^B}(x) \mathrm{d}x \\ &= M \left(\sum_{j=1}^{K} \frac{(K)!}{(K-j)!j!} \left(\frac{1}{M}\right)^j \left(\frac{M-1}{M}\right)^{K-j} \right. \\ &\times \Big(\sum_{i=1}^{N} \frac{F_{\gamma_{i,1:M}}(\alpha_i)^j - F_{\gamma_{i,1:M}}(\alpha_{i-1})^j}{F_{\gamma_{i,1:M}}(\alpha_i) - F_{\gamma_{i,1:M}}(\alpha_{i-1})} \int_{\alpha_{i-1}}^{\alpha_i} \log_2(1+x) p_{\gamma_{i,1:M}}(x) \mathrm{d}x \\ &\left. + \left(\frac{M-1}{M}\right)^k \frac{1}{M-1} \sum_{j=2}^{M} \int_0^\infty \log_2(1+x) p_{\gamma_{i,j:M}}(x) \mathrm{d}x \right). \end{aligned} \tag{7.71}$$

BBI strategy

Based on the mode of operation of the BBI strategy, the SINR of the user assigned to the mth beam, γ_m^B in (7.10), may follow two different types of distribution. More specifically, if there is at least one user requesting the mth beam, then this beam will be the best beam of the selected user. Therefore, γ_m^B is the largest among M beam SINRs for a user, i.e. $\gamma_m^B = \gamma_i^*$, whose PDF is given in (7.53). On the other hand, when no user requests the mth beam and that beam is assigned

to a randomly chosen user, γ_m can be any one of M beam SINRs, except for the largest one, for the selected user. Therefore, the PDF of γ_m^B for this case was given in (7.59), in terms of the PDF of the jth largest beam SINR for a user $f_{\gamma_{i,j:M}}(\cdot)$.

Let N_a denote the number of beams that are requested by at least one user. Clearly, N_a is a discrete random variable, taking values $1, 2, \cdots, M$. We can easily see that the probability that only one beam is active, i.e. $N_a = 1$ is equal to the probability that all k users feed back the same beam index, which can be calculated as

$$\Pr[N_a = 1] = \binom{M}{1} \left(\frac{1}{M}\right)^K. \tag{7.72}$$

The probability of exactly two beams being active can be calculated by subtracting from the probability that at most two beams are active, which is given by $\binom{M}{2}\left(\frac{2}{M}\right)^K$, the probability of only one of those two beams is active, which is equal to $\binom{M}{2}\binom{2}{1}\left(\frac{1}{M}\right)^K$. Therefore, we have

$$\Pr[N_a = 2] = \binom{M}{2}\left[\left(\frac{2}{M}\right)^K - \binom{2}{1}\left(\frac{1}{M}\right)^K\right]. \tag{7.73}$$

Similarly, the probability that exactly three beams are active can be calculated by subtracting from the probability that at most three beams are active, the probabilities that not all three beams are active. Hence, the probability of $N_a = 3$ is given by

$$\begin{aligned}\Pr[N_a = 3] = \binom{M}{3}\Bigg\{&\left(\frac{3}{M}\right)^K - \binom{3}{2} \cdot \\ &\left[\left(\frac{2}{M}\right)^K - \binom{2}{1}\left(\frac{1}{M}\right)^K\right] - \binom{3}{1}\left(\frac{1}{M}\right)^K\Bigg\}.\end{aligned} \tag{7.74}$$

In general, the probability that exact m beams out of M available beams are active given that k users feed back their best beam indexes can be recursively calculated as

$$\begin{aligned}\Pr[N_a = m] = \binom{M}{m}\Bigg\{&\left(\frac{m}{M}\right)^K \\ &- \sum_{j=1}^{m-1}\binom{m}{j}\frac{\Pr[N_a = j]}{\binom{M}{j}}\Bigg\},\ m = 1, 2, \cdots, M.\end{aligned} \tag{7.75}$$

We also can prove by induction that (7.75) can be simplified to the following compact expression

$$\Pr[N_a = m] = \frac{1}{M^K}\binom{M}{m} \cdot \sum_{q=1}^{m}(-1)^{m-q}\binom{m}{q}q^K,\ m = 1, 2, \cdots, M. \tag{7.76}$$

It is easy to verify that (7.76) holds for the $i = 1$ case. Assume that (7.76) holds for all $1 \le i \le m-1$, then we have

$$\Pr[N_a = i] = \frac{1}{M^K}\binom{M}{i}\cdot \sum_{q=1}^{i}(-1)^{i-q}\binom{i}{q}q^K,\ i = 1, 2, \cdots, m-1. \tag{7.77}$$

We now consider the case of $i = m$. From (7.75), we have

$$\Pr[N_a = m] = \binom{M}{m}\left\{\left(\frac{m}{M}\right)^k - \sum_{j=1}^{m-1}\binom{m}{j}\frac{\Pr[M_a = j|N_f = k]}{\binom{M}{j}}\right\}. \tag{7.78}$$

Substituting (7.77) into (7.78), we have

$$\begin{aligned}
&\Pr[M_a = m|N_f = k] \\
&= \frac{1}{M^k}\binom{M}{m}\left\{m^k - \sum_{j=1}^{m-1}\binom{m}{j}\sum_{q=1}^{j}(-1)^{j-q}\binom{j}{q}q^k\right\} \\
&\overset{(a)}{=} \frac{1}{M^k}\binom{M}{m}\left\{m^k - \sum_{q=1}^{m-1}\left\{\sum_{j=q}^{m-1}(-1)^j\binom{m}{j}\binom{j}{q}\right\}(-1)^q q^k\right\} \\
&\overset{(b)}{=} \frac{1}{M^k}\binom{M}{m}\left\{m^k - \sum_{q=1}^{m-1}\left\{\sum_{j=q}^{m-1}(-1)^j\binom{m-q}{j-q}\right\}(-1)^q\binom{m}{q}q^k\right\} \\
&\overset{(c)}{=} \frac{1}{M^k}\binom{M}{m}\left\{m^k - \sum_{q=1}^{m-1}\left\{\sum_{j=0}^{m-q-1}(-1)^j\binom{m-q}{j}\right\}\binom{m}{q}q^k\right\} \\
&\overset{(d)}{=} \frac{1}{M^k}\binom{M}{m}\left\{m^k + \sum_{q=1}^{m-1}(-1)^{m-q}\binom{m}{q}q^k\right\} \\
&= \frac{1}{M^k}\binom{M}{m}\left\{\sum_{q=1}^{m}(-1)^{m-q}\binom{m}{q}q^k\right\}
\end{aligned}$$

where

(a) follows by change order of summation;

(b) follows since $\binom{m}{j}\binom{j}{q} = \binom{m}{q}\binom{m-q}{j-q}$, which can be proven by direct calculation;

(c) follows by the change of variable;

(d) follows from the formula $\sum_{j=0}^{m}(-1)^j\binom{m}{j} = 0$, which results from the binomial expansion of $(1-1)^m$. Therefore, (7.76) holds in general.

Finally, the sum rate of a RUB-based multiuser MIMO system with BBI strategy can be obtained, by conditioning on the number of beams that have been

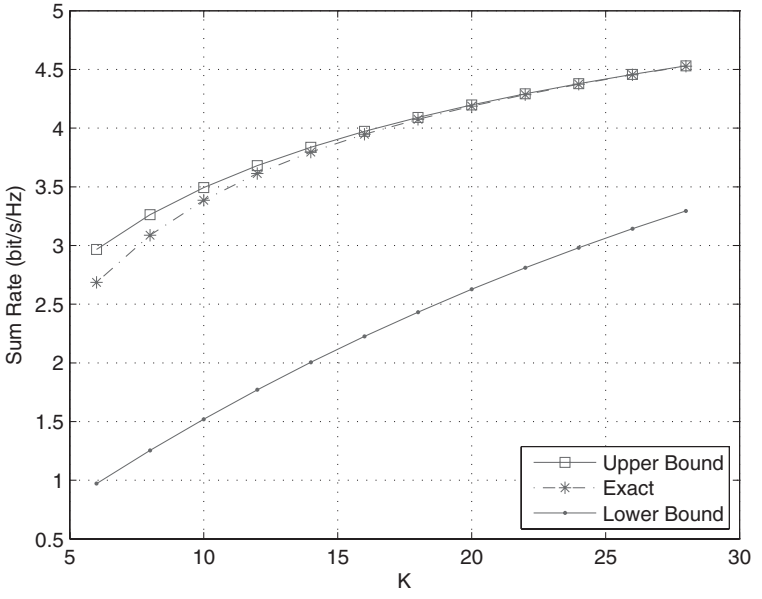

Figure 7.7 Sum-rate capacity in comparison with upper and lower bounds ($M = 4$, $P = 5$ dB).

requested by at least one user, as

$$R^{BBI} = \sum_{i=1}^{M} \Pr[N_a = i] \Big(i \int_0^{\infty} \log_2(1+x) p_{\gamma_i^*}(x) \mathrm{d}x + \frac{M-i}{M-1} \sum_{j=2}^{M} \int_0^{\infty} \log_2(1+x) p_{\gamma_{i,j:M}}(x) \mathrm{d}x \Big), \tag{7.79}$$

where $\Pr[N_a = i]$ is given in (7.76).

In Fig. 7.7, we plot the exact sum rate of the MIMO broadcast channel with BBSI-based RUB as given in (7.66) as the function of the number of users under consideration. On the same figure, we also plot the upper and lower bound derived in [20] for the asymptotic sum-rate analysis. As we can see, the upper bounds are much closer to the exact sum rate, especially when the number of users is large. We also notice that when the number of users is small, there is also a noticeable gap between the upper bound and the exact sum rate. As such, the analytical sum-rate expression provides a valuable tool to predict the system performance when the number of users in the system is limited.

In Fig. 7.8, we plot the sum-rate performance of the MIMO broadcast channel with BBSI-based RUB as given in (7.66) as a function of the average SNR for a different number of active users K and a different number of antennae (or, equivalently, the number of beams) M. First of all, we can observe a common

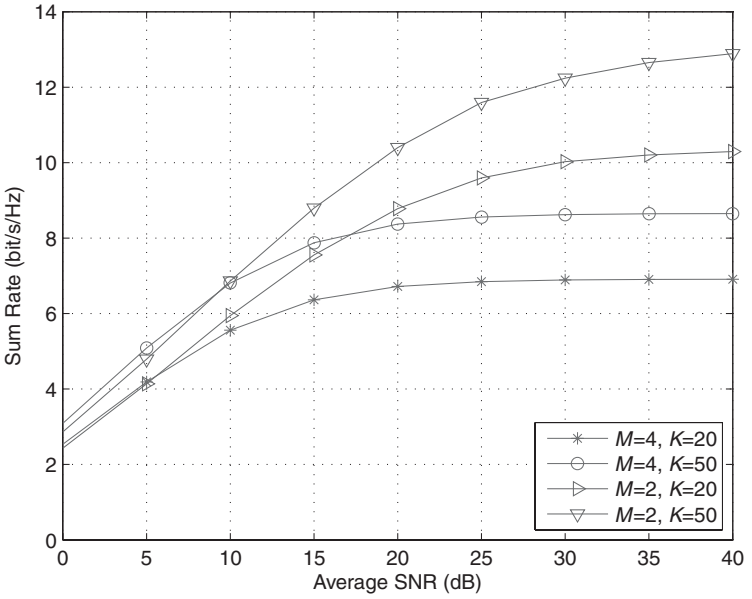

Figure 7.8 Sum-rate performance for a different number of transmit antennae and/or number of users.

trend that, when SNR increases, the sum rate of RUB systems increases over the low SNR region but saturate in the high SNR region. If we compare the curves with the same K value but different M values, we can see that while using more antennae, i.e. transmitting to more users simultaneously, helps slightly increase the total sum rate over the low SNR region, activating fewer beams leads to a much better sum-rate performance in the high SNR region. These behaviors can be explained as follows. Over the high SNR region, the multiuser interference becomes a dominant factor in terms of limiting the system sum rate. Note that a user for the $M = 2$ case will only experience a third of the amount of multiuser interference experienced by uses for the $M = 4$ cases. In addition, with the same total transmitting power constraint, the users in the $M = 2$ case enjoy twice the transmitting power as the users in the $M = 4$ cases, which contributes further to the sum-rate advantage of the $M = 2$ case over the high SNR region. On the other hand, noise is the major limiting factor over the low SNR region whereas the multiuser interference can be negligible. As such, transmitting to more users translates to approximately a linear increase in the system sum rate and can overcome the power loss due to the total power constraint.

In Fig. 7.9 we compare the sum-rate performance of different RUB schemes considered in this work for the case of four transmit antennae and a total of 20 users. The sum rate of BBSI schemes with quantized SINR feedback (QBBSI), which leads to lower feedback load, is presented. Note that if $N = 2^r$ SINR

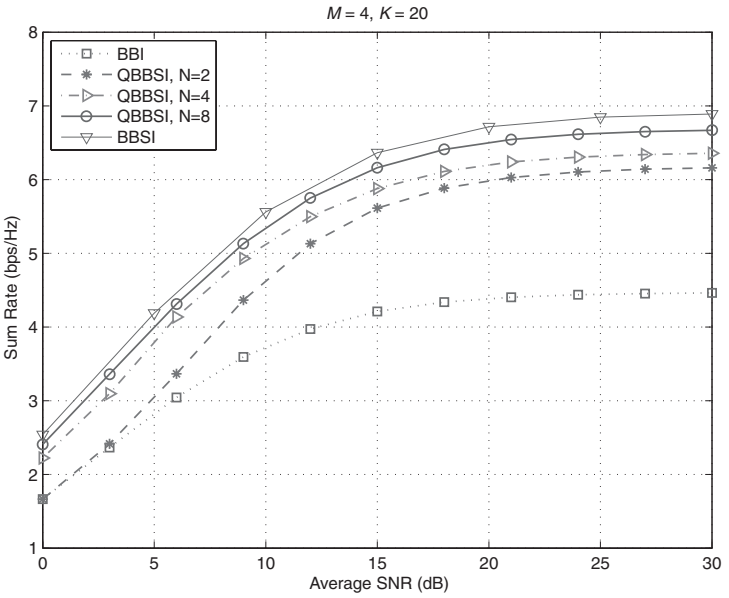

Figure 7.9 Sum-rate performance of different RUB schemes as the function of average SNR (SINR thresholds for QBBSI: 3 dB for $N = 2$; –5, 0 and 5 dB for $N = 4$; –6, –3, 0, 3, 6, 9, and 12 dB for $N = 8$).

intervals are used, then each user needs to feed back r additional bits for its best-beam SINR feedback. As we can see, the sum-rate performance of all three schemes improves as average SNR increases and saturate in the high SNR region, as expected. On the other hand, the sum rate of the BBI-based RUB scheme converges to a much smaller value than other schemes. It is worth noting that the QBBSI-based scheme offers a much larger sum-rate capacity than the BBI scheme over high SNR, even with $N = 2$ SINR intervals, i.e. one additional bit feedback for quantized best-beam SINR. We also notice that when the number of quantization levels increases, the sum rate of the QBBSI scheme improves and quickly approaches that of the BBSI scheme. Note that the sum rate of QBBSI with $N = 8$ intervals is within 0.3 bps/Hz to that of the BBSI scheme.

As a final numerical example, we plot the sum-rate of different RUB schemes as a function of the number of active users in the system in Fig. 7.10. We assume that the total transmitting power budget is fixed to 10 dB with four transmit antennae. The SINR threshold values for QBBSI schemes are arbitrarily selected to be the same as the ones used in Fig. 7.9. As we can clearly observe, while the sum-rate of BBSI and QBBSI-based RUB schemes increases as the number of active users increases, that of BBI scheme quickly saturates at a small value (≈ 3.8 bps/Hz). This is because without any knowledge of SINR values, the BBI scheme cannot fully explore the multiuser diversity gain. We also see from

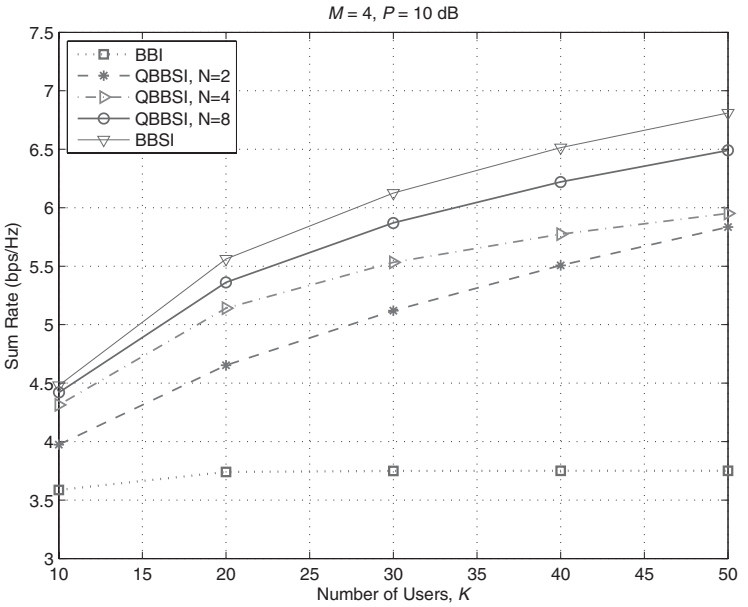

Figure 7.10 Sum-rate performance of different RUB schemes as a function of the number of active users (SINR thresholds for QBBSI: 3 dB for $N = 2$; –5, 0 and 5 dB for $N = 4$; –6, –3, 0, 3, 6, 9, and 12 dB for $N = 8$).

Fig. 7.10, the sum rate of QBBSI increases at a higher rate as K increases when the number of quantization levels becomes larger.

7.5 RUB with conditional best-beam index feedback

In this section, we present another low-feedback user scheduling strategy for a RUB-based multiuser MIMO system, termed adaptive beam activation based on conditional best-beam index feedback (ABA-CBBI) [31]. In general, feedback thresholding is a commonly adopted mechanism to reduce the feedback load in multiuser systems [21, 28, 32]. For a multiuser MIMO system, it was suggested in [21,28] to only allow those users with best-beam SINR greater than a threshold to feed back their best beam information. With the ABA-CBBI scheme, similar to the strategy proposed in [28], only those users with their largest SINR greater than a threshold will feed back their best-beam indexes. When the threshold is high and/or the number of users is moderate, it may be that a beam is not requested by any user. When this happens, previous work [21, 28] suggests randomly selecting a user for those beams. Note that this random user selection for an unrequested beam cannot guarantee high SINR for a selected user and will introduce more interuser interference. With the ABA-CBBI scheme, however,

only those beams that are requested by at least one user will be active for transmission. We study the sum-rate performance of the ABA-CBBI strategy through accurate statistical analysis. In particular, we derive the distribution of the number of active beams and the distribution of their resulting SINR, which are then applied to obtain the exact analytical expression of the overall system sum rate. We also accurately quantify the average feedback load of the ABA-CBBI scheme. Based on these analytical results, we study the effects of the feedback threshold on the sum-rate performance and its optimization. We show that the resulting ABA-CBBI scheme can effectively explore multiuser diversity gain and control interuser interference for sum-rate performance benefit.

7.5.1 Mode of operation and feedback load analysis

At the beginning of the scheduling period, each user will determine the instantaneous SINR on the available beams while assuming that all M beams will be active. Specifically, with the knowledge of beamforming vector set $\mathcal{U}$ and the estimated channel vector $\mathbf{h}_k$, the SINR of user k on the jth beam can be calculated as

$$\gamma_{k,j} = \frac{\frac{P}{M}|\mathbf{h}_k^T \mathbf{u}_j|^2}{\frac{P}{M}\sum_{m=1,m\neq j}^{M}|\mathbf{h}_k^T \mathbf{u}_m|^2 + 1},\ k = 1, 2, \cdots, K,\ j = 1, 2, \cdots, M. \quad (7.80)$$

The users will then perform some comparison to determine their best beams j^*, which achieve the maximum SINR among all beams, namely $j^* = \arg\max_j(\gamma_{k,j})$. The corresponding SINR, denoted by γ_{k,j^*}, is called the best-beam SINR of user k. Each user compares its best-beam SINR with an SINR threshold, denoted by β. Only when its best-beam SINR is greater than β will the user feed back its best-beam index, which results in a feedback of $\log_2(M)$ bits per user. After collecting the best-beam indexes fed back from qualified users, the base station will assign a beam randomly to a user requesting it. If a beam is not requested by any feedback user, the base station will simply turn off that beam and redistribute the power to other beams. In this case, the number of active beams (or selected users) M_a will be less than the number of available beams M. Since ABA-CBBI randomly assigns a beam to one of the users requesting it, this strategy has lower operational complexity than the scheme proposed in [20], which ranks the SINRs of all users requesting that beam first and then assigns it to the user achieving the maximum SINR on it.

The feedback load of the proposed ABA-CBBI strategy varies over time as the number of qualified users changes with the channel condition. We can quantify the average feedback load of this strategy as

$$F = KP_f \log_2 M, \quad (7.81)$$

where P_f is the probability that a user is qualified to feed back. Based on the mode of operation above, P_f is equal to the probability that the best-beam SINR of a user while assuming all M beams are active, γ_{k,j^*}, is greater than

the threshold β, i.e. $P_f = \Pr[\gamma_{k,j^*} < \beta]$. With the homogeneous Rayleigh fading assumption, it can be shown that γ_{k,j^*} are identically distributed with the common PDF given by

$$p_{\gamma_{j^*}^{(M)}}(x) = \frac{M}{(M-2)!}\int_0^\infty (M/P+z)e^{-x(\frac{M}{P}+z)-z}\times \sum_{j=0}^{M-1}\binom{M-1}{j}(-1)^j\big(z-jx(\frac{M}{P}+z)\big)^{M-2}\mathrm{U}\big(z-jx(\frac{M}{P}+z)\big)\mathrm{d}z, \tag{7.82}$$

where $\mathrm{U}(\cdot)$ denotes the unit step function. As such, the average feedback load with the proposed ABA-CBBI strategy is given by[2]

$$F = K\log_2 M\int_\beta^\infty p_{\gamma_{j^*}^{(M)}}(x)\mathrm{d}x. \tag{7.83}$$

Distribution of the number of active beams

A unique feature of the proposed ABA-CBBI strategy is no random user selection for unrequested beams. As a result, the number of selected users/active beams, M_a, becomes a discrete random variable taking values in $[1, 2, \cdots, M]$. Note that if every user feeds back, the probability of a beam not being requested by any user will be small and even negligible, as long as the number of users is large enough. However, with conditional feedback strategies, this probability becomes larger as the number of feedback users can be small due to the feedback thresholding. In the following, we derive the probability mass function (PMF) of M_a, which will be applied to the sum-rate analysis of the proposed scheme in the next section.

With the ABA-CBBI strategy, the number of users that are qualified to feed back, denoted by N_f, is random. The probability of $N_f = k$ is given by

$$\Pr[N_f = k] = \binom{K}{k}P_f^k(1-P_f)^{K-k},\ k = 0, 1, \cdots, K. \tag{7.84}$$

Given that k users feed back their best-beam indexes, the probability that only one beam is active, i.e. $M_a = m$, can be calculated, by following the similar derivation in a previous section, as

$$\Pr[M_a = m|N_f = k] = \binom{M}{m}\Bigg\{\Big(\frac{m}{M}\Big)^k - \sum_{j=1}^{m-1}\binom{m}{j}\frac{\Pr[M_a = j|N_f = k]}{\binom{M}{j}}\Bigg\},\ m = 1, 2, \cdots, M. \tag{7.85}$$

which can be simplified to the following compact expression

$$\Pr[M_a = m|N_f = k] = \frac{1}{M^k}\binom{M}{m}\cdot\sum_{q=1}^{m}(-1)^{m-q}\binom{m}{q}q^k,\ m = 1, 2, \cdots, M. \tag{7.86}$$

[2] This result corrects an error in [28, eq. (13)] as the SINR of a user for different beams are correlated random variables.

Finally, combining (7.84) and (7.86), the probability that exact m beams are active can be obtained by applying the total probability theorem as

$$\begin{aligned}\Pr[M_a = m] &= \sum_{k=1}^{K} \Pr[N_f = k] \Pr[M_a = m | N_f = k] \\ &= \binom{M}{m} \sum_{q=1}^{m} (-1)^{m+q} \binom{m}{q} \left[\left(1 - \frac{M-q}{M} P_f\right)^K - (1-P_f)^K \right],\end{aligned} \tag{7.87}$$

where the feedback probability P_f is given in (7.83).

7.5.2 Sum-rate analysis

In this section, we investigate the performance of the proposed ABA-CBBI strategy by analytically deriving the exact sum-rate expression for the resulting multiuser MIMO systems. Conditional on the number of active beams, the average sum rate with ABA-CBBI strategy can be calculated as

$$\mathbf{E}[R] = \sum_{m=1}^{M} \Pr[M_a = m] \mathbf{E}\left[\sum_{i=1}^{m} \log_2(1+\gamma_i) \right], \tag{7.88}$$

where $\Pr[M_a = m]$ was given in (7.87) and γ_i is the SINR of the ith selected user. Based on the mode of operation of the proposed strategy, the SINR of users on different active beams are identically distributed. As such, we can rewrite the sum rate as

$$\mathbf{E}[R] = \sum_{m=1}^{M} \Pr[M_a = m] m \int_0^{\infty} \log_2(1+x) p_{\gamma_B^{(m)}}(x) \mathrm{d}x, \tag{7.89}$$

where $f_{\gamma_B^{(m)}}(\cdot)$ denotes the common PDF of the SINR of selected users given that exactly m beams are active.

We now proceed to derive the PDF $f_{\gamma_B^{(m)}}(\cdot)$. Based on the mode of operation of the proposed ABA-CBBI strategy, $\gamma_B^{(m)}$ is also the best-beam SINR of a feedback user when m beams are active. Meanwhile, the best-beam SINR of such a user when assuming all M beams are active, $\gamma_B^{(M)}$, must be greater than the threshold β. Therefore, the SINR distribution for active beams with the ABA-CBBI strategy is the conditional distribution of $\gamma_B^{(m)}$ given $\gamma_B^{(M)} > \beta$. It follows that the cumulative distribution function (CDF) of the SINR of the selected users when m beams are active can be determined as

$$F_{\gamma_B^{(m)}}(x) = \frac{\Pr[\gamma_B^{(m)} < x, \gamma_B^{(M)} > \beta]}{\Pr[\gamma_B^{(M)} > \beta]}. \tag{7.90}$$

To proceed further, we note that a beam becomes the best beam for a particular user if and only if the user's channel vector has the largest projection norm

square ($|\mathbf{h}_k^T \mathbf{u}_j|^2$) on that beam direction. Therefore, we can rewrite $\gamma_B^{(m)}$ as

$$\gamma_B^{(m)} = \begin{cases} \frac{\alpha_{1:M}}{z_{m-1}+m/P}, & 1 < m \le M, \\ P\alpha_{1:M}, & m = 1, \end{cases} \tag{7.91}$$

where $\alpha_{1:M} = \max\{|\mathbf{h}_i^T \mathbf{u}_j|^2, j = 1, 2, \cdots, M\}$ is the largest projection norm squares onto all M possible beam directions and z_{m-1} is the sum of arbitrary $m-1$ projection norm squares out of the remaining $M-1$ ones. As such, the joint probability in (7.90) can be rewritten as

$$\begin{aligned} &\Pr[\gamma_B^{(m)} < x, \gamma_B^{(M)} > \beta] \\ &= \begin{cases} \Pr[P\alpha_{1:M} < x, \frac{\alpha_{1:M}}{z_{M-1}+M/P} > \beta], & m = 1; \\ \Pr[\frac{\alpha_{1:M}}{z_{m-1}+m/P} < x, \frac{\alpha_{1:M}}{z_{m-1}+z_{M-m}+M/P} > \beta], & 1 < m < M; \\ \Pr[\beta < \frac{\alpha_{1:M}}{z_{M-1}+M/P} < x], & m = M, \end{cases} \end{aligned} \tag{7.92}$$

where we define $z_{M-m} = z_{M-1} - z_{m-1}$ for the case of $1 < m < M$. Consequently, the joint probability of the case of $m = 1$ can be calculated using the joint PDF of $\alpha_{1:M}$ and z_{M-1} as

$$\begin{aligned} &\Pr[\gamma_B^{(m)} < x, \gamma_B^{(M)} > \beta] \\ &= \int_0^{x/P} \mathrm{d}y \int_0^{\min\{y/\beta - M/P, (M-1)y\}} \mathrm{d}u p_{\alpha_{1:M}, z_{M-1}}(y, u), \end{aligned} \tag{7.93}$$

where the joint PDF $p_{\alpha_{1:M}, z_{M-1}}(y, u)$ is given by

$$\begin{aligned} &p_{\alpha_{1:M}, z_{M-1}}(y, u) = p_{\alpha_{1:M}}(y) p_{z_{M-1}|\alpha_{1:M}=y}(u) \\ &= M e^{-y-u} \sum_{j=0}^{M-1} \binom{M-1}{j} \frac{(-1)^j (u - jy)^{M-2}}{(M-2)!} \mathrm{U}(u - jy), \\ &\quad y > 0, u < (M-1)y. \end{aligned} \tag{7.94}$$

The joint probability of the cases of $1 < m < M$ can be calculated using the joint PDF of $\alpha_{1:M}$, z_{m-1}, and z_{M-m} as

$$\begin{aligned} \Pr[\gamma_B^{(m)} < x, \gamma_B^{(M)} > \beta] = \int_0^{\infty} \mathrm{d}y \int_{y/x - m/P}^{y/\beta - M/P} \mathrm{d}u \\ \int_0^{y/\beta - u - M/P} \mathrm{d}v p_{\alpha_{1:M}, z_{m-1}, z_{M-m}}(y, u, v). \end{aligned} \tag{7.95}$$

The joint PDF of $\alpha_{1:M}$, z_{m-1} and z_{M-m} can be determined by following the Bayesian approach. It has been shown that the unordered projection norm squares $|\mathbf{h}_i^T \mathbf{u}_j|^2$, $j = 1, 2, \cdots, M$, are i.i.d. χ^2 random variables with two degrees of freedom [18]. Due to the ordering process, $\alpha_{1:M}$, z_{m-1} and z_{M-m} are correlated random variables. On the other hand, it can be shown that given $\alpha_{1:M} = y$, z_{m-1} and z_{M-m} are the sum of $m-1$ and $M-m$ i.i.d. random variables with truncated distribution on the right at y, respectively, and as such are independent.

Specifically, the joint PDF of $\alpha_{1:M}$, z_{m-1} and z_{M-m} can be written as

$$\begin{aligned} p_{\alpha_{1:M},z_{m-1},z_{M-m}}(y,u,v) &= p_{\alpha_{1:M}}(y)p_{z_{m-1}|\alpha_{1:M}=y}(u)p_{z_{M-m}|\alpha_{1:M}=y}(v) \\ &= p_{\alpha_{1:M}}(y)p_{\sum_{j=1}^{m-1}\alpha_j^-}(u)p_{\sum_{j=m+1}^{M}\alpha_j^-}(v), \end{aligned} \tag{7.96}$$

where α_j^- are i.i.d. random variables with PDF for the Rayleigh fading scenario under consideration given by

$$p_{\alpha_j^-}(x) = \frac{e^{-x}}{1-e^{-y}}, \qquad 0 < x < y. \tag{7.97}$$

After some mathematical manipulations, we can obtain the closed-form expression for the joint PDF of $\alpha_{1:M}$, z_{m-1} and z_{M-m} as

$$\begin{aligned} p_{\alpha_{1:M},z_{m-1},z_{M-m}}(y,u,v) &= Me^{-y-u-v}\sum_{j=0}^{m-1}\binom{m-1}{j}\frac{(-1)^j(u-jy)^{m-2}}{(m-2)!}\mathrm{U}(u-jy) \\ &\times \sum_{k=0}^{M-m}\binom{M-m}{k}\frac{(-1)^k(v-ky)^{M-m-1}}{(M-m-1)!}\mathrm{U}(v-ky), \\ &y>0, u<(m-1)y, v<(M-m)y. \end{aligned} \tag{7.98}$$

The joint probability for the case of $m = M$ can be calculated using the PDF of $\gamma_B^{(M)}$ given in (7.82) as

$$\Pr[\gamma_B^{(m)} < x, \gamma_B^{(M)} > \beta] = \int_\beta^x p_{\gamma_B^{(M)}}(y)\mathrm{d}y. \tag{7.99}$$

After proper substitutions and taking derivatives, we obtain the PDF of active beam SINR $\gamma_B^{(m)}$ as

$$p_{\gamma_B^{(m)}}(x) = \tag{7.100}$$
$$\frac{1}{P_f}\begin{cases} \int_0^{\frac{x}{P\beta}-\frac{M}{P}} \frac{1}{P}p_{\alpha_{1:M},z_{M-1}}(\frac{x}{P},u)\mathrm{d}u, & m=1; \\ \int_0^\infty\int_0^{\frac{y}{\beta}-\frac{y}{x}-\frac{M-m}{P}} \frac{y}{x^2}p_{\alpha_{1:M},z_{m-1},z_{M-m}}(y,\frac{y}{x}-\frac{m}{P},v)\mathrm{d}v\mathrm{d}y, & 1<m<M; \\ f_{\gamma_B^{(M)}}(x)\mathrm{U}(x-\beta), & m=M. \end{cases}$$

Finally, the exact sum-rate expression for RUB-based multiuser MIMO systems with ABA-CBBI strategy can be obtained by substituting (7.87) and (7.100) into (7.89). The final expression can be readily evaluated using mathematical software such as Maple and Mathematica.

We now study the sum-rate performance of the proposed ABA-CBBI scheduling strategy through selected numerical examples. In particular, we compare its performance and complexity with some well-known user scheduling strategies for RUB-based multiuser MIMO systems. Table 7.2 summarizes the key features of the different user scheduling strategies under consideration. Figure 7.11 illustrates the effects of random user selection for unrequested beams on the sum-rate performance. In particular, we plot the sum rate of ABA-CBBI and conventional CBBI as a function of SNR. As we can see, with the same threshold value, the

Table 7.2 Features of different strategies [31]. © 2009 IEEE.

	SINR thresholding	SINR value feedback	Random selection
BBSI	No	Yes	Yes
CBBI	Yes	No	Yes
ABA-CBBI	Yes	No	No
BBI	No	No	Yes

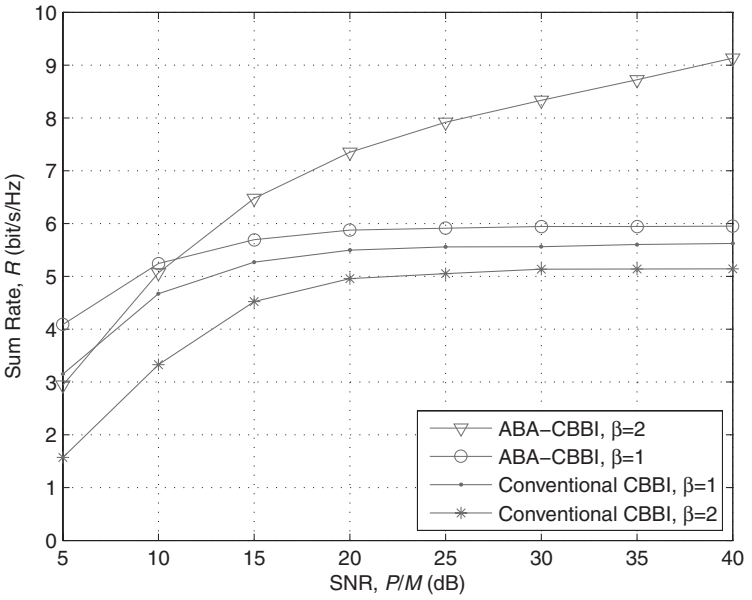

Figure 7.11 Effect of random user selection on sum rate performance ($K = 20$) [31]. © 2009 IEEE.

sum rate of ABA-CBBI is always greater than that of conventional CBBI, which shows that the RUB-based system is not benefiting from random user selection. We also notice from Fig. 7.11 that ABA-CBBI with different threshold values has a better sum-rate performance over different SNR ranges. Therefore, to achieve the best sum-rate performance, we should use the optimal value of the feedback threshold β.

In Fig. 7.12, we plot the sum rate of the proposed ABA-CBBI strategy as a function of the feedback threshold β. For a fixed SNR, there exists an optimal value of β maximizing the sum rate, which is marked in the figure. Intuitively, when β is very small, almost all users will feed back their best-beam indexes to the base station. Since the base station randomly assigns a beam to one of the users requesting it, that beam may be assigned to a user that does not achieve high SINR, which leads to relatively poorer sum-rate performance. On the other hand, when β is very large, few users will be qualified to feed back and some

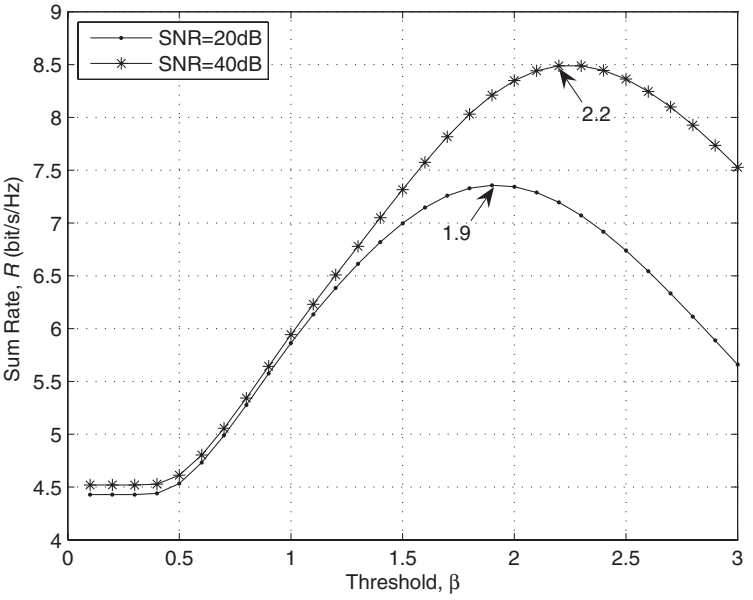

Figure 7.12 Sum rate of ABA-CBBI as a function of SINR threshold for different SNR values (K =20) [31]. © 2009 IEEE.

beams may not be requested. As such, not enough spatial multiplexing gain will explored, which also causes poorer sum-rate performance.

In Fig. 7.13, we compare the sum-rate performance of the proposed ABA-CBBI strategy with two strategies without thresholding, BBSI and BBI. As we can see, the sum rate of ABA-CBBI with optimal threshold values approaches that of BBSI over low SNR region and as SNR increases, ABA-CBBI considerably outperforms BBSI. This somewhat surprising behavior can be explained as follows. While the sum rate of the BBSI strategy saturates over high SNR regions due to multiuser interference, ABA-CBBI manages to reduce multiuser interference by increasing the threshold value and then selecting fewer users to serve. As a result, the selected users will experience less multiuser interference, a bottleneck to achieving better sum-rate performance at high SNR for conventional RUB-based user scheduling schemes. By comparison, BBI has the worst performance due to its complete lack of a mechanism to guarantee the high SINR of selected users.

7.6 RUB performance enhancement with linear combining

We investigate the performance enhancement of RUB-based multiuser MIMO systems multiple receive antennae at each mobile user. Specifically, we assume

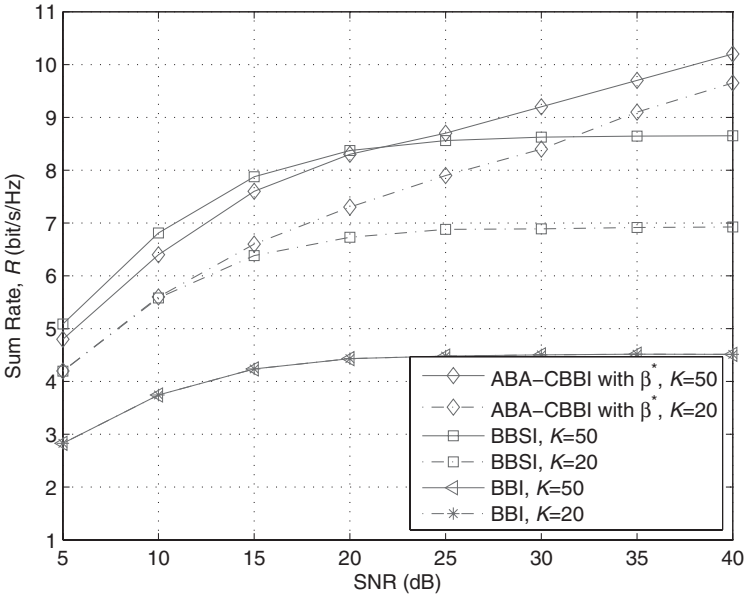

Figure 7.13 Sum-rate comparison between ABA-CBBI, BBSI and BBI strategies [31]. © 2009 IEEE.

that each mobile user has N $(N > 1)$ antennae. A conventional approach to exploit multiple receive antennae is to treat each antenna independently and let each user feed back the best-beam indexes and corresponding SINR values for all its receive antennae [20]. Intuitively, this approach would improve the sum-rate performance since it is equivalent to increasing the number of single-antenna users in the system to NK. The main disadvantage with this approach is, however, that the selected receiver will only use one designated antenna for reception and the received signals at other receive antennae are simply disgarded, which leads to inefficient utilization of the multiple receive antennae.

Alternatively, we can apply linear combining technique to fully explore the multiple receive antennae at each mobile [33,34]. In this section, we present and investigate two different feedback strategies for a RUB-based multiuser MIMO system with linear combining. In particular, we first present the system model, then describe the model of operation, and finally study their sum-rate performance through either asymptotic or exact statistic analysis. We consider the selection combining (SC) [35] and optimum combining (OC)[3] [36–38] schemes here.

[3] We omit the maximum ratio combining (MRC) scheme because MRC is optimal only in the noise-limited environment.

7.6.1 System and channel model

We consider the downlink transmission of a single-cell wireless system. The base station is equipped with M antennae and each mobile terminal is equipped with N antennae, where $N < M$ due to the size and cost limitations of the mobiles. We assume that there are a total of K active users in the cell where $K \gg M$. With RUB, the base station utilizes M random orthonormal vectors generated from an isotropic distribution [18] to transmit to as many as M selected users simultaneously. We denote the vector set as $\mathcal{U} = \{\mathbf{u}_1, \mathbf{u}_2, \cdots, \mathbf{u}_M\}$. The transmitted signal vector from M antennae over one symbol period can be written as

$$\mathbf{x} = \sum_{m=1}^{M} \mathbf{u}_m s_m, \tag{7.101}$$

where s_m is the information symbol for the mth selected user. The transmitted signal vector $\mathbf{x}$ has an average power constraint of $\mathbf{E}(\mathbf{x}^H \mathbf{x}) \leq P$, where P is the maximum average transmitting power, $\mathbf{E}(\cdot)$ denotes the statistical expectation, and $(\cdot)^H$ stands for the Hermitian transpose.

We adopt a homogeneous flat fading channel model for analytical tractability. Specifically, the channel gains from each transmit antenna to each receive antenna of users follow i.i.d. zero-mean complex Gaussian distribution with unit variance. The channel gain from the mth transmit antenna to the nth receive antenna of the kth mobile users is denoted by $h_{nm}^{(k)}$. As such, the $N \times M$ channel matrix for the kth user is constructed as

$$\mathbf{H}_k = \begin{pmatrix} h_{11}^{(k)} & h_{12}^{(k)} & \cdots & h_{1M}^{(k)} \\ h_{21}^{(k)} & h_{22}^{(k)} & \cdots & h_{2M}^{(k)} \\ \vdots & \vdots & \ddots & \vdots \\ h_{N1}^{(k)} & h_{N2}^{(k)} & \cdots & h_{NM}^{(k)} \end{pmatrix} \tag{7.102}$$

with the nth row, denoted by $\mathbf{h}_n^{(k)}$, being the instantaneous MISO channel for the nth receive antenna of the kth user.

The received signal vector over a symbol period at the ith selected user, when the jth beam is assigned to it, can be written as

$$\mathbf{y}_j^{(i)} = \mathbf{H}_i \mathbf{x} + \mathbf{n}_i = \mathbf{H}_i \mathbf{u}_j s_j + \sum_{m=1, m \neq j}^{M} \mathbf{H}_i \mathbf{u}_m s_m + \mathbf{n}_i, \tag{7.103}$$

where $\mathbf{n}_i$ is the $N \times 1$ additive Gaussian noise vector, whose entries follow independent complex Gaussian distribution with zero mean and variance σ_n^2. Note that $\mathbf{H}_i \mathbf{u}_j s_j$ is the desired signal for user i while $\sum_{m=1, m \neq j}^{M} \mathbf{H}_i \mathbf{u}_m s_m$ acts as interference.

The mobile receivers apply linear diversity combining techniques, such as SC and OC, to combine the signal received from N different receive antennae. When beam j is assigned to the ith user, the combined signal at user i can be written

as

$$z_j^{(i)} = \mathbf{w}_{ij}^H \mathbf{y}_j^{(i)} = \mathbf{w}_{ij}^H \mathbf{H}_i \mathbf{u}_j s_j + \mathbf{w}_{ij}^H \sum_{m=1, m\neq j}^{M} \mathbf{H}_i \mathbf{u}_m s_m + \mathbf{w}_{ij}^H \mathbf{n}_i, \tag{7.104}$$

where $\mathbf{w}_{ij}$ denotes the weighting vector of user i for the jth beam. Assuming that the transmit power is allocated equally among M selected users, the SINR of the combined signal at the user i when the jth beam is assigned to it can be shown to be given by

$$\gamma_j^{(i)} = \frac{|\mathbf{w}_{ij}^H \mathbf{H}_i \mathbf{u}_j|^2}{\sum_{m=1, m\neq j}^{M} |\mathbf{w}_{ij}^H \mathbf{H}_i \mathbf{u}_m|^2 + \rho \|\mathbf{w}_{ij}\|^2}, \tag{7.105}$$

where $\rho = \frac{M\sigma_n^2}{P}$ is the normalized transmit SNR. We assume that users have the perfect knowledge of their downlink channel matrix through the channel estimation process. Applying (7.105), user i calculates the SINRs after beam-specific combining for all M available beams, $\gamma_j^{(i)}, j = 1, 2, \cdots, M$.

7.6.2 M beam feedback strategy

With this strategy, each mobile evaluates the resulting SINR for each beam at the beginning of each time slot, after linearly combining the received signals on all antennae with either SC or OC. Then, the mobile will return the information of M effective beam SINRs to the BS. The incurred feedback load with this strategy is M real numbers per mobile. Note that OC performs active interference suppression by exploiting the interference structure, whereas SC simply selects the beam with the best SINR. It will be shown later that this characteristic interference-suppression feature enables OC to considerably outperform SC with higher implementation complexity. After receiving the effective SINR information from all mobiles, the BS schedules and starts data transmission to the mobiles that reported the largest effective SINRs on different beams. The selected mobile will combine the received signals from all antennae before data detection.

We now apply an asymptotic approach to analyze the performance of this strategy based on the limiting distribution of the beam SINR [33]. It is worth noting that the probability of awarding multiple beams to the same mobile is rather small, when the number of mobiles K is large. As such, the SINR of the jth beam after user selection is equal to $\gamma_j^B = \max\{\gamma_j^{(1)}, \gamma_j^{(2)}, \cdots, \gamma_j^{(i)}\}$, where $\gamma_j^{(i)}$, $i = 1, 2, \cdots, K$, are the resulting SINR at user i for the beam j after applying diversity combining. With the homogeneous fading assumption, we can show that the CDF of γ_j^B is given by

$$F_{\gamma_j^B}(x) = [F_{\gamma_j^{(i)}}(x)]^K. \tag{7.106}$$

In the following, we develop the limiting distribution of γ_j^B and use it to examine the asymptotic throughput and sum-rate scaling laws of different combining schemes. To make the analysis easy to follow, we focus on the case of four transmit antennae $M = 4$ and two receive antennae per mobile $N = 2$.

Selection combining
For SC, we first obtain the CDF of the resulting SINR after beam-specific combining as

$$F_{\gamma_j^{(i)}}(x) = \left(1 - \frac{e^{-\rho x}}{(1+x)^3}\right)^2. \tag{7.107}$$

It follows that the PDF of $\gamma_{i,j}$ is given by

$$p_{\gamma_j^{(i)}}(x) = 2\left(1 - \frac{e^{-\rho x}}{(1+x)^3}\right)\frac{e^{-\rho x}}{(1+x)^4}\left(\rho(1+x)+3\right). \tag{7.108}$$

We can then verify easily that the following condition is satisfied

$$\lim_{x\to+\infty} \frac{1 - F_{\gamma_j^{(i)}}(x)}{p_{\gamma_j^{(i)}}(x)} = 1/\rho > 0, \tag{7.109}$$

which implies that the limiting distribution of γ_j^B exists and follows the Gumbel type. More specifically, the limiting distribution of γ_j^B when K approach infinity is given by

$$\lim_{K\to+\infty} F_{\gamma_j^B}(x) = \exp\left(-e^{-\frac{x-b_K}{a_K}}\right), \tag{7.110}$$

where a_K and b_K are normalizing factors, which can be determined by solving numerically the equations $1 - F_{\gamma_j^{(i)}}(b_K) = 1/K$ and $1 - F_{\gamma_j^{(i)}}(a_K + b_K) = 1/(eK)$.

Starting from this limiting distribution, it can be shown that the corresponding scaling law for SC scheme is given by [33]

$$\lim_{K\to+\infty} \frac{C^{\mathrm{SC}}}{4\log b_K} = 1. \tag{7.111}$$

When $\rho = 1$, we can approximate b_K as

$$b_K \approx \log 2K - 2\log(1 + \log 2K). \tag{7.112}$$

Optimal combining
The resulting SINR after applying OC for a particular beam is equivalent to the combined SINR with OC in the presence of $M - 1$ interfering sources, the CDF of which has been derived in [39]. For the four transmit antennae and two receive antennae case under consideration, the CDF specializes to

$$F_{\gamma_j^{(i)}}(x) = 1 - \frac{e^{-\rho x}}{(1+x)^3}(1 - 3x - \rho x). \tag{7.113}$$

It follows that the PDF is given by

$$p_{\gamma_j^{(i)}}(x) = \frac{xe^{-\rho x}}{(1+x)^4}[(3\rho - \rho^2)x + (6 + 6\rho + \rho^2)]. \tag{7.114}$$

Again, based on these results, it can be shown that the limiting distribution of γ_j^B is also following the Gumbel type. Following the similar procedure of the SC case, we can show that that the corresponding scaling law for OC scheme is given by [33]

$$\lim_{K\to+\infty} \frac{C^{\mathrm{OC}}}{4\log b_K} = 1. \tag{7.115}$$

When $\rho = 1$, we can approximate b_K as

$$b_K \approx \log 4K - 2\log\log K. \tag{7.116}$$

7.6.3 Best-beam feedback strategy

In this section, we investigate the sum-rate performance of RUB systems with linear combining when each user only feeds back the best-beam information. Specifically, the user first calculates the output SINR after beam-specific combining for each of the M available beams. Then, the user selects its best beam among M beams, i.e. the one that achieves the largest combiner output SINR. Let b_i denote the index of the best beam for user i. Mathematically, b_i is given by $b_i = \arg\max_j \gamma_j^{(i)}$. The index of the best beam b_i and its corresponding output SINR $\gamma_{b_i}^{(i)}$ are fed back to the base station. Note that the feedback load with receiver combining techniques is one integer (for best-beam index) and one real number (for best-beam output SINR) per user, which is much lower than that of the M beam feedback strategy discussed in the previous subsection.

The base station assigns a beam to the user that feeds back the largest SINR value among all users requesting for that beam. Specifically, let $\mathcal{K}_m$ denote the user index set containing all users who feed back beam index m, i.e. $b_k = m$ if and only if $k \in \mathcal{K}_m$. If $\gamma_m^{(\hat{k})}$ is the largest among all $\gamma_m^{(k)}$, $k \in \mathcal{K}_m$, then the mth beam will be assigned to user $\hat{k}$ and the SINR of the mth beam γ_m^B will be equal to $\gamma_m^{(\hat{k})}$. If a particular beam is not requested by any user, i.e. the set $\mathcal{K}_m$ is empty for such a beam, then the base station knows that this beam is not the best one for any user and will allocate it to a randomly chosen user. The selected user will then apply proper weights to combine the signal from different antennae.

In what follows, we analyze the sum-rate performance of the resulting system through accurate statistical analysis. Unlike the limiting distribution approach adopted in a previous section, which applies only when the number of users is very large, this analysis applies to an arbitrary number of users. In particular, we derive the exact statistics of the feedback SINR for the SC scheme, based on which we arrive at the exact expression of its sum rate. By following a geometric approach, we also develop the statistics of the OC output SIR over high SNR

region, which is then used to obtain an upper bound for the sum rate. The upper bound is shown to be tight for a moderate number of users, but the number of users must be at least five times the number of transmit antennae.

Selection combining

With the SC scheme, the combined SINR at user i for the jth beam is equal to the largest SINR among N ones corresponding to different receive antennae for this beam. Specifically, the SINR on user i's nth receive antenna, while assuming beam j is assigned to it, can be written as

$$\gamma_{n,j}^{(i)} = \frac{|(\mathbf{h}_n^{(i)})^T \mathbf{u}_j|^2}{\sum_{m=1,m\neq j}^{M} |(\mathbf{h}_n^{(i)})^T \mathbf{u}_m|^2 + \rho}, \ 1{\leq}n{\leq}N, \ 1{\leq}j{\leq}M, \tag{7.117}$$

where $\mathbf{h}_n^{(i)}$ is the $M{\times}1$ channel vector from M transmit antennas to the nth receive antenna of user i. The combined SINR for the jth beam is then given mathematically by $\gamma_j^{(i)} = \max\{\gamma_{1,j}^{(i)}, \gamma_{2,j}^{(i)}, \cdots, \gamma_{N,j}^{(i)}\}$. If a user is selected for data reception on a certain beam, the user will use only the best receive antenna for this beam during reception, which constitutes the main complexity advantage of the SC scheme.

The sum-rate performance of the resulting multiuser MIMO system can be analyzed following a similar approach as in a previous section while treating each user as a single antenna receiver. On the other hand, because of the antenna selection process at the mobile users, the statistics of the feedback SINR is different from the single receive antenna case. In particular, $\gamma_{b_i}^{(i)}$ is the largest of M i.i.d. combined SINRs, i.e. $\gamma_{b_i}^{(i)} = \max\{\gamma_1^{(i)}, \gamma_2^{(i)}, \cdots, \gamma_M^{(i)}\}$. Equivalently, the feedback SINR $\gamma_{b_i}^{(i)}$ can be viewed as the largest among N best-beam SINRs, i.e. $\gamma_{b_i}^{(i)} = \max\{\gamma_{1,j^*}^{(i)}, \gamma_{2,j^*}^{(i)}, \cdots, \gamma_{N,j^*}^{(i)}\}$, where $\gamma_{n,j^*}^{(i)} = \max\{\gamma_{n,1}^{(i)}, \gamma_{n,2}^{(i)}, \cdots, \gamma_{n,M}^{(i)}\}$ denotes the best-beam SINR for the nth antenna at user i, whose PDF was obtained as

$$p_{\gamma_{n,j^*}^{(i)}}(x) = \sum_{j=0}^{M-1} \frac{(-1)^j M(M-1)}{(M-j-1)!j!} \int_0^{\infty} (\rho+z) \tag{7.118}$$
$$\times((1-jx)z - jx\rho)^{M-2} e^{-(1+x)z - x\rho} U((1-jx)z - jx\rho)\mathrm{d}z.$$

Therefore, the common PDF of the feedback SINRs $\gamma_{b_i}^{(i)}$ can be obtained as

$$p_{\gamma_{b_i}^{(i)}}(x) = N F_{\gamma_{n,j^*}^{(i)}}(x)^{N-1} p_{\gamma_{n,j^*}^{(i)}}(x), \tag{7.119}$$

where $F_{\gamma_{n,j^*}^{(i)}}(x) = \int_0^x p_{\gamma_{n,j^*}^{(i)}}(z)\mathrm{d}z$ is the CDF of $\gamma_{n,j^*}^{(i)}$.

Based on the mode of operation for user selection, a certain beam will be assigned to a randomly selected user if no user feeds back the index of such a beam. In this case, the user will choose the best antenna, i.e. the receive antenna that leads to the largest SINR on this beam, for data reception. As such, the beam SINR for such a beam will be equal to the largest SINR among N i.i.d.

ones, whose PDF is given by

$$f_{\gamma^R}(x) = N\big(F_{\gamma_{n,j}^{(i)}}(x)\big)^{N-1} p_{\gamma_{n,j}^{(i)}}(x), \tag{7.120}$$

where $f_{\gamma_{n,j}^{(i)}}(x)$ and $F_{\gamma_{n,j}^{(i)}}(x)$ denote the PDF and CDF of $\gamma_{n,j}^{(i)}$ in (7.117), respectively. The closed-form expression of $f_{\gamma_{n,j}^{(i)}}(x)$ is given by [20, eq. (14)]

$$p_{\gamma_{n,j}^{(i)}}(x) = \frac{e^{-x/\rho}}{(1+x)^M}\left(\frac{x+1}{\rho} + M - 1\right). \tag{7.121}$$

Finally, following the similar analytical approach of the previous section, while noting that the PDF of user feedback SINR is given in (7.118) and the PDF of randomly assigned beam SINR in (7.121), the sum rate of RUB system with SC at receivers can be calculated as

$$\begin{aligned} R^{SC} &= \int_0^\infty \log_2(1+x) p_{\gamma_{b_i}^{(1:K)}}(x)\mathrm{d}x \\ &+ \sum_{m=2}^{M}\sum_{i=m}^{K}\left(P_i^m \int_0^\infty \log_2(1+x)\; p_{\gamma_{b_i}^{(i:K)}}(x)\mathrm{d}x\right. \\ &+ \left.\left(\frac{m-1}{M}\right)^{K-1}\int_0^\infty \log_2(1+x) p_{\gamma^R}(x)\mathrm{d}x\right), \end{aligned} \tag{7.122}$$

where P_i^m denotes the probability that the mth beam is assigned to the user with the ith largest feedback SINR, i.e. $\gamma_m^B = \gamma_{b_i}^{(i:K)}, i = m, m+1, \cdots, K$, which is given by,

$$P_i^m = \sum_{\substack{\sum_{j=1}^{m-1} n_j = i-m \\ n_j \in \{0,1,\cdots,i-m\}}} \left[\prod_{j=1}^{m-1}\left(\frac{j}{M}\right)^{n_j}\left(1-\frac{j}{M}\right)\right],\ i = m, m+1, \cdots, K, \tag{7.123}$$

and $p_{\gamma_{b_i}^{(i:K)}}(x)$ represents the PDF of the ith user feedback SINR, given in terms of $f_{\gamma_{b_i}^{(i)}}(x)$ as

$$p_{\gamma_{b_i}^{(i:K)}}(x) = \frac{K!}{(K-i)!(i-1)!} F_{\gamma_{b_i}^{(i)}}(x)^{K-i}[1 - F_{\gamma_{b_i}^{(i)}}(x)^M]^{i-1} p_{\gamma_{b_i}^{(i)}}(x). \tag{7.124}$$

Optimum combining

With the OC scheme [35,36], it can be shown that the optimal weighting vector of user i for the jth beam is given by

$$\mathbf{w}_{ij}^* = \left(\sum_{m=1, m\neq j}^{M} \mathbf{H}_i \mathbf{u}_m (\mathbf{H}_i \mathbf{u}_m)^H + \rho \mathbf{I}\right)^{-1} \mathbf{H}_i \mathbf{u}_j, \tag{7.125}$$

and the corresponding maximum SINR of the combined signal is given by

$$\gamma_j^{(i)} = (\mathbf{H}_i\mathbf{u}_j)^H\mathbf{w}_{ij}^* = (\mathbf{H}_i\mathbf{u}_j)^H\left(\sum_{m=1,m\neq j}^{M}\mathbf{H}_i\mathbf{u}_m(\mathbf{H}_i\mathbf{u}_m)^H+\rho\mathbf{I}\right)^{-1}\mathbf{H}_i\mathbf{u}_j, \tag{7.126}$$

where $\mathbf{I}$ denotes the identity matrix. After proper comparison, user i will feed back the best-beam index b_i and the corresponding combined SINR, $\gamma_{b_i}^{(i)}$, to the base station for user selection. If the user is selected for data reception on the b_ith beam, the user will combine the signal from different antennae using weights $\mathbf{w}_{ib_i}^*$ calculated using (7.125) for data detection.

After some mathematical manipulation, the optimal weight vector and the corresponding output SINR are simplified to

$$\mathbf{w}_{ij}^* = \frac{(\mathbf{H}_i\mathbf{H}_i^H+\frac{1}{\rho}\mathbf{I})^{-1}\mathbf{H}_i\mathbf{u}_j}{1-(\mathbf{H}_i\mathbf{u}_j)^H(\mathbf{H}_i\mathbf{H}_i^H+\frac{1}{\rho}\mathbf{I})^{-1}\mathbf{H}_i\mathbf{u}_j}, \tag{7.127}$$

and

$$\gamma_j^{(i)} = \frac{(\mathbf{H}_i\mathbf{u}_j)^H(\mathbf{H}_i\mathbf{H}_i^H+\frac{1}{\rho}\mathbf{I})^{-1}\mathbf{H}_i\mathbf{u}_j}{1-(\mathbf{H}_i\mathbf{u}_j)^H(\mathbf{H}_i\mathbf{H}_i^H+\frac{1}{\rho}\mathbf{I})^{-1}\mathbf{H}_i\mathbf{u}_j}, \tag{7.128}$$

respectively. Note that each user needs only to calculate the inversion of a single matrix $(\mathbf{H}_i\mathbf{H}_i^H+\frac{1}{\rho}\mathbf{I})$ now. Although the statistics of the combined SINR for a single beam can be obtained [39, 40], because of the dependence between SINRs for different beams, it is very difficult, if not impossible, to derive the statistics of the feedback SINR with the OC scheme. Therefore, we focus on the sum rate upper bound analysis over a high SNR region in what follows.

When the SNR is very high and the system becomes interference-limited, the optimal weighting vector can be approximately given by, after setting ρ in (7.127) to infinity,

$$\mathbf{w}_{ij}^* = \frac{(\mathbf{H}_i\mathbf{H}_i^H)^{-1}\mathbf{H}_i\mathbf{u}_j}{1-(\mathbf{H}_i\mathbf{u}_j)^H(\mathbf{H}_i\mathbf{H}_i^H)^{-1}\mathbf{H}_i\mathbf{u}_j}. \tag{7.129}$$

It follows that $\mathbf{w}_{ij}^*$ is proportional to the least square solution of $\mathbf{H}_i^H\mathbf{w}=\mathbf{u}_j$ [39, 41]. Therefore, with the optimal weighting vector, the angle between the effective MISO channel for user i, $\mathbf{H}_i^H\mathbf{w}_{ij}^*$, and the jth beam, $\mathbf{u}_j$ is minimized, which is equal to the angle between $\mathbf{u}_j$, and the range space of $\mathbf{H}_i^H$, denoted by $\mathcal{R}(\mathbf{H}_i^H)$.

Lemma 1. *Over a high SNR region, the maximum output SINR at user i after performing optimal combining with respect to the jth beam is given by*

$$\gamma_{i,j}^* = |\cot(\theta_{ij})|^2, \tag{7.130}$$

where θ_{ij} is the angle between $\mathbf{u}_j$ and $\mathcal{R}(\mathbf{H}_i^H)$.

Proof. Let ρ in (7.128) go to infinity, the maximum output SINR at user i over high SNR region becomes

$$\gamma_{i,j}^{*} = \frac{(\mathbf{H}_i\mathbf{u}_j)^H(\mathbf{H}_i\mathbf{H}_i^H)^{-1}\mathbf{H}_i\mathbf{u}_j}{1-(\mathbf{H}_i\mathbf{u}_j)^H(\mathbf{H}_i\mathbf{H}_i^H)^{-1}\mathbf{H}_i\mathbf{u}_j}. \tag{7.131}$$

Since $\mathbf{H}_i^H(\mathbf{H}_i\mathbf{H}_i^H)\mathbf{H}_i$ is the projection matrix onto $\mathcal{R}(\mathbf{H}_i^H)$, we have

$$|\cos(\theta_{ij})|^2 = (\mathbf{H}_i\mathbf{u}_j)^H(\mathbf{H}_i\mathbf{H}_i^H)^{-1}\mathbf{H}_i\mathbf{u}_j. \tag{7.132}$$

The lemma is proved after substituting (7.132) into (7.131). □

Since $\cot(\cdot)$ is a monotonically decreasing function, each user can feed back the index and SINR value of the beam that forms the smallest angle with $\mathcal{R}(\mathbf{H}_i^H)$.

It can be shown that the random variable $|\cos(\theta_{ij})|^2$, where θ_{ij} is the angle between a random vector of length M and a space spanned by N independent random vectors of the same length, follows the beta distribution parameterized by N and $M-N$, with PDF and CDF given by [17]

$$f_{|\cos(\theta)|^2}(x) = (M-N)\binom{M-1}{N-1}x^{N-1}\cdot(1-x)^{M-N-1}, \quad 0\leq x\leq 1 \tag{7.133}$$

and

$$F_{|\cos(\theta)|^2}(x) = \mathrm{I}(x;N,M),\ 0\leq x\leq 1, \tag{7.134}$$

respectively. To derive an upper bound of the system sum rate, we assume that every beam of the base station is requested by at least one user. In this case, since a user can only be assigned to one beam, the SINR of the jth assigned beam can be shown to be equal to the largest among $K-j+1$ combined SINRs on that beam for the remaining $K-j+1$ users ($j-1$ users have been previously assigned). Mathematically speaking, the SINR of the jth assigned beam is equal to $|\cot(\theta_j^*)|^2$, where θ_j^* is the smallest angle among $K-j+1$ ones. Correspondingly, $|\cos(\theta_j^*)|^2$ will be the largest one among $K-j+1$ independent Beta distributed random variables. The PDF of $|\cos(\theta_j^*)|^2$ is thus given by [27]

$$f_{|\cos(\theta_j^*)|^2}(x) = (K-j+1)\big(F_{|\cos(\theta)|^2}(x)\big)^{K-j}f_{|\cos(\theta)|^2}(x), \quad 0\leq x\leq 1. \tag{7.135}$$

Noting that $\log_2(1+|\cot(\theta_j^*)|^2) = -\log_2(1-|\cos(\theta_j^*)|^2)$, we obtain a sum rate upper bound for the proposed scheme over the high SNR region as

$$R^{\mathrm{OC}} = \sum_{j=1}^{M} -(K-j+1)\int_0^1 \log_2(1-x)\big(F_{|\cos(\theta)|^2}(x)\big)^{K-j}f_{|\cos(\theta)|^2}(x)\mathrm{d}x. \tag{7.136}$$

As this upper bound is derived based on the assumption that all beams are requested, it will be tight as long as the probability of all beams being requested is close to 1. In [31], we showed that the probability that each of M available

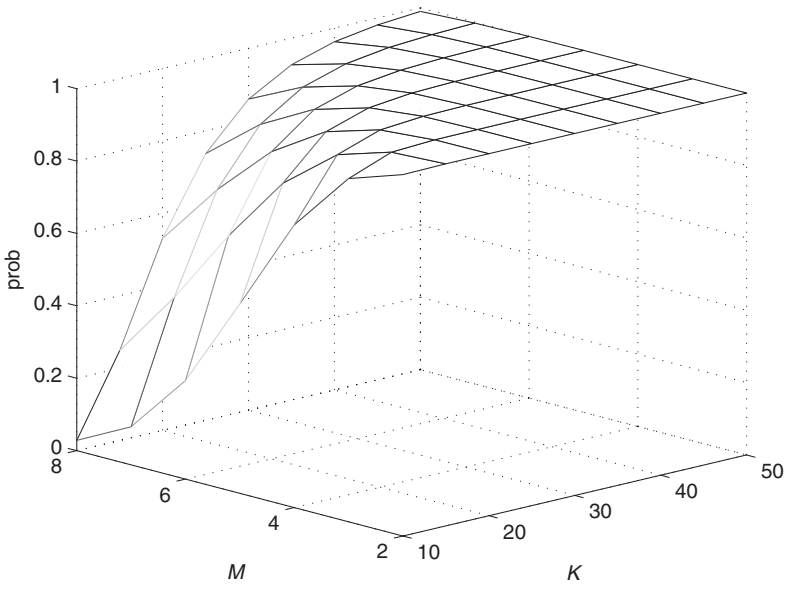

Figure 7.14 Probability of all beams being requested [34]. © 2010 IEEE.

beam is requested by at least one user is given by

$$\Pr[\text{every beam requested}] = \sum_{q=1}^{M} (-1)^{M-q} \binom{M}{q} \left(\frac{q}{M}\right)^{K}. \tag{7.137}$$

This probability is plotted as a function of the number of users K and the number of beams M in Fig. 7.14. As we can see, when K is more than five times M, which is usually the case in practice, every beam will be requested with probability very close to 1.

In Fig. 7.15, we plot the sum rate of SC-based systems as a function of SNR for a different number of users. We set $M = 4$ and $N = 2$ here. The sum rate of the conventional approach, which treats a user's receive antennae independently, is also plotted for comparison. Although requiring only $1/N$ of the feedback load of the conventional approach, SC is shown to achieve nearly the same sum-rate performance. In Fig. 7.15, we also compare our analytical results given by (7.123) to simulation results. The perfect match verifies the analytical approach adopted in this work.

In Fig. 7.16, the sum rate of the OC-based system is plotted as a function of SNR for a different number of users. The sum rate of the conventional approach, M beam feedback (the scheme considered in [33, 40]), and the analytical upper bound given by (7.136) are also plotted. As expected, the analytical upper bound developed for OC-based system is shown to be tight over the high SNR region. Compared to the conventional approach, OC achieves noticeably better

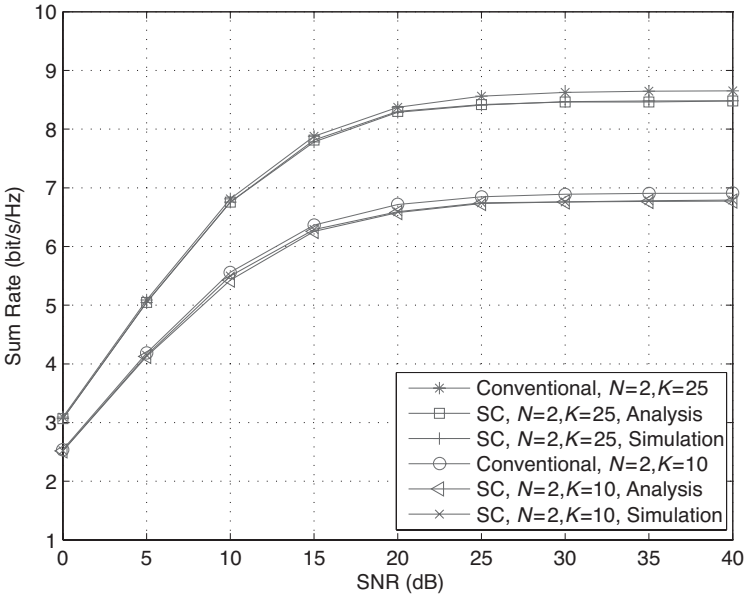

Figure 7.15 Sum-rate performance of RUB systems with SC scheme ($M = 4$) [34]. © 2010 IEEE.

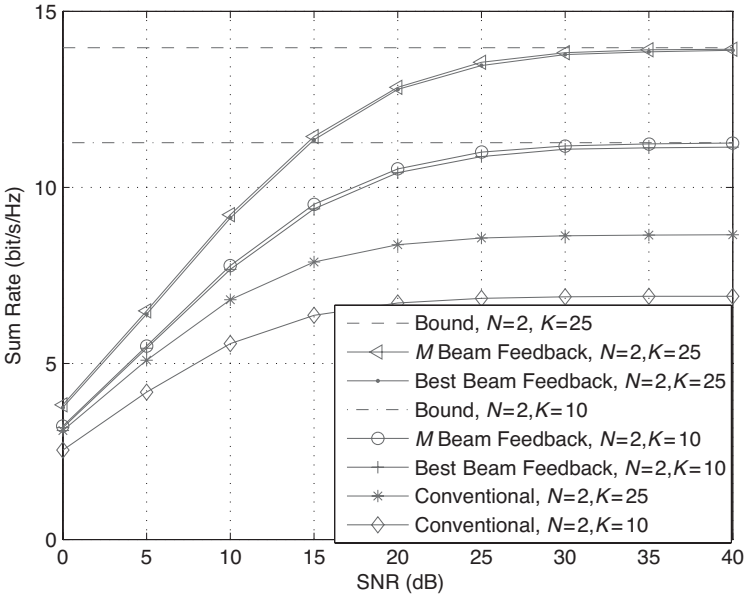

Figure 7.16 Sum-rate performance of RUB systems with OC scheme ($M = 4$) [34]. © 2010 IEEE.

sum-rate performance while requiring less feedback load. We further observe that the proposed OC-based scheme offers nearly the same performance as the M beam feedback scheme in [33, 40], which mandates M real numbers per user feedback load. It is worthwhile mentioning that the advantages of OC come at the cost of additional processing complexity of channel matrix inversion when calculating the combining weights and output SINR.

7.7 Summary

In this chapter, we focused on the low-complexity beamforming/user scheduling schemes for multiuser MIMO systems. While ZFBF can completely eliminate the interuser interference when operating in multiuser MIMO channels, RUB schemes incur much lower feedback load, as the users need not feed back the complete channel gain vectors. As it is usually sufficient for the users to feed back their best-beam SINR information, we applied the order statistics results to obtain the exact statistics of users' best-beam SINR, which found applications in the analysis of several user scheduling schemes for RUB systems. Finally, we showed that the receiver combining approach can offer significant performance gain for the multiple antennae per user case.

7.8 Bibliography notes

For a more thorough discussion on point-to-point MIMO systems, including the transceiver design and decoding algorithms, the reader may refer to [11,12]. The capacity of multiuser MIMO systems and its achieving with DPC was investigated in [6,8]. The optimality of the ZFBF scheme over multiuser MIMO channel is examined in [17, 42], whereas that for the RUB scheme can be found in [20]. Refs [43–46] present some additional user scheduling scheme with limited feedback for multiuser MIMO systems. A beamforming schemes with limited feedback for multiple access channel was considered in [47]. Finally, more details for optimal combining can be found in [35].

References

[1] G. J. Foschini and M. J. Gans, "On limits of wireless communications in a fading environment when using multiple antennas," *Wireless Personal Commun.*, vol. 6, no. 3, pp. 311–335, March 1998.

[2] I. Emre Telatar, "Capacity of multi-antenna Gaussian channels," *European Trans. Telecomm.*, vol. 10, no. 6, pp. 585–595, November–December 1999.

[3] G. J. Foschini, D. Chizhik, M. Gans, C. Papadias and R. A. Valenzuela, "Analysis and performance of some basic spacetime architectures," *IEEE J. Select. Areas Commun.*, vol. 21, pp. 303–320, April 2003.

[4] D. Gesbert, "Robust linear MIMO receivers: a minimum error-rate approach," *IEEE Trans. Signal Processing*, vol. 51, pp. 2863–2871, November 2003.

[5] M. Sellathurai and G. J. Foschini, "Stratified diagonal layered spacetime architectures: signal processing and information theoretic aspects," *IEEE Trans. Signal Processing*, vol. 51, pp. 2943–2954, November 2003.

[6] G. Caire and S. Shamai, "On the achievable throughput of a multiantenna Gaussian broadcast channel," *IEEE Trans. Inform. Theory*, vol. IT-49, no. 7, pp. 1691–1706, July 2003.

[7] H. Viswanathan, S. Venkatesan and H. Huang, "Downlink capacity evaluation of cellular networks with known-interference cancellation," *IEEE J. Select. Areas Commun.*, vol. 21, no. 5, pp. 802–811, June 2003.

[8] P. Viswanath and D. Tse, "Sum capacity of the vector Gaussian broadcast channel and uplink–downlink duality," *IEEE Trans. Inform. Theory*, vol. IT-49, no. 8, pp. 1912–1921, August 2003.

[9] S. Vishwanath, N. Jindal and A. Goldsmith, "Duality, achievable rate and sum-rate capacity of Gaussian MIMO broadcast channels," *IEEE Trans. Inform. Theory*, vol. IT-49, no. 10, pp. 2659–2668, October 2003.

[10] H. Weingarten, Y. Steinberg and S. Shamai, "The capacity region of the Gaussian multiple-input multiple-output broadcast channel," *IEEE Trans. Inform. Theory*, vol. IT-52, no. 7, pp. 3936–3964, September 2006.

[11] A. Paulraj, R. Nabar and D. Gore, *Introduction to Space-Time Wireless Communications*, 1st ed., Cambridge: Cambridge University Press, 2003.

[12] E. Biglieri, R. Calderbank, A. Constantinides, A. Goldsmith, A. Paulraj and H. V. Poor, *MIMO Wireless Communications*. Cambridge: Cambridge University Press, 2007.

[13] D. Gesbert, M. Shafi, D. S. Shiu, P. Smith and A. Naguib, "From theory to practice: an overview of MIMO space-time coded wireless systems," *IEEE J. Select. Areas Commun.*, vol. 21, no. 4 pp. 281–302, April 2003.

[14] M. Costa, "Writing on dirty paper," *IEEE Trans. Inform. Theory*, vol. IT-29, no. 5, pp. 439–441, May 1983.

[15] N. Jindal and A. Goldsmith, "Dirty-paper coding versus TDMA for MIMO broadcast channels," in *IEEE Trans. Inform. Theory*, vol. IT-51, no. 5, pp. 1783–1794, March 2005. See also *Proc. of IEEE Conf. on Communications (ICC'2004)*, Paris, France, June 2004.

[16] W. Rhee, W. Yu and J. M. Cioffi, "The optimality of beamforming in uplink multiuser wireless systems," *IEEE Trans. Wireless Commun.*, vol. TWC-3, no. 1, pp. 86–96, January 2004.

[17] T. Yoo and A. Goldsmith, "On the optimality of multi-antenna broadcast scheduling using zero-forcing beamforming," *IEEE J. Select. Areas Commun.*, vol. SAC-24, no. 3, pp. 528–541, March 2006.

[18] B. Hassibi and T. L. Marzetta, "Multiple-antennas and isotropically random unitary inputs: the received signal density in closed form," *IEEE Trans. Inform. Theory*, vol. IT-48, no. 6, pp. 1473–1484, June 2002.

[19] K. K. J. Chung, C.-S. Hwang and Y. K. Kim, "A random beamforming technique in mimo systems exploiting multiuser diversity," *IEEE J. Select. Areas Commun.*, vol. SAC-21, no. 5, pp. 848–855, June 2003.

[20] M. Sharif, and B. Hassibi, "On the capacity of MIMO broadcast channels with partial side information," *IEEE Trans. Inform. Theory*, Vol. IT-51, no. 2, pp. 506–522, February 2005.

[21] H. Wang, A. B. Gershman, and T. Kirubarajan, "Random unitary beamforming with partial feedback for multi-antenna downlink transmission using multiuser diversity," in *Proc. of IEEE Veh. Technol. Conf. (VTC'Spring 2005)*, June 2005, pp. 216–220.

[22] K. Zhang and Z. Niu, "Random beamforming with multibeam selection for MIMO broadcast channels," in *Proc. of IEEE Intl. Conf. Commun. (ICC'2006)*, Istanbul, Turkey, June 2006, pp. 4191–4195.

[23] T. Yoo and A. Goldsmith, "Sum-rate optimal multi-antenna downlink beamforming strategy based on clique search," *Proc. IEEE Global Telecomm. Conf.* (*Globecom' 2005*), St. Louis, Missouri, vol. 3, pp. 1510–1514, December 2005.

[24] J. Kim, S. Park, J. H. Lee, J. Lee and H. Jung, "A scheduling algorithm combined with zero-forcing beamforming for a multiuser MIMO wireless system," *Proc. IEEE Semiannual Veh. Tech. Conf. (VTC' 2005)*, Dallas, Texas, vol. 1, pp. 211–215, September 2005.

[25] A. M. Toukebri, S. Aissa and M. Maier, "Resource allocation and scheduling for multiuser MIMO systems: a beamforming-based strategy," *Proc. IEEE Global Telecomm. Conf. (Globecom' 2006)*, San Francisco, California, November 2006.

[26] G. Dimic and N. D. Sidiropoulos, "On downlink beamforming with greedy user selection: performance analysis and a simple new algorithm," *IEEE Trans. Sig. Pro.*, vol. 53, no. 10, pp. 3857–3868, October 2005.

[27] H. A. David, *Order Statistics*. New York, NY: John Wiley & Sons, Inc., 1981.

[28] J. Diaz, O. Simeone, O. Somekh and Y. bar-Ness, "Scaling law of the sum-rate for multiantenna broadcast channels with deterministic or selective binary feedback," in *Proc. of Inform. Theory Workshop (ITW'2006)*, Punta del Este, Uruguay, March 2006, pp. 298–301.

[29] J. Diaz, O. Simeone and Y. bar-Ness, "Sum-rate of MIMO broadcast channels with one bit feedback," in *Proc. of Int. Symp. Inform. Theory (ISIT'2006)*, Seattle, Washington, July 2006, pp. 1944–1948.

[30] Y.-C. Ko, H.-C. Yang, S.-S. Eom and M.-S. Alouini, "Adaptive modulation with diversity combining based on output-threshold MRC," *IEEE Trans. Wireless Commun.*, vol. TWC-6, no. 10, pp. 3728–3737, October 2007.

[31] P. Lu and H.-C. Yang, "A simple and efficient user scheduling strategy for RUB-based multiuser MIMO systems and its sum rate analysis," *IEEE Trans. Veh. Tech.*, vol. 58, no. 9, pp. 4860–4867, November 2009.

[32] D. Gesbert and M.-S. Alouini, "How much feedback is multi-user diversity really worth?" in *Proc. of IEEE Int. Conf. on Commun. (ICC'2004)*, Paris, France, June 2004, pp. 234–238.

[33] M. O. Pun, V. Koivunen and H. V. Poor, "SINR analysis of opportunistic MIMO-SDMA downlink systems with linear combining," *Proc. of IEEE Int. Conf. Commun. (ICC'2008)*, Beijing, China, May 2008.

[34] P. Lu and H.-C. Yang, "Performance analysis for RUB-based multiuser MIMO systems with antenna diversity techniques," *IEEE Trans. Veh. Tech.*, vol. 59, no. 1, pp. 490–494, January 2010.

[35] M. K. Simon and M. S. Alouini, *Digital Communication over Fading Channels*, 2nd ed. Newark, NJ: John Wiley & Sons, Inc., 2004.

[36] J. H. Winters, "Optimum combining in digital mobile radio with cochannel interference," *IEEE Trans. Veh. Technol.*, vol. 33, no. 3, pp. 144–155, August 1984.

[37] A. Shah and A. M. Haimovich, "Performance analysis of optimum combining in wireless communications with Rayleigh fading and cochannel interference," *IEEE Trans. Commun.*, vol. 46, no. 4, pp. 473–479, April 1998.

[38] M. Chiani, M. Z. Win, A. Zanella, R. K. Mallik and J. H. Winters, "Bounds and approximations for optimum combining of signals in the presence of multiple cochannel interferers and thermal noise," *IEEE Trans. Commun.*, vol. 51, no. 2, pp. 296–307, February 2003.

[39] H. S. Gao, P. J. Smith and M. V. Clark, "Theoretical reliability of MMSE linear diversity combining in Rayleigh-fading additive interference channels," *IEEE Trans. Commun.*, vol. 46, no. 5, pp. 666–672, May 1998.

[40] M. O. Pun, V. Koivunen and H. V. Poor, "Opportunistic scheduling and beamforming for MIMO–SDMA downlink systems with linear combining," *Proc. of Int. Symp. Personal, Indoor and Mobile Radio Commun. (PIMRC' 2007)*, Athens, Greece, September 2007.

[41] S. Haykin, "Adaptive filter theory," *Information and System Sciences*, Englewood Cliffs, NJ: Prentice Hall, 1986.

[42] N. Jindal, "MIMO broadcast channels with finite feedback," in *IEEE Trans. Inform. Theory*, vol. IT-52, no. 11, pp. 5045–5059, November 2006. See also *Proc. of IEEE Global Telecomm. Conf. (Globecom'2005)*, St. Louis, MO, November 2005.

[43] C. Anton-Haro, "On the impact of PDF-matched quantization on orthogonal random beamforming," *IEEE Commun. Letters*, vol. 11, no. 4, pp. 328–330, April 2007.

[44] S. Y. Park, D. Park, and D. J. Love, "On scheduling for multiple-antenna wireless networks using contention-based feedback," *IEEE Trans. Commun.*, vol. 55, no. 6, pp. 1174–1190, June 2007.

[45] J. So and J. M. Cioffi, "Multiuser diversity in a MIMO System with opportunistic feedback," *IEEE Trans. Veh. Tech.*, vol. 58, no. 9, pp. 4909–4918, November 2009.

[46] M. Pugh and B. D. Rao, "Reduced feedback schemes using random beamforming in MIMO broadcast channels," *IEEE Trans. Signal Process.*, vol. 58, no. 3, pp. 1821–1832, March 2010.

[47] W. Dai, B. C. Rider and Y. E. Liu, "Joint beamforming for multiaccess MIMO systems with finite rate feedback," *IEEE Trans. Wireless Commun.*, vol. 8, no. 5, pp. 2618–2628, May 2009.

[48] P. Lu and H.-C. Yang. "Sum-rate analysis of multiuser MIMO system with zero-forcing transmit beam forming," *IEEE Trans. Commun.*, vol. 57, no. 9, pp. 2585–2589, September 2009.

References

M. Abramowitz and I. A. Stegun, *Handbook of Mathematical Functions.* New York, NY: Dover Publications, 1972.

A. A. Abu-Dayya and N. C. Beaulieu, "Analysis of switched diversity systems on generalized-fading channels," *IEEE Trans. Commun.*, vol. COM-42, no. 11, pp. 2959–2966, November 1994.

A. A. Abu-Dayya and N. C. Beaulieu, "Switched diversity on microcellular Ricean channels," *IEEE Trans. Veh. Technol.*, vol. VT-43, no. 4, pp. 970–976, November 1994.

S. M. Alamouti, "A simple transmitter diversity scheme for wireless communications," *IEEE J. Select. Areas Commun.*, vol. 16., pp. 1451–458, October 1998.

Y. S. Al-Harthi, A. H. Tewfik and M.-S. Alouini, "Multiuser diversity with quantized feedback," *IEEE Trans. Wireless Commun.*, vol. 6, no. 1, pp. 330–337, January 2007.

M.-S. Alouini and A. J. Goldsmith, "Adaptive modulation over Nakagami fading channels," *Kluwer J. Wireless Commun.*, vol. 13, nos. 1–2, pp. 119–143, 2000.

M.-S. Alouini and M. K. Simon, "An MGF-based performance analysis of generalized selective combining over Rayleigh fading channels," *IEEE Trans. Commun.*, vol. COM-48, no. 3, pp. 401–415, March 2000.

M.-S. Alouini and M. K. Simon, "Performance of coherent receivers with hybrid SC/MRC over Nakagami-m fading channels," *IEEE Trans. Veh. Technol.*, vol. VT-48, no. 4, pp. 1155–1164, July 1999.

M.-S. Alouini and H.-C. Yang, "Minimum estimation and combining generalized selection combining (MEC-GSC)," in *Proc. IEEE Int. Symposium Inform. Theory (ISIT'05)*, Adelaide, Australia, September 2005. Full paper revised for *IEEE Trans. Wireless Commun.*

A. Annamalai, G. Deora and C. Tellambura, "Unified analysis of generalized selection diversity with normalized threshold test per branch," in *Proc. of IEEE Wireless Commun. and Networking Conf. (WCNC'03)*, New Orleans, Louisiana, vol. 2, March 2003, pp. 752–756.

A. Annamalai and C. Tellambura, "Analysis of hybrid selection/maximal-ratio diversity combiners with Gaussian errors," *IEEE Trans. Wireless Commun.*, vol. 1, no. 3, pp. 498–511, July 2002.

C. Anton-Haro, "On the impact of PDF-matched quantization on orthogonal random beamforming," *IEEE Commun. Letters*, vol. 11, no. 4, pp. 328–330, April 2007.

N. Balakrishnan and C. R. Rao, *Handbook of Statistics 17: Order Statistics: Applications*, 2nd ed. Amsterdam: North-Holland Elsevier, 1998.

N. Belhaj, N. Hamdi, M.-S. Alouini and A. Bouallegue, "Low-power minimum estimation and combining with adaptive modulation," in *Proc. of the Eighth IEEE International Symposium on Signal Processing and its Applications (ISSPA'2005)*, Sydney, Australia, August 2005.

N. Belhaj, N. Hamdi, M.-S. Alouini and A. Bouallegue, "Adaptive modulation and combining for bandwidth efficient communication over fading channels," in *Proc. of the IEEE Personal Indoor Mobile Radio Conference (PIMRC'2005)*, Berlin, Germany, September 2005.

E. Biglieri, R. Calderbank, A. Constantinides, A. Goldsmith, A. Paulraj and H. V. Poor, *MIMO Wireless Communications*. Cambridge: Cambridge University Press, 2007.

M. A. Blanco and K. J. Zdunek, "Performance and optimization of switched diversity systems for the detection of signals with Rayleigh fading," *IEEE Trans. Commun.*, vol. COM-27, no. 12, pp. 1887–1895, December 1979.

Z. Bouida, N. Belhaj, M.-S. Alouini and K. A. Qaraqe, "Minimum selection GSC in independent Rayleigh fading," *IEEE Trans. Wireless Commun.*, vol. 7, no. 7, pp. 2492–2501, 2008.

G. Caire and S. Shamai, "On the achievable throughput of a multiantenna Gaussian broadcast channel," *IEEE Trans. Inform. Theory*, vol. IT-49, no. 7, pp. 1691–1706, July 2003.

C.-J. Chen and L.-C. Wang, "A unified capacity analysis for wireless systems with joint multiuser scheduling and antenna diversity in Nakagami fading channels," *IEEE Trans. Commun.*, vol. 54, no. 3, pp. 469–478, March 2006.

Z. Chen, "Asymptotic performance of transmit antenna selection with maximal-ratio combining for generalized selection criterion," *IEEE Commun. Lett.*, vol. 8, no. 4, pp. 247–249, April 2004.

Y. Chen and C. Tellambura, "A new hybrid generalized selection combining scheme and its performance over fading channels," *Proc. IEEE Wireless Commun. Net. Conf. (WCNC'04)*, vol. 2, pp. 926–932.

M. Chiani, M. Z. Win, A. Zanella, R. K. Mallik and J. H. Winters, "Bounds and approximations for optimum combining of signals in the presence of multiple cochannel interferers and thermal noise," *IEEE Trans. Commun.*, vol. 51, no. 2, pp. 296–307, February 2003.

K. Cho and D. Yoon, "On the general BER expression of one- and two-dimensional amplitude modulation," *IEEE Trans. Commun.*, vol. 50, no. 7, pp. 1074–1080, July 2002.

S. Choi, M.-S. Alouini, K. A. Qaraqe and H.-C. Yang, "Soft handover overhead reduction by RAKE reception with finger reassignment," *IEEE Trans. on Commun.*, vol. 56, no. 2, pp. 213–221, February 2008.

S. Choi, M.-S. Alouini, K. A. Qaraqe and H.-C. Yang, "Fingers replacement method for RAKE receivers in the soft handover region," *IEEE Trans. on Wireless Commun.*, vol. 7, no. 4, pp. 1152–1156, April 2008.

S. Choi, Y.-C. Ko and E. J. Powers, "Optimization of switched MIMO systems over Rayleigh fading channels," *IEEE Trans. Veh. Technol.*, vol. 56, no. 1, pp. 103–114, January 2007.

S. Choi, H.-C. Yang and Y.-C. Ko, "Performance analysis of transmit diversity systems with antenna replacement," *IEEE Trans. Veh. Technol.*, vol. 57, no. 4, pp. 2588–2595, July 2008.

K. K. J. Chung, C.-S. Hwang and Y. K. Kim, "A random beamforming technique in mimo systems exploiting multiuser diversity," *IEEE J. Select. Areas Commun.*, vol. SAC-21, no. 5, pp. 848–855, June 2003.

M. Costa, "Writing on dirty paper," *IEEE Trans. Inform. Theory*, vol. IT-29, no. 5, pp. 439–441, May 1983.

W. Dai, B. C. Rider and Y. E. Liu, "Joint beamforming for multiaccess MIMO systems with finite rate feedback," *IEEE Trans. Wireless Commun.*, vol. 8, no. 5, pp. 2618–2628, May 2009.

H. A. David, *Order Statistics.* New York, NY: John Wiley & Sons, Inc., 1981.

J. Diaz, O. Simeone, O. Somekh and Y. bar-Ness, "Scaling law of the sum-rate for multiantenna broadcast channels with deterministic or selective binary feedback," in *Proc. of Inform. Theory Workshop (ITW'2006)*, Punta del Este, Uruguay, March 2006, pp. 298–301.

J. Diaz, O. Simeone and Y. bar-Ness, "Sum-rate of MIMO broadcast channels with one bit feedback," in *Proc. of Int. Symp. Inform. Theory (ISIT'2006)*, Seattle, Washington, July 2006, pp. 1944–1948.

G. Dimic and N. D. Sidiropoulos, "On downlink beamforming with greedy user selection: performance analysis and a simple new algorithm," *IEEE Trans. Sig. Pro.*, vol. 53, no. 10, pp. 3857–3868, October 2005.

X. Dong and N. C. Beaulieu, "Average level crossing rate and average fade duration of selection diversity," *IEEE Commun. Lett.*, vol. 5, no. 10, pp. 396–398, October 2001.

T. Eng, N. Kong and L. B. Milstein, "Comparison of diversity combining techniques for Rayleigh-fading channels," *IEEE Trans. Commun.*, vol. 44, no. 9, pp. 1117–1129, September 1996.

T. Eng, N. Kong and L. B. Milstein, "Correction to 'Comparison of diversity combining techniques for Rayleigh-fading channels'," *IEEE Trans. Commun.*, vol. COM-46, no. 9, p. 1111, September 1998.

G. Femenias, "Performance analysis of generalized sort, switch, and examine combining," *IEEE Trans. Commun.*, vol. COM-54, no. 12, pp. 2137–2143, December 2006.

G. J. Foschini and M. J. Gans, "On limits of wireless communications in a fading environment when using multiple antennas," *Wireless Pers. Commun.*, vol. 6, no. 3, pp. 311–335, March 1998.

G. J. Foschini, D. Chizhik, M. Gans, C. Papadias and R. A. Valenzuela, "Analysis and performance of some basic spacetime architectures," *IEEE J. Select. Areas Commun.*, vol. 21, pp. 303–320, April 2003.

M. J. Gans, "The effect of Gaussian error in maximal ratio combiners," *IEEE Trans. Commun. Technol.*, vol. COM-19, no. 4, pp. 492–500, August 1971.

H. S. Gao, P. J. Smith and M. V. Clark, "Theoretical reliability of MMSE linear diversity combining in Rayleigh-fading additive interference channels," *IEEE Trans. Commun.*, vol. 46, no. 5, pp. 666–672, May 1998.

D. Gesbert and M.-S. Alouini, "How much feedback is multi-user diversity really worth?" in *Proc. of IEEE Int. Conf. on Commun. (ICC'04)*, Paris, France, June 2004, pp. 234–238.

D. Gesbert, "Robust linear MIMO receivers: a minimum error-rate approach," *IEEE Trans. Signal Processing*, vol. 51, pp. 2863–2871, November 2003.

A. Ghrayeb and T. M. Duman, "Performance analysis of MIMO systems with antenna selection over quasi-static fading channels," *IEEE Trans. Veh. Technol.*, vol. 52, no. 2, pp. 281–288, March 2003.

A. J. Goldsmith, *Wireless Communications*. New York, NY: Cambridge University Press, 2005.

A. J. Goldsmith and S.-G. Chua, "Adaptive coded modulation for fading channels," *IEEE Trans. Commun.*, vol. COM-46, no. 5, pp. 595–602, May 1998.

D. A. Gore and A. J. Paulraj, "MIMO antenna subset selection with space-time coding," *IEEE Trans. Signal Processing*, vol. 50, no. 10, pp. 2580–2588, October 2002.

I. S. Gradshteyn and I. M. Ryzhik, *Table of Integrals, Series, and Products*, 6th ed. San Diego, CA: Academic Press, 2000.

D. Gesbert, M. Shafi, D. S. Shiu, P. Smith and A. Naguib, "From theory to practice: an overview of MIMO space-time coded wireless systems," *IEEE J. Select. Areas Commun.*, vol. 21, no. 4 pp. 281–302, April 2003.

P. Gupta, N. Bansal and R. K. Mallik, "Analysis of minimum selection H-S/MRC in Rayleigh fading," *IEEE Trans. Commun.*, vol. COM-53, no. 5, pp. 780–784, May 2005. See also the conference version in *Proc. of IEEE Int. Conf. on Commun. (ICC'05)*.

S. B. Halima, M.-S. Alouini and K. A. Qaraqe, "Joint MS-GSC combining and downlink multiuser diversity scheduling," *IEEE Trans. Wireless Commun.*, vol. 8, no. 7, pp. 3536–3545, July 2009.

S. Haykin, "Adaptive filter theory," *Information and System Sciences*. Englewood Cliffs, NJ: Prentice Hall, 1986.

K.J. Hole, H. Holm and G. E. Øien, "Adaptive multidimentional coded modulation over flat fading channels," *IEEE J. Select. Areas Commun.*, vol. SAC-18, no. 7, pp. 1153–1158, July 2000.

H. Holma and A. Toskala, *WCDMA for UMTS*, revised ed. New York, NY: John Wiley & Sons, 2001.

G. B. Holter, M.-S. Alouini, G. E. Øien and H.-C. Yang, "Multiuser switched diversity transmission," in *Proc. IEEE Vehicular Technology Conf. (VTC'04-Fall)*, Los Angeles, CA, 2004, pp. 2038–2043.

B. Hassibi and T. L. Marzetta, "Multiple-antennas and isotropically random unitary inputs: the received signal density in closed form," *IEEE Trans. Inform. Theory*, vol. IT-48, no. 6, pp. 1473–1484, June 2002.

J. Hömäläinen and R. Wichman, "Capacities of physical layer scheduling strategies on a shared link," *Wireless Pers. Commun.*, vol. 39, no. 1, pp. 115–134, October 2006.

W. C. Jakes, *Microwave Mobile Communication*, 2nd ed. Piscataway, NJ: IEEE Press, 1994.

N. Jindal and A. Goldsmith, "Dirty-paper coding versus TDMA for MIMO broadcast channels," in *IEEE Trans. Inform. Theory*, vol. IT-51, no. 5, pp. 1783–1794, March 2005. See also *Proc. of IEEE Conf. on Communications (ICC'2004)*, Paris, France, June 2004.

N. Jindal, "MIMO broadcast channels with finite feedback," in *IEEE Trans. Inform. Theory*, vol. IT-52, no. 11, pp. 5045–5059, November 2006. See also *Proc. of IEEE Global Telecomm. Conf. (Globecom'2005)*, St. Louis, MO, November 2005.

S. W. Kim, D. S. Ha and J. H. Reed, "Minimum selection GSC and adaptive low-power RAKE combining scheme," in *Proc. of IEEE Int. Symp. on Circuits and Systems. (ISCAS'03)*, Bangkok, Thailand, May 2003, pp. 357–360.

S. W. Kim, Y. G. Kim and M. K. Simon, "Generalized selection combining based on the log-likelihood ratio," *IEEE Trans. Commun.*, vol. COM-52, no. 4, pp. 521–524, April 2004.

K. J. Kim, S. Y. Kwon, E. K. Hong and K. C. Whang, "Comments on 'Comparison of diversity combining techniques for Rayleigh-fading channels'," *IEEE Trans. Commun.*, vol. COM-46, no. 9, pp. 1109–1110, September 1998.

J. Kim, S. Park, J. H. Lee, J. Lee and H. Jung, "A scheduling algorithm combined with zero-forcing beamforming for a multiuser MIMO wireless system," *Proc. IEEE Semiannual Veh. Tech. Conf.* (VTC' 2005), Dallas, Texas, vol. 1, pp. 211–215, September 2005

R. Knopp and P. Humblet, "Information capacity and power control in single-cell multiuser communications," in *Proc. IEEE Int. Conf. Commun. (ICC95)*, Seattle, WA, vol. 1, pp. 331–335, June 1995.

Y.-C. Ko, M.-S. Alouini and M. K. Simon, "Analysis and optimization of switched diversity systems," *IEEE Trans. Veh. Technol.*, vol. VT-49, no. 5, pp. 1569–1574, September 2000. See also Y.-C. Ko, M.-S. Alouini, and M. K. Simon, "Correction to 'Analysis and optimization of switched diversity systems'," *IEEE Trans. Veh. Technol.*, vol. VT-51, p. 216, January 2002.

Y.-C. Ko, H.-C. Yang, S.-S. Eom and M.-S. Alouini, "Adaptive modulation with diversity combining based on output-threshold MRC," *IEEE Trans. Wireless Commun.*, vol. TWC-6, no. 10, pp. 3728–3737, October 2007.

N. Kong, T. Eng and L. B. Milstein, "A selection combining scheme for RAKE receivers," in *Proc. IEEE Int. Conf. Univ. Personal Comm. (ICUPC'95)*, Tokyo, Japan, November 1995, pp. 426–429.

R. Kwan and C. Leung, "Downlink scheduling optimization in CDMA networks," *IEEE Commun. Letters*, vol. 8, pp. 611–613, October 2004.

G. W. Lank and L. S. Reed, "Average time to loss of lock for an automatic frequency control loop with two fading signals and a related probability density function," *IEEE Trans. Inf. Theory*, vol. IT-12, no. 1, pp. 73–75, January 1966.

J.-P. M. G. Linnartz and R. Prasad, "Threshold crossing rate and average nonfade duration in a Rayleigh-fading channel with multiple interferers," *Archiv Fur Elektronik und Ubertragungstechnik Electonics and Communication*, vol. 43, no. 6, pp. 345–349, November/December 1989.

D. J. Love and R.W. Heath, "Diversity performance of precoded orthogonal space-time block codes using limited feedback," *IEEE Commun. Lett.*, vol. 8, no. 5, pp. 305–307, May 2004.

P. Lu and H.-C. Yang, "Performance analysis for RUB-based multiuser MIMO systems with antenna diversity techniques," *IEEE Trans. Veh. Technol.*, vol. 59, no. 1, pp. 490–494, January 2010.

P. Lu and H.-C. Yang, "A simple and efficient user scheduling strategy for RUB-based multiuser MIMO systems and its sum rate analysis," *IEEE Trans. Veh. Technol.*, vol. 58, no. 9, pp. 4860–4867, November 2009.

P. Lu, H.-C. Yang and Y.-C. Ko, "Sum-rate analysis of MIMO broadcast channel with random unitary beamforming," in *Proc. of IEEE Wireless Commun. and Networking Conf. (WCNC'08)*, Las Vegas, Nevada, March 2008.

Q. Ma and C. Tepedelenlioglu, "Practical multiuser diversity with outdated channel feedback," *IEEE Trans. Veh. Technol.*, vol. 54, no. 4, pp. 1334–1345, July 2005.

Y. Ma and C. C. Chai, "Unified error probability analysis for generalized slection combining in Nakagami fading channels," *IEEE J. Select. Areas Commun.*, vol. 18, no. 11, pp. 2198–2210, November 2000.

Y. Ma and J. Jin, "Unified performance analysis of hybrid-selection/equal-gain combining," *IEEE Trans. Veh. Technol.*, vol. VT-56, no. 4, pp. 1866–1873, July 2007.

Y. Ma, J. Jin and D. Zhang, "Throughput and channel access statistics of generalized selection multiuser scheduling," *IEEE Trans. Wireless Commun.*, vol. 7, no. 8, pp. 2975–2987, August 2008.

Y. Ma and S. Pasupathy, "Efficient performance evaluation for generalized selection combining on generalized fading channels," *IEEE Trans. Wireless. Commun.*, vol. 3, no. 1, pp. 29–34, January 2004.

Y. Ma, D. Zhang and R. Schober, "Capacity-maximizing multiuser scheduling for parallel channel access," *IEEE Signal Processing Letters*, vol. 14, pp. 441–444, July 2007.

R. K. Mallik, D. Gupta and Q. T. Zhang, "Minimum selection GSC in independent Rayleigh fading," *IEEE Trans. Veh. Technol.*, vol. 54, no. 3, pp. 1013–1021, May 2005.

R. K. Mallik and M. Z. Win, "Analysis of hybrid selection/maximal-ratio combining in correlated nakagami fading," vol. COM-50, no. 8, pp. 1372–1383, August 2002.

A. F. Molisch, M. Z. Win and J. H. Winters, "Capacity of MIMO systems with antenna selection," in *Proc. of IEEE Int. Conf. on Commun. (ICC'01)*, Helsinki, Finland, vol. 2, June 2001, pp. 570–574.

A. F. Molisch, M. Z. Win and J. H. Winters, "Reduced-complexity transmit/receive-diversity systems," *IEEE Trans. Signal Processing*, vol. 51, no. 11, pp. 2729–2738, November 2003.

H. Nam and M.-S. Alouini "Multiuser switched diversity scheduling systems with per-user threshold," *IEEE Trans. on Commun.*, vol. 58, no. 5, pp. 1321–1326, May 2010.

S. Nam, M.-S. Alouini and H.-C. Yang, "An MGF-based unified framework to determine the joint statistics of partial sums of ordered random variables," in *IEEE Trans. on Inform. Theory*, vol. IT-56, no. 11, pp. 5655–5672, November 2010.

S. Nam, M.-S. Alouini and H.-C. Yang, "Impact of interference on the performance of selection based parallel multiuser scheduling," in *Proc. of IEEE International Symposium on Information Theory and its Applications (ISITA'08)*, Auckland, New Zealand, December 2008.

S. Nam, M.-S. Alouini, H.-C. Yang and K. A. Qaraqe, "Threshold-based parallel multiuser scheduling," *IEEE Trans. on Wireless Commun.*, vol. 8, no. 4, pp. 2150–2159, April 2009.

S. Nam, H.-C. Yang, M.-S. Alouini and K. A. Qaraqe, "Performance evaluation of threshold-based power allocation algorithms for down-link switched-based parallel scheduling," *IEEE Trans. on Wireless Commun.*, vol. 8, no. 4, pp. 1744–1753, April 2009.

A. H. Nuttall, "Some integrals involving the Q_M function," *IEEE Trans. on Inform. Theory*, no. 1, pp. 95–96, January 1975.

A. H. Nuttall, "An integral solution for the joint PDF of order statistics and residual sum," NUWC-NPT, Technical Report, October 2001.

A. H. Nuttall, "Joint probability density function of selected order statistics and the sum of the remaining random variables," NUWC-NPT, Technical Report, January 2002.

A. H. Nuttall and P. M. Baggenstoss, "Joint distributions for two useful classes of statistics, with applications to classification and hypothesis testing," *IEEE Trans. Signal Processing*, submitted for publication. [Online]. Available: http://www.npt.nuwc.navy.mil/Csf/papers/order.pdf

K.-H. Park, Y.-C. Ko and M.-S. Alouini, "Joint adaptive combining and multiuser downlink scheduling," *IEEE Trans. Veh. Technol.*, vol. 57, no. 5, pp. 2958–2968, September 2008.

S. Y. Park, D. Park and D. J. Love, "On scheduling for multiple-antenna wireless networks Using contention-based feedback," *IEEE Trans. Commun.*, vol. 55, no. 6, pp. 1174–1190, June 2007.

A. J. Paulraj, D. A. Gore, R. U. Nabar and H. Blcskei, "An overview of MIMO communications. A key to gigabit wireless," *Proc. IEEE*, vol. 92, no. 2, pp. 198–218, February 2004.

A. Paulraj, R. Nabar and D. Gore, *Introduction to Space-Time Wireless Communications*. Cambridge: Cambridge University Press, 2003.

R. Prasad, *OFDM for Wireless Communication Systems*. Boston, MA: Artech House Publishers, 2004.

M. Pugh and B. D. Rao, "Reduced feedback schemes using random beamforming in MIMO broadcast channels," *IEEE Trans. Signal Process.*, vol. 58, no. 3, pp. 1821–1832, March 2010.

M. O. Pun, V. Koivunen and H. V. Poor, "SINR analysis of opportunistic MIMO-SDMA downlink systems with linear combining," *Proc. of IEEE Int. Conf. Commun.* (ICC'2008), Beijing, China, May 2008.

M. O. Pun, V. Koivunen and H. V. Poor, "Opportunistic scheduling and beamforming for MIMO–SDMA downlink systems with linear combining," *Proc. of Int. Symp. Personal, Indoor and Mobile Radio Commun.* (PIMRC' 2007), Athens, Greece, September 2007.

W. Rhee, W. Yu and J. M. Cioffi, "The optimality of beamforming in uplink multiuser wireless systems," *IEEE Trans. Wireless Commun.*, vol. TWC-3, no. 1, pp. 86–96, January 2004.

Y. Roy, J.-Y. Chouinard and S. A. Mahmoud, "Selection diversity combining with multiple antennas for MM-wave indoor wireless channels," *IEEE J. Select. Areas Commun.*, vol. SAC-14, no. 4, pp. 674–682, May 1998.

S. Sanayei and A. Nosratinia, "Opportunistic downlink transmission with limited feedback," *IEEE Trans. Inform. Theory*, vol. 53, no. 11, pp. 4363–4372, November 2007.

M. Sellathurai and G. J. Foschini, "Stratified diagonal layered spacetime architectures: signal processing and information theoretic aspects," *IEEE Trans. Signal Processing*, vol. 51, pp. 2943–2954, November 2003.

A. Shah and A. M. Haimovich, "Performance analysis of optimum combining in wireless communications with Rayleigh fading and cochannel interference," *IEEE Trans. Commun.*, vol. 46, no. 4, pp. 473–479, April 1998.

M. Sharif and B. Hassibi, "On the capacity of MIMO broadcast channels with partial side information," *IEEE Trans. Inform. Theory*, Vol. IT-51, no. 2, pp. 506–522, February 2005.

M. K. Simon and M.-S. Alouini, "Performance analysis of generalized selection combining with threshold test per branch (T-GSC)," *IEEE Trans. Veh. Technol.*, vol. VT-51, no. 5, pp. 1018–1029, September 2002.

M. K. Simon and M.-S. Alouini, *Digital Communications over Generalized Fading Channels: A Unified Approach to Performance Analysis*. New York, NY: John Wiley & Sons, 2000.

J. So and J. M. Cioffi, "Feedback reduction scheme for downlink multiuser diversity," *IEEE Trans. Wireless Commun.* , vol. 8, no. 2, pp. 668–672, February 2009.

J. So and J. M. Cioffi, "Multiuser diversity in a MIMO System with opportunistic feedback," *IEEE Trans. Veh. Technol.*, vol. 58, no. 9, pp. 4909–4918, November 2009.

G. L. Stüber, *Principles of Mobile Communications*, 2nd ed. Norwell, MA: Kluwer Academic Publishers, 2000.

P. V. Sukhatme, "Tests of significance for samples of the population with two degrees of freedom," *Ann. Eugenics*, vol. 8, p. 5256, 1937.

A. I. Sulyman and M. Kousa, "Bit error rate performance of a generalized diversity selection combining scheme in Nakagami fading channels," in *Proc. of IEEE Wireless Commun. and Networking Conf. (WCNC'00)*, Chicago, Illinois, September 2000, pp. 1080–1085.

T. Tang and R. W. Heath, "Opportunistic feedback for downlink multiuser diversity," *IEEE Commun. Lett.*, vol. 9, no. 10, pp. 948–950, October 2005.

V. Tarokh, N. Seshadri and A. R. Calderbank, "Spacetime codes for high data rate wireless communication: performance criterion and code construction," *IEEE Trans. Inform. Theory*, vol. 44, no. 2, pp. 744–765, March 1998.

I. Emre Telatar, "Capacity of multi-antenna Gaussian channels," *European Trans. Telecomm.*, vol. 10, no. 6, pp. 585–595, November–December 1999.

C. Tellambura, A. Annamalai and V. K. Bhargava, "Unified analysis of switched diversity systems in independent and correlated fading channel," *IEEE Trans. Commun.*, vol. COM-49, no. 11, pp. 1955–1965, November 2001.

S. Thoen, L. V. der Perre, B. Gyselinckx and M. Engels, "Performance analysis of combined transmit-SC/receive-MRC," *IEEE Trans. Commun.*, vol. 49, no. 1, p. 58, January 2001.

B. R. Tomiuk, N. C. Beaulieu and A. A. Abu-Dayya, "General forms for maximal ratio diversity with weighting errors," *IEEE Trans. Commun.*, vol. COM-47, no. 4, pp. 488–492, April 1999. See also *Proc. IEEE Pacific Rim Conf. on Communications, Computers and Signal Processing (PACRIM'99)*, Victoria, BC, Canada, pp. 363–368, May 1995.

A. M. Toukebri, S. Aissa and M. Maier, "Resource allocation and scheduling for multiuser MIMO systems: a beamforming-based strategy," *Proc. IEEE Global Telecomm. Conf. (Globecom' 2006)*, San Francisco, California, November 2006.

D. N. C. Tse, "Optimal power allocation over parallel Gaussian channels," in *Proc. Int. Symp. Inform. Theory (ISIT97)*, Ulm, Germany, p. 27, June 1997.

N. T. Uzgoren, "The asymptotic developement of the distribution of the extreme values of a sample," in *Studies in Mathematics and Mechanics Presented to Richard von Mises*. New York, NY: Academic, 1954, pp. 346–353.

S. Vishwanath, N. Jindal and A. Goldsmith, "Duality, achievable rate and sum-rate capacity of Gaussian MIMO broadcast channels," *IEEE Trans. Inform. Theory*, vol. IT-49, no. 10, pp. 2659–2668, October 2003.

P. Viswanath, D. Tse and R. Laroia,"Opportunistic beamforming using dumb antennas," *IEEE Trans. Inform. Theory*, vol. 48, pp. 1277–1294, June 2002.

P. Viswanath and D. Tse, "Sum capacity of the vector Gaussian broadcast channel and uplink–downlink duality," *IEEE Trans. Inform. Theory*, vol. IT-49, no. 8, pp. 1912–1921, August 2003.

H. Viswanathan, S. Venkatesan and H. Huang, "Downlink capacity evaluation of cellular networks with known-interference cancellation," *IEEE J. Select. Areas Commun.*, vol. 21, no. 5, pp. 802–811, June 2003.

H. Wang, A. B. Gershman and T. Kirubarajan, "Random unitary beamforming with partial feedback for multi-antenna downlink transmission using multiuser diversity," in *Proc. of IEEE Veh. Technol. Conf. (VTC'Spring 2005)*, June 2005, pp. 216–220.

H. Weingarten, Y. Steinberg and S. Shamai, "The capacity region of the Gaussian multiple-input multiple-output broadcast channel," *IEEE Trans. Inform. Theory*, vol. IT-52, no. 7, pp. 3936–3964, September 2006.

M. Z. Win and Z. A. Kostić, "Virtual path analysis of selective Rake receiver in dense multipath channels," *IEEE Commun. Letters*, vol. 3, no. 11, pp. 308–310, November 1999.

M. Z. Win and J. H. Winters, "Analysis of hybrid selection/maximal-ratio combining in Rayleigh fading," *IEEE Trans. Commun.*, vol. COM-47, no. 12, pp. 1773–1776, December 1999. See also *Proceedings of IEEE International Conference on Communications (ICC'99)*, pp. 6–10, Vancouver, British Columbia, Canada, June 1999.

M. Z. Win and J. H. Winters, "Virtual branch analysis of sysmbol error probability for hybrid selection/maximal-ratio combining Rayleigh fading," *IEEE Trans. Commun.*, vol. 49, no. 11, pp. 1926–1934, 2001.

J. H. Winters, "Optimum combining in digital mobile radio with cochannel interference," *IEEE Trans. Veh. Technol.*, vol. 33, no. 3, pp. 144–155, August 1984.

L. Xiao and X. Dong, "Unified analysis of generalized selection combining with normalized threshold test per branch," *IEEE Trans. Wireless Commun.*, vol. 5, no. 8, pp. 2153–2163, August 2006.

Y. Xue and T. Kaiser, "Exploiting multiuser diversity with imperfect one-bit channel state feedback," *IEEE Trans. Veh. Technol.*, vol. 56, no. 1, pp. 183–193, January 2007.

H.-C. Yang and M.-S. Alouini, "Markov chain and performance comparison of switched diversity systems," *IEEE Trans. Commu.*, Vol. COM-52, no. 7, pp. 1113–1125, July 2004.

H.-C. Yang and M.-S. Alouini, "Performance analysis of multibranch switched diversity systems," *IEEE Trans. Commun.*, vol. COM-51, no. 5, pp. 782–794, May 2003.

H.-C. Yang and M.-S. Alouini, "Improving the performance of switched diversity with post-examining selection," *IEEE Trans. Wireless Commun.*, vol. TWC-5, no. 1, pp. 67–71, January 2006.

H.-C. Yang and M.-S. Alouini, "Generalized switch and examine combining (GSEC): a low-complexity combining scheme for diversity rich environments," *IEEE Trans. Commun.*, vol. COM-52, no. 10, pp. 1711–1721, October 2004.

H.-C. Yang and L. Yang, "Tradeoff analysis of performance and complexity on GSECps diversity combining scheme," *IEEE Trans. on Wireless Commun.*, vol. TWC-7, no. 1, pp. 32–36, January 2008.

H.-C. Yang, "New results on ordered statistics and analysis of minimum-selection generalized selection combining (GSC)," *IEEE Trans. Wireless Commun.*, vol. TWC-5,

no. 7, July 2006. See also the conference version in *Proc. of IEEE Int. Conf. on Commun. (ICC'05)*.

L. Yang and M.-S. Alouini, "Performance analysis of multiuser selection diversity," *IEEE Trans. Veh. Technol.*, vol. 55, pp. 1003–1018, May 2006.

H.-C. Yang and M.-S. Alouini, "MRC and GSC diversity combining with an output threshold," *IEEE Trans. Veh. Technol.*, vol. TVT-54, no. 3, pp. 1081–1090, May 2005.

T. Yoo and A. Goldsmith, "On the optimality of multi-antenna broadcast scheduling using zero-forcing beamforming," *IEEE J. Select. Areas Commun.*, vol. SAC-24, no. 3, pp. 528–541, March 2006.

T. Yoo and A. Goldsmith, "Sum-rate optimal multi-antenna downlink beamforming strategy based on clique search," *Proc. IEEE Global Telecomm. Conf. (Globecom' 2005)*, St. Louis, Missouri, vol. 3, pp. 1510–1514, December 2005.

X. Zhang and N. C. Beaulieu, "SER and outage of thresholdbased hybrid selection/maximal-ratio combining over generalized fading channels," *IEEE Trans. Commun.*, vol. 52, no. 12, pp. 2143–2153, December 2004.

K. Zhang and Z. Niu, "Random beamforming with multibeam selection for MIMO broadcast channels," in *Proc. of IEEE Intl. Conf. Commun. (ICC'2006)*, Istanbul, Turkey, June 2006, pp. 4191–4195.

Index